Genosensors:

Design

and

characterisation

Edna P. Williams (BSc)
PhD candidate
November 2002

I hereby certify that this material,
which I now submit for assessment on the program of study
leading to the award of a PhD thesis is entirely my own work
and has not been taken from the work of others save and
to the extent that such work has been cited and
acknowledged within the text of my work.

Signed:_____.

ID No_____98970593_____.

Date_____15/11/02_____.

Acknowledgements

First and foremost I would like to thank Prof. Robert Forster for his support, understanding and useful discussions throughout my PhD, but especially for teaching the lesson that everything can be learned, thank you. I would also like to thank both Dr. Donal Leech, national university Galway, and Prof. Salvador Alegret, UAB, Barcelona for giving me the chance to work with them within their research groups and also for giving me the opportunities to explore new places.

To the technical staff of DCU, Veronica, Mick, Ambrose, Vinny and for helpful assistance on many levels. To the past and present members of the Robert Forster research group, thanks for the wide variety of music and conversations supplied throughout the lab day, good luck with your futures.

Thanks to Clodagh, Marco, Fiona, and Jenny *et al* for the interesting coffee discussions and for providing moments of sanity in a sometimes, insane world. To various friends for technical support when it looked like everything was lost and about to be abandoned. All those people that I met in DCU, Dublin and beyond during those college days, it was a great pleasure, sorry the names are too numerous to mention but conversations and nights are remembered.

Finally to those I love, my parents and family for their constant support and patience throughout my *long* college stay, I hope it will be worth it! And to George for his companionship and for travelling over past few years, thanks it has been an adventure.

"Every search begins with beginners luck.
And every search ends with the
victor being severely tested"

Paul Choelho "Alchemist"

Abstract:

Edna P. Williams (BSc)

A sensor capable of detecting specific sequence of DNA was designed by bulk modification of a graphite epoxy composite electrode with either avidin or streptavidin (2% w/w). Avidin or streptavidin are used to capture a biotinylated DNA strand and immobilize this capture DNA onto the surface of the electrode. Subsequent hybridisation is achieved between this biotin DNA strand and a target DNA sequence. The rapid binding kinetics of avidin/ streptavidin–biotin allow a one step immobilization and hybridisation procedure. Detection of this DNA duplex is achieved through use of a small antibody labelled DNA strand. Immersion of DNA electrode in a solution containing a horseradish peroxidase labelled antigen allows electrochemical detection to be achieved in the presence of H_2O_2 and an electron mediator hydroquinone. Optimization of the sensor design, percentage modifier, immobilization and hybridisation times, was achieved using a simple nucleotide sequence and detection limits of 150 picomolar are reported. Regeneration of the sensor is achieved by using a simple polishing procedure, and shows good reproducibility. A two percent avidin–graphite epoxy composite gave the best performance, lowest non-specific adsorption, greater reproducibility and stability. Subsequently a genosensor was prepared that was capable of detecting a gene, *mec*A, specific to Methicillin Resistant *Staphylococcus aureus* (MRSA).

A characterization of these graphite epoxy composite electrode is also reported. This characterization involved an electrochemical and microscopic study. Results indicate that these composite electrodes exhibit properties similar to a random assembly of microelectrodes, as they possess characteristics such as generation of steady state current at short times, capability of being use in highly resistive media. Scanning electron microscopy illustrates that these electrodes are heterogeneous in nature. Resistance measurements indicate these electrodes have a resistance of 11.45 Ω that is comparable with glassy carbon electrode, 10.18 Ω. The RC time constant was calculated to be 0.07 s. Using the Nicholson–Shain model for the measurement of the rate of heterogeneous electron transfer show that these graphite epoxy composite electrodes posses a sluggish rate of electron transfer. 0.35×10^{-3} cm s^{-1} and scan rates no greater than 20 Vs^{-1} can be employed.

To study the influence various physiological buffers exert on the electrochemical response polymer modified electrodes (PMEs) were prepared using a glassy carbon electrode by drop-casting 40 μl of a metallopolymer, $[Os(dime(bpy)_2PVI_{10}Cl]PF_6,(Os–PVI_{10})$ where dime(bpy) is 2'2 dimethyl–bipyridyl and PVI in poly–N–vinylimidazole. This metallopolymer was synthesized from the $[Os(dime(bpy)_2Cl]^{2+/3+}$ and PVI. Characterisation of the synthesised product was achieved using HPLC, UC-visible and elemental analysis and indicate good purity. To investigate the influence of a biocomponent progesterone was incorporated within the PME. Electrochemical characterization involved cyclic voltammetry to determine the value of the diffusion coefficient and to compare the values with those obtained from chronoamperometry. Results indicate that the rate of charge transport is slower in buffered systems but shows the best response in phosphate buffer. An investigation into the rate of heterogeneous electron transfer for Os–PVI_{10} and progesterone modified show rates of 1.55×10^5 and 0.51×10^5 cm s^{-1} respectively.

Table of contents

Abbreviations

AIBN:	2,2´-azobisisobutylonitrile
Anti-dig-HRP:	antidigoxigenin labelled horse radish peroxidase
bpy:	bipyridine
CME	chemically modified electrode
CPE:	Carbon paste electrode
CPSV:	constant potential stripping voltammetry
C_o:	concentration of oxidized species
C_R:	concentration of reduced species
dime(bpy)$_2$:	4,4'–dimethyl–2,2'–dipyridyl
Dig-DNA:	digoxigenin labelled DNA
DMF:	dimethyl formamide
DNA:	Deoxyribonucleic acid
dsDNA:	double stranded DNA
EIA:	enzyme immunoassay
ELISA:	enzyme linked immunosorbent assay
EP:	ephedrine
EQCM:	electrochemical quartz crystal microbalance
FADH$_2$:	Flavinadenonine dehydrogenase
FWHM:	full width half maximum
GC:	gas chromatography
GO:	Glucose oxidase
HMDE:	hanging mercury drop electrode
HPLC:	high performance liquid chromatography
HOMO:	highest occupied molecular orbital
HRP:	horseradish peroxidase
K$_D$:	kilo Dalton
LC:	liquid chromatography
LUMO:	lowest unoccupied molecular orbital
Mab:	Monoclonal antibody
MLCT:	metal to ligand charge transfer reaction
MRSA:	methicillin resistant *Staphylococcus aureus*
MTEOS:	methyltriethoxysilane
NNISSS:	National Nosocomial Infections Surveillance System

NADH: nicotine adenine dehydrogenase

PBS/BSA: phosphate buffered saline/bovine serum albumin

PCR: polymerase chain reaction

PEG(DGE):   poly ethylene glycol (diglycidyl-ether)

PFGE: pulse field gel electrophoresis

PME: polymer modified electrode

Prog.:   progesterone

PVP: poly(N-vinyl-pyridine)

PVI: Poly(N–vinylimidazole)

O: species oxidized at the electrode surface

R: species reduced at the electrode surface

SEM: scanning electron microscopy

s/n: signal: noise ratio

ssDNA: single stranded DNA

TCQN: 7,7´8,8´tetracyanoquinodimethane

TBAF$_4$:   tetrabutylammonium tetra fluoride

TMB: Trimethylbenzene

Tris:

UME: ultramicroelectrode

UV/Vis: Ultra violet visible

Symbols

E_e: equilibrium potential (V)

E: Potential (V)

E_F: formal potential (V)

$E_{initial}$: initial applied potential (V)

E^{θ}:   standard potential (V)

E_p: peak potential (V)

ΔE_p: difference in peak to peak splitting (V)

n: number of electrons being transferred

F: Faraday's constant

T: temperature (K or °C)

$G^{\neq}$:	Gibbs free energy
i_{ss}:	steady state current (Amp)
k'_f:	rate constant for the forward reaction (cm s^{-1})
k'_b:	rate constant for the forward reaction (cm s^{-1})
K:	Boltzmann constant
η:	over potential
α:	symmetry factor
k°:	standard rate of heterogeneous electron transfer (cm s^{-1})
R:	universal gas constant
Q:	charge (C)
Γ:	surface coverage (mol cm^{-2})
RC:	cell time constant
V:	Voltage (V)
R:	resistance (Ω)
r_s:	radius of sphere (μm)
D_O/D_R:	ratio of diffusion coefficient for the oxidation vs. reduction process

Chapter 1

Literature Survey:

Polymer Modified Electrodes

1.1   Introduction

Chemically modified electrodes (CME) represent a highly developed and investigated class of chemically integrated systems. Faulkner[1] described chemically modified electrodes as *"this lovely assembly is not a technological object. But it is an artistic one for a scientific clientele. And it shows beautifully the level of control of both structure and function that can be imposed on an electrode"*. These modified electrodes result from the purposeful manipulation of a conductive substrate to produce an electrode suited to a particular function and whose properties are different from those of the unmodified substrate. The strong and sometimes irreversible, adsorption of species onto an electrode surface has long been known to alter the electrochemical behaviour of an electrode surface. Some well-known examples of this phenomenon are the adsorption of CN^- onto the surface of platinum electrode, which results in a negative shift in the potential at which hydrogen evolves.[2] This effect has the advantage of broadening the working potential range to more negative potentials for electroanalytical work.[2]

The interest in modifying electrode surfaces though chemical means with subsequent characterisation began in the 1970s. It was the potential number of applications that could theoretically arise, which drove this interest. For example, an electrode of an inexpensive and rugged material could be utilised for fuel cells if oxygen could be reduced to water at a reasonable rate near the thermodynamic potential. Moreover, examples exist of surface films capable of emitting light upon electrochemical oxidation.[3] These would have the potential to be used in active displays.[4] The area of most interest to analytical scientists involves the modification of an electrode with a biological species to form what is known as a biosensor.[5] This approach exploits the exquisite sensitivity of biological materials such as antibodies and DNA to confer selectivity of the electrode response.

When dealing with chemically modified electrodes, it is essential to remember that by adsorbing a species onto the surface of the electrode, one is deliberately attempting to manipulate its surface such that it will exhibit the chemical, electrochemical, and spectral properties of the immobilized species. For electroanalytical applications, such as those considered here, the choice of modifying material is determined principally by the analyte of interest, and, is chosen on the basis that it will enhance/improve the selectivity, sensitivity, or dynamic range of the electrochemical response.

In addition to expanding electroanalytical measurements, these electrodes also provide a good insight as to how surface-confined species behave with respect to their solution phase counterparts. If there are no lateral interactions between adsorbed species on the surface of the electrode, these confined species ought to exhibit the same behaviour as their free counterparts.[6] Possibly, one of the most useful of all chemically modified electrodes, CMEs, involves modifying films that are themselves electroactive. If a surface-confined species is capable of exchanging electrons with the electrode surface, this allows the thermodynamics and kinetics of electron transfer to be studied in unprecedented detail.

The decision to create a CME starts with the choice of electrode material that must have high electrical conductivity, with a good resistance to corrosion. Electrodes should be both mechanically and chemically stable. Both platinum and gold exhibit the required chemical stability and inertness. However, due to the relative expense of these materials a more popular choice of substrate is carbon.

In addition to the low cost, its popularity is due to its surface activity that facilitates the attachment of organic groups. Typical surface functional groups include hydroxyl, carboxyl and quinones. A wide variety of physical and chemical forms of carbon exist ranging from graphite, pyrolytic graphite, glassy carbon, and a wide range of polycrystalline materials with varying degrees of porosity.

The ability of carbon electrodes to form CMEs is due to the high π-electron density of carbon, which allows for extensive Van-der-Waals or Coulombic interactions between the substrate and the adsorbed film. Of the methods that exist for modification of an electrode, possibly one of the most popular is film deposition. One class of film deposited electrodes, which demonstrates many advantages, is known as a polymer-modified electrode (PME). These PMEs consist of polymers, which are either electroactive on their own, or, contain electroactive groups being modified on to an electrode surface; examples of these types of polymers can be seen in Figure 1.1. The most common are those containing electroactive groups, which have been synthetically incorporated into their backbone.

One of the main advantages of this approach, in which the metallopolymer is preformed rather than polymerised in-*situ* onto the electrode surface, is the capability of characterising and manipulating the polymer with respect to its redox behaviour. It is possible to achieve such manipulation by altering the backbone or the redox centre loading without affecting the redox properties of the PME.

Another advantage associated with film deposition is the ability to form relatively thick layers of controlled thickness as opposed to the other methods that often form monolayers.[2] This capability is important since layer thickness may play an important role in efficiency, charge transport rates, and stability of the modified layer. Modification of an electrode surface with a polymer can be achieved simply and reproducibly by three different methods. The first method is known as polymer casting and involves dissolution of the polymer in a volatile solvent, and, then transferring a small quantity (usually μl) to the electrode surface where the solvent evaporates leaving a formed PME. The drying method, e.g., vacuum assisted solvent evaporation can influence the layer morphology.[2] Hence, this is an important aspect as for analytical measurements the greater the available surface area the more enhanced the analytical response.

Other methods similar to drop casting involve dip coating and spin coating. The spin-coating technique allows control over the layer thickness by controlling the rotation speed and solvent viscosity at which the polymer is deposited from solution.

An alternative approach to forming PMEs is to use a monomer that can be electro-oxidised or photo-polymerised onto the surface of the electrode.[7] In the case of electro-polymerisation, modification of the electrode surface is achieved in a single step by creating radical intermediates electrochemically near the electrode. The rate of initiation is controlled by electrode potential. Typically, a heavily cross-linked polymer layer forms, resulting in problems of slow charge transport and irregular surface morphology.[8,9] Additionally, it is difficult to guarantee that all the radicals formed produce polymers at the electrode surface and also control of the chain length is difficult to achieve.

Choices of polymers available for modification of the surface of an electrode range from electroactive polymers;[10] these contain redox species within the polymer backbone, typical examples were shown in Figure 1.1. Ion-exchange polymers[11] contain charged sites, which are capable of incorporating species via an ion exchange process; typical examples of these are Nafion® and polystyrene sulphonate polymers. Another alternative is electronically conductive polymers[12] such as polyaniline or polypyrrole. Coordinating polymers[13] such as poly(vinyl pyridine) or poly(vinylimidazole) contain groups capable of coordinating with metal ions, such as osmium or ruthenium bipyridyl complexes, and permanently entrapping them into the polymer matrix.

This chapter reviews past literature dedicated to the deliberate modification of electrode surfaces, in particular carbon electrode surfaces. The theory of dynamic electrochemistry is also examined especially with regards to the overall of range of sensing systems available

Electroactive polymers

Poly(vinylferrocene)

$$—(CH_2—CH)_n—$$
$$|$$
$$FeCp_2$$

Poly[Ru(vbpy)$_3^{2+}$][b]

$$—(CHCH_2)_n—$$
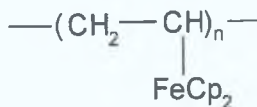
Ru(vbpy)$_2$
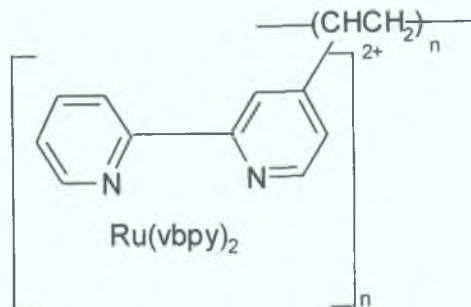
Ion-exchange polymers (polyelectrolytes)

Nafion

$$—(CF_2CF_2)_x(CFCF_2)_y—$$
$$|$$
$$O—C_3F_6—O—CF_2CF_2—SO_3^- Na^+$$
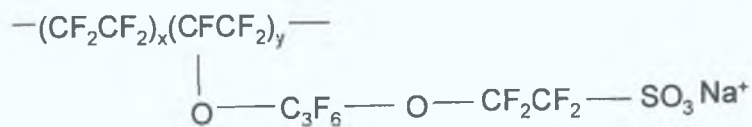
Quaternized poly
(4-vinylpyridium)

$$—(CH_2—CH^-)_n—$$

N+

Me
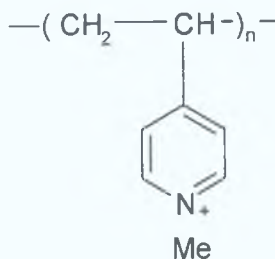
Coordinating Polymer

Poly(4-vinylpyridine)

$$—(CH_2—CH)_n—$$

N
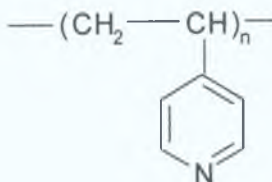
Figure 1.1. Typical polymers used for electrode modification.
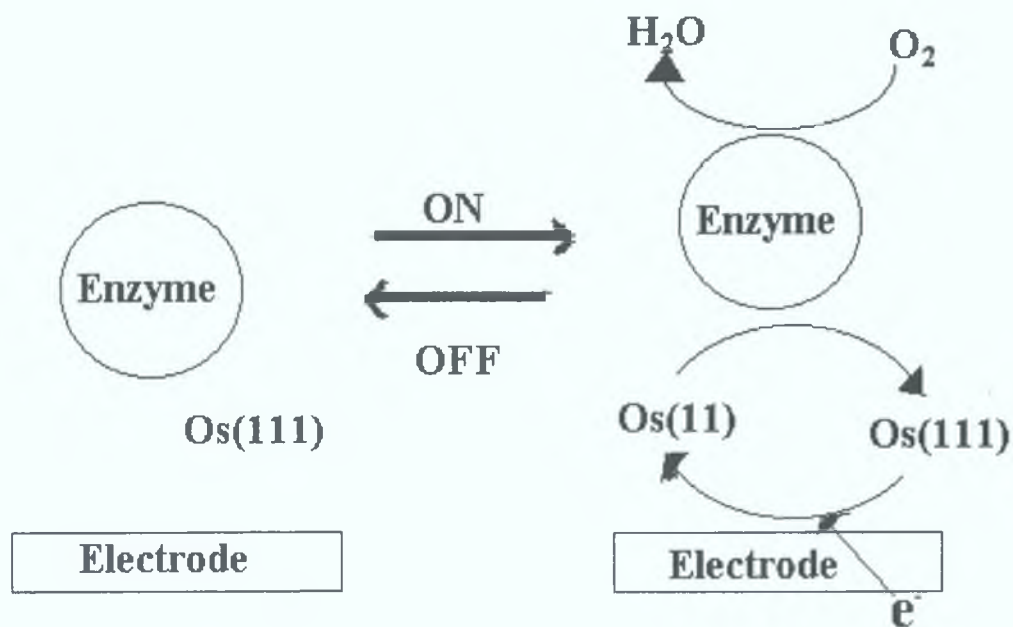
Figure 1.2. Catalytic scheme for the activity of the co-immobilised enzyme and osmium redox mediator in a hydro-gel on a glassy carbon electrode surface

1.3   Biosensors and polymer modified electrodes

One of the main reason for extensive research into the area of sensors is the diagnosis and management of disease, e.g., diabetes. Diabetes monitoring requires a fast, efficient, reliable, and cheap method for the analysis of glucose levels in blood. When one considers the highly complex nature of the blood matrix, a highly selective method of analysis is required. The obvious choice of method for detection involved the use of the highly specific enzyme responsible for the breakdown of glucose known as glucose oxidase/glucose oxidoreductase. Glucose oxidase (GO–FAD) is compose of two identical sub-units covalently linked to each other by disulphide bonds; each sub-unit consists of one molecule of iron and FAD.[14] In the presence of glucose, the reaction seen in Equation 1.2 occurs with the regeneration GO-FAD in the presence of oxygen.

$$GO\text{-}FAD + Glucose \rightarrow GO\text{-}FADH_2 + Gluconolactone$$
$$GO\text{-} FADH_2 + O_2 \rightarrow GO\text{-}FAD + H_2O_2 \qquad \textbf{Equation 1.2}$$
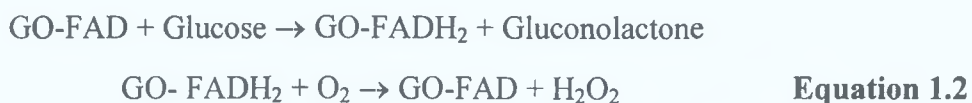
It was recognised that electron transfer was occurring in the above reaction, making it feasible to use electrochemistry as a method of analysis. From Equation 1.2, it can be seen that the decrease in O_2 with an oxygen electrode or an increase in H_2O_2 with a platinum electrode may used to determine the presence of glucose.

In 1977, Suzuki et al[15] immobilised glucose oxidase onto the surface of a poly-vinyl chloride (PVC) membrane that was then attached to the surface of an electrode. The use of the PVC membrane was necessary to ensure that the enzyme remained in close proximity to the electrode surface. However, there are many problems associated with this method of detection of glucose. Firstly, the concentration of O_2 is an extremely difficult parameter to measure accurately. In addition, H_2O_2 degrades the enzyme; therefore, not an ideal method of detection. Another problem, is that the measurement of H_2O_2 requires a highly catalytic electrode (increases cost) and a positive working potential for the detection of the reversible $FAD/FADH_2$ redox couple. This positive potential results in high background current, increasing the limit of detection and triggering enzyme degradation. In addition to these aforementioned problems, the use of a PVC selective membrane increased the cost of the electrode preparation, while also creating problems associated with leaching of enzyme through the membrane resulting in low stability of the electrode. Although much research was
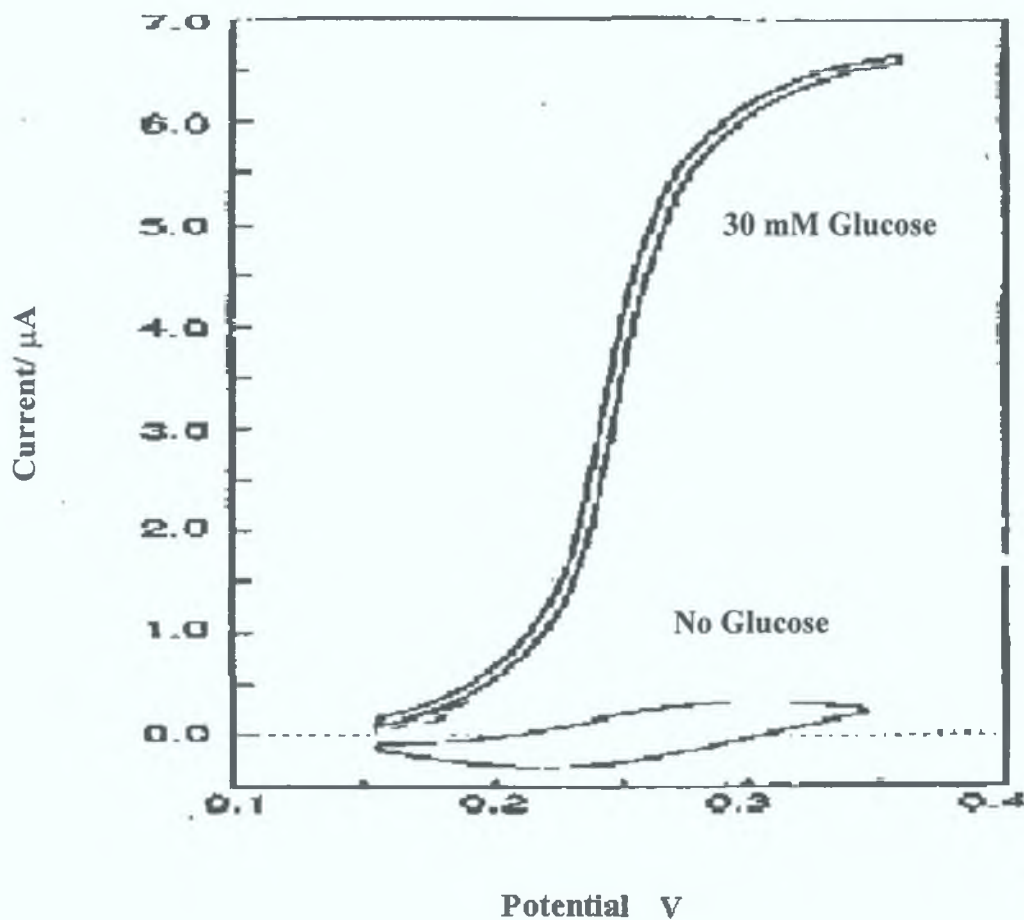
Figure 1.4. Cyclic voltammogram for glucose oxidase enzyme electrode. In the absence of (lower curve) and presence (upper curve), 0.15 M NaCl and with 30 mM glucose. The enzyme electrode is made with a copolymer of (poly(vinyl pyridine-Os(bpy)$_2$Cl) and poly(vinyl-N-methylpyridinium chloride). 3 mm in diameter glassy carbon electrodes and a scan rate of 0.002 Vs^{-1}

capable of detecting levels of azide as low as 1 μM in solution. Interestingly, studies on a slow electron transfer enzymes, such as Ceruloplasmin, show that no catalytic currents are observed. These results indicate the suitability of using fast electron exchange mediators to probe rapid electron exchange reactions, between the enzyme redox centre and redox polymer homogeneous rate constants, while also indicating the unsuitability of these mediators for slow electron exchange reactions.

Apart from the development of biosensors incorporating enzymes, another important area of analysis requiring the use of a rapid sensitive detection system involves the detection of neurotransmitters such as epinephrine. Epinephrine is an important compound involved in message transfer in the mammalian central nervous system. Many diseases are known to be associated with changing concentrations of epinephrine within the brain. For this reason it was under taken to design a suitable method of detection.[30] Traditional detection of epinephrine involved liquid chromatography[31] and visible spectroscopy.[32] The electroactive nature of this molecule means that it can be detected using electrochemistry.[33,34] A major problem in accurately determining its concentration is the presence of interferences. Work presented by Ni *et al*,[30] overcomes these problems by use of a Nafion® layer and an osmium redox polymer. Incidences where it is necessary to use a semi-permeable membrane, and resulting in a loss of sensitivity, a fast redox mediator can be used, counteracting the loss in sensitivity with slight improvements in detection limits at the same time. By using a semi-permeable membrane and an osmium polymer, a lower limit of detection was achieved in comparison with previous attempts by the same group, which developed sensors using other modifiers such as methylene green. In both incidences ephedrine was detected by its electrocatalytic oxidation according to Equation 1.3 below, where EP is ephedrine and Os-PVP$_{10}$ is an osmium polyvinyl pyridine mediator.

$$2[\text{Os-PVP}_{10}]^{2+} + \text{EP}_{red} \rightarrow 2[\text{Os-PVP}_{10}]^+ + \text{EP}_{ox} \qquad \textbf{(Equation 1.3)}$$

Rather than using conventional macroelectrodes, Huangxian *et al*[35] used carbon fibre microelectrodes modified with the same polymer as was used previously.[29] These modified electrodes showed electrocatalytic activity for the oxidation of Nicotinamide Adenine Dinucleotide (Phosphate) Dehydrogenase (NAD(P)H). NAD(P)H are key central electron carriers in biological redox reactions, which relate to approximately 300 dehydrogenase enzymes, thus selective determination of NADH, or

NADPH co-factors is significant. Numerous mediators for modified electrode surfaces have been developed for the electrochemical determination of NADH[36, 37, 38, 39] However, the use of an osmium polymer allows a simple and sensitive method for detection of NADH.

The high selectivity of enzymes coupled with modern technology should theoretically result in an electrochemical sensor capable of detecting single biochemical species in a complex matrix. However, there are complications with this approach as the nature of the substance being analysed must be considered. When one is talking about biological molecules, it must be remembered that the structure can sometimes be very complex. Indeed this is the case with glucose oxidase, where the redox centre is buried deep within the protein folds of the enzyme. In such a case direct communication between the redox centre and a metal electrode surface is impeded.

Despite the enormous potential of CMEs for chemical analysis, such devices are rarely used for routine monitoring and are not widely available for commercial use. This sparse commercial exploitation is in part is due to the mode of preparation of CMEs, which involves the attachment of a modifier to the bare electrode surface by means of covalent bonding, chemisorption or polymer coatings. While these approaches yield the desired effects, they suffer drawbacks from the practical difficulties that limit the ease with which the resulting electrodes can be routinely prepared, used, and renewed for subsequent reuse. Shaw and Creasy[40] described a class of CMEs prepared by co-polymerisation of styrene and divinyl-benzene, in the presence of the modifier and carbon black based on the more traditional carbon paste electrodes (CPE) developed by Adams *et al.*[41] Such a scheme resulted in the development of robust and polishable (renewable) bulk modified electrodes, as desired for many practical applications. While the concept of these bulk modified is very attractive, difficulties arise due to complex fabrication procedure, short shelf life and low success rate. Wang *et al*[42] developed graphite epoxy modified electrodes, which exhibited the desired characteristics for "real life" applications. Experiments involved the use of commercially available graphite filled epoxy resin. Modification of this epoxy resin is easily accomplished by mixing the desired quantity of the modifier within the resin, Figure 1.5.
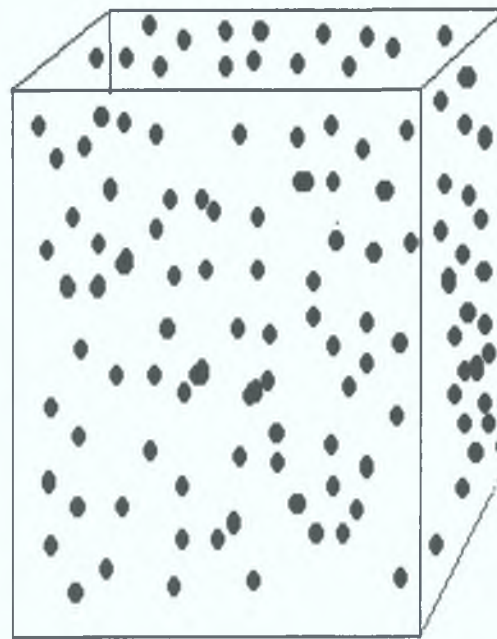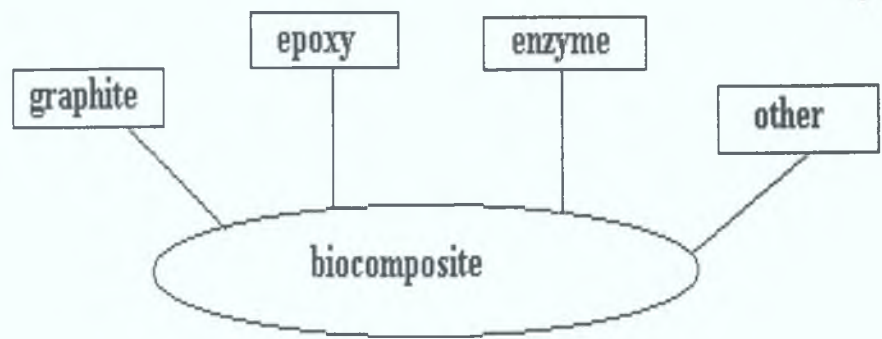
Figure. 1.5. Schematic representation of a carbon – polymer – biocomposite

Extensive study into the electrochemical nature of the carbon paste electrodes or soft carbon polymer biocomposites has been carried out.[40–43] These studies show that the traditional carbon paste electrodes suffer many drawbacks when compared with the traditional glassy carbon electrode. Such drawbacks are the complex heterogeneous nature of the surface of the electrode, which influences the double layer capacitance and hence affects the sensitivity of the electrode. The presence of the pasting liquid results in decreasing the rate of electron transfer when compared with traditional homogeneous electrodes. The lipophilic nature of the pasting liquid enhances the electrode overpotential (potential required to drive the reaction). This is due to the marked hydrophobicity of the liquid that hinders the approach of the analyte towards the surface. When compared with solid graphite or noble metal electrodes these carbon paste electrodes have a low background current, the magnitude of which drops with increasing quantity of pasting liquid in the paste. However, this lower background current is often accompanied by a decrease in sensitivity of the electrode. In addition to this these problems, the electrodes suffer many drawbacks associated with oxygen that is trapped within the carbon particles. Additional problems associated with these carbon paste electrodes arise due to the physical nature of these materials, which are mechanically soft and not amenable to mechanised surface polishing. Additionally, enzyme or modifier loss is high with these materials and problems arise when these electrodes need to be used in non-aqueous media, further limiting the use of these materials as biosensors.

The improved epoxy based sensors developed by Wang *et al*[42] resulted in a matrix that could be moulded prior to curing so that sensors of different shapes and sizes can be constructed and adapted to any machineable configuration. This construction procedure brought novel and attractive advantages to enzyme based biosensor development. The simplicity of fabrication rendered these biosensors amenable to mass production as they are produced in a dry environment.

Céspedes *et al*[43] showed an alternative method for the development of rigid carbon polymer composites. In their method a conductive non-commercial epoxy and graphite particles, 50 µm in diameter, are modified with a biocomponent to give rise to a biocomposite, giving added advantage of further manipulation of the biocomposite. A composite by definition is a combination of two or more phases of different natures whereby each phase maintains its individual characteristics, but the mixture may show new physical, chemical or biological properties. For instance, if one phase is an

electrical conductor, the overall electrical properties of the conducting composite will be determined by the nature, relative content and distribution of each phase.

A characteristic of the electrode types is that in reducing the active surface area of the electrode there is an improved signal-to-noise ratio (s/n). In accordance with Oldham *et al.*,[44] the perimeter of the surface has a greater influence on the signal, as is the case of a microelectrode. By means of this edge effect, non-linear diffusion is established and the quality of the signal is enhanced. A higher s/n and a lower limit of detection show this enhancement.

In the case of composite electrodes, which are composed of very small conductive particles dispersed within a polymer matrix, microelectrode behaviour may be observed for some loadings. This factor, in combination with the ease of preparation, makes such systems very attractive for practical applications. Ease of modification of these composites is associated with the plasticity of the matrix prior to curing. Modifying fillers can be blended into the matrix conferring another advantage of composite electrodes, i.e., the ease of manipulation of the surface for bulk modification.

A variety of rigid carbon polymer biocomposites has been developed. The first type involves biosensors based on carbon–polymer–enzyme biocomposites that have been used for the detection of acetylthiocholine,[45] phenol[46] and glucose.[47] The enzyme included in the biocomposite catalyses a reaction that generates an electrochemically active species. Other examples are GO–FAD [48, 49, 50] and electrodes for urea analysis involving incorporation of urease enzyme.[51] In each of these cases, the working potential of each biosensor depends on the oxidation or reduction potential of the species generated by biocatalysis. In general, however, the applied potential needs to be substantially positive, and the number of interfering species can be significant depending on the sample under analysis. The absence of membranes reduces the size of the diffusion profiles and produces a useful signal quickly as the electroactive species are generated close to the conducting sites on the surface of the biosensor. Some enzymes such as peroxidases contain active centres like haem C that can be oxidised and reduced directly at the surface of the sensor.

The physical and electrochemical characteristics of the biocomposites facilitate direct communication between the redox centres of the enzyme and the conductive sites of the biomaterial. An example of this direct communication is a biocomposite that contains a peroxidase enzyme that is regenerated by direct reduction on the surface of the biosensor; such regeneration would not be possible if the active site

was not in close proximity with the conducting particles, similar to what can be observed in Figure 1.3.

Carbon–polymer–enzyme biocomposites modified with electrocatalysis: In this case the modifiers added to the composites, by bulk modification as illustrated in Figure 1.5, are one or several transition metal particles like Au, Pd or their oxides[52,53] and Pt.[54]. Although, there is no electron mediator between the enzyme and the transducer, the electrocatalytic action of the nanoparticles lowers the working potential and hence reduces the range of interferences. However, problems associated with interferences still exist.

Carbon–polymer–enzyme biocomposites modified with redox mediators: The suitability of redox mediators was realised previously for their incorporation into PME and these principles also apply to biocomposites. These mediators compete with the natural co-substrate to regenerate the enzyme by the transfer of electrons between them and undergoing the regeneration on the surface of the electrode. The main advantages of using mediators are the independence of the analytical signal in relation to the concentration of the natural co-substrates present in the working solution. Such an interaction is possible due to the close proximity of the mediator to the enzymes redox site, and, hence facilitating direct electrical communication, that was observed above with PMEs described previously,[18–35] between the mediator and the active site of the enzyme. Also as with the PMEs described above[18–35] an additional advantage of these redox mediators is the reduction in working potential.

Carbon paste electrodes; Another type of biosensor developed by Alegret *et al*[55] was for the determination of organo-phosphorus and carbamate pesticides. This is an important area for environmental monitoring as it can affect aquatic life amongst other things. In this case the enzyme used for detection was acteylcholinesterase as it is known that pesticides inhibit the activity of such enzymes. As in all other incidences a mediator was used in this case 7,7'8,8-tetracyanoquinone (TCQN) again a fast electronic mediator.

Carbon–polymer–enzyme biocomposites modified with another enzyme. In some cases, immobilising another enzyme results in a higher indirect analytical selectivity towards the measured substrate.[56] The immobilisation of two enzymes is simple for biocomposites in comparison to wet chemistry techniques as the co-immobilisation occurs under dry conditions.

Carbon– polymer–enzyme biocomposites modified with cofactors. Some dehydrogenase enzymes require the presence of cofactors such as NADH or FAD for the catalysis of the chemical reaction. The cofactor has been used as a component of the solution with an ensuing loss after analysis cycling. Recently, biocomposites based on these enzymes have incorporated the cofactor into their matrices. Examples of such a biosensor is one for the detection of glucose which incorporates the enzyme glucose dehydrogenase–Nicotinamide Adenine Dinucleotide Phosphate (GDH–NADP$^+$) into the biocomposite, this results in a reduction in the working potential in a method similar to that described for redox materials.[57]

Carbon–polymer–biocomposite based on antibodies. In addition to the development of enzyme based biosensors using biocomposite materials, there is reports of amperometric immunosensors.[58,59] For example, immunoglobin (Ig) is immobilised within the composite material. The resulting immunomaterial acts as a reservoir of immunological component. An analytical signal is produced by the oxidation/reduction of a product of the reaction in the presence of a substrate. A typical example of this is an antigen specific to Ig is labelled with the enzyme horse radish peroxidase (HRP)) in the presence of hydrogen peroxide a signal is produced.

In all cases of the above mentioned biocomposites, the sensors showed added advantages which were not available by the previously mentioned PMEs. Firstly, there is a renewable surface upon polishing showing excellent reproducibility. Additionally, the preparation of these electrodes is in a dry environment introducing the possibility of mass production of these electrodes.

1.4   Genosensors

As previously stated, the 1980s witnessed a surge in publications dealing with the creation of a perfect glucose biosensor.[60] This increased interest was fuelled as much by the demand of increasing incidences in diabetes as it was by the advancements in areas of technology – providing instruments capable of sub-micromolar detection. Likewise, the 1990s has experienced the same surge in publications relating to the development of the perfect genosensor – devices that combine a biological recognition agent to a electrode surface resulting in the selective and sensitive determination of sequence specific DNA. These advancements are in part contributed to the accumulated knowledge through trial and error practices relating to the perfection of the glucose biosensor – especially enzyme labelled detection methods. However, the main reason for progress in this area of analytical biochemistry can be attributed to developments in genetics, in particular the development of polymerase chain reaction (PCR).[61, 62, 63]

PCR is an amplification technique that is capable of replicating a predetermined genetic sequence in a matter of minutes, offering unsurpassed advantages regarding the rapid identification of disease causing pathogens. Although, the development of PCR has improved the possibilities for rapid DNA analysis, actual determination of the amplified PCR product is limited to more traditional time consuming techniques such as southern blotting and pulse field gel electrophoresis amongst others.[61–63]

This problem of time was especially evident in recent outbreaks of foot and mouth in the U.K.,[64] where the time between testing a suspected animal and official results was 48 hrs. Given the success of the glucose biosensor for rapid real time analysis, electrochemistry is one of the areas which is dedicating much time and research into the development of a rapid real time sensor capable of detecting the presence of sequence specific DNA.

The concept of using electrochemistry for detecting specific DNA sequences is not a new one. In fact, the original pioneering work was first proposed as early as 1958 by Palecek,[65] who demonstrated the ability of sequence specific nucleic acids to strongly adsorb onto the surface of a hanging mercury drop electrode, (HMDE) forming monomolecular compact films. Only DNA bases can undergo redox processes, as neither the attached deoxyribose sugars nor the phosphate groups attached to DNA are

electroactive. This guarantees that the electrochemical response is arising from adsorbed DNA. Extensive research, over the following years by Palecek and co-workers,[66] [67], [68], [69], [70] into the possible differentiation between oxidation of double stranded DNA (dsDNA) and single stranded DNA (ssDNA) demonstrated a potential difference in the oxidation peak, occurring at -1.2 V and -1.4 V for ssDNA and dsDNA, respectively. However, later reports by Palecek[71] suggest that no significant hybridisation takes place at the mercury electrode possibly due to hydrophobic interaction between the probe bases and the surface of the mercury electrode with the phosphate sugar backbone being more exposed in solution than the DNA bases. As a result of this hydrophobic interaction there is poor accessibility of the probe bases for hybridisation and subsequent detection. In addition to the poor accessibility for hybridisation is the unsuitability of using HMDE for routine analysis.

A perusal of literature shows that the development of a genosensor can essentially be divided into three experimental stages; immobilisation of a capture probe onto the electrode surface, hybridisation of the capture probe to a sequence specific target analyte and finally detection of this hybridisation event through electrochemical means.

1.4.1 Immobilisation procedure;

Current methods available for attachment of a ssDNA capture probe, are summarised below.

Adsorption

Membrane adsorption;

Of the immobilisation procedures that are available, the most straightforward one is the adsorption of the capture probe onto a membrane as the need for special nucleic acid modifications is not required.[72],[73],[74],[75],[76], [77], [78], [79] Materials reported in literature for this adsorption approach include; nitrocellulose, nylon, polystyrene, metal oxides or carbon/carbon paste electrodes. Figure 1.6*a* shows the adsorption of ssDNA onto a Nafion membrane.

The disadvantages associated with this technique are related to poor hybridisation efficiency and desorption of the nucleic acid due to hybridisation conditions. Apart from these initial reports[72-78] very little other work has been carried out using membrane technology for the development of a genosensor.

Electrochemical pretreatment step:

One suggested method of overcoming the issues of desorption involved the use of an electrochemical pretreatment step. As illustrated in Figure 1.6b holding a freshly polished carbon paste electrode at a potential of +1.8 V[73] results in a roughening of the electrode surface thereby increasing its hydrophilicity. Subsequent electrochemical adsorption of a capture probe was achieved by holding the electrode potential at +0.5 V, for a preset time. This potential of +0.5 V is known to increase the stability of the immobilised probe through electrostatic attraction between the positively charged carbon surface and the negatively charged hydrophilic sugar phosphate backbone.[70] Palecek *et al*[70] observed that using this electrochemical pretreatment step results in the exposure or opening out of the DNA bases in solution, making them ready for hybridisation with a target probe, and overcoming problems reported for the HMDE.

Although electrochemical pretreatment of an electrode surface overcomes many of the original problems associated with desorption, the DNA sensor appears difficult to reuse under the reported denaturing conditions.[80]

Adsorption without electrochemical pre-treatment step:

Another possibility for the immobilisation of DNA to an electrode surface has been demonstrated using physical adsorption techniques.[81, 82, 83] The most common reported method involves dropping a small volume of ssDNA solution onto a glassy carbon electrode and leaving the electrode to dry overnight. Others report using physical adsorption on pyrolytic graphite carbon. Additionally, as illustrated in Figure 1.6c, glassy carbon electrodes previously coated with the conducting polymer polypyrrole have been used.[83] The advantages of a polypyrrole coated electrode is due to electrostatic attractions occurring between the positively charged polymer and the negatively charged DNA, resulting in the formation of a stable DNA film. Adsorption of DNA onto the surface of a gold electrode also exists. In this incidence, a small volume of DNA was dropped on the surface of the electrode. The electrode was then left to dry in air overnight, with subsequent washing a buffered solution to remove unadsorbed DNA.[84]

The problem associated with these physical adsorption methods is that the sequence specific DNA must contain a high percentage of guanine base pairs, as these have the lowest ionisation energy and have proved to form the more stable non-

chemically confined DNA sensors. Such a property limits the application of target DNA sequences which can be used.

Armistead et al[85] report the adsorption of DNA onto the surface of an indium tin oxide electrode. Unlike previously reported methods, adsorption is thought to occur through a metal phosphate interaction. This method shows great promise as the resulting film is reported to be stable at high temperatures.

Covalent attachment:

A more stable method for immobilising a DNA capture probes onto an electrode surface involves the use of covalent bonds.[86, 87, 88, 89, 90, 91] Again, this method depends on the type of electrode surface.

By electrochemically oxidizing a glassy carbon electrode in an acidic solution, followed by a dry adsorption procedure using a water soluble carbodiimide (ECD) and a N-hydroxysulfosuccinimide (NHS) an electrode surface which is capable of reacting selectively with DNA is produced.[86-91] The stability of the assembly is related to the guanine content of the DNA sequence. A report by Liu et al,[91] demonstrate a similar method of covalent attachment of DNA to the surface of an electrode. In this case, a graphite carbon electrode is used and is chemically modified with primary amino groups using EDC. Placement of the capture probe into a hybridisation solution containing the target sequence and ethidium bromide (EB) after a prehybridisation incubation step results in the formation of a dsDNA probe.

Gold electrodes have demonstrated success using covalent attachment methods. This success can be attributed to work by Abrūna et al[92], in relation to the spontaneous assembly of alkanethiol ($SH-(CH_2)_n$) functionalised ssDNA to assemble on a gold electrode surface. It is well documented that thiols adsorb rapidly onto the surface of a gold electrode through the sulphur atom resulting in the formation of a $Au-S-(CH)_n$ bond. Despite the attractive nature of this method[92] problems of forming closely packed surface due to the large hydrophilic nucleic acid groups raise issues of stability. A more precise control of the gold electrode surface was achieved using a two step approach, as illustrated in Figure 1.6d. In this incidence, a mixed monolayer is created by using a thiol derivitised capture probe and a lateral spacer thiol, mercaptohexanol, was used and reports indicate that a compact layer can be formed.[93, 94, 95]

a) Membrane adsorption

Direct adsorption of
ssDNA

Nafion membrane

electrode

b) Electrochemical pretreatment

Electrode held at +1.8 V
for 5 min

electrode then immersed in a
sample containing capture DNA and
held at +0.5V for a preset time
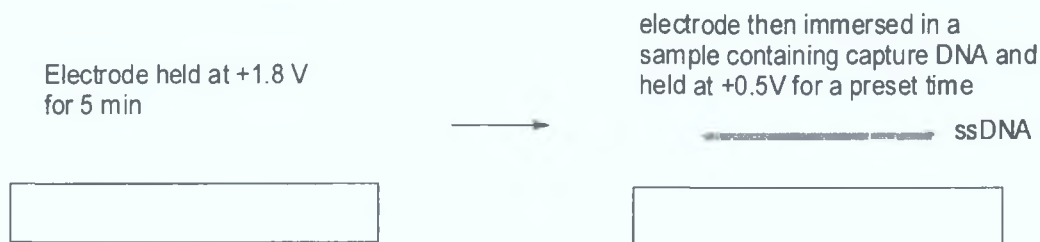
ssDNA

c) adsorption via modified electrode surface

Electropolymerisation

Py, Py $\sim\!\!\!\wedge$

$-[PPy \sim\!\!\!\wedge]_n$

$NH_2....DNA$

$-[PPy \sim\!\!\!\wedge]_n NH_2....DNA$

d) Covalent attachment

step 1

Gold electrode

$SH-(CH_2)_n-DNA$

$-S-(CH_2)_n-DNA$

$-S-(CH_2)_n-DNA$

$-S-(CH_2)_n-DNA$

step 2

$S-(CH_2)_n$

$-S-(CH_2)_n-DNA$
$-S-(CH_2)_n$
$-S-(CH_2)_n-DNA$
$-S-(CH_2)_n$
$-S-(CH_2)_n-DNA$
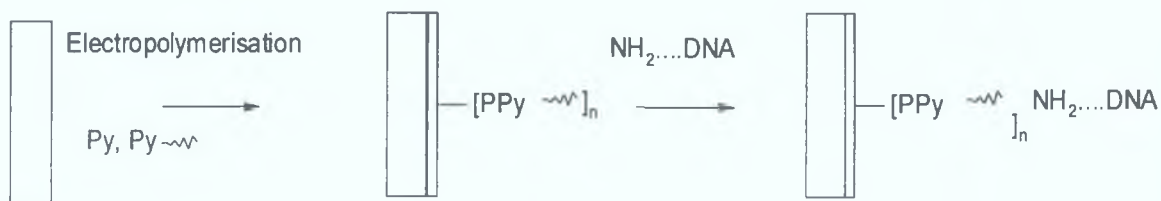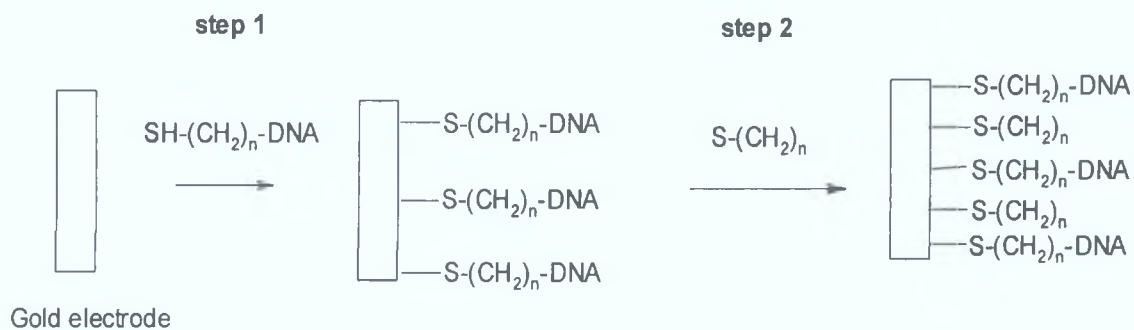
Electrode is immersed in a solution
containing thiolated DNA for a preset time

Figure 1.6. Illustrating various methods of immobilizing ssDNA to an electrode surface
allowing subsequent attachment of a capture probe.

From the above reports, it can be seen that many problems exist with the immobilisation of a DNA capture probe to the surface an electrode either because of slow desorption of the capture probe, the necessity of multiple chemical pretreatment steps or electrochemical pretreatment of the electrode surface. All this results in a complicated protocol that is both time consuming and relies on skilled personnel.

As was stated by Wang *"besides the introduction of new sensing/hybridisation systems it is essential to develop improved schemes for the immobilising the DNA layer, and, obtaining a better understanding of the confirmation and arrangement of the surface layer"*. One positive step in this direction has been the increased use of biotin–streptavidin/avidin recognition elements. The chemistry of this ligand receptor molecule is known for its unique properties; tetravalent binding ability, one of the strongest known non-covalent interactions and increase thermal stability upon binding.

Examples of successful genosensor applications of biotin–avidin interactions were first reported by Pantano *et al.*[96] However, this report also incorporates an electrochemical pretreatment step. Kleinjung *et al*[97] improved on this by using an overnight drying procedure which was stabilized by crosslinking the dried avidin with gluteraldehyde for a further 3 hrs. This electrode was then exposed to a biotinylated DNA probe, resulting in a stable film, however, the overnight drying process lengthens the procedure

While the stability of biotin–streptavidin/avidin is well known, the necessity[98, 99] of forming a stable layer still proves to be an issue requiring an a chemical pretreatment step. Shamansky *et al,*[100] overcame the need for chemical pretreatment by using a photoactive biotin derivative that is immobilised to the surface of an electrode by exposure to UV–light, however this is a novel attempt, which awaits further publication to determine its success.

In light of the problems associated with immobilisation of DNA through physical and chemical adsorption, it appears that any successful attempts at producing a genosensor may lie in an improvement in a biotin–avidin/streptavidin approach. This opinion is supported by the success of biotin–avidin/streptavidin in the development of many other sensors, both chemical and biological.

1.4.2 Hybridisation of sequence specific DNA

Hybridisation of DNA is a well-known procedure due to applications in genetics and biology for numerous years. The more common method of hybridisation that is employed in genosensor applications involves the immersion of the DNA probe in a hybridisation solution for a predetermined time, usually 1 hr., this step is then followed by a gentle washing procedure. Reports[74-80] also exist using an electrochemical hybridisation of target DNA to the capture probe. In this instance the probe coated electrode is immersed in a hybridisation solution, again for a predetermined time, while holding the potential at +0.5 V vs. Ag/AgCl reference electrode. Problems of non-specific adsorption of non-complimentary DNA onto the electrode surface have been reported.

In both methods, the most important factor to control is temperature to ensure that a dsDNA duplex forms.

1.4.3 Detection of the DNA duplex

There are three possible methods for detection of the DNA hybridisation event; use of an electroactive indicator, an enzyme labelling method or to detect the guanine oxidation signal, a label free method of detection. These methods of detection are described in greater detail below.

Electroactive intercalators

In this case the duplex formation is detected by using an appropriate electroactive hybridisation indicators containing planar aromatic ligands, such as cationic metal complexes, e.g., $Co(phen)_3^{3+}$, $Co(bpy)_3^{3+}$, $Ru(bpy)_3^{3+}$, $Fe(phen)_3^{2+}$, $Fe(bpy)_3^{2+}$, $Cu(phen)_2^{2+}$, and $Cu-(TAAB)^{2+ii}$. Also organic compounds such as acridine orange, anthracyclines, phenothiazines and ethidium bromide have been used.[101, 102, 103] All these compounds interact in different ways with ssDNA or dsDNA but preferentially with the dsDNA by undergoing reversible electrostatic interaction with the minor groove or displaying a double helical intercalative binding ability, as shown in Figure 1.7 below. Once the duplex is formed using the methods mentioned in Section 1.4.2,

---

[i] Phenanthroline

[ii] Tetraza macrocyclic ligand

the dsDNA electrode is immersed in a solution containing an intercalating compound for example $Co(phen)_3^{3+}$, $Co(bpy)_3^{3+}$, and held at +0.5 V for ~2 min., upon which binding to the dsDNA duplex via the planar aromatic groups stacking between base pairs occurs. Subsequent detection is achieved using cathodic potential stripping voltammetry (CPSV)

Another procedure used by Marrazza *et al*,[75] involved the use of daunomycin hydrochloride, a species which has known intercalation properties with dsDNA. Surface accumulation of daunomycin hydrochloride is also measured using CPSV at a constant current. An important parameter to consider in the use of intercalators is the issue of non-specific adsorption of electroactive species on to the electrode surface resulting in a false positive result. Another problem with this method of DNA duplex detection associated with the oxidation signals of DNA electroactive indicators is that for carbon electrodes poorly defined signals are observed and there are only small differences between ssDNA and dsDNA molecules. Palecek *et al*[74] observed that in order to differentiate between dsDNA and ssDNA large concentrations of target DNA are required thus increasing time, cost, and reducing the value of electrochemistry as a sensitive analytical method.
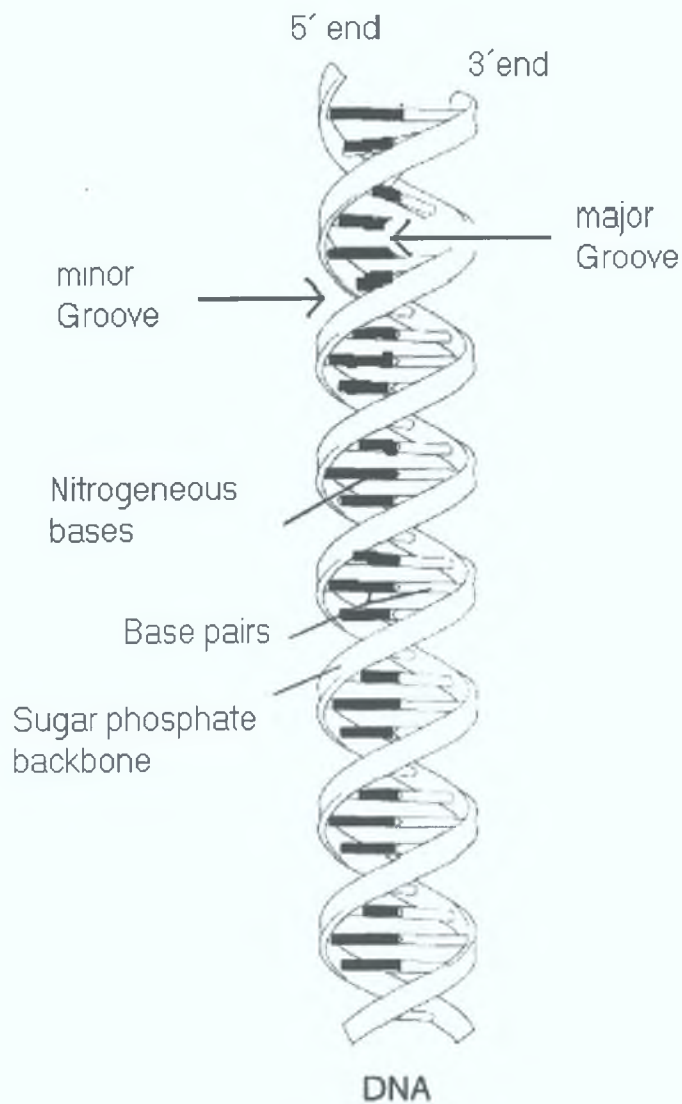
Figure 1.7. Binding sites of intercalators occurs either through the major or minor groove.

Enzyme labelling method

A method that can be used to overcome the aforementioned problem of non-specific adsorption of electroactive markers onto the electrode surface is to chemically or otherwise attach an electrochemical marker to a small complementary DNA probe that will hybridise with the target probe. The obvious advantage of this method is that one is not limited to electroactive species that are capable of interacting with DNA electrostatically, therefore extending the range of possible markers that may be used. [104–109]

Although many compounds have been reported including osmium[104] and aminoferrocene,[105] possibly the most commonly employed is the enzyme horseradish peroxidase (HRP).[106] HRP is an enzyme label that has been frequently used in various biosensor designs. Chen *et al*[106] report the capability of directly detecting the presence HRP on an electrochemical surface without use of an electron mediator, as described in Section 1.2. In this report, the technique cyclic voltammetry is used, with a reduction potential of –0.208 V vs. Ag/AgCl, the rate of this electron transfer process is slow and is not recommended for an efficient method of analysis. Another possible method of detection involves the incorporation of a fast electron redox mediator as discussed above in Section 1.3, allowing, the use of constant potential chronoamperometry. In brief, common redox mediators that have been employed for the detection of a DNA–HRP duplex are; $Os(dime(bpy)_2Cl)^{2+/3+,[107]}$ and hydroquinone,[108] with hydroquinone being the more suitable. The most common method for incorporation of HRP involve the use of an antibody or biotin labelled DNA with subsequent reaction of an antigen/streptavidin labelled–HRP enzyme.

Indicator free electrochemical monitoring

In this method of detection of a hybridised DNA duplex detection can be achieved by using the chronoamperometric oxidation peak of guanine. This oxidation occurs at 1.03 V vs. Ag/AgCl that decreases in intensity upon hybridisation.[77] The reasons for this decrease in current upon hybridisation are still not clear but it is thought that upon hybridisation the nucleobases are on the inside of the double helix resulting in steric hindrance by the surrounding sugar bases.[109]

From the above literature review it may be concluded that the most suitable method of immobilisation would involve taking advantage of the strong and stable binding chemistry of biotin–avidin/streptavidin. For hybridisation of the target DNA

problems associated with non-specific adsorption, suggest that simple immersion of the immobilised DNA probe in a hybridisation solution containing the target DNA is more appropriate. While detection of the DNA duplex can be achieved using an specifically labelled complementary strand with subsequent attachment using an enzyme labelled antibody.

1.5   Dynamic electrochemistry

Dynamic electrochemistry is either concerned with the study of electron transfer reactions between electrodes and reactant molecules in solution or adsorbed onto the electrode surface. Many parameters have been found to influence the dynamics of an electrode reaction including the electrode potential, transport of material between the electrode and bulk solution, the reactivity of the redox species and the nature of the electrode surface.   Prior to understanding the influence of these factors on the electrochemical response, a grasp of the equilibrium electrochemistry and homogeneous electron transfer must first be established.[110]

1.5.1   Equilibrium electrochemistry:

Electrode processes involve the transfer of electrons (charge), across the interface of the electrode surface, to the solution species as in the reaction below, (Equation 1.4). This reaction can only occur under suitable conditions. The transfer of this charged particle (electron) occurs between two distinct phases, the metal phase (m) of an electrode and the aqueous phase (aq) of the reaction species.

$$Fe^{3+}(aq) + e^{-}(m) \leftrightarrow Fe^{2+}(aq) \qquad \textbf{(Equation 1.4)}$$
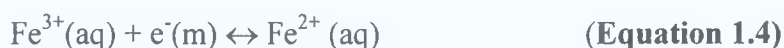
An approach towards equilibrium results in a net charge separation being developed between the electrode and solution. This charge separation creates a potential difference at the electrode/solution ($\Delta\phi_{m/s}$) interface. Equation 1.5 shows the difference in potential that arises at the electrode/solution interface as a result of this potential difference:

$$\Delta\phi_{m/s} = \Delta\phi_{m} - \Delta\phi_{s} \qquad \textbf{(Equation 1.5)}$$

where, $\Delta\phi_{m}$ is the potential at the metal interface and $\Delta\phi_{s}$ is the potential at the solution interface. Measurement of $\Delta\phi_{m/s}$ requires a complete electrical circuit with the presence of an additional electrode (reference electrode) that provides a constant potential against which the observed potential difference between the two electrodes can be measured (Equation 1.6).

$$E = (\Delta\phi_m - \Delta\phi_s) + \text{constant} \qquad \textbf{(Equation 1.6)}$$

Providing that no current is drawn through the cell, the potential attains a steady state value known as the equilibrium potential that depends on the relative concentrations of the redox species. Nernst showed that the potential established under equilibrium conditions is given by Equation 1.7, also known as the Nernst Equation:

$$E = E^\circ - \frac{RT}{nF} \ln \frac{C_o}{C_R} \qquad \textbf{(Equation 1.7)}$$

where the equilibrium potential (E_e) of the electrode results from the standard electrode potential (E^θ) of the reaction and C_O and C_R are the concentrations of O and R at the electrode surface, which, under equilibrium conditions, is the same as their values in bulk solution.

The ability to establish equilibrium in electrochemistry allows thermodynamic measurements such as entropies, enthalpies and rate constants to be obtained.

Applying a potential other than E_e to the electrochemical circuit results in current flow from electron exchange between the electrode and the molecules in solution. In this way, the redox composition of a thin layer of solution adjacent to the electrode is altered. Depending on the direction of the current flow either reduction (Equation 1.8) or oxidation (Equation 1.9) of the redox species is occurring.

$$Fe^{3+} + e^- \rightarrow Fe^{2+} \qquad \textbf{(Equation 1.8)}$$

$$Fe^{2+} - e^- \rightarrow Fe^{3+} \qquad \textbf{(Equation 1.9)}$$

For solution phase species, the magnitude of current obtained is given by the Equation 1.10

$$i = Afj \qquad \textbf{(Equation 1.10)}$$

where i is current, j is the Flux i.e. the quantity of material reaching the electrode surface per second, A is the area of the electrode and F is known as Faraday's constant.

In the act of a current flowing and the conversion of Fe^{3+} to Fe^{2+} the concentration of Fe^{3+} at the electrode surface is no longer the same as that in solution. The reason for this concentration difference is that the rate of depletion is faster than the rate at which the reactant can diffuse from bulk solution to the surface of the electrode. From this analysis, the current depends not only on the rate of heterogeneous electron transfer from the electrode to the reactant species but also the rate at which reactant diffuses to the electrode surface.

1.5.2   *Homogeneous electron transfer and the activated complex theory*

The suitability of electrochemistry as an analytical technique is best understood by making comparisons with solution phase homogeneous chemical reactions as seen in equation below, Equation 1.12:

$$Fe^{3+}_{(aq)} + e^- \leftrightarrow Fe^{2+}$$ **(Equation 1.12)**

By considering the simplified version of the activated complex theory, Figure 1.6 –an important theory for describing the energetics of any chemical reaction – it is possible to learn what is occurring at the electrode interface in a systematic manner. According to this theory, an Arrhenius dependence is assumed for the forward rate constant, k'_f, on the chemical free energy of activation, $\Delta G^{\neq}$, Equation 1.13.

$$k'_f = \frac{kT}{h} \exp\left[\frac{-G_f^{\neq}}{RT}\right]$$ **(Equation 1.13)**

where, k, T, h, and R are Boltzmann constant, temperature, Planck and gas constant respectively. From Equation 1.13 and Figure 1.6 it can be seen that in order for a chemical reaction to proceed the reactant's internal energy must change by $\Delta G^{\neq}$ which can be accomplished either by a change in temperature or of the reactant's structure.
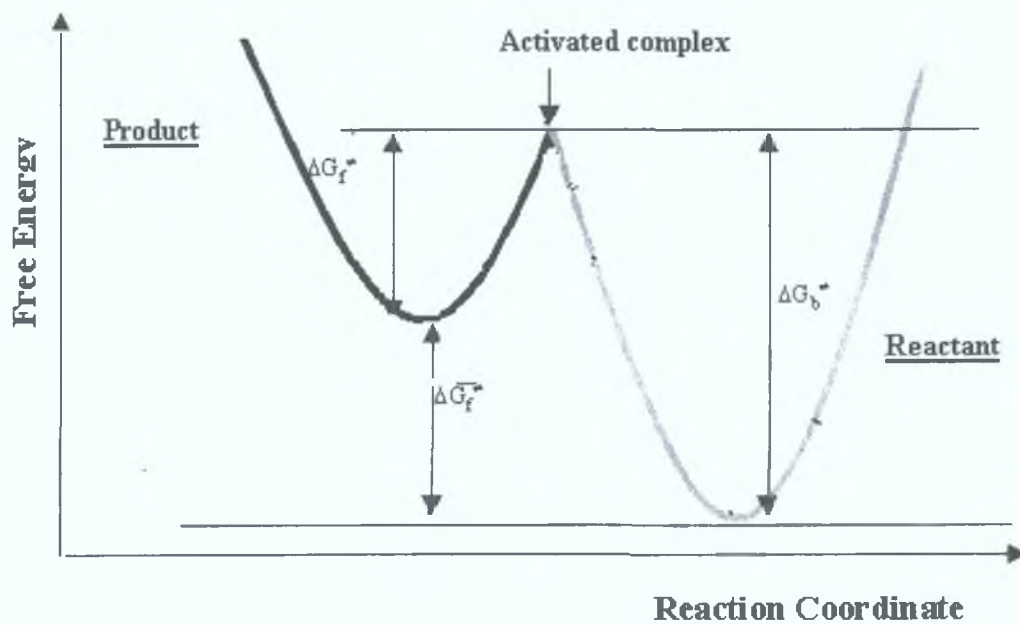
Figure 1.6. Free energy changes during a reaction. The activated complex is the configuration of maximum free energy.

1.5.3 Effect of applying a potential to an electrode

The next issue that needs to be considered is what occurs when an electron is accepted/donated from a metal electrode to a redox species in solution. Metals contain a lattice of closely packed atoms. The overlap of atomic orbitals within these lattices ensures that electrons are free to move about. The maximum energy that these electrons occupy is known as the Fermi Level. In the case of metal electrodes application of a potential results in either an increase or decrease of this energy level as shown in Figure 1.7a.

In Figure 1.7b(i) a reactant molecule, O, capable of undergoing charge transfer has been introduced. Some of the energy states of O are depicted and, in particular, it has its lowest unoccupied molecular orbital (LUMO) at an energy level higher than that of the metal electrode's Fermi Level. When, as in this incidence, the LUMO has a higher energy level higher than the Fermi Level of the electrode, electron transfer reaction will be thermodynamically unfavourable. However when a potential is applied that increases the Fermi level of the electrode the reaction becomes thermodynamically favourable and electron transfer occurs as shown in Figure 1.7b(ii).

The exact magnitude of the potential required to drive the reaction is known as the overpotential, η, and is described in Equation 1.14. The magnitude depends greatly on the electrode material and redox species being reduced.

$$\eta = E - E^{\circ'}$$

(Equation 1.14)
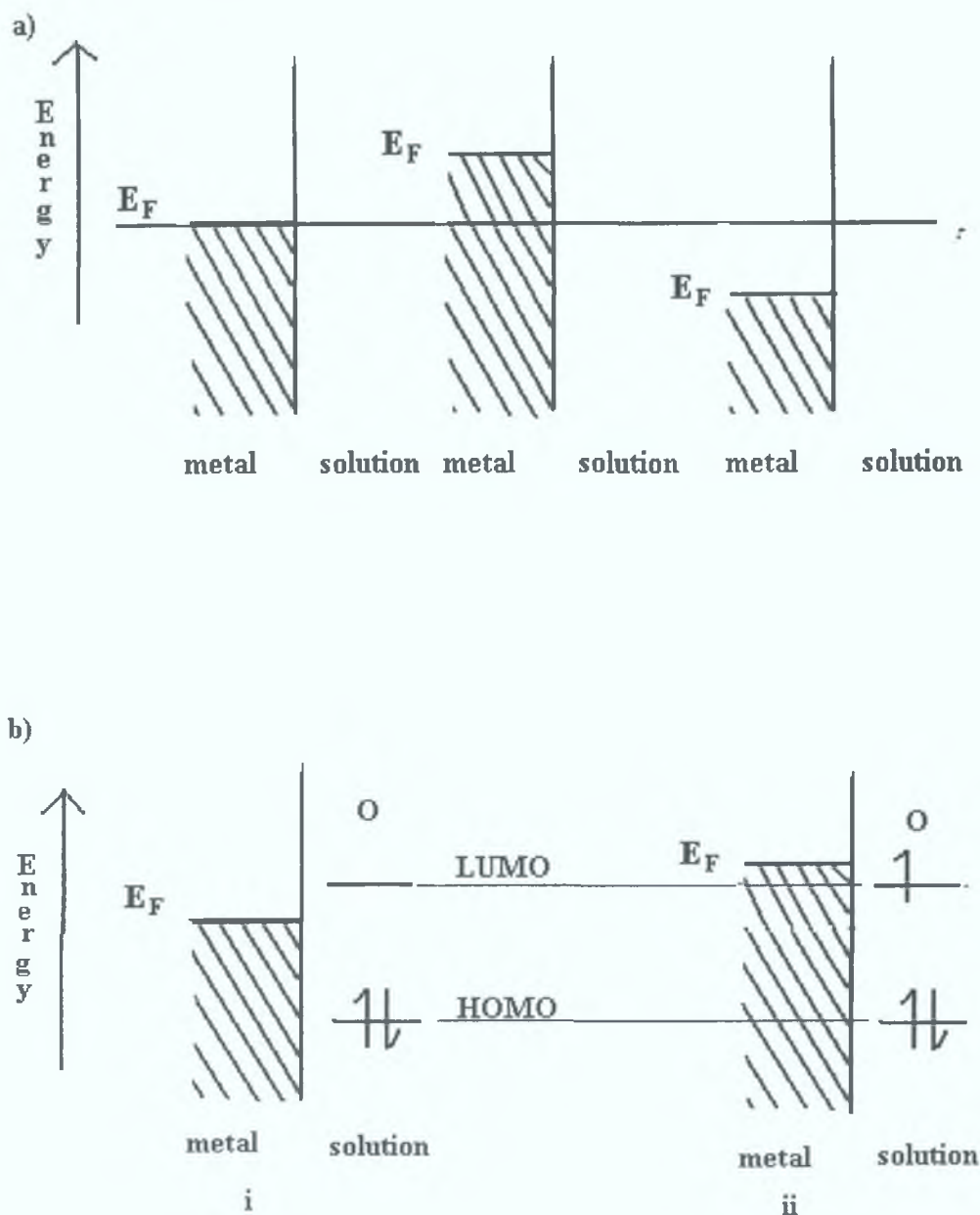
Figure 1.7. a) The influence of potential on the Fermi level in a metal and b) Electron transfer and energy levels (i) insufficient electrode potential to drive the reduction of O to R and (ii) at a more reductive potential where the reduction process becomes thermodynamically favourable.

1.5.4   Effect of potential on activated complex theory; Butler-Volmer model

As it is known that the reaction of redox complexes is influenced by a change in the interfacial potential, it is possible to discuss electrochemical dynamics in terms of the activated complex theory, previously mentioned in Section 1.5.2, for homogeneous chemical reactions. However, in contrast to chemical reactions, electrochemistry uses as its driving force potential, with $\Delta G^{\neq}$ of Equation 1.13 above becoming $\Delta \bar{G}_f^{\neq}$ allowing the rate constant for a forward reaction to be described as seen in Equation 1.15.

$$k_f = \frac{kT}{h} \exp\left[\frac{-\Delta \bar{G}_f^{\neq}}{RT}\right] \qquad \textbf{(Equation 1.15)}$$

In this case both chemical and electrochemical components contribute to the electrochemical free energies of activation. These changes can be seen in the changes in the activation complex theory for an electrochemical reaction, Figure 1.8 that can also be represented in the form illustrated in Figure 1.9. As can be seen from Figure 1.8, both chemical and electrical components contribute to the electrochemical free energies of activation. The dashed line in Figure 1.8 illustrates that a shift in potential of the electrode to a value E results in a change in the energy barrier by amount -nFE. Under electrochemical conditions the barrier for oxidation may be described as $\Delta G^{\neq} - \Delta \bar{G}_f^{\neq}$. This fraction of energy change nFE may also be described as 1-α, where α is also known as the symmetry factor or the transfer co-efficient and lies between 0 and 1, depending on the shape of the free energy curves in the intersection region of Figure 1.8. It is now possible to represent the free energies of activation as seen in equation 1.16 and 1.17 for the forward and back reaction respectively.

$$\Delta G_f^{\neq} = \Delta \bar{G}_f^{\neq} - \alpha nFE \qquad \textbf{(Equation 1.16)}$$

$$\Delta G_b^{\neq} = \Delta \bar{G}_b^{\neq} - (1-\alpha)nFE \qquad \textbf{(Equation 1.17)}$$

By substituting Equation 1.16 and 1.17 into Equation 1.13 it is possible to determine the potential dependence of redox reactions, which is given by Equation 1.18 and 1.19, for the oxidation and reduction processes respectively.

$$k_f = \frac{kT}{h} \exp\left(\frac{-\Delta G_f^{\neq}}{RT}\right) \exp\left(\frac{-\alpha n F E}{RT}\right) \qquad \textbf{(Equation 1.18)}$$

$$k_b = \frac{kT}{h} \exp\left(\frac{-\Delta G_b^{\neq}}{RT}\right) \exp\left(\frac{(1-\alpha)n F E}{RT}\right) \qquad \textbf{(Equation 1.19)}$$

As can be seen from Equations 1.18 and 1.19 above, the first term is independent of potential and hence may be describes as k_f° and k_b° representing the rate constants for the reaction at equilibrium. It is important to remember that when a system is at equilibrium the amounts of both oxidized and reduced species present in solution is equal, and hence, the standard heterogeneous electron transfer rate constant is simply designated as k°. Equations 1.20 and 1.21 below, account for this potential independent step, the dynamics of the system are described by k° and its units are cm s^{-1} and s^{-1} for solution phase and surface confined species respectively

Taking all these factors into account the heterogeneous rate constant can be represented as seen in Equation 1.20 for the forward reaction and Equation 1.21 for the back reaction.

$$k_f = k^{\circ} \exp\left[\frac{-\alpha n F (E - E^{\circ})}{RT}\right] \qquad \textbf{(Equation 1.20)}$$

$$k_b = k^{\circ} \exp\left[\frac{(1-\alpha)n F (E - E^{\circ})}{RT}\right] \qquad \textbf{(Equation 1.21)}$$

Free Energy

E = 0

$(1-\alpha)\,nFE$

$\Delta G_f^{\neq}$

αnFE

$\Delta G_b^{\neq}$

$\Delta \overline{G_b}^{\neq}$

nFE

$\Delta \overline{G_f}^{\neq}$

RED

Ox + ne

Reaction Coordinate
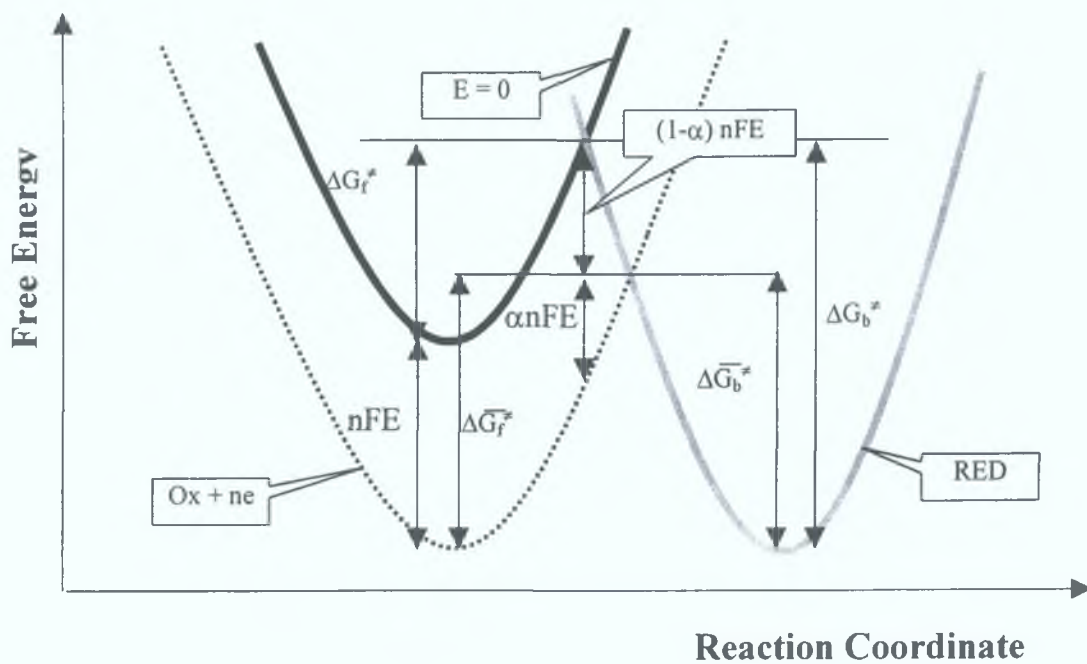
Figure 1.8. Showing influence of potential of the free energies of activated complex theory. As can be seen in the presence of applied potential the free energy of activation required for this reaction is reduced by the amount nFE.
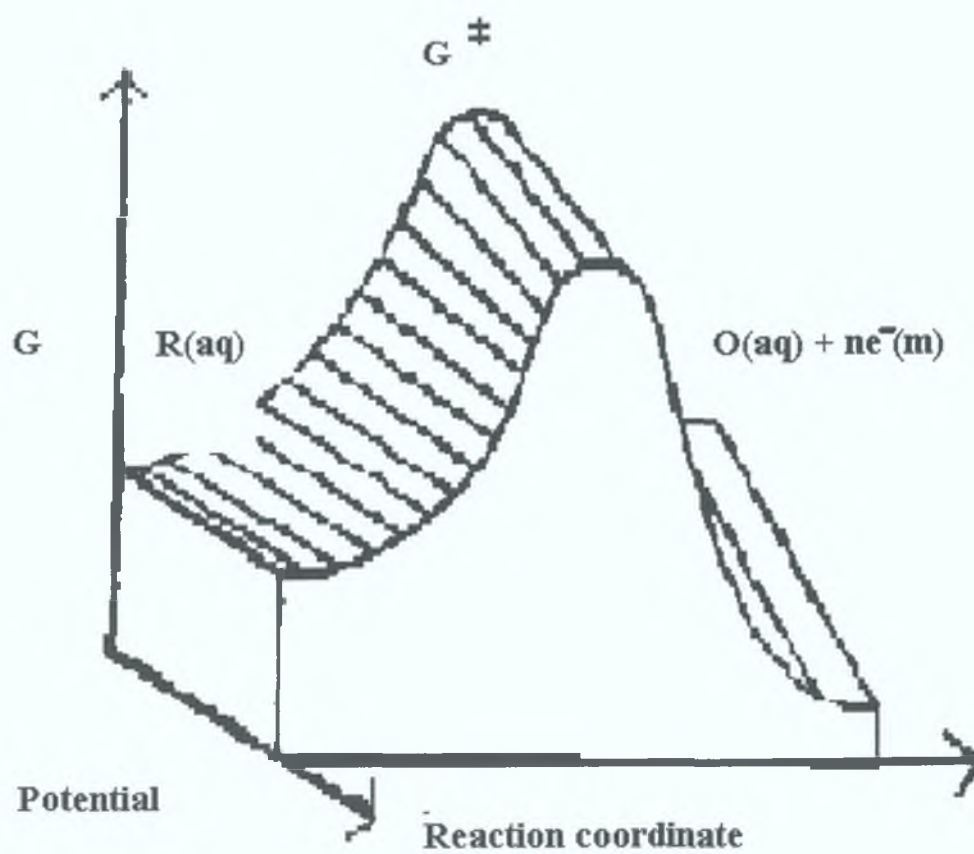
Figure 1.9. Free energy potential surface for $\alpha = 0.5$, G is Gibbs free energy, R reduced species and O oxidised species

These equations, Equation 1.20 and 1.21, are known as the Butler–Volmer equations and allow for macroscopic treatment of heterogeneous electron transfer. The dynamics of the system are described according to $k°$. According to this treatment of electron transfer a large value for $k°$ is retrieved for a reversible redox couple which established equilibrium conditions according to the Nernst Equation, Equation 1.7.

In most incidences where electrochemistry is used, the quantitative information is retrieved in the form of net current, i, flowing at the working electrode surface. Therefore, it is necessary to establish a relationship between Equations 1.20 and 1.21 and Equation 1.10. This relationship is shown in Equation 1.22 below

$$i_0 = i_0 \left(\frac{[R]_0}{[R]_{bulk}} \exp\left\{ \frac{(1-\alpha)F\eta}{RT} \right\} - \frac{[O]_0}{[O]_{bulk}} \exp\left\{ \frac{-\alpha F\eta}{RT} \right\} \right) \qquad \textbf{(Equation 1.22)}$$

Equation 1.22 is used to predict how the observed current varies as a function of the overpotential and the transfer coefficient. In conditions where the concentration of species at the electrode surface are equal to the concentration in bulk solution i.e., $[R]_0 = [R]_{bulk}$ and $[O]_0 = [O]_{bulk}$, it is possible to simplify Equation 1.22 above to Equation 1.23

$$i = i_. \left[\exp\left(\frac{(1-\alpha)nF\eta}{RT} \right) - \exp\left(\frac{-\alpha n F\eta}{RT} \right) \right] \qquad \textbf{(Equation 1.23)}$$

A variation of current may be seen in Figure 1.11 where two limiting cases are considered corresponding to both large and small values of i_0. In both cases it is expected that no current will flow when $\eta = 0$. The difference in current will occur in response to the imposition of small overpotentials.

When i_0 is large and reversible, known as a reversible electrochemical reaction, little or no applied overpotential is required to drive the reaction and current flows readily in both anodic and cathodic directions according to the sign of the overpotential applied. In addition, because the i_0 is large, the net current i will have significant contributions from both i_a and i_c except at large positive(negative) overpotentials where the cathodic (anodic) component ultimately becomes negligible. In cases where i_0 is small a high overpotential is required to induce the current flow, this is known as irreversible electrochemical reaction. Both reversible and irreversible

47

reactions are illustrated in Figure 1.11. For the irreversible reaction when the overpotential is increased to a value at which the oxidative (anodic) process is driven, then the corresponding reductive component is vanishingly small with the opposite being true for the reverse case.

As to whether or not a given system is reversible, when electron transfer is a fast process, or irreversible, when rate of electron transfer is a sluggish process, it can be seen to depend on whether or not i_o is large or small. However all these terms are relative and signify the time scale of the electrode kinetics relative to transport of material in and out of the interfacial region.
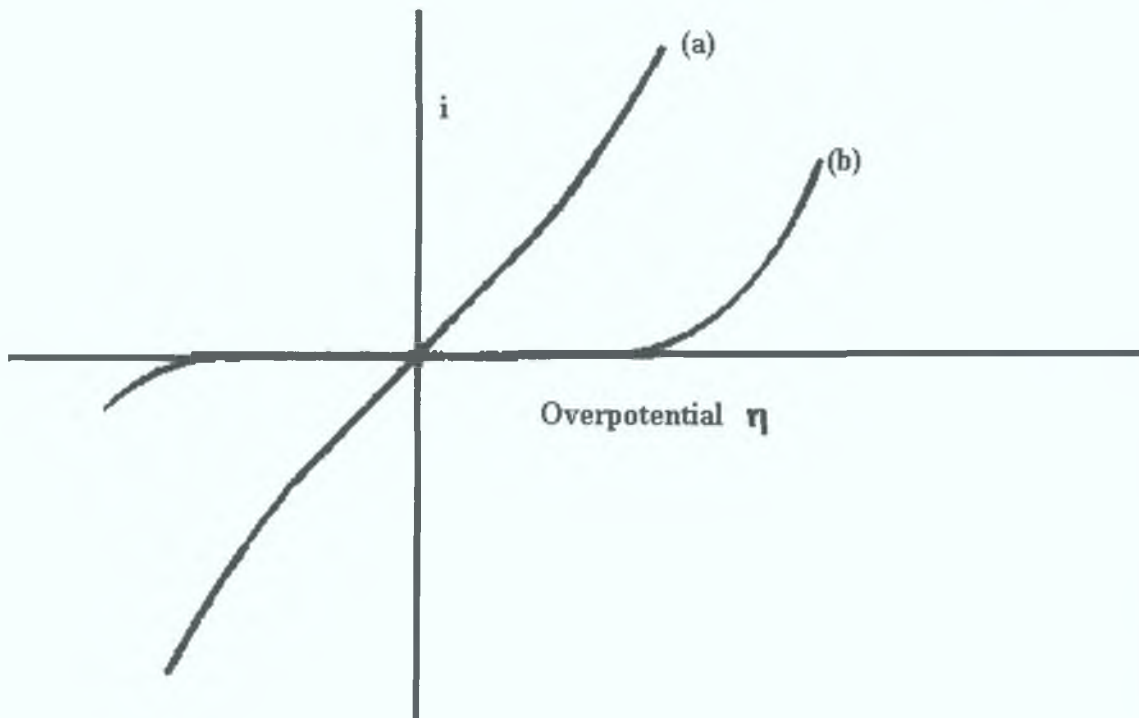
Figure 1.11. Illustrating the variation of current as a function of overpotential (η), for (a) a reversible and (b) an irreversible electrode reaction.

Although, the Butler–Volmer theory provides an experimental theory for the nature of heterogeneous electron transfer it is not an accurate description of what is occurring at the electrode interface, but rather a macroscopic explanation of a microscopic phenomena. The shortfalls of the Butler–Volmer equation can be seen by the prediction for a simple electron transfer reaction the rate constant should increase exponentially with increasing η – this is true only for a limited range in potentials.[112] In addition, the Butler–Volmer does not account for the distance dependence of heterogeneous electron transfer rate constants. Also, it does not describe how changes in the redox centre's structure will alter as a consequence of the solvent choice, $k°$.

Further study into the origin of these transfer reactions was carried out by Marcus.[111] The transition state theory, used to describe the above processes and as illustrated in Figure 1.8, focuses on the intersection or crossover point of the free energy curves for the oxidized and reduced forms. According to this transition model there is an assumption that rate of reaction depends on the number of moles with sufficient energy to reach the transition state at a particular instant in time and the probability with which they cross over the transition state. The number of molecules at the transition state depends on the free energy of activation, $\Delta G°$. Accordingly, Equation 1.24 gives the heterogeneous electron transfer rate constant:

$$k^0 = v\sigma \exp\left(\frac{\Delta G^0}{RT}\right)$$
(Equation 1.24)

where v is a frequency factor (s^{-1}) used to describe the rate at which reactants cross this energy barrier, and σ is the reaction layer thickness in cm. According to the Marcus theory, the energy of activation of the redox centre acts like a simple harmonic oscillator such that the solvent energy depends quadratically on the charge density of the molecule.[112] According to this model, the free energies of both outer sphere solvent reorganisation, ΔG_{os}, and inner sphere vibrations, ΔG_{is}, contribute to the overall energy of activation, ΔG_{Total}, as described by Equation 1.25.

$$\Delta G_{Total} = \Delta G_{os} + \Delta G_{is}$$
(Equation 1.25)

Marcus predicted that in order for electron transfer to occur the product R must firstly possess the same molecular shape (bond lengths, bond angles etc), inner

sphere energy of activation, and solvation shell structure as pertained to the reactant O in the instant prior to the electron being transferred. In addition, since no loss or gain of energy can occur, R must be formed with an energy that matches the sum of the energy of the electron in its Fermi level and the energy of O in the instant preceding the electron transfer. Using this theory it is possible to study the different patterns of the reversible and irreversible behaviour at the molecular level. For example, Forster *et al*[113] applied the Marcus theory of electron transfer between glassy carbon electrodes and osmium metallopolymers showing highly reproducible results for the rate of this outer sphere one electron transfer reaction, in various solvents of varying ionic strength. If one considers that the transfer of electrons between the electrode and the oxidised species, O, involves the quantum mechanical tunnelling of electrons between the two locations. This process is highly sensitive to the distance between the two locations and necessitates that the oxidised species is in the plane of closest approach.

The simultaneous operation of both constraints requires that the O molecule must be become energetically excited and that the R molecule formed is energetically excited. This activated state of O as seen in *Figure 1.6* is the transition state representing the structure in which O and R have the same geometry, i.e., both shape and solvation and satisfy the energy conservation restriction mentioned above in Equations 20 and 21.

A good example of such a fast electrode processes can be seen for the oxidation of MnO_4^- to MnO_4^{2-}, will occur due to both the R and O form having a tetrahedral shape and similar bond lengths. In addition to this the charge in both cases is relatively delocalised and hence the solvation state is not dissimilar.

To date the Marcus theory of heterogeneous electron transfer is the most accurate model that allows a description of what is occurring at the electrode/electrolyte interface.

Mass Transport: As was previously stated in the case of solution electrochemistry another factor which affects the current observed for an electrochemical reaction, is the rate at which a species reaches the surface of the electrode. However, in the case of a surface-confined species, especially relatively thick polymer films a mass transport limitation may be observed because counterions must diffuse from bulk solution and within the film itself in order to maintain electroneutrality. Hence, since the overall rate of reaction will be governed by its slowest step it is important to consider mass transport

limitations even for adsorbed species. As was seen in the previously in Section 1.5.3 the rate of electron transport can be controlled by electrode potential and may vary by several orders of magnitude for a small increment in the potential. Hence, in situations where electrode reactions are occurring rapidly factors such as mass transport become important for correct interpretation of experimental results. There are three influencing types of mass transport diffusion, migration and convection.

Diffusion – Diffusion involves the spontaneous movement of a species under the influence of concentration gradient, i.e., from regions of high concentration to regions of low concentration with the aim of minimising the concentration difference. The rate of diffusion at a given point in solution depends upon the concentration gradient at that particular location. *Convection* – transport to the electrode by gross physical movement either by forced convection, e.g., gas bubbling through the solution, or natural convection. *Migration* – influence of the applied electrode potential results in an electrostatic force being exerted on the electrolyte solution i.e. the movement of charge particles along an electric field.

It is however possible to eliminate some of these effects such as migration through the use of chemically and electrochemically inert background electrolytes which are added to the solution in high concentrations. Adding a background electrolyte provide several important advantages including an increase in solution conductivity which makes it less resistive to the flow of current. Moreover, the use of a high background electrolyte concentration results in an increase in contribution of current arising from the double layer. A potential gradient is absent outside of a very thin interfacial region meaning migrational effects are eliminated. This double layer is approx. 10 - 20 A thick, under equilibrium conditions. In conclusion, for quiescent solutions containing a high concentration of electrolyte, diffusion represents the dominant mass transport mechanism.

1.6 References

1. Faulkner, L. *Chem. Eng. News*, **1984**, 27, 28

2. Faulkner, L .; Bard, A.J.; *Electrochemistry Fundamental and applications*. Publisher, place of publication,year, volume, Chapter 14.

3. Chen, X.; Yi, C.; Li, M.; Lu, X.; Li, X.; Li, P.; Wang, X. *Anal. Chim. Acta.,* **2002,** *466*, 79

4. Sanders, C.A.; Rodriguez, M.; Greenbaum, E. *Biosens. Bioelectron.* **2001**

5. Meyerhoff, M.E.; Fraticelli, Y.M. *Anal. Chem.,* **1982**, *54*, 27

6. Wang, J. *Analytical Electrochemistry*, VCH publishers, New York, 1994

7. Teiter, S.; Habermuller, K.; Schuhman, W. *Sensors and Actuators B*, **2001,** *79*, 150.

8. Kelly-Basetti, B. M.; Krodkiweska, I.; Sasse, W. H. F.; Savage, G. P.; Simpson, G.W. *Tetrahedron Lett.*, **1995**, *36*, 327

9. Collins, J. E.; Lamba, J. J. S.; Love, J. C.; McAlvin, J. E.; Ng, C.; Peters, B. P.; Wu. X.; Fraser, C. L. *Inorg. Chem.,* **1999**, *38,* 2020

10. Sadik, O. A.; Van Emon, J. M. *Biosens. Bioelectron.* **1996,** *11*, 8.

11. Nistor, C.; Emmneus, J.; Gorton, L.; Ciucy, A. *Anal. Chim. Acta*, **1999,** *387*, 309

12. Ferloni, P.; Mengje, L.; *Electrochimica Acta*, **1996**, *41*, 27

13. Forster, R. J.; Vos, J. G. *Macromolecules*, **1990**, *23*, 4372

14. White, D. C.; White, J. S. *Source Book of Enzymes*, CRC Press LLC, New York, **1998**

15. Suzuki, S.; Karube, I.; Saton, I. *Biomedical Applications of Immobilised Enzyme and Proteins*, Plenum Press, New York, 1977, Vol II

16. Sansen, W.; De Wachter, D.; Callewaert, L.; Lambrechts, M.; Claes, A. *Sensors and Actuators B*: **1990**, *1–6*, 298

17. Talaie, A.; *Polymer*, 1997, *38*, 1145

18. Dengani, Y.; Heller, A. *J. Am. Chem. Soc*, **1989**, *111*, 2357.

19. Gough, D.A.; Leypoldt, J.K. *Anal. Chem.*, **1979**, *51*, 439,

20. Vreeke, M. S.; Rocca, P.; Heller, A. *Anal. Chem.*, **1995**, *67*, 303

21. Vreeke, M. S.; Yony, T.; Heller, A.; *Anal. Chem.*, **1995**, *67*, 4247

22. Wang, D. L.;. Heller, A. *Anal. Chem.*, **1993**, *65*, 1069

23.   Ikawa, M.; Phillips, N.; Haney, J. F.; Sasner, J.J.; *Toxicon*, **1999**, *37*, 923

24.   Muller, L. D. J. Pharm. *Biomed. Anal.*, **2001**, *25*, 985,

25.   Gregg, A. *J. Phys. Chem.*, **1991**, *95*, 5970

26.   Delange, D. .; Bravo, L. G. *J. Chrom. B*, **2001**, *762*, 43

27.   Mcgrath, M.J.; Iwuoha, E.I.; Diamond, D.; Smyth, M.R. *Biosens. Bioelectron.*, **1995**, *10*, 937

28.   Park, T.M.; Iwuoha, E.I.; Smyth, M.R.; Freaney, R.; McShane, A.J. *Talanta*, **1997**, *44*, 973

29.   Daigle, F.; Trudea, F.; Robinson, G.; Smyth, M. R.; Leech, D. *Biosens. Bioelectron.*, **1998**, *13*, 417

30.   Ni, J.A.; Ju, H.-X.; Chen, H.-F.; Leech, D.; *Anal. Chim. Acta*, **1999,** *378*, 151

31.   Cooper, B. R.; Wightmann, R. M.; Jogenson, J. W. *J. Chrom. B*, **1994**, *653*, 25

32.   Salem, F. B.; Alexandria, A.; *J. Pharm. Sci.*, **1995,** *9*, 334

33.   Schenk, J. O.; Miller, E.; Adams, R. N. *J. Chem. Ed.*, **1993,** *60*, 311

34.   Hasebe, Y.; Hirano, T.; Uchiyama, S. *Sens.Actuators, B*, **1995**, *24*, 94

35.   Huangxian, J,; Leech, D.; *Anal. Chim. Acta*, **1997**, *345*, 51

36 .   Vreeke, M.; Maidan, R.; Heller, A. *Anal. Chem.*, **1992**, *64*, 3084

37.   Ohsaka, T.; Tanaka, K.; Tokudda, K. *J. Chem. Soc. Comm.*, **1993**, *222*

38.   Willner, I.; Riklin, K. *Anal. Chem.*, **1994,** *66*, 1535

39.   Kulys, J. *Biosens. Bioelectron.*, **1986,** *2*, 3

40.   Shaw, R.; Creasy, K. E. *Anal. Chem.*, **1988**, *60*, 1241

41.   Adams, R. N. *Anal. Chem.*, **1958**, *30*, 1576

42.   Wang, J. ; Golden, T.; Varughese, K.; El-Rayes, I. *Anal. Chem.*, **1989**, *61*, 508

43.   Céspedes, F.; Martinez-Fabregas, E.; Bartroli, J.; Alegret, S. *Anal. Chim. Acta*, **1993,** *273*, 409

44.   Oldham, K. B. *J. Electroanal. Chem.*, **1981**, *122*, 1

45.   Martorell, D.; Cespedes, F.; Martinez-Fabregas, E.; Alegret, S. *Anal. Chim. Acta*, **1997**, 290, 343.

46.   Alegret, S.; Cespedes, F.; Fabregas, E.; Martorell, D.; Morales, A.; Centelles, E.; Munoz, J.; *Biosens. Bioelectron.,* **1996,** *11*, 35.

47.   Onnerfjord, P.; Emmeus, J.; Marko-Varga, G.; Gorton, L.; Ortega, F.; Dominguez, E. *Biosens. Bioelectron.,* **1995**, *10,* 607

48.   Céspedes, F.; Valero, F.; Martinínez-Fàbregas, F.; Bartrolí, J.; Alegret, S. *Analyst,* **1995**, *120,* 2255

49.   Alegret, S.; Céspedes, F.; Martinínez-Fàbregas, E.; Martorell, D.; Morales, A. *Biosens. Bioelectron.,* **1996**, *11,* 35

50.   Alegret, S.; Alonso, J.; Bartrolí, J.; Céspedes, F.; Martinínez-Fàbregas, E.; del Valle, M. *Sensors and Materials,* **1996**, *8,* 147

51.   Jurkiwictz, M.; del Valle, M.; Alegret, S.; Martinínez-Fàbregas, E. *Anal. Chim. Acta,* **1996**, *327,* 243

52.   Céspedes, F.; Fabregas, E.; Alegret, S. *Anal. Chim. Acta,* **1993**, *284,* 21

53.   Mareike, E.S.; Domínguez, E. *Electroanalysis,* **1996**, *8,* 117

54.   Morales, A.; Céspedes, F.; Muñoz, J.; Fábregas, E.; Alegret, S. *Anal. Chim. Acta.,* **1996**, *332,* 131

55.   Martorell, D.; Céspedes, F.; Martinínez-Fàbregas, E.; Alegret, S. *Anal. Chim. Acta,* **1997**, *337,* 305

56.   del Cerro, M. A. Cayuela, G.; Reviejo, A. J.; Pingarrón J. M.; Wang, J. *J. Electroanal.* **1997**, *9,* 1113

57.   Morales, A.; Céspedes, F.; Martinínez-Fàbregas, E.; Alegret, S. *Electrochim. Acta,* **1998**, *43,* 3575

58.   Santandreu, M.; Céspedes, F.; Alegret, S.; Martinínez-Fàbregas, E. *Anal. Chem.,* **1997**, *69,* 2080

59.   Santandreu, M.; Solé, S.; Fàbregas, E.; Alegret, S. *Biosens. Bioelectron.,* **1998**, *13,* 7

60.   **News,** *Biosens.* **1987**, *3,* 317

61.   Sugawara, K.; Kobayashi, D.; Saito, K.; Furuya, E.; Araake, H.; Yagihashi, A.; Yajima, T.; Hosoda, K. Kamimura, T.; Watanabe, N. *Clinica Chimica Acta,* **2000**, *299,* 45.

62.   Guiver, M.; Borrow, R.; Marsh, J.; Gray, S. J.; Kaczmarski, E. B.; Howells, E.; Boseley, P.; Fox, A. J. *FEMS Immunology and Medical Microbiology,* **2000**, *28,* 173

63.   Navas-Castillo, J.; Díaz, A.; Sánchez-Campos, S.; Moriones, E. *J. Virol. Methods,* **1998**, *75,* 195

64. Crowther, J. R.; Reckziegel, P. O.; Prado, J. A. *Vaccine,* **1995**, *13,* 1064

65. Palecek, E. *Naturwiss,* **1958**, 45, 186.

66. Berg, H. *Biochem. Z.* **1957**, 329, 274.

67. Palecek, E. Coll. *Czech. Chem. Commun.,* **1960**, *25,* 2283.

68. Janik, B.; Palecek, E. *Z. Naturforsch.,* **1966**, *21b,* 1117.

69. Janik, B. Elving, P. J. *Chem. Rev.,* **1968**, *68,* 295

70. Palecek, E.; Fojta, M.; Tomschik, M.; Wang, J. *Biosens. Bioelectron.,* **1998**, *13,* 621

71. Palecek, E. *Talanta,* **2002**, *56,* 809

72. Marrazza, G., Chianella, L., Mascini, M. *Biosens. Bioelectron.,* **1999**, *14,* 43

73. Wang, J.; Cai, X.; Fernandes, J. R.; Grant, D. H.; Ozsoz, M. *Anal. Chem.,* **1997**, *69,* 4056

74. Wang, J.; Cai, X.; Rivas, G.; Shiraishi, H.; Dontha, N. *Biosens. Bioelectron.* **1997**, *12,* 587

75. Wang, L.; Rivas, G.; Cai, X. *Electroanalysis,* **1997**, *9,* 395

76. Wang, J.; Rivas, G.; Cai, X.; Chicharro, M.; Parrado, C.; Dontha, N.; Begleiter, A.; Mowat, M.; Palecek, R.; Nielsen, P. E. *Anal. Chim. Acta,* **1997**, *344,* 111

77. Wang, L.; Rivas, G.; Cai, X.; Palecek, E.; Nielsen, R.; Shirishi, H.; Dontha, R.; Luo, D.; Parrado, C.; Chicharro, M.; Fanias, P. A. M.; Valera, F.S.; Grant, D. H.; Ozsoz, M.; Flair, M. N. *Anal. Chim. Acta,* **1997**, *347,* 1

78. Wang, J., Fernandes, J. R., Kubota, L. T. *Anal. Chem.,* **1998**, *70,* 3699

79. Babkina, S. S.; Medyantseva, E. P.; Budnikov, H. C.; Tyshlek, M. P. *Anal. Chem.,* **1996**, *68,* 3827

80. Liu, S.; Ye, L.; He, P.; Fang, Y. *Anal. Chim. Acta.;* **1996**, *335,* 239

81. Armistead, P. M.; Thorp, H. H. *Anal. Chem.,* **2000**, *72,* 3764

82. Brett, O.; Macedo, A. M.; Raimundo, T. R. A.; Marques, E.; Serrano, S. H. P. *Biosens. Bioelectron.,* **1998**, *13,* 861

83. Labuda, L.; Buckova, M.; Vanic, C.; Mattusch, M.; Wennrich, R. *Electroanalysis,* **1999**, *11,* 101

84. Pang, D. W.; Abruna, H. D. *Anal. Chem.,* **1998**, *70,* 3162

85. Millan, K. M.; Spurmanis, A. L.: Mikkelsen, S. K. *Electroanalysis,* **1992**, *4,* 929

86. Millan, K. M.; Mikkelsen, S. K. *Anal.. Chem.*, **1993**, *65*, 2317

87. Millan, K. M.; Saraullo, A.; Mikkelsen, S. K. *Anal. Chem.*, **1994**, *66*, 2943

88. Mikkelsen, S. K. *Electroanalysis*, **1996**, *8*, 15

89. Yang, M.; McGovern, M. E.; Thompson, M. *Anal. Chim. Acta*, **1997**, *346*, 259

90. Herne, T. M.; Tarlov, M. J. *J. Am. Chem. Soc.*, **1997**, *119*, 8916

91. Liu, S.; Ye, L.; He, P.; Fang, Y. *Anal. Chim. Acta*, **1996**, *335*, 239

92. Pang, D. W.; Abruna, H. D. *Anal. Chem.*, **1998**, *70*, 3162

93. Nuzzo, R. G.; Allara, D. L. *J. Am. Chem. Soc.*, **1983**. *105*, 4481

94. Bain, C. D.; Troughton, E. B.; Tao, Y.-T.; Evall, J.; Whitesides, G. M.; Nuzzo, R. G. *J. Am. Chem. Soc.* **1989**, *111*, 321

95. Steel, A. R.; Herne, T. M.; Tarlov, M. J. *Anal. Chem.*, **1998**, *70*, 4670

96. Pantano, P.; Morton, T. H.; Kuhr, W. G. *J. Am. Chem. Soc.*, **1991**, *113*, 1832

97. Kleinjung, F.; Klussmann, S.; Erdmann, V. A.; Scheller. F. W.; Ful, J. P.; Furste, Bier, F. F. *Anal. Chem.*, **1998**, *70*, 328

98. Jordona, C. E.; Frutos, A. G.; Thoe,; A. J.; Corn, R. M. *Anal. Chem.*, **1997**, *69*, 4939

99. Caruso, F.; Rodda, E.; Furlong, D. N. *Anal. Chem.*, **1997**, *69*, 2043

100. Shamansky, L. M.;Brandon-Davis, C.; Stuart, J. K.; Kuhr, W. G. *Talanta*. **2001**, *55*, 909

101. Carter, M. T.; Rodriguez, M.; Bard, A. L. *J. Am. Chem. Soc.*, **1989**, *111*, 8901

102. Pang, D. W.; Abruna, H. D. *Anal. Chem.*, **1998**, *70*, 3162

103. Labuda, L.; Buckova, M.; Ikova, M.; Mattusch, L.; Wennrich, R. *Electroanalysis*, **1999**, *11*, 101

104. Palecek, E.; Fojta, M.; Jelen, F. *Biochem.*, **2002**, uncorrected proof

105. Chetcuti, A. F.; Wong, D. K. Y. *Anal. Chem.*, **1999**, *71*, 4088

106. Chen, X.; Ruan, C.; Kong, J.; Deng, J. *Anal. Chim. Acta*, **2000**, *412*, 89

107. de Lumney-Woodyear, T.; Campbell, C. N.; Freeman, E.; Freeman, F.; Georgiou, G.; Heller, A *Anal. Chem.*, **1999**, *71*, 535

108. Xu, C.;.Cai, H.; He, P. *Analyst.* **2001**, *126*, 62

109. Singhal, P.; Kuhr, W. G. *Anal. Chem.*, **1997**, *69*, 4828

110. A.C. Fisher. *Electrode Dynamics*, Oxford University Press, Oxford Publishers, UK, 1996

111. Marcus, R. A.; *J. Phys. Chem.,* **1963**, *67*, 853

112. Forster, R. J. *Interface*, **2000**, *9*, 24.

113. Forster, R. J.; Vos, J. G. *J Chem. Soc. Faraday Trans.*, **1991**, *87*, 3769

Chapter 2

Synthesis and

Electrochemical Characterisation

of Redox Polymers in Buffered Systems

2.1   Introduction

Electroactive monolayer and thicker films on conductive substrates are frequently known as chemically modified electrodes.[1] These electrodes are often prepared by modification of a conductive substrate to produce an electrode suited to a particular function, whose properties differ from those of the unmodified substrate.

Interest in modified electrodes is based mainly on the broad range of possible applications, as reviewed in Section 1.3. One area of particular interest is the capability of modified electrodes to function as an analytical sensor, i.e., the commercially significant glucose biosensor.[2] Additionally, while these modified electrodes are of interest to the analytical chemist they are also of great interest to the electrochemist in terms of electron and mass transfer reactions.[3]

This chapter reports on the synthesis and characterisation of metal ion chelating polymers, specifically poly(N-vinyl-imidazole) (PVI), and poly(4-vinyl-pyridine) (PVP). The advantage of such polymers is their capability to co-ordinate species like metal ions and biocomponents and irreversibly bind them within the polymer matrix. These materials can subsequently be used to modify an electrode surface.

Here, the metal complexes incorporated within PVP and PVI are $[Os(bpy)_2Cl]^{2+/3+}$ and $[Os(dime(bpy)_2Cl]^{2+/3+}$ respectively. The choice of osmium as the metal ion is twofold. First, extensive electrochemical characterisation of these osmium based polymers has been conducted.[4,9] From this characterisation it is known that these species possess all the desirable characteristics of an electron mediator between an enzyme redox site and the electrode surface, since in most incidence the enzyme redox site is located deep within the protein structure therefore demanding the use of a mediator to achieve electron transfer. The most important characteristics that these metal ions possess in relation to use as an electron mediator are fast electron transfer, chemical stability and electrochemical reversibility over a broad pH. In addition to these advantages the formal potential is close to 0.000 V with respect to the Ag/AgCl reference electrode, hence minimising interferences due to electro-oxidation of interfering substances.

As previously mentioned an extensive characterisation of these metal-polymer complexes has been carried out in various electrolytes that differ both in ionic

strength and pH.[4] However, it is striking that there have been no studies characterising these modified electrodes in pH buffered systems. Therefore, an investigation into the redox properties of these PMEs is made. Moreover, in an effort to extend the range of analytes that can be detected with these PMEs, the osmium based polymers were modified with progesterone through a simple reaction which can occur at room temperature. This is an improvement on previous attempts[21] that required a tedious temperature controlled process to ensure that modification occurred. To ensure that the progesterone is present within the PME an indirect enzyme immunoassay was employed. Following this modification procedure, an electrochemical characterisation of the basic redox properties is reported. This characterisation demonstrated that the presence of a biocomponent significantly affects the electrochemical properties of the PME.

2.2 Apparatus

Ultraviolet-visible (UV/Vis) spectra were recorded using a Shimadzu UV-3100 spectrophotometer. High performance liquid chromatography (HPLC) was carried out on a Waters 510 HPLC using a Waters 990 photodiode array detector equipped with a NEC PAC III detector, a 20 µl injector loop and a Partisil SCX radial PAK cartridge. Electrochemical methods were performed using CH Instruments Model 600 and 660 electrochemical workstations. CHN analysis were performed by Microanalytical Laboratories, UCD,. Potentials were measured versus Ag/AgCl or a silver wire where indicated. The counter electrode was a 1 cm^2 platinum flag. All electrochemical measurements were carried out at 22° $\pm$ 3 °C.

2.3 Experimental

2.3.1 Preparation of Poly(4-vinyl pyridine)

Poly(4-vinyl pyridine) was provided by Conor Hogan and was prepared as follows. First, the hydroquinone preservative was removed by vacuum distillation of the monomer at 70 °C. The colourless monomer was then degassed with nitrogen and bulk polymerised for 4 hr., using the free radical initiator 2,2′-azobisisobutylonitrile (AIBN) at a mole ratio of 500:1 (monomer: initiator). The product was purified by repeated

precipitation in diethyl ether from methanol and dried under vacuum. Viscometry was carried in ethanol was used in order to determine the molecular weight of the polymer

2.3.2   Preparation of Poly(N–vinylimidazole).

The monomer N–vinylimidazole, 99% (Aldrich) was purified by vacuum distillation, using a short path vacuum distillation Kugelrohr apparatus (Buchi Gkr-5, Germany). This procedure removed the hydroquinone that inhibits polymerisation of the monomer. The colourless monomer was then degassed using nitrogen and bulk polymerisation was carried out using a free radical initiator AIBN at a mole ratio of 1:500 (monomer: AIBN) and dissolved in 10 cm^3 methanol. This solution was then refluxed to achieve bulk polymerisation for approx. 4 hrs. The resulting solution was filtered and the filtrate was then redissolved in methanol. This solution was precipitated in diethyl ether (X2) and filtered. The white polymer was dried overnight under vacuum. Characterisation of Poly(N–vinylimidazole), PVI, was carried out using viscometry, by dissolving the PVI in ethanol and application of the Mark–Houwink equation.

2.3.3   Preparation of [Os(dime(bpy)$_2$)PVI$_{10}$Cl](PF$_6$)$_2$]

The metallopolymer, [Os(dime(bpy)$_2$)PVI$_{10}$Cl](PF$_6$)$_2$] was synthesised according to Equations 2.1 and 2.2

$$K_2[OsCl_6] + 2 \text{ dime(bpy)} + 2H_2O \rightarrow [Os(dime(bipy)_2Cl_2]Cl.2H_2O + 2KCl + \text{Products}$$

(Equation 2.1)

$$[Os(dime(bipy)_2Cl_2]Cl.2H_2O + Na_2S_2O_4 \rightarrow 2[Os(dime(bipy)_2)Cl_2] + 2H_2SO_4 + 2H_2O$$

(Equation 2.2)
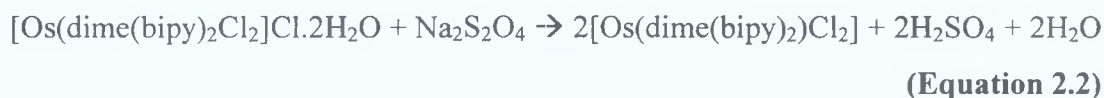
Potassium hexachloroosmium (IV) (1g, 2.7 mmol) was heated to 120 °C, in 20 cm^3 DMF, in a round-bottomed flask until it completely dissolved. Then, 0.75 g (4.14 mmol) of 4,4'–dimethyl–2,2'–dipyridyl (dime(bpy)$_2$) dissolved in 5 cm^3 of DMF was added in small aliquots. The mixture was heated at reflux with continuous stirring for approx. 1 hr. Equation 2.1 demonstrates that upon reflux side products are formed, these products are filtered while still hot using Whatman filter paper, 100 µm porosity. When the solution had cooled to room temperature the complex was precipitated by

drop-wise precipitation into a diethyl ether, which was rapidly stirred (approx. 1 cm^3 of complex to 100 cm^3 of diethyl ether was used). Once all of the precipitate was filtered using a sinter glass funnel, it was allowed to dry overnight in a dessicator.

As shown in Equation 2.2, this Os^{3+} complex was then reduced using dithionite as follows: Bis(2,2'-dime(bipy)$_2$ dichloro-osmium chloride dihydrate (0.75g, 1.07 mmol) was dissolved in 10 cm^3 methanol and 4 cm^3 of DMF in a large beaker, placed in an icebath. To this solution sodium-dithionite (0.186g, 1.07mmol) disolved in 10 cm^3 of HPLC grade water, was added slowly over a period of 30 mins with continious stirring,. Stirring was continued for an additional 15 mins after the sodium dithionite was added to this mixture. The solution was placed in an icebath and left to crystallise overnight at 4 °C. To check the purity of the synthesised product HPLC was carried out using adetection wavelength was 280 nm. The chromatography was achieved using a mobile phase, which consisted of acetonitrile/water, 80/20 (v/v) containing 0.08 M LiClO$_4$. The flow rate was 1.8 cm^3 min^{-1}. HPLC of the product revealed only a single peak at 1.73 min, thus indicating the formation of a single product.

The next stage involved binding of the osmium complex to the poly(N-vinylimidazole).[4,5] This binding reaction is summarised below in Equation 2.3

$$[Os(dime(bipy)_2)Cl_2] + PVI \rightarrow [Os(dime(bipy)_2PVI_{10}](PF_6)_2 + products$$

(Equation 2.3)

A typical synthesis of a metallopolymer involved adding 0.4 g (0.69 mmol) of Os[dime(bipy)$_2$Cl$_2$] to 30 cm^3 ethanol, allowing it to reflux for approx. 30 min. PVI (0.75 g (6.9 mmol)) was dissolved in 5cm^3 of ethanol, and was added dropwise to the reaction vessel. The desired redox loading of osmium to polymer is 1:10, hence the quaties chosen will ensure such a loading is obtained. The solution was refluxed for another 72 hrs, and monitored continously with cyclic voltammetry. Isolation of [Os(dime(bipy)$_2$PVI$_{10}$Cl]$^{2+/3+}$ was achieved by precipitation in diethyl ether. Addtion of the the Os–PVI$_{10}$ to a solution containing NH$_4$PF$_6$ resulted in the precipitation of the complex as a the PF$_6^-$. Elemental analysis(UCD) results show values of C–45.6%, N–8.8% and H–3.6% which are in satisfactory agreement with the theoretical values of C–45.8%, N–8.9% and H–3.8%.

2.3.4 Synthesis of [Os(bpy)$_2$PVP$_{10}$](PF6)$_2$

Both the Os(bpy)$_2$Cl$_2$ and poly(4-vinylpyridine) were supplied by Conor Hogan and made in accordance with Buckingham et al.[6] The general reaction scheme is shown in Equations 2.4 and 2.5,

$$[Os(bpy)_2Cl_2] + H_2O \rightarrow [Os(bpy)_2Cl\ H_2O]^+ + Cl^- \qquad \textbf{(Equation 2.4)}$$

$$[Os(bpy)_2Cl\ H_2O]^+ + PVP \rightarrow [Os(bpy)_2PVP_{10}Cl]^{2+/3+} \qquad \textbf{(Equation 2.5)}$$

0.2 g (0.35 mmol) of [Os(bpy)$_2$Cl$_2$] was dissolved in 20 cm^3 of ethanol and was refluxed for approximately 20 min. to ensure that the entire complex dissolved as shown in Equation 2.4. In accordance with Equation 2.5, 0.38 g (3.5 mmol) of PVP dissolved in 10 cm^3 of ethanol was added slowly, in 1ml aliquots, to the reflux vessel with the intention of forming a complex that yields a 1:10 ratio of Osmium: PVP. This solution was refluxed for another 72 hrs, and monitored continously with cyclic voltammetry, the rest of the procedure follows the same as Section 2.3 above for synthesis/purification of PVI$_{10}$–Os.

Elemental analysis of the percentage of C, N, and H shows that the amount of carbon was C–41.5%, H–2.7% and N–9.6% for the [Os(bipy)$_2$Cl$_2$] which is in satisfactory agreement with the theoretical values C–41.9%, N–9.80% and H–2.8%. CHN. Apart from elemental analysis, to ascertain the purity of the complex UV–Vis were carried out, conditions were the same as those used in Section 2.3.3.

2.3.5 Modified Electrodes

A metallopolymer film was formed by drop casting a constant volume of 40 µl, onto the surface of the electrode using a micropipette. The electrode was dried in an upright position in a solvation chamber, which contained Milli–Q water to a depth of 1 cm, over a period of 48 hrs. Incorporation of progesterone into the PVI$_{10}$–Os was achieved by taking equal volumes of diamino-propane (13.5 µmol), polyethyleneglycol (PEG) (2.3 µmol), progesterone (50 µmol) and 50 µmol of PVI$_{10}$–Os. Modification of PVP$_{10}$–Os with progesterone occurs in the same manner as above with the addition of a hydrophilic carbodiimide (5.9µmol) which reacts with the pendent amine on the PVP polymer. The addition of this hydrophilic agent ensures the solubility of PVP$_{10}$–Os in

water. All chemicals were dissolved in water except progesterone, which was dissolved in ethanol. This solution was allowed to react for approx. 1 hr. and was always prepared on the same day as the electrodes. Again, a 40 µl sample is then micro-pippetted onto the surface of a freshly polished glassy carbon electrode and left drying in an upright position for 48 hrs. in a dessicator.

2.3.6   *Enzyme immunoassay for detection of the presence of progesterone*

An indirect immunoassay was used to confirm that progesterone is present and active within the PME. This assay is essential, as progesterone contains no redox active centres. To achieve this objective, a PME was immersed in a solution containing a monoclonal antibody (Mab) for one hour. The Mab used is known to have react specifically with the progesterone incorporated within the PME, and was supplied by the Department of Biochemistry and the National Diagnostics Centre Bioresearch Ireland, NUI, Galway.[7] The electrode was removed and washed with a phosphate buffered saline/bovine serum albumin (PBS/BSA). The electrode was then immersed in a solution of enzyme labelled antibody, rabbit-antimouse horseradish peroxidase (RAM/HRP) after one hour when it was removed and washed with the PBS/BSA solution. The modified electrode was then immersed into a plastic cuvette containing 1cm^3 of TMB, for 15 min. After 15 min. have elapsed the reaction is stopped by adding 0.1cm^3 of 0.1 M H_2SO_4. Following this a single wavelength UV-vis spectrometer set at 450 nm was used to obtain an absorbance reading. The control experiments were carried out with respect to this immunoassay were:

i.   Electrodes modified with the metallopolymer alone.

ii.   Electrodes modified with all "wiring components" except progesterone.

iii. Electrodes modified with a greater concentration of progesterone, i.e., between 2–10mg/ml of progesterone.

All experiments were carried both with and without washing with the PBS/BSA solution.

65

2.4   Results and Discussion

2.4.1   Characterisation of synthesised metal complexes and metallopolymer.

Absorption spectroscopy: Electronic spectroscopy has proved useful in the characterisation of metallopolymers.[8]   Of particular interest is the position of the absorption maxima in the visible region, that varies with the ligand composition and generally is used for identification of complexes.[9] Figure 2.1 shows the UV-vis spectra of both PVI_{10}–Os and PVP_{10}–Os in methanol. These osmium complexes exhibit intense absorbance bands in the visible region of the spectrum because of the metal centred electrons that are transferred to the organic ligands when the complex is irradiated with a suitable wavelength of light. Such an electronic transfer is known as a metal to ligand charge transfer (MLCT). From Figure 2.1 the λ_{max} values for MLCT are approximately, 431, 486 and 730 nm for the Os–PVP complex while the Os–PVI complex shows transitions at approximately 431, and 524 nm. The λ_{max} observed at 364 nm for both metallopolymers is associated with a metal–centred charge transfer. Neither the PVI and PVP metallopolymers exhibit significant emission which agrees with Forster et al.[4]

Viscometry: Both polymers were characterised using viscometry in accordance with the Mark-Houwink equation, $[\eta] = KM_v^a$. Viscometry is a hydrodynamic technique which relates polymer viscosity to molecular weight, $[\eta]$ is the intrinsic viscosity at an infinite dilution, η/η^* is the viscosity of the solution divided by the viscosity of the pure solvent (effective eflux times are substituted for this value). K and a are the Flory constants and are available from literature,[10,11,12,] and are related to the identity of the solution and the polymer.   For these experiments, both PVI and PVP were dissolved in ethanolic solution in the concentration range of 0.2 % to 1.0% (w/v). The flow time of each polymer through a viscometer is measured at 25 ± 0.5 °C. A plot of $[(\eta/\eta^*)-1]$/concentration vs. concentration allows data to be extrapolated and subsituted into the Mark-Houwink equation. It was found that PVI has a molecular weight of 110,000 g/mol while PVP has a molecular weight of 430,000 g/mol.
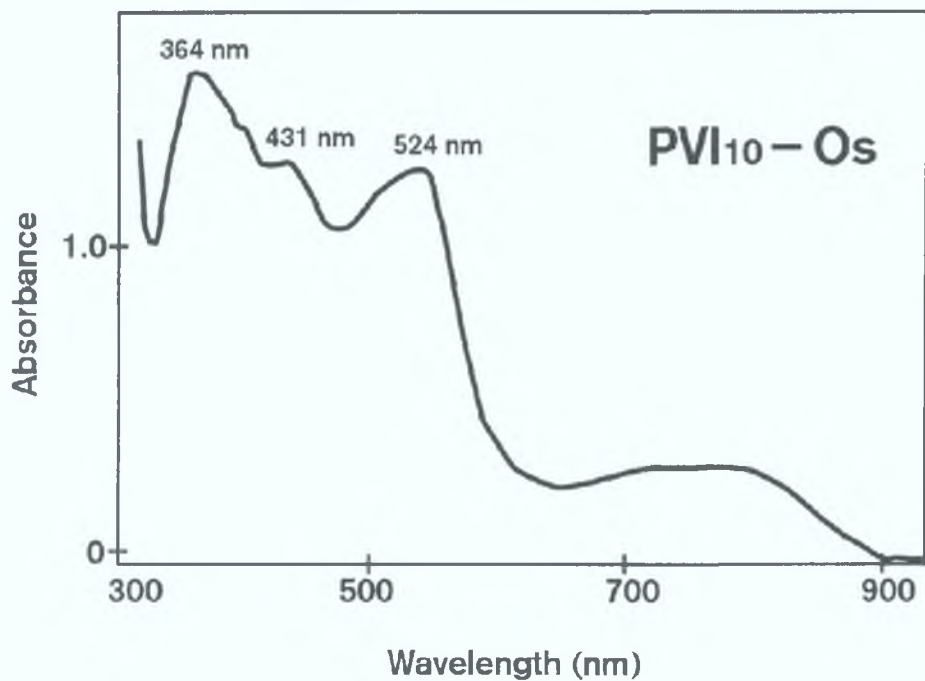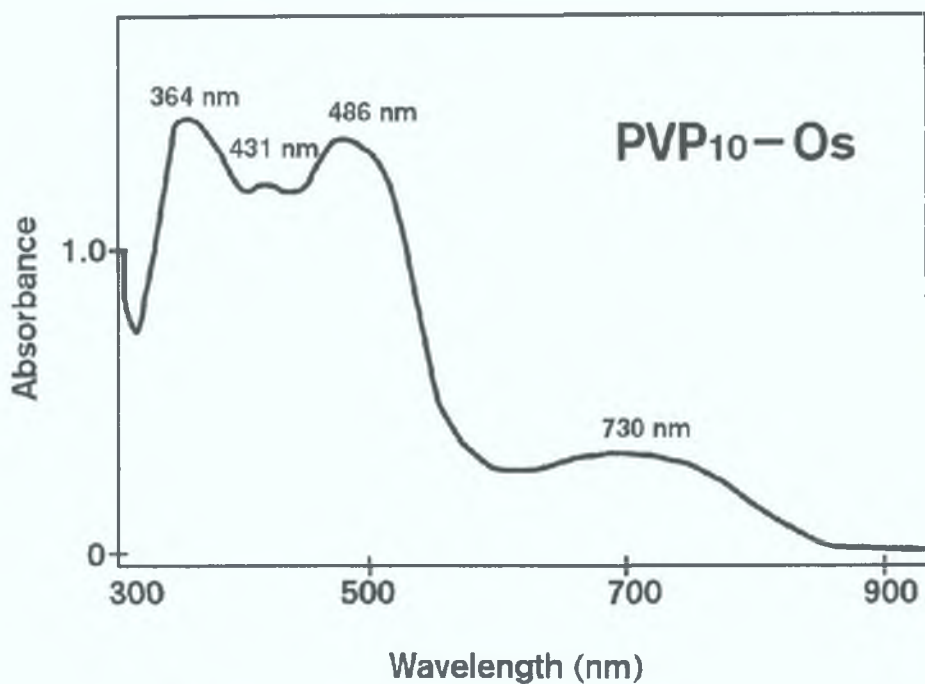
Figure 2.1. UV-vis spectra of PVP_{10}–Os peaks can be seen at 364, 431, 486 and 730 nm and PVI_{10}–Os, (1.5 mM). λ_{max} may be observed at 364, 431 and 524 nm. In both cases, the solvent used was ethanol.

2.4.2   Cyclic Voltammetry

Cyclic voltammetry is a widely used electroanalytical technique for characterising redox active systems. This is because of its ability to rapidly provide information on the thermodynamics of redox processes, the location of the formal potentials of the redox species and the kinetics of heterogeneous electron transfer reactions. For this reason, cyclic voltammetry is often the first experiment performed in an electroanalytical study. By scanning linearly the potential of a stationary-working electrode, using a triangle potential waveform, Scheme 2.1, analytical data is retrieved. It is during the potential sweep, that the potentiostat measures the current resulting from the applied potential. The resulting plot is known as a cyclic voltammogram
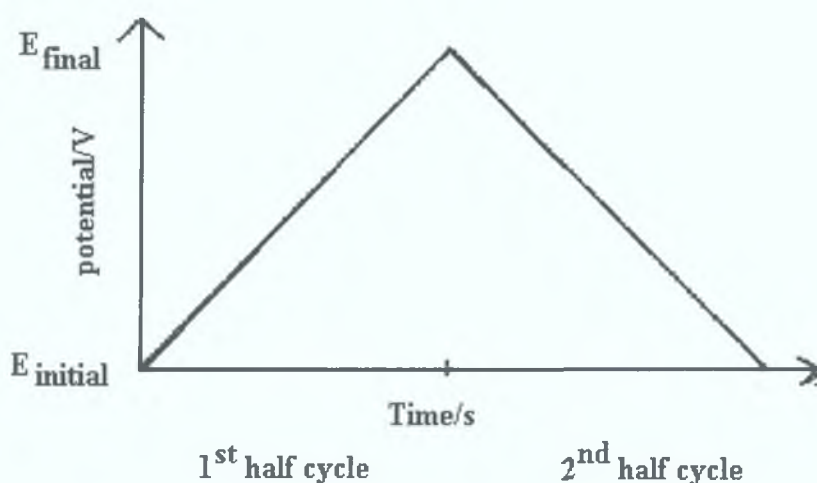
Scheme 2.1. Triangular waveform potential

Initially, it is assumed that only the oxidised species are present, hence a negative going potential scan is chosen for the first half cycle, starting from a potential value where no oxidation/reduction occurs. When the applied potential approaches the characteristic E° a cathodic current begins to flow, until a peak is reached. After passing the region where the reduction occurs the direction of the potential sweep is reversed. During the reverse cycle the initially reduced molecules are re-oxidised, and an anodic peak results. These characteristic peaks for a reversible electrode reaction, which are seen in Figure 2.2 are caused by the formation of a diffusion layer near the surface of

68

the electrode. A continuous change in surface concentration is coupled to the expansion of the diffusion layer thickness. The resulting current peaks reflect this continuous change of the concentration gradient with time. By using the Randles–Sevcik equation, Equation 2.6, it is possible to characterise the diffusion co-efficient for a fast redox reaction by measuring the peak current obtained from a cyclic voltammetry experiment.

$$i_p = (2.69 \times 10^5)n^{3/2}ACD_0^{1/2}v^{1/2}$$
(Equation 2.6)

In this equation, v is the scan rate, n is the number of electrons transferred in the electrochemical reaction, A is the area of the electrode, D_0 is the diffusion co-efficient and C is the concentration of the electroactive species. According to Equation 2.6 the current is directly proportional to the concentration redox species at the surface of the electrode and increases with the square root of the scan rate. For a simple one electron reversible couple the ratio of the forward peak to reverse peak $i_{p,f} / i_{p,r}$ is close to unity. However, this peak ratio can be greatly affected by chemical reactions, which may be coupled to the redox process. Positioning of peaks on the potential axis is related to the formal potential of the redox process. Equation 2.7, shows how in the case of a reversible couple the formal potential is centred between E_{pa} and E_{pc}, anodic and cathodic peak potential respectively.

$$E° = \frac{E_{pa} + E_{pc}}{2}$$
(Equation 2.7)

For a reversible redox couple the separation between peaks, ΔE_p is given by Equation 2.8. From this equation, it can be seen that the peak separation may be used to determine the number of electrons transferred. In the case of a fast one electron process a ΔE_p of approx. 0.059 V is obtained, assuming a switching potential of at least 0.09 V beyond the value of E_p with both the cathodic and anodic peak potentials being independent of scan rate.

$$\Delta E_p = E_{pa} - E_{pc} = \frac{0.059}{n}V$$
(Equation 2.8)

2.4.3   *Electrochemical Characterisation of Polymers and Complexes*

While carrying out the reflux synthesis described in Sections 2.3.3 and 2.3.4, small volumes (0.5 cm^3) were periodically taken from the reaction vessel and dissolved in acetonitrile containing 0.1 M TBAF$_4$.

A solution phase voltammogram of the starting material [Os(dime(bipy)$_2$Cl$_2$] in acetonitrile containing 0.1 M TBAF$_4$ is shown in Figure 2.2. A single redox couple is observed with a formal potential, $E^{0'}$ of –0.175 V. This redox active couple is characteristic of a reversible one electron transfer. In Figure 2.3, the substitution one of the chloride ions for PVI results in a shift in $E^{0'}$ from –0.175 to approximately 0.07 V. As can be seen in Figure 2.4 there are four methyl groups on the bpy ligand, and two nitrogen atoms on the imidazole polymer, both of which contain lone pairs. Because of these electronegative groups are within the redox polymer, application of a potential results in easier removal of an electron and consequently, an $E^{0'}$ closer to zero is observed.

It is perhaps easier to demonstrate the effects electronegative groups have on $E^{0'}$ by studying the ligand substitution reaction of [Os(bpy)$_2$Cl$_2$] with PVP to produce the redox polymer (PVP$_{10}$-Os). As can be seen from Figure 2.5 the PVP$_{10}$–Os complex does not have any methyl groups attached to the bpy ligand in addition the PVP only contains one nitrogen atom and hence one set of lone pairs. Similar to what was observed in Figure 2.2 substituting one of the chloride ions for PVP results in a shift in $E^{0'}$ from 0.192 V at 1 hr. to 0.272 V at 45 hrs. to 0.432 V at 70 hrs. The differences in $E^{0'}$ can be seen in Figure 2.6 that compared both PVI$_{10}$–Os with PVP$_{10}$–Os, at a scan rate of 0.1 Vs^{-1}. The higher values of $E^{0'}$ for PVP$_{10}$–Os when compared with PVI$_{10}$–Os is associated with the fewer electron donating/electronegative groups being present.
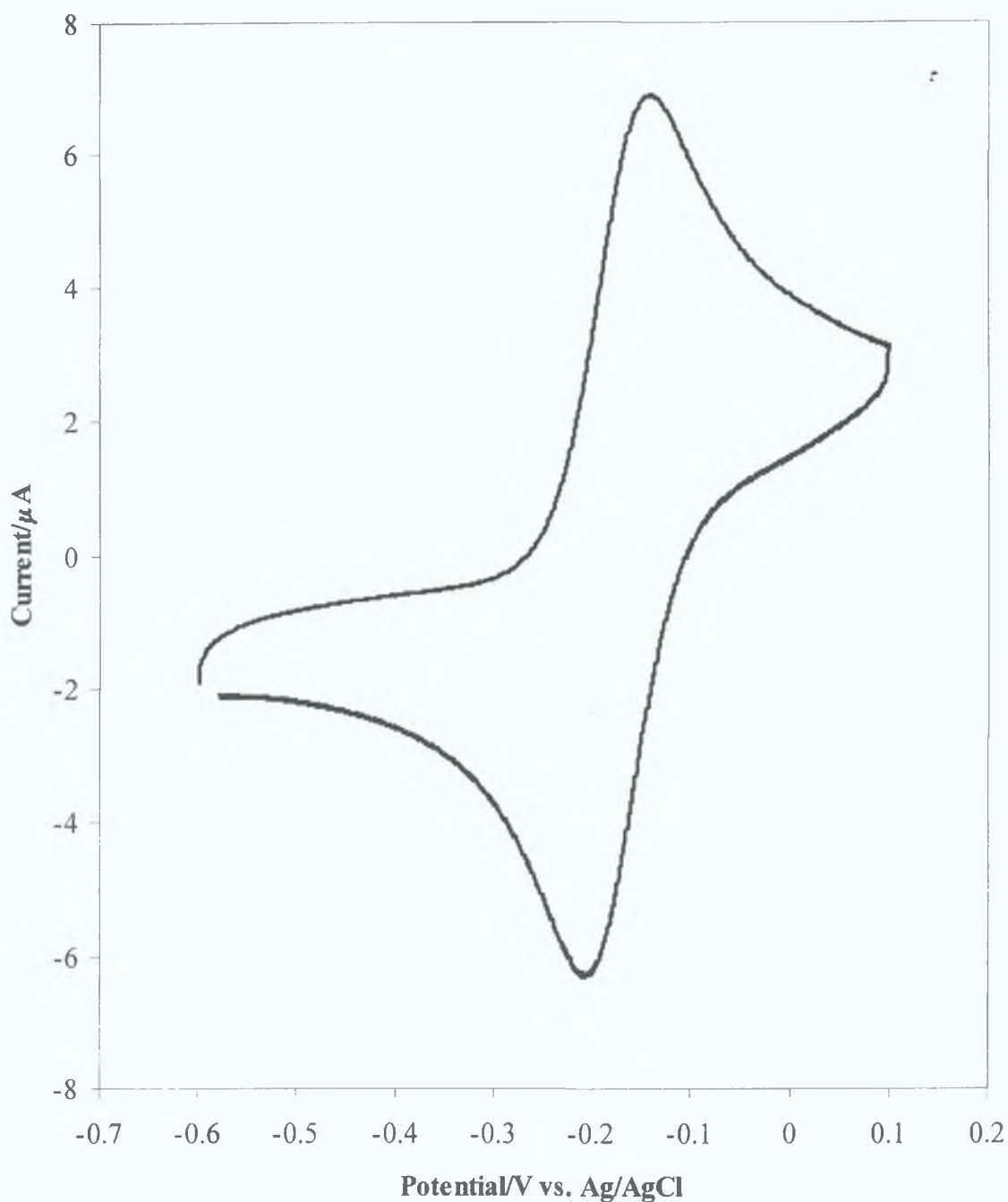
Figure 2.2 Solution phase cyclic voltammogram of a 1 mM solution of [Os(dime(bpy)$_2$Cl$_2$] in acetonitrile with 0.1 M TBAF$_4$ as the electrolyte. The scan rate was 0.1 Vs^{-1} and a 1.5 mm radius glassy carbon electrode was used. The initial potential was –0.6 V.
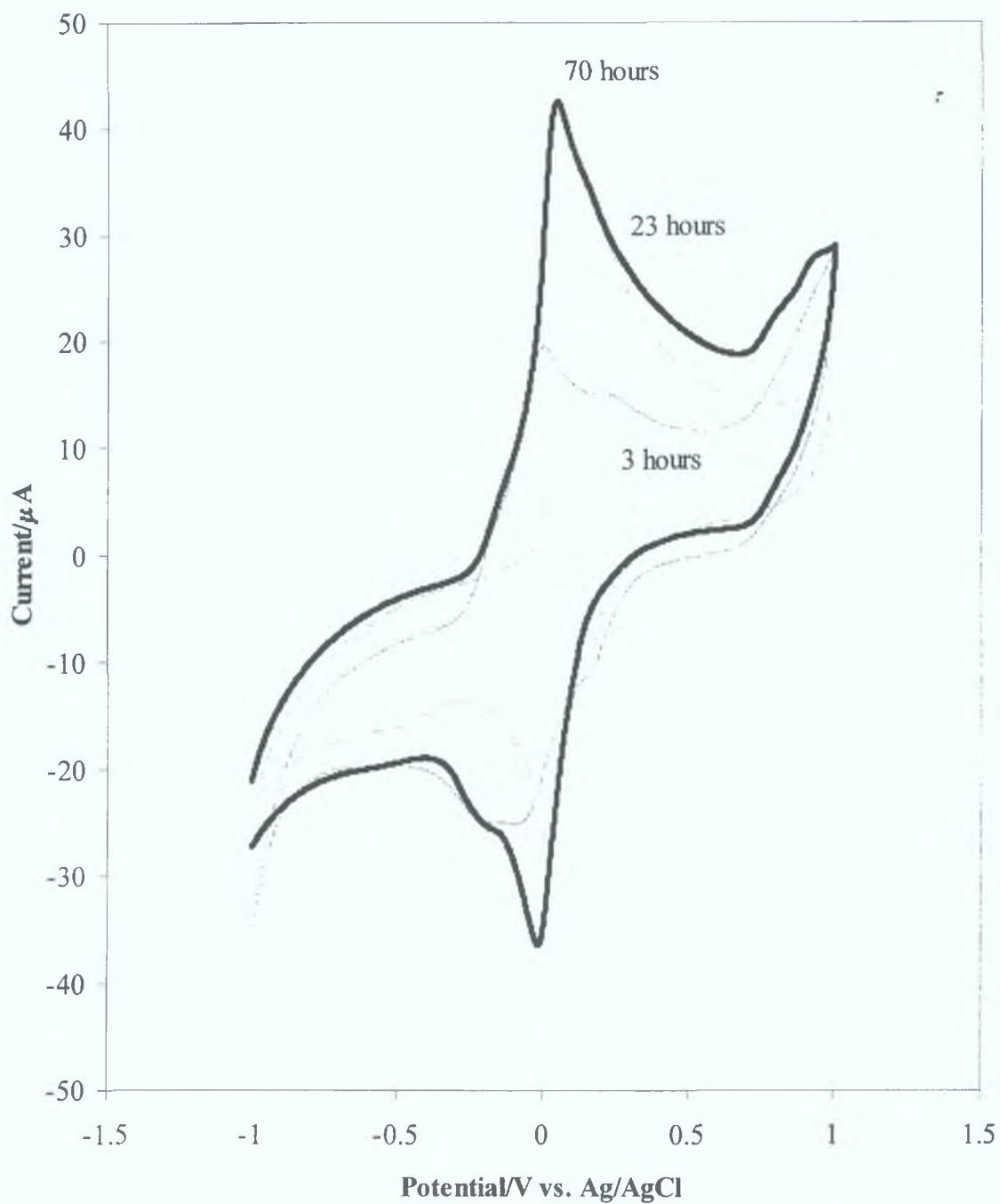
Figure 2.3. Cyclic voltammogram of (PVI$_{10}$-Os) at various stages of reflux, as highlighted, in 0.1M TBAF$_4$ acetonitrile. The scan rate was 0.1 Vs^{-1} and a 1.5 mm radius glassy carbon electrode was used. The initial potential was −1.0 V.
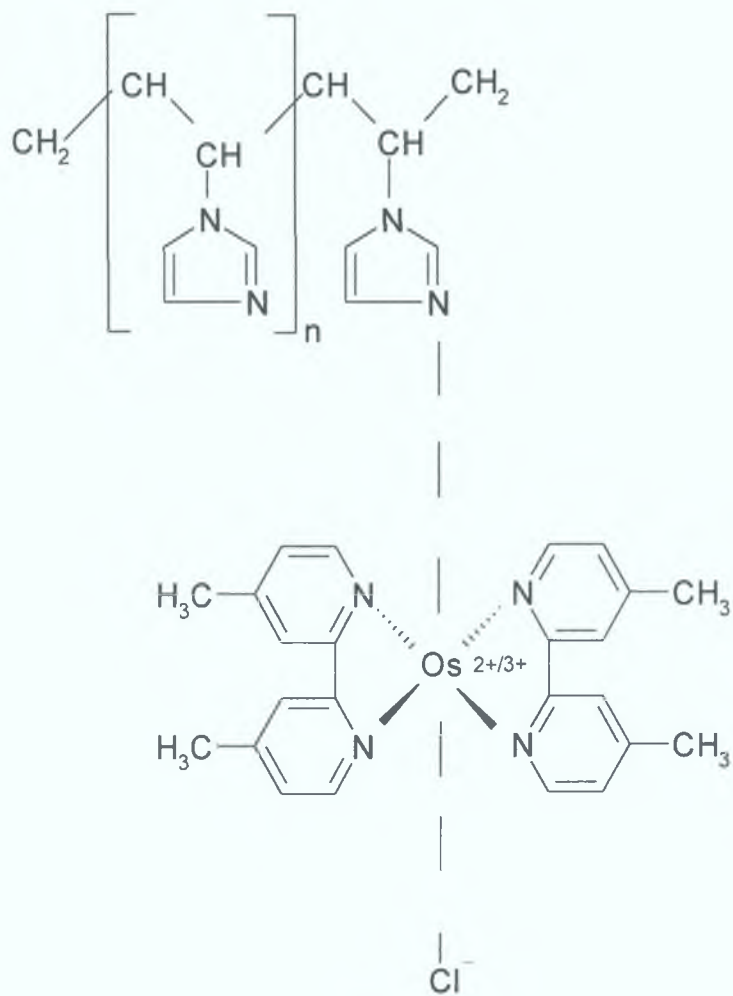
Figure 2.4. Chemical structure of Os(dime(bpy)₂Cl complexed to poly(1–vinylimidazole), n = 9
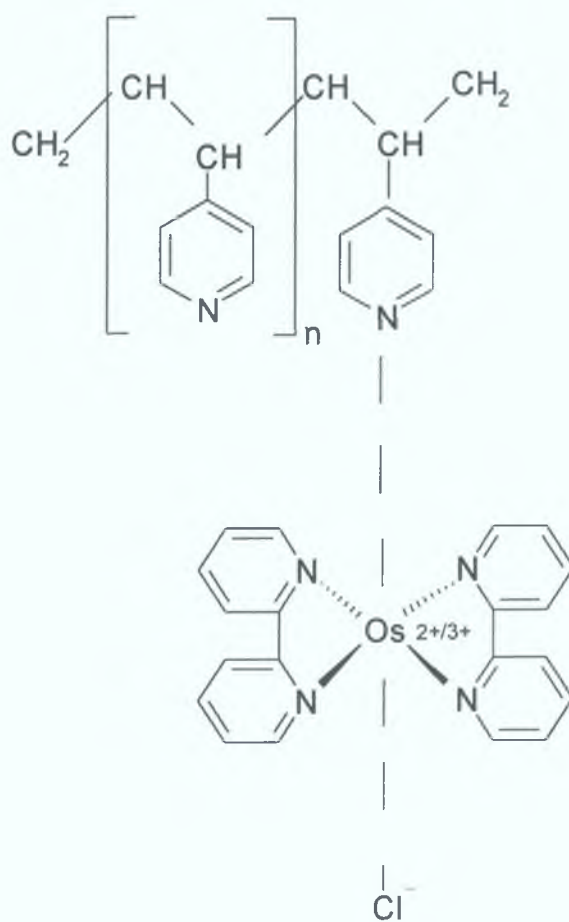
Figure 2.5. Chemical structure of Os(bpy)₂Cl complexed to poly(vinyl pyridine), n= 9
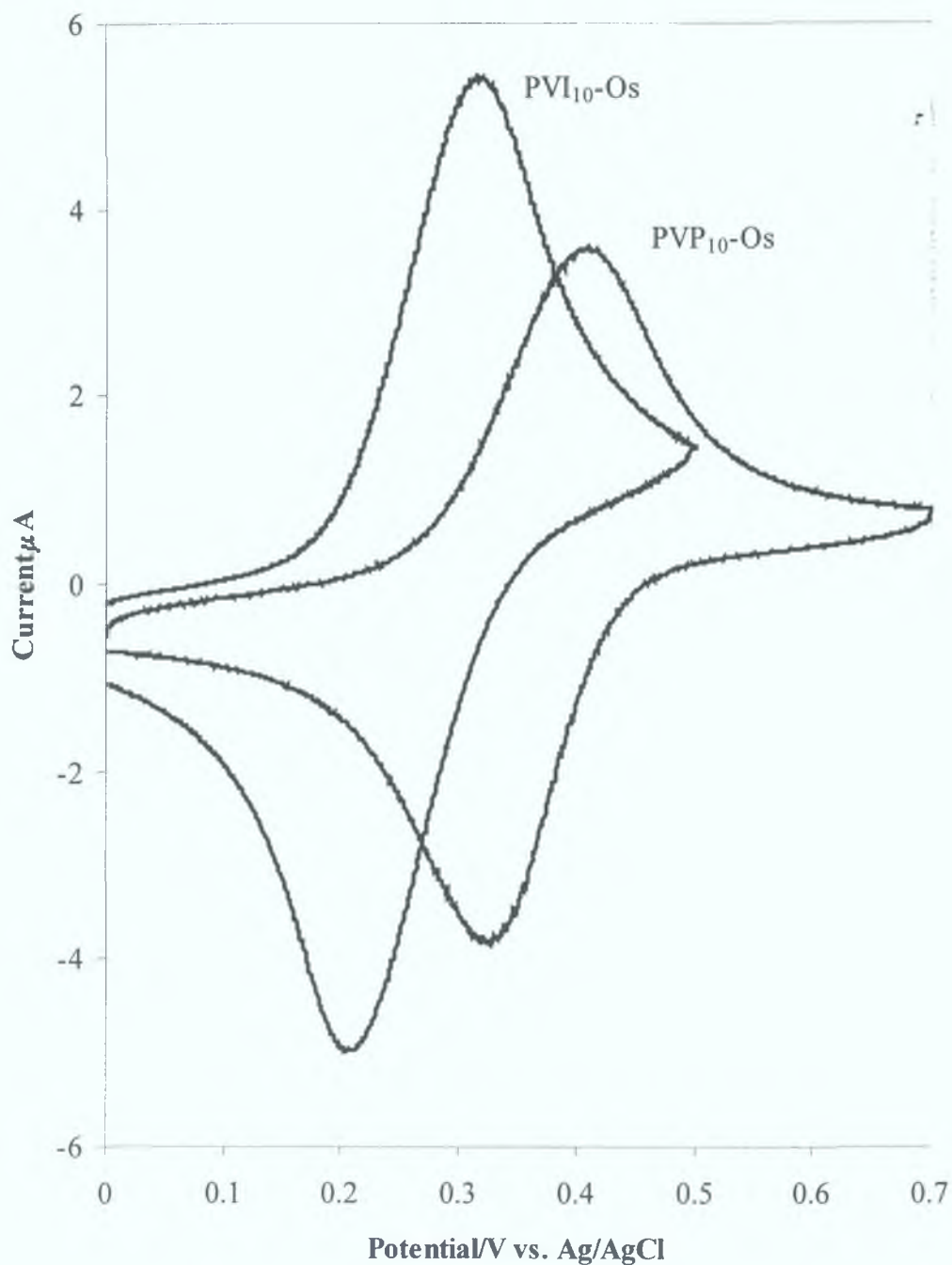
Figure 2.6. Cyclic voltammogram of PVI_{10}-Os and PVP_{10}-Os in aqueous 0.05 M phosphate buffer, pH 7.4, with 0.1 M KCl. The scan rate was 0.1 Vs^{-1} and a 1.5 mm radius glassy carbon electrode was used. The initial potential was 0.000 V.

### 2.4.4 General Redox Properties of Polymer Modified Electrodes

The electrochemical behaviour of osmium redox species is well defined irrespective of whether they are in solution, exist as surface confined monolayers or take the form of polymer films.[13,14,15,16,17] However, the response of these species in buffered medium has not yet been reported. An electrochemical characterisation of these PMEs was carried out using cyclic voltammetry.

Figure 2.7 shows a typical cyclic voltammogram of an PVI_{10}–Os PME in 0.05 M phosphate buffer containing 0.1 M KCl at a scan rate of 0.002 Vs^{-1}. Figure 2.8 shows the electrochemical response at the faster scan rate of 0.5 Vs^{-1}.

At slow scan rates shown in Figure 2.7 a number of characteristics expected for surface bound redox species can be seen, including symmetrical oxidation and reduction waves, a linear dependence of peak current (i_p) on scan rate (v). From Figure 2.7 the value of $E^{0'}$ is estimated at 0.211 V, ΔE_p is 0.012 V $\pm$ 0.002 V and a full width half maximum (FWHM) of 0.100 V. Theoretically, for a surface confined reversible Nernstian species a ΔE_p of 0.00 V and a FWHM of 0.096 V is expected. Figure 2.8, shows characteristics similar to a solution phase redox species where, ΔE_p is 0.072 V, while the FWHM is 0.135 V. Figure 2.9 shows a linear dependence of i_p on $v^{1/2}$. The electrochemical response is very similar to that expected for an electrochemically reversible solution phase redox species, i.e., independence of E_p on scan rate, dependency of i_p on $v^{1/2}$. The only deviation from an ideal solution phase response is the value of ΔE_p being 0.072 V as opposed to a theoretical value of 0.059.

Such combined surface and solution phase responses have been observed previously[18] for PMEs containing more than one monolayer of surface-active species. Koide et al[19] observed evidence of the dependence of peak current on $v^{1/2}$. Elmgren et al[20] studied the rate of charge propagation through a PME using [Os(bpy)$_2$PVP/polyamine] polymer matrix, from their studies it was observed that at slow scan rates the modified electrode system shows thin layer characteristics however as the scan rate increases quasi-reversible behaviour is seen. Quasi-reversible systems are characterised by the influence of both charge transfer and mass transport on peak current, with a smaller peak current being observed and a greater ΔE_p that what should be expected i.e. $\Delta E_p > 0.059$ V.[1]

Typical key processes that occur for surface confined film can be observed in Figure 2.10, whereby unlike a solution phase reaction the redox species are not free to diffuse to the electrode surface but are confined to it. All redox species present are oxidised and to balance this; extra positive charge that has been created by the oxidation process, counter ions from solution diffuse from bulk solution into the modified electrode. In the case of phosphate buffer, the reaction of $Os^{2+} + e^- \rightarrow Os^{3+}$ requires the diffusion of PO_4^{2-} counterions to maintain the electroneutrality of the film. This ion transport process can be a major factor influencing both the shape and size of the current potential response and the extent of the diffusional tailing observed, and is responsible for the deviation from ideal surface confined behaviour.

The objective which is being sought in the following experiments is to determine the influence buffered electrolytes exert on modified electrode systems, especially with respect to the diffusional processes and also to look at the influence of incorporating a biological species and its effects on the electrochemical response.
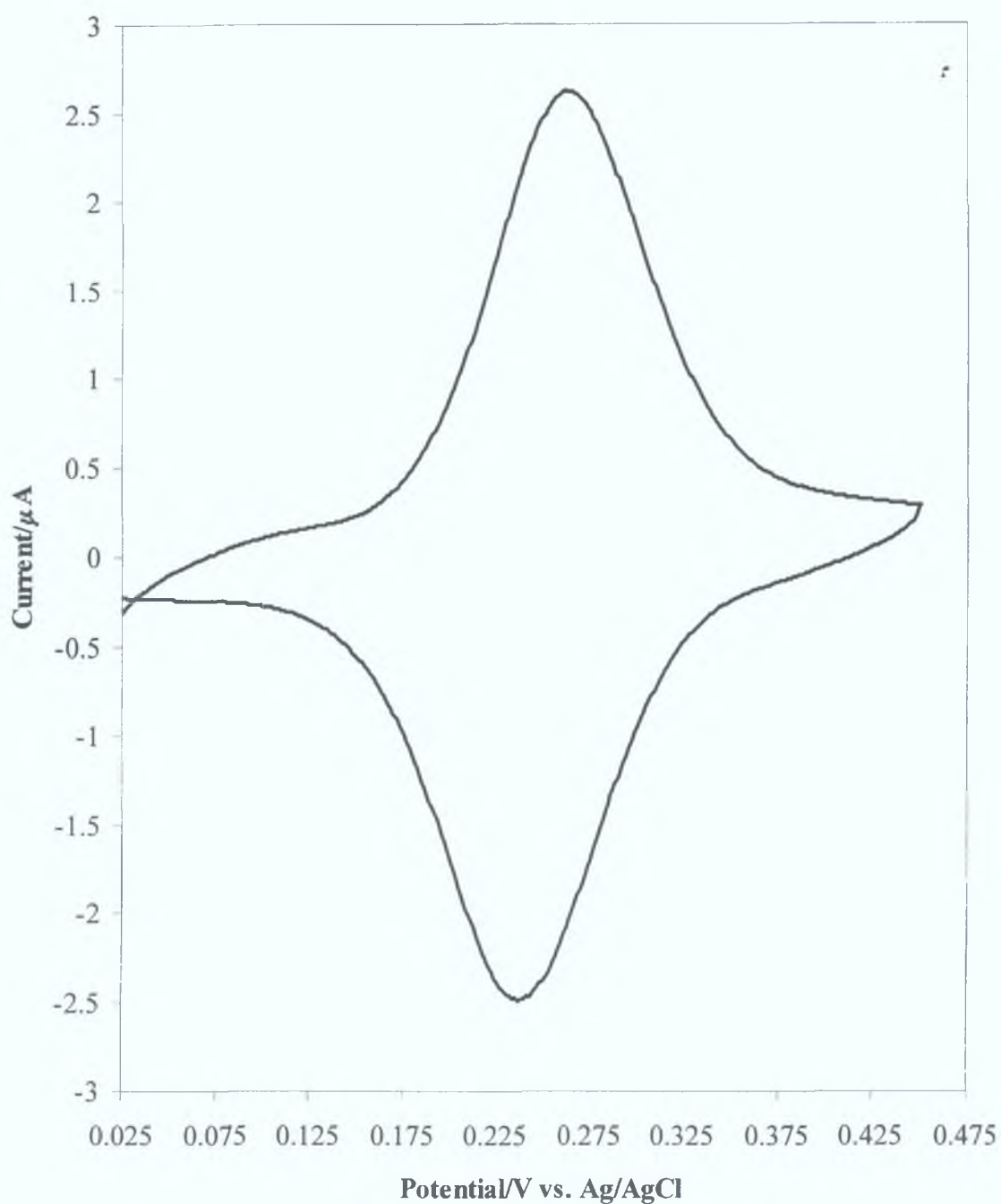
Figure 2.7. Cyclic voltammogram of PVI_{10}-Os, in aqueous 0.05 M phosphate buffer, pH 7.4, with 0.1 M KCl supporting electrolyte. The scan rate was 0.002 Vs^{-1} and a 1.5 mm radius glassy carbon electrode was used. The initial potential was 0.025 V, in a positive direction. Surface coverage is 2.05 x 10^{-8} mol cm^{-2}.
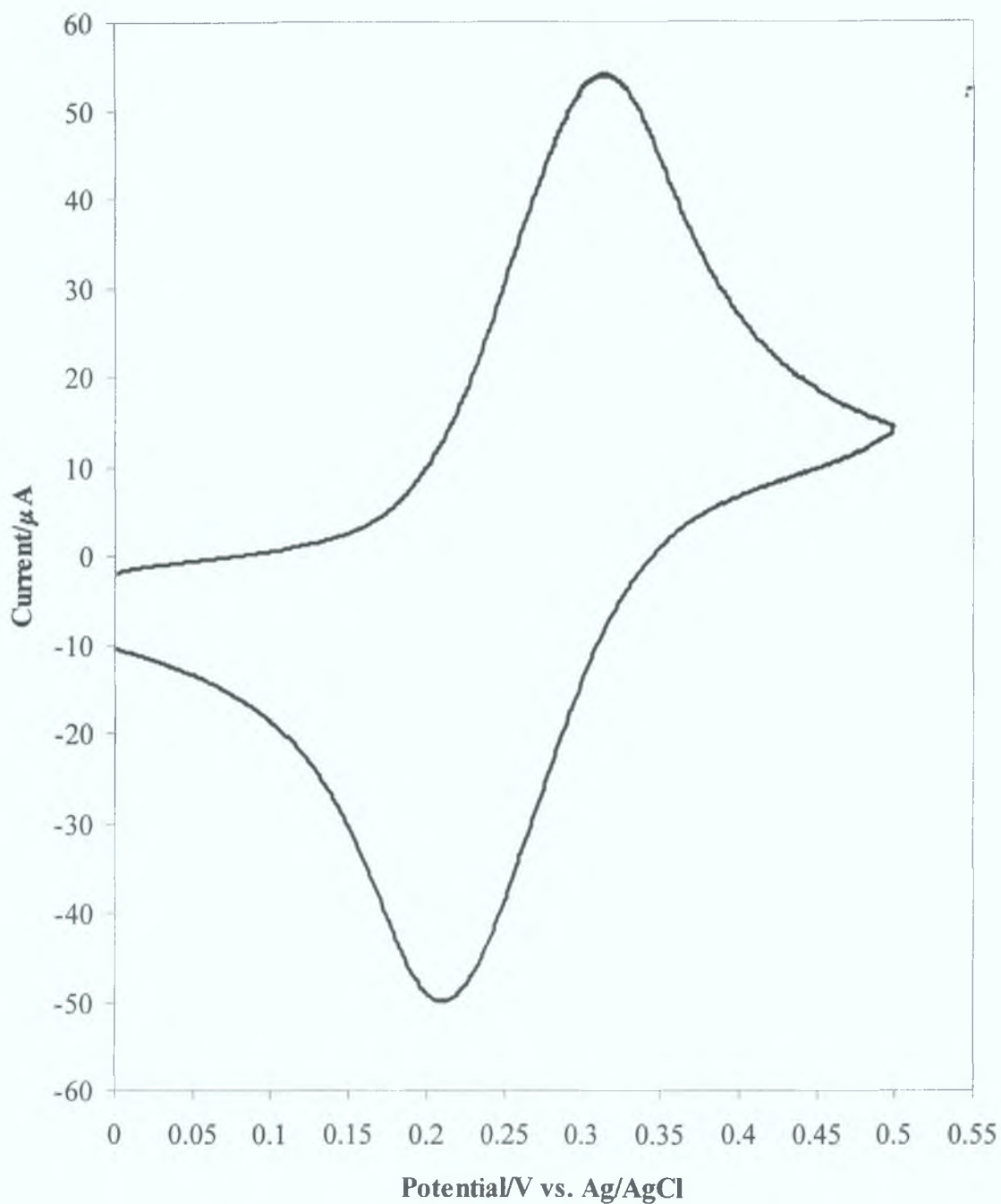
Figure 2.8. Cyclic voltammogram of PVI_{10}-Os, in aqueous 0.05 M phosphate buffer, pH 7.4, with 0.1 M KCl supporting electrolyte. The scan rate was 0.5 Vs^{-1} and a 1.5 mm radius glassy carbon electrode was used. The initial potential was 0.000 V. Surface coverage is 2.05 x 10^{-8} mol cm^{-2}
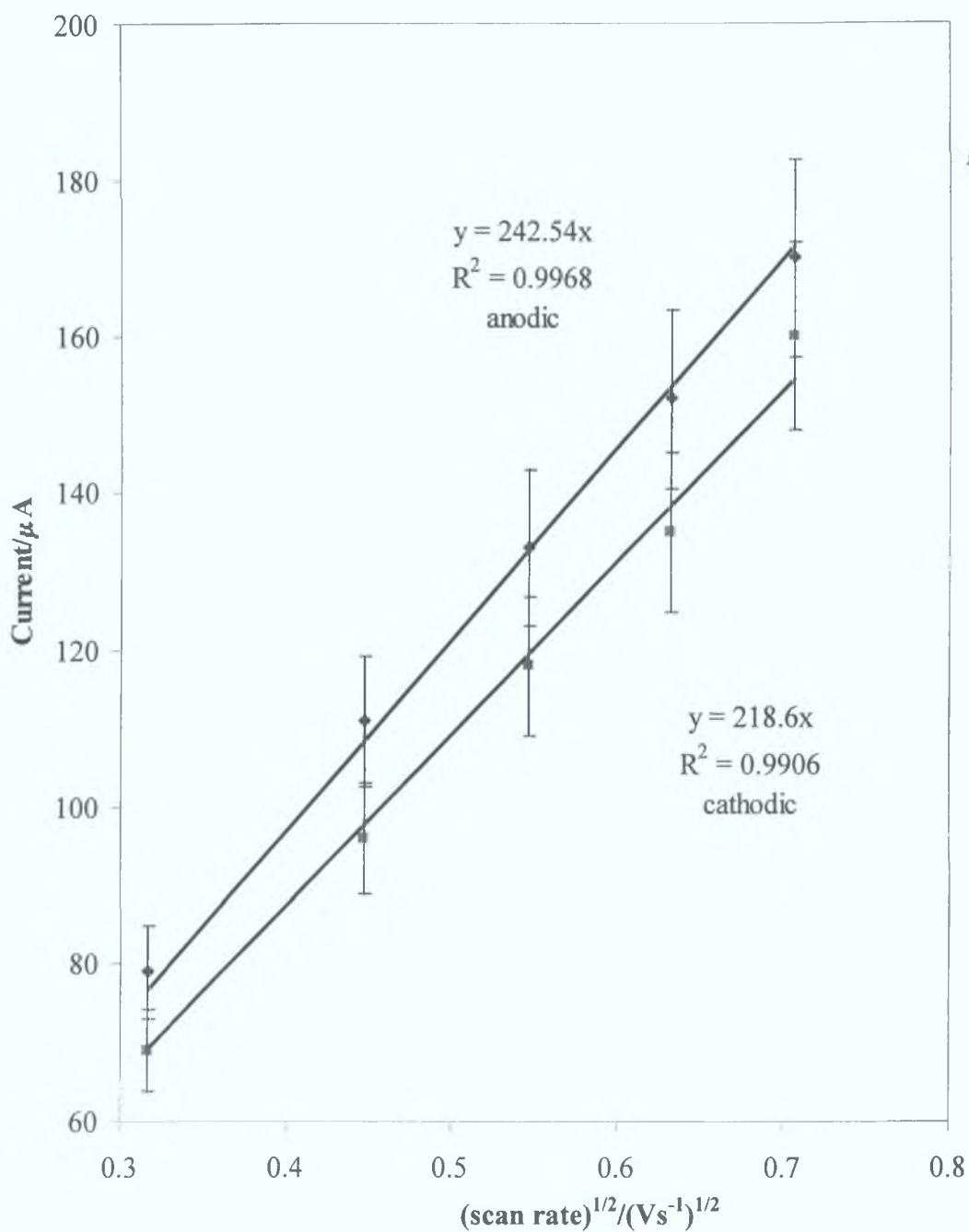
Figure 2.9. Plot of $v^{1/2}$ $(Vs^{-1})^{1/2}$ vs. current (μA), obtained when cyclic voltammograms experiments were employed at various scan rates, in aqueous 0.05 M phosphate buffer, pH 7.4, containing 0.1 M KCl supporting electrolyte.

Polymer modified electrode film

Mass transfer of counterions from bulk solution required to maintain electroneutrality
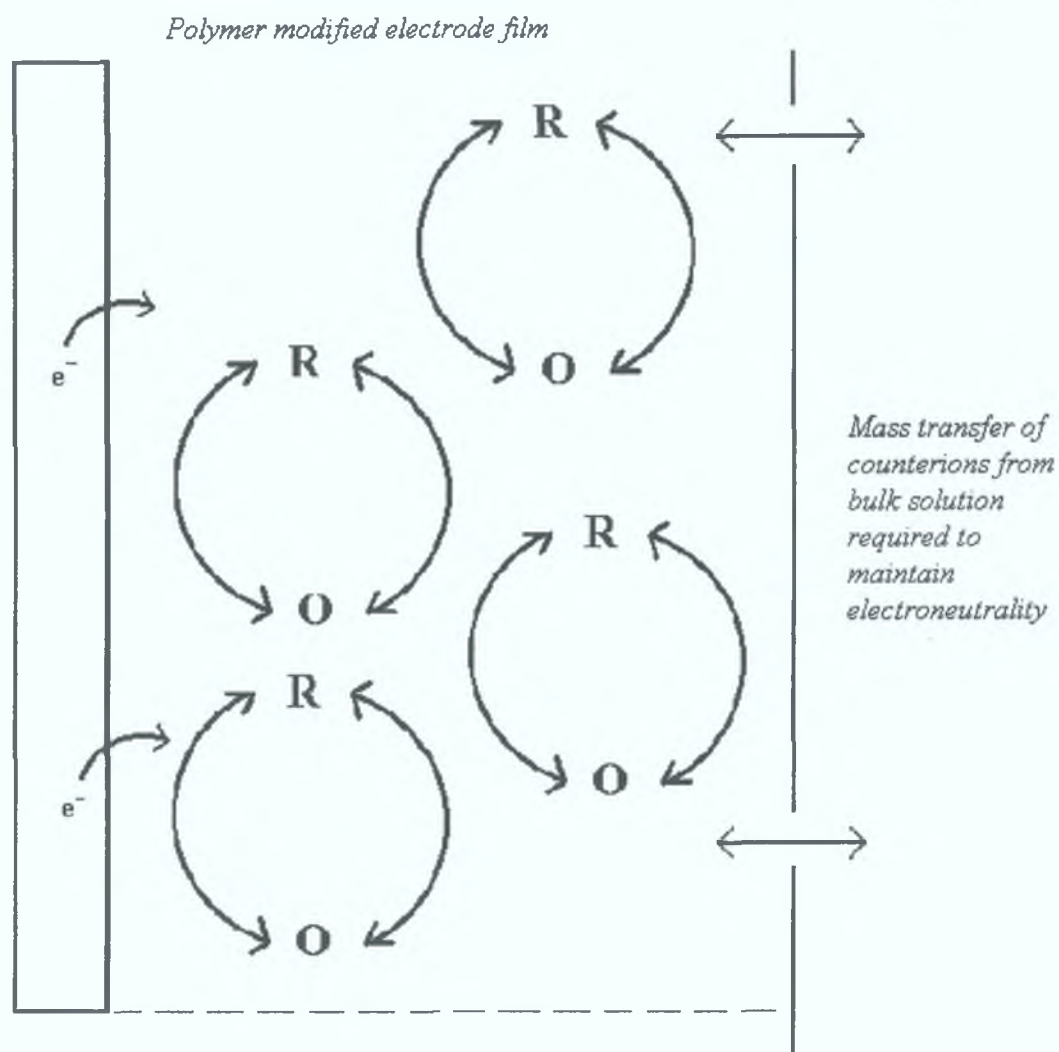
Figure 2.10. Key electron transfer reactions occurring for a redox species confined within a PME.

2.4.5   Determination of surface coverage

As the metallopolymer film is oxidised, charge compensating counterions must ingress into the film to maintain electroneutrality. In the case of phosphate buffer, while it is difficult to be completely certain as to the identity of the charge compensating counterions, it is likely that when the redox species is oxidised i.e. $O + ne^- \rightarrow R$, PO_4^{2-} ions diffuse into the film. As the objective of this work is to establish the effects that various buffers, and, hence their anions have on the overall electrochemical response, the first parameter investigated was the extent of electroactivity within the polymer film. To achieve this a series of PMEs were prepared as described in Section 2.3.5, and allowed to equilibrate for 30 min, in an electrolyte containing 0.1 M KCl, dissolved in the most commonly employed buffers, whose pH range is within that of physiological pH. These buffers were: phosphate, Tris–HCl and HEPES. In all cases, the buffers were aqueous, pH of 7.4, 0.05 M in concentration. After the electrode has equilibrated a slow scan rate of 0.002 Vs^{-1} was applied.

As was previously stated, these PMEs do not show the ideal Nernstian behaviour i.e., a $\Delta E_p = 0$ mV and a FWHM of 90.6 mV was not observed. Hence, for an accurate determination of surface coverage Equation 2.9 is used:

$$\Gamma = \frac{Q}{nFA}$$

(Equation 2.9)

where, Γ is surface coverage in mol cm^{-2}, Q is the area under the curve, coulombs, n is the number of electrons transferred, F is Faraday's constant and A is the electrode area, cm^2.

Figure 2.11, shows three voltammograms in various buffers at a scan rate of 0.002 Vs^{-1}. The variation in electrochemical response of all three identical PMEs suggests the influence of electrolyte choice on the stability of the electrode and the current obtained. The determination of surface coverage was achieved by integrating the charge (Q, Coulombs), under the curve.
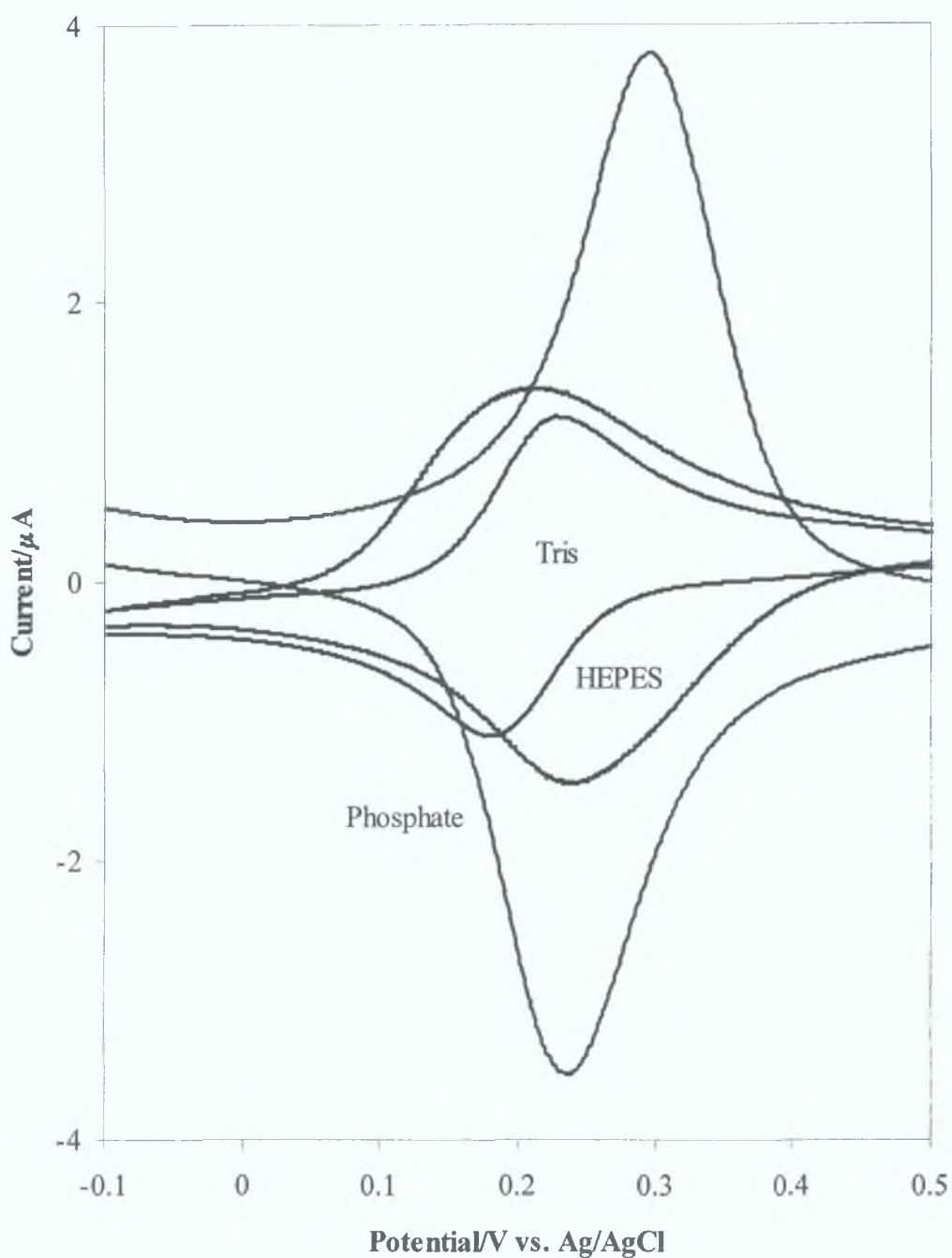
Figure 2.11. Cyclic voltammogram of PVI_{10}-Os, in aqueous 0.05 M phosphate, HEPES and Tris buffer, pH 7.4. The scan rate was 0.002 Vs^{-1} and a 1.5 mm radius glassy carbon electrode was used. The initial potential was –0.1 V, in a positive direction. Surface coverage is 0.088, 0.19 and 0.091 x 10^8 mol cm^{-2} respectively.

To explain why there is a difference in the observed E^{0} and i_p, it is necessary to examine the properties of the charge compensating ions which diffuse through the PME to balance the charge created by the oxidation and reduction process. The chemical structures of both HEPES and Tris are shown below in Schemes 2.2 and 2.3 as can be seen the cations and anions of these buffers vary in sizes: SO_3^- has an atomic radii of approx. 4.83 Å whereas there the PO_4^{3-} has an atomic radii of approx. 3.52 Å. It is possibly as a result, of this increased bulk and reduced charge of the SO_3^- ion that both the HEPES and Tris, in a varying electrochemical response when compared with the when compare with the phosphate buffer.
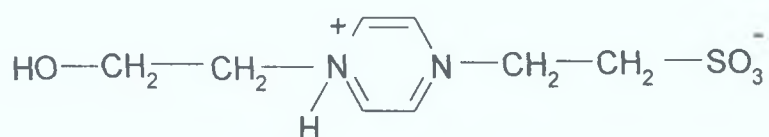
Scheme 2.2. HEPES structure
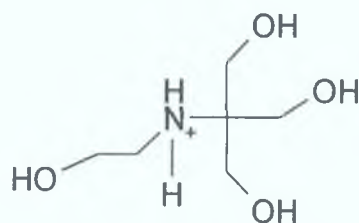
Scheme 2.3. Tris structure

In Table 2.1 below the values of surface coverage are shown. If one considers that the total number of moles deposited on the electrode surface is 2.47×10^{-7} mol cm^{-2} of PVI_{10}–Os while for PVP_{10}–Os it is 2.91×10^{-7} mol cm^{-2} are deposited on the electrode surface it can be seen that only a very small percentage of the total PME is electroactive.

Table 2.1. Results for surface coverage of the two different polymer complexes in various buffers of concentration of 0.05 M. Scan rate of 0.002 Vs^{-1} was used.

	HEPES	Phosphate	Tris
$10^8 \; \Gamma \; PVI_{10}-Os$	$0.\,88 \pm 0.03$	2.05 ± 0.02	0.091 ± 0.03
$10^8 \; \Gamma \; PVP_{10}-Os$	2.5 ± 0.5	1.5 ± 0.3	0.97 ± 0.24

The large error bars seen in Table 2.1 led to an investigation into the stability of these PMEs. For these experiments, the electrodes were equilibrated for 30 min. to avoid any effects of initial film swelling. A scan rate of 0.1 Vs^{-1} was employed and continuous cycling of 50 scans proved to be sufficient to achieve a time invariant response. Results are presented in Tables 2.2 and 2.3 compare the loss of electroactivity in the form of reduction in peak current between the second full cycle and the last full cycle for both polymer complexes. From these, it can be seen that irrespective of the buffer used there is a greater reduction in i_p for the electrode containing the $PVP_{10}-Os$ than $PVI_{10}-Os$. In the case of $PVI_{10}-Os$ phosphate buffer results in the more constant i_p as the maximum loss in i_p is 0.2 %.

Table 2.2, PVP_{10}-Os percentage loss from the surface of the electrode after scanning for 50 repetitive scans at a scan rate of 0.1Vs^{-1} all buffers were aqueous and 0.05 M and were purged with N_2 to remove any dissolved oxygen.

Electrolyte	Electrode 1	Electrode 2
HEPES	1%	3%
Tris	3%	2%
Phosphate	16%	14%

Table 2.3. PVI_{10}-Os percentage loss from the surface of the electrode after scanning for 50 repetitive scans at a scan rate of 0.1Vs^{-1} all buffers were 0.05 M in concentration and were purged with N_2 to remove any dissolved oxygen.

Electrolyte	Electrode 1	Electrode 2
HEPES	0.5%	0.3%
Tris	6.0%	6.0%
Phosphate	0.1%	0.2%

2.4.6 'Wiring' of progesterone to the redox polymer

The immobilisation of biological species, especially enzymes, within polymers either covalently or electrostatically has been an extensive area of interest to analytical chemists.[21-29] In addition to the advantage of heterogeneous catalysis, the immobilisation procedure can lead to an increased stabilisation in the biological species by:

i. Protection against attack by proteases, e.g., in the case of the glucose biosensors.

ii. Physical confinement of the biological species can retard thermal denaturation.

iii. Incorporation of a redox mediator has the advantage of narrowing the potential window and hence avoiding complications which may arise with the use of high overpotential, i.e., interference due to other electroactive species in solution, choice of electrolyte, etc.

Although species can be immobilised by various methods, in this study, a method proposed by O Hara et al[21] was used to immobilise a biological molecule into an electrically active polymer.

This electrical wiring is achieved by using PEG and di-epoxide resin, both of which are highly water-soluble. This hydrophilicity in addition with the use of a long cross-linking reagent, approximately 40 Å in length, results in a highly swollen gel like redox polymer for the PVI_{10}–Os. The combination of epoxy–amine network forming reaction results in a tough hydrophilic redox conducting epoxy cement that is strongly absorbed onto carbon electrodes.

In contrast to the method proposed by Heller,[21] who quaternised the PVP polymer, to ensure its solubility in water, in warm (60 °C) dimethyl formamide (DMF) under a constant flow of N_2, the wiring of both PVP and PVI took place 22 ± 2 °C.

In both cases, the reaction between the epoxide and the amine proceeds slowly in a neutral aqueous solution and takes place only after the surface has dried, hence, the electrodes are left to dry over 48 hrs in a dessicator. Scheme 2.4–2.6, illustrate the cross-linking reaction between a water-soluble di-epoxide, in this case

Poly(ethyleneglycol) diglycidyl ether, and the pendant amine function on both the progesterone and the vinyl–imidazole.
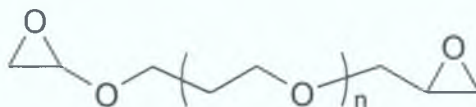
Scheme 2.4. Chemical structure of poly(ethyleneglycol) diglycidyl ether, n = 9

Scheme 2.5. Reaction of an epoxide with an amine.
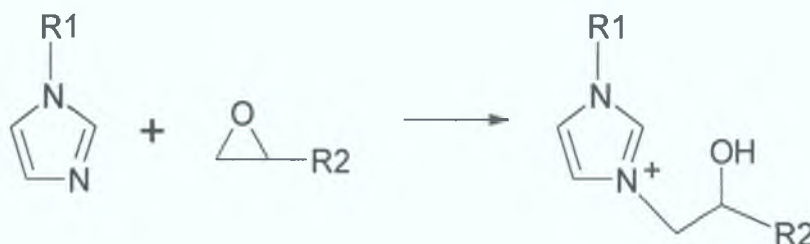
Scheme 2.6. Reaction of epoxide with imidazole.

The total concentration of redox polymer is 0.5×10^{-7} mol cm^{-2}, for the PVI$_{10}$–Os this concentration was 2.47×10^{-7} mol cm^{-2}. This is evident by examining Figure 2.12, where at a scan rate of 0.002 Vs^{-1} a peak current of 1.95 and 0.58 µA was obtained for PVI$_{10}$–Os–PEG and PVI$_{10}$–Os–progesterone respectively. Comparing the PVI$_{10}$–Os, shown in Figure 2.11, where a peak current of 3.84 µA is obtained with Figure 2.12 it can be seen that there is a difference in the availability of metal redox centre within these PMEs. A calculation of the surface coverage of PVI$_{10}$–Os–progesterone, PVI$_{10}$–Os and PVI$_{10}$–Os–wiring chemicals may be seen in Table 2.4 where a scan rate of 0.002 Vs^{-1} is employed.

The electrochemical response of the PME containing all wiring components apart from progesterone shows a response similar to that observed for PVI$_{10}$–Os, as seen in Figure 2.13, for slow scan rates in 0.05 M phosphate buffer, pH 7.4. For both of these experiments, an almost symmetrical wave is seen indicative of reversible surface bound couple with a ΔEp of 0.030 V, a FWHM of 0.102 V, and an $E^{0'}$ of 0.151 V. In

the case of the pure polymer where the onset of semi-infinite linear diffusion process was observed at scan rates greater than 30 mVs^{-1}, the diffusional processes are observed at scan rates greater than 5 mVs^{-1} with a linear dependence on $v^{1/2}$, diffusional tailing seen and peak splitting is substantially increased being observed. This can be seen in Figure 2.12 which shows a comparison of the PVI$_{10}$–Os–PEG with PVI$_{10}$–Os–progesterone 0.1 Vs^{-1} As can be seen from Figure 2.12 the influence of diffusion can be observed at slower scan rates; this will be dealt with in the Chapter 3 in greater detail. A similar behaviour was observed by Gregg and co-workers[23-30] with [Os(bpy)$_2$PVI$_{10}$] modified with glucose molecule.

Table 2.4. Surface coverage of PVI$_{10}$–Os–progesterone compared with PVI$_{10}$–Os and PVI$_{10}$–Os–wiring components. All results obtained from second cycle in aqueous 0.05M phosphate buffer at a scan rate of 0.002 Vs^{-1}.

	With Progesterone	No Progesterone	PVI only
$10^8 \, \Gamma$ Os–PVI$_{10}$	0.60 ±0.20	1.54 ±0.30	2.05 ±0.06
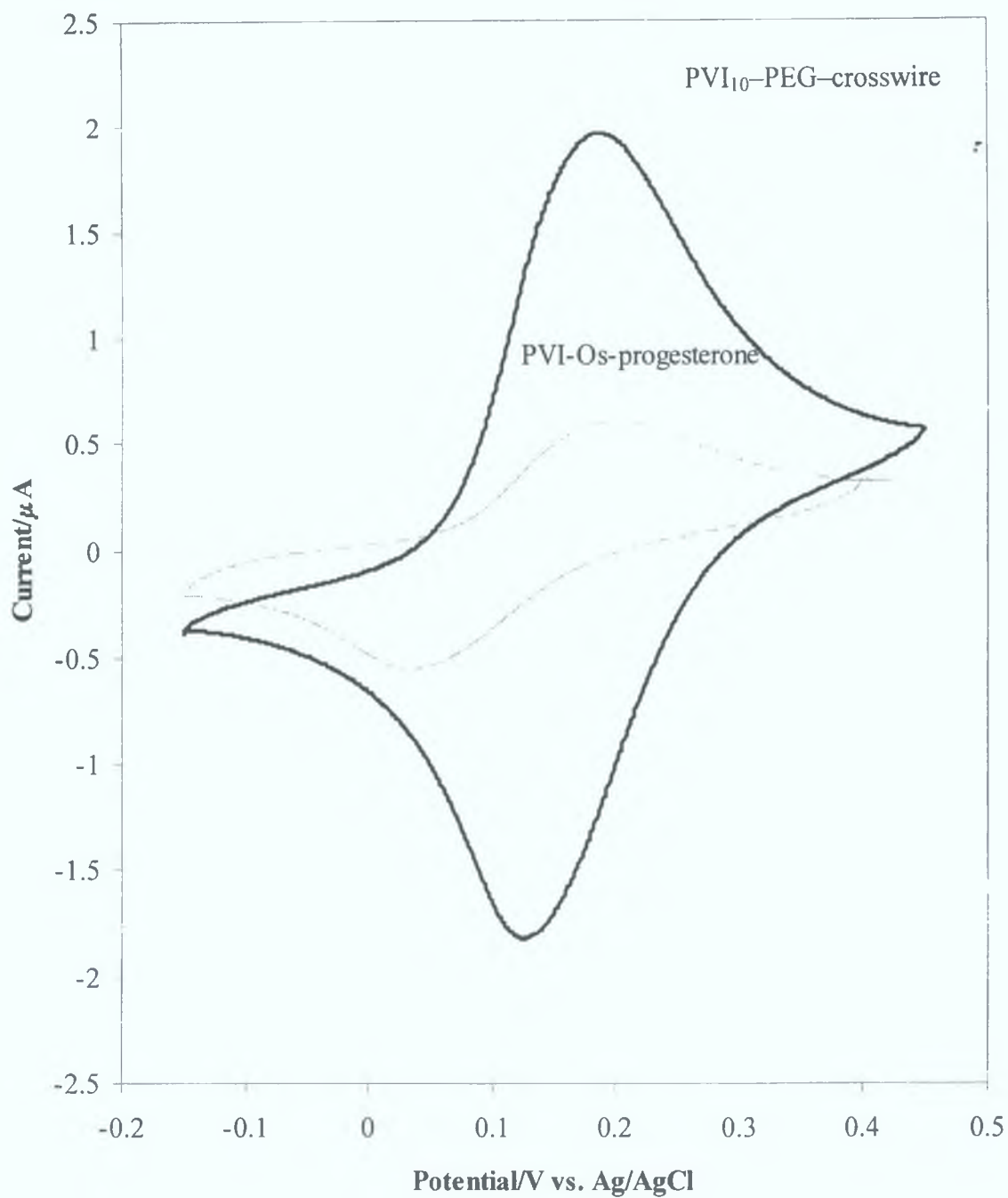
Figure 2.12. Comparison of PVI_{10}–Os–PEG (—) with PVI_{10}–Os–progesterone(—), in 0.05M phosphate buffer pH 7.4, with 0.1 M KCl supporting electrolyte. Scan rate was 0.002 Vs^{-1}, starting potential was –0.15 V. Surface coverage is 1.54 and 0.6 x 10^{-8} mol cm^{-2}
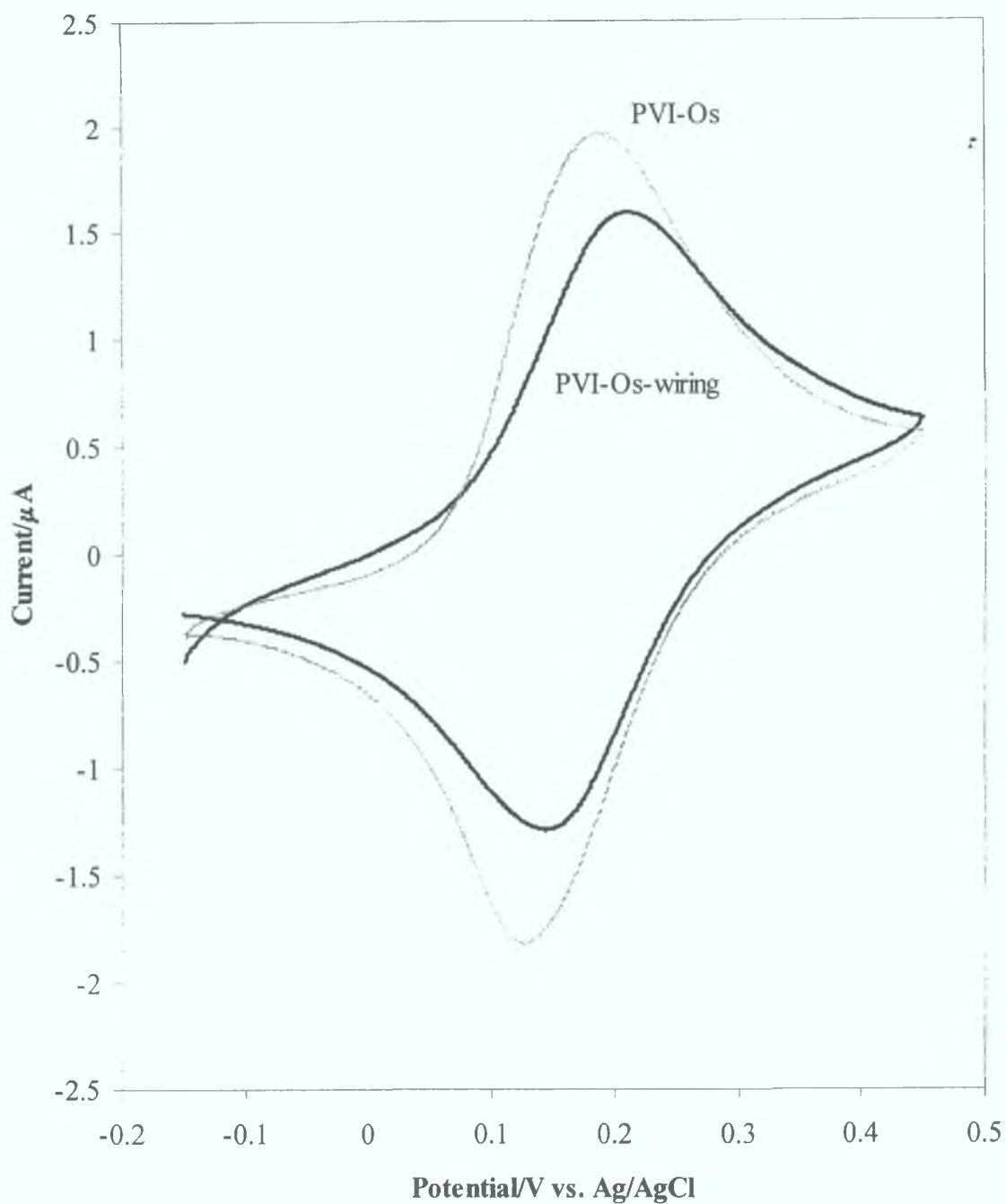
Figure 2.13 Comparison of a glassy carbon electrode containing PVI_{10}–Os and PVI_{10}-Os–wiring in aqueous 0.05 M phosphate buffer, pH 7.4, with 0.1 M KCl supporting electrolyte. Scan rate was 0.1 Vs^{-1}, starting potential was –0.15 V. Surface coverage is 0.6 x 10^{-8} and 3.14 mol cm^{-2} for PVI_{10}–Os and PVI_{10}-Os–wiring respectively.
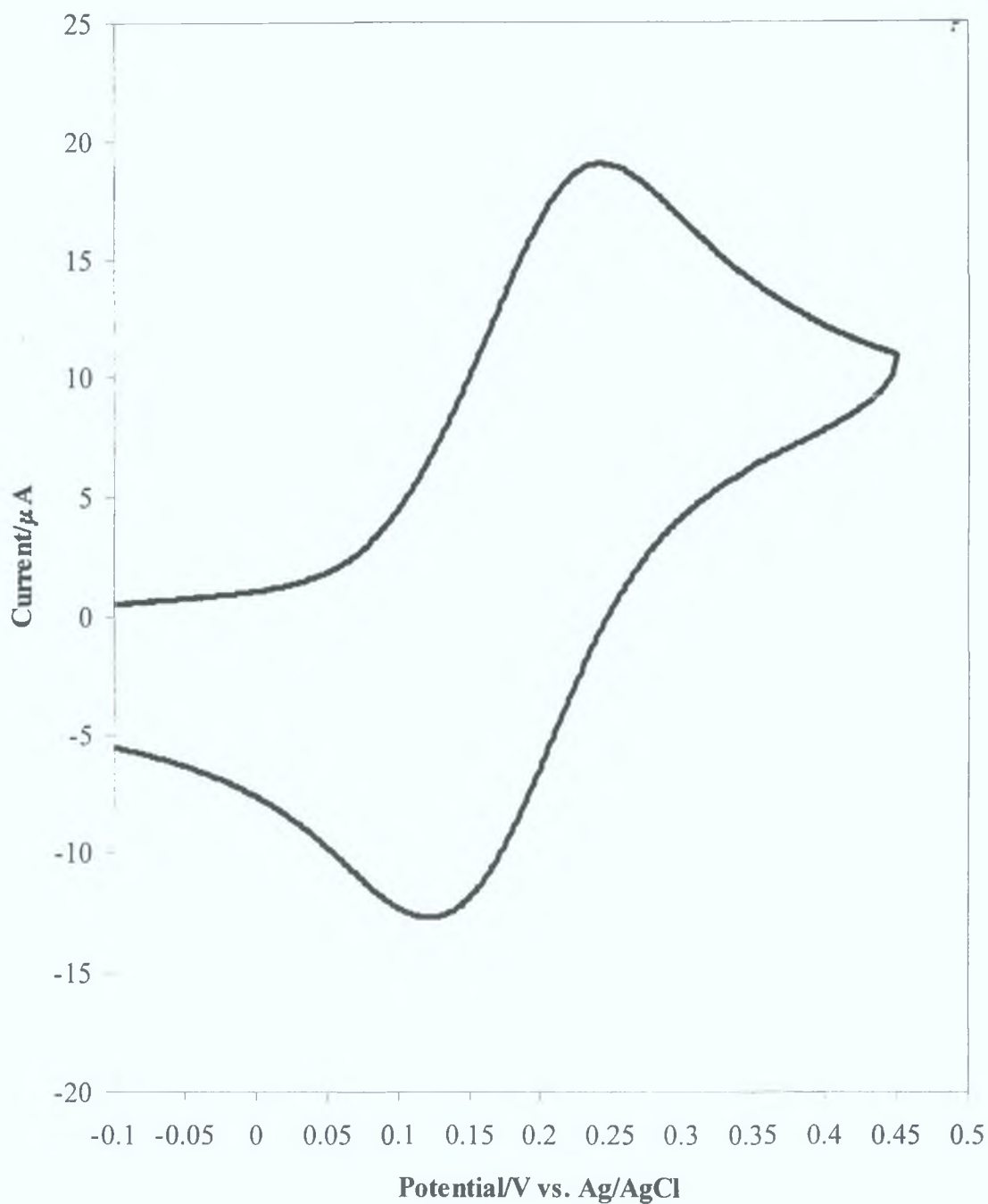
Figure 2.14. Stability of a completely modified electrode aqueous 0.05 M phosphate buffer, pH 7.4, with 0.1 M KCl supporting electrolyte. A scan rate of 0.1 Vs^{-1}, starting potential was 0.1 V in a positive direction. Out scan is the initial and inner scan is scan number 20.

2.4.7   Enzyme immunoassay:

Usually, it is possible to detect the presence of a biocomponent within a redox polymer through electrochemistry, e.g., glucose is reduced to gluconolactone in the presence of the enzyme glucose oxidase resulting in the transfer of electrons that are detected using an electron mediator, such as osmium.   However, here the progesterone is neither oxidised nor reduced requiring that another detection method is used, to ensure the progesterone is indeed present and active within the PME. In this incidence, the method of detection used is an indirect enzyme immunoassay (EIA). As with all immunoassays the problem of non-specific adsorption is a problem that needs to be addressed. For this reason PBS/BSA is used as a blocking agent to prevent non-specific adsorption of Mab onto the surface of the electrode. The Mab used is known[7] to be specific to the type of progesterone used in this experiment, whereby it attaches on to the progesterone within the PME as seen in Figure 2.14*a*.

Attachment of the RAM/HRP is illustrated in Figure 2.14b, followed by immersion in the solution of TMB. The use of TMB provides a colorimetric method of detection due to TMB oxidising the HRP giving rise to a blue colour. It should be noted that although it would be possible to detect the presence of HRP using the redox mediator, EIA, due to ease of detection and the need for only a qualitative result.
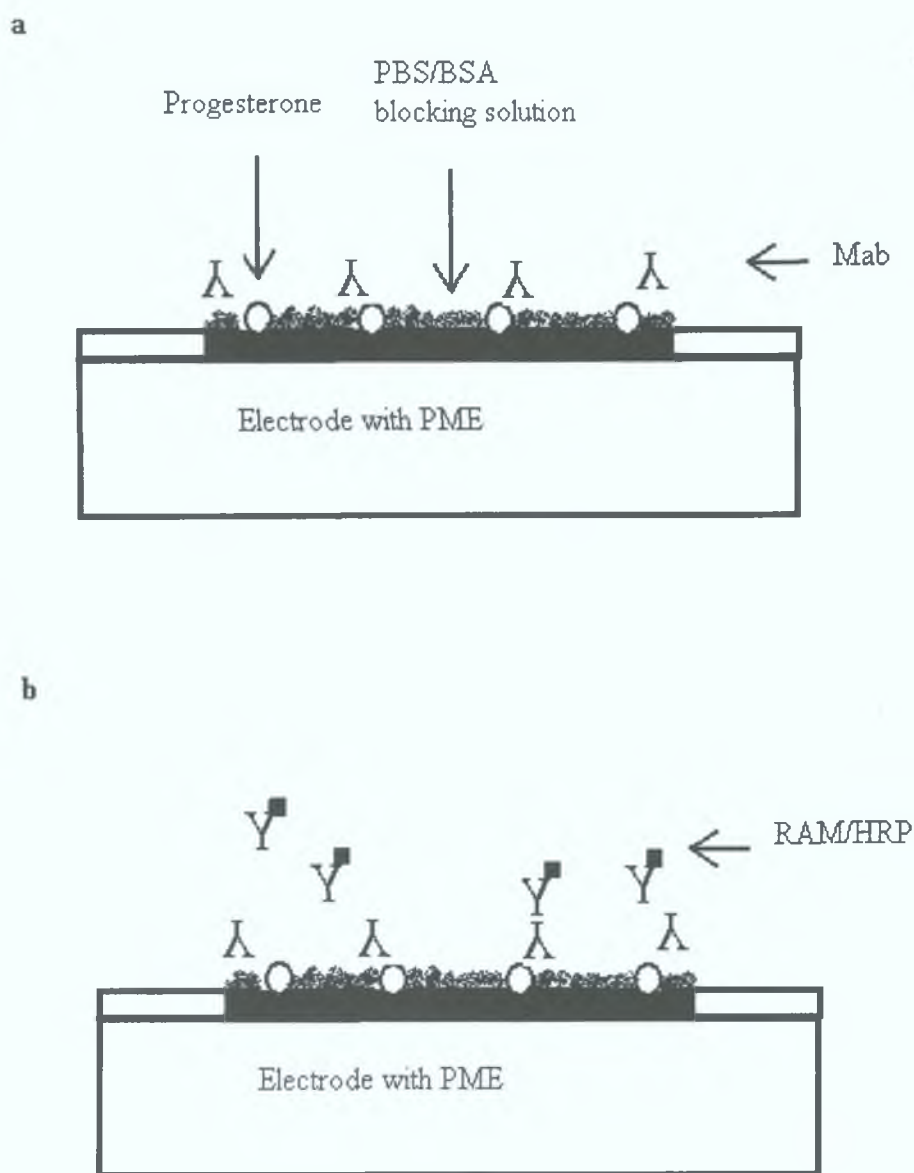
Figure 2.14. Enzyme immunoassay used to detect the presence of progesterone within the PME. (a) attachment of the Mab specific to the progesterone modified within the PME, and (b) attachment of the RAM/HRP to the Mab.

While the EIA used for these experiments is only intended to be a qualitative assay, to ascertain that the progesterone is indeed present within the PME, results shown in Figure 2.15 indicate that increasing the progesterone concentration within the PME has a linear response. This response however is not linear over the entire range shown above, possibly due to saturation at the 5mg/ml concentration. As can be seen there is an increase in the error as the concentration of progesterone increases within the PME. This behaviour is expected since there is no way of controlling exactly where the progesterone is within the PME, and since not all the progesterone in the modified electrode is available at the surface of the electrode for binding with the Mab, a variation in results is expected. The presence of progesterone is detected due to reaction of TMB with HRP labelled antibody to produce a blue colour which is subsequently stopped to produce a yellow colour. This yellow colour absorbs visible light in the region of 450 nm.

Although not shown here additional control experiments carried out at a later stage show that after carrying out an entire set of electrochemical experiments where there was a variation in the progesterone concentration, these again show a linear response, emphasising the stability of the biological component within the PME.

Non-specific adsorption, that can arise due to random adsorption of the Mab to the PME and not specifically the progesterone molecule was investigated. The results presented in Table 2.5, show that when no washing procedure is used NSA is a definite problem. By washing with PBS/BSA, NSA is was kept to a minimum and may be attributed to the Mab adsorbing onto the Teflon shroud, which surrounds these glassy carbon electrodes.

Table 2.5. Absorbance reading for enzyme immunoassay, comparison between washing and no washing procedures.

	PBS/BSA	No PBS/BSA
PVI_{10}-Os	0.15	0.6
Modified with all except Progesterone	0.20	0.85
Bare Carbon electrode	0.05	0.25
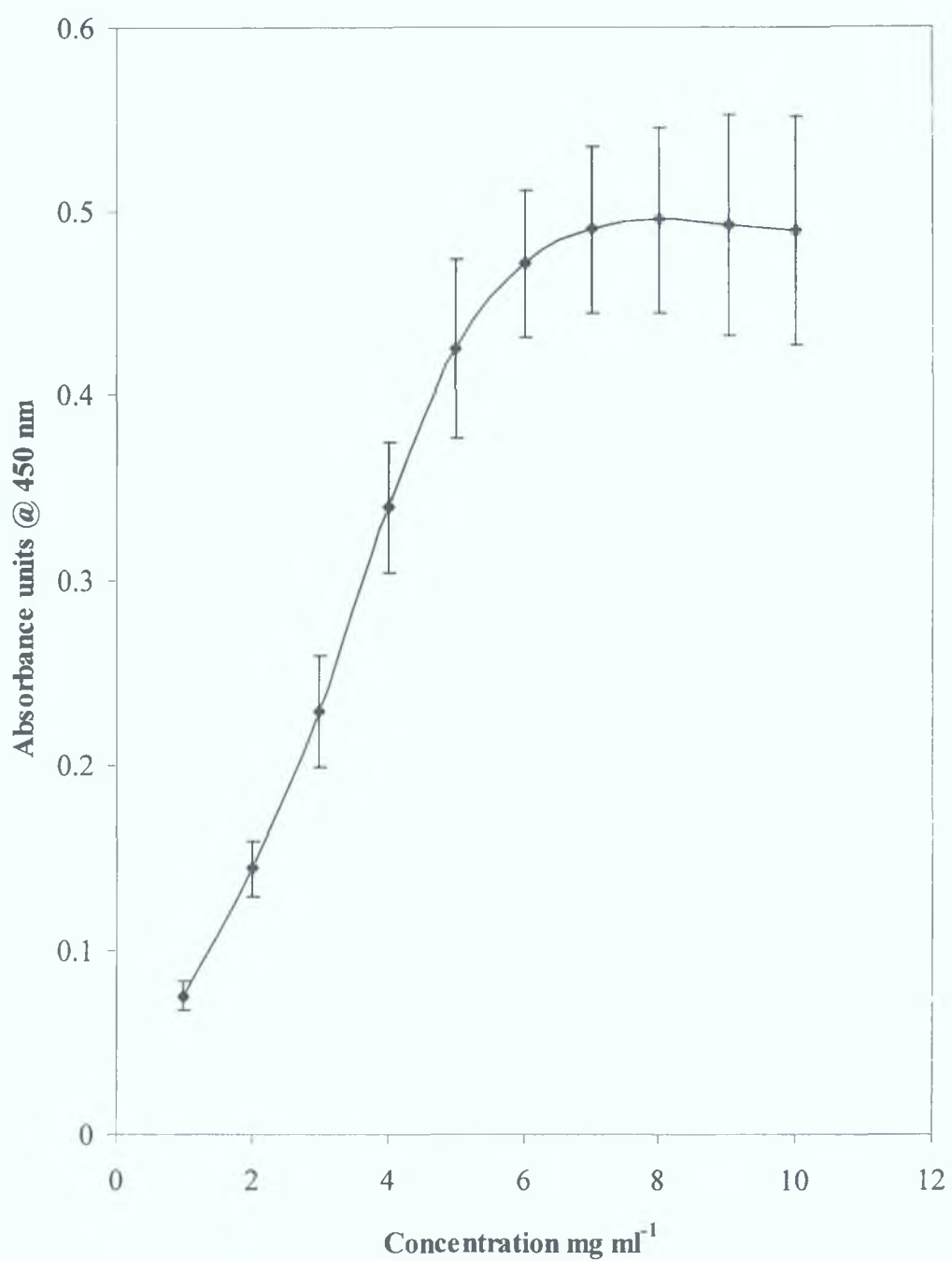
**Figure 2.15.** Plot of absorbance at 450 nm vs. progesterone concentration, mg ml^{-1}, contained within the PME, in 1ml TMB and 0.1 cm^3 H$_2$SO$_4$.

2.5   Conclusions:

Metallopolymers based on poly-N-vinylimidazole and poly-4-vinylpyridine were successfully synthesised and analysed using UV-vis spectroscopy, HPLC electrochemistry and elemental analysis. The electrochemical properties of both metallopolymers were studied. At long experimental time scales these PMEs exhibit properties characteristic of a surface confined monolayer. However, as the experimental time scale was decreased, it was observed that their behaviour was similar to their solution phase counterparts where the response is dominated by semi-infinite linear diffusion. Studies, regarding the stability of these molecules, show that PVI_{10}-Os exhibits greater stability, ease of preparation, and a more reproducible electrochemical response compared to PVP_{10}-Os. In addition, the closer proximity of the $E^{0'}$ to 0 V results in a more ideal electrochemical response, since the further away from 0 V the greater the chances of interferences due to electro-oxidation of species present in the supporting electrolyte medium. Significantly, the influence of buffers on the electrochemical behaviour using three of the most commonly employed buffers, phosphate, Tris and HEPES, illustrated that phosphate buffer resulted in the best performance, while the PVI_{10}–Os gave the more stable response.

Modification of PVI_{10}–Os with progesterone was achieved using a cross linking reaction which occurred at room temperature. The presence of progesterone was confirmed using an EIA; results indicate that this modification procedure was successful. Comparative studies between an unmodified PME and progesterone resulted in the onset of diffusional behaviour at lower scan rates, indicating that a bio-component plays a major role in many electrochemical features of a PME. The next chapter will focus on the influence of a bio-component.

2.6 References

1.   Bard A. J.; Faulkner, L. R. *Electrochemical Methods, Fundamentals and Applications,* Wiley, New York, 1999, p. 580

2.   Ikawa, M.; Phillips, N.; Haney, J. F.; Sasner, J. *J. Toxicol.,* **1999**, *37*, 923

3.   Roto, R.; Villemure, G. *J. Electroanal. Chem.,* **2002**, *527,* 123

4.   Forster, R. J.;Vos, J. G. *Marcomolecules*, **1990**, *23*, 4372

5.   Doherty, A. P.; Buckley, T.; Kelly, D. M.; Vos, J. G. *Electroanal.,* **1994**, *6*, 553

6.   Buckingham, D. A.; Dwyer, F. P.; Goodwin, H. A.; Sargeson, A. M. *Aust. J. Chem.,* **1964**, *17*, 325

7.   O'Rorke, A.; Kane, M. M.; Gosling, J. P.; Tallon, D. F.; Fottrell, P. F. *Clin. Chem.,* **1994**, *40*, 454

8.   *Modern Chemical Techniques: For Teachers and Students*, Royal Society of Chemistry, London, U.K. 1989

9.   Geraty, S. M.; Vos, J. G. *J. Chem. Soc. Dalton Trans.,* **1987**, 3073

10.   Wilson, R. W.; Cibitt, R.; Glodñe, A.; Hillman, A. R.; Saville, P. M.; Vos, J. G.; *Electrochim. Acta*, **1999**, *44*, 3536

11.   Berokwitz, J. B.; Yamin M.; Fuoss, R. M. *J. Polym. Sci.,* **1958**, *28*, 69

12.   Bamford, C. H.; Schofield, E. *Polymer*, **1981**, *22*, 1227

13.   *Analytical electrochemistry,* J. Wang, VCH, New York, USA, 1994

14.   Brett, C. M. A.; Brett, A. O. *Electrochemistry*, Principles, Methods and Applications, Oxford University Press Inc. New York, USA, 1983

15.   Fisher, A. C. *Electrode Dynamics*, Oxford Science Publications, Oxford University Press Inc. New York, USA, 1996

16.   Antropov, L. I. *Theoretical Electrochemistry*, Mir publication, Moscow, 1972

17.   Bard A. J.; Faulkner, L. R. *Electrochemical Methods, Fundamentals and Applications*, Wiley, New York, 1980

18.   Hogan, C. F.; Forster, R. J. *Anal. Chim. Acta*, **1999**, *39*, 613

19.   Koide, S.; Yokoyama, K. *J. Electroanal. Chem.,* **1999**, *468*, 193

20.   Elmgren, E.; Linquist, S. E. *J Electroanal. Chem.,* **1993**, *362*, 227

21. Ohara, T. J.; Rajagopalan, R.; Heller, A. *Anal. Chem.*, **1994**, *66*, 2451

22. Ohara, T. J.; Rajagopalan, R.; Heller, A. *Anal. Chem.*, **1993**, *65*, 351232

23. Gregg, B. A. *Phys. Chem.*, **1991**, *95*, 5970

24. *Methods in Enzymology*, K. Mosbach, (Ed.) Academic Press. New York, 1987.

25. Trevan, M. D. *Immobilised Enzymes,* Wiley, New Work, 1980

26. Gregg, B. A. *Anal. Chem.*, **1990**, *62*, 258

27. Kawai, T.; Keuwabara, T.; Wang, S.; Yosino, K. *J. Electrochem. Soc.*, **1990**, *137*, 3793

28. Astsushi, A.; Rajagopalan, R.; Heller, A. *J. Phys Chem.*, **1995**, *99*, 5102

29 Gregg, B. A. *J. Phys. Chem.*, **1991**, *95*, 5976

30 . Ohara, T. J.; Rajagopalan, R.; Heller, A. *Anal. Chem.*, **1993**, *65*, 351232

Chapter 3

Charge Transport and
Heterogeneous Electron Transfer

3.1 Introduction

The current trend in technology towards miniaturisation[1] is resulting in a revival in techniques that were optimised and studied extensively in the latter part of the last century. Much of the recent success in nano-technology can be attributed to a coming together of various disciplines, ranging from engineers, chemists to life scientist, and the application of the knowledge gained from all these separate disciplines resulting in enhanced technological devices capable of probing time domains.[2]

Another very good example of this is the use of microelectrodes, which were only of interest to a devoted physical chemist whose interest lay in the probing of thermodynamic issues occurring at the electrode/ electrolyte interface. However, the improvements in design and performance of microelectrodes gave rise to an interest from neuroscientists and analysts, as it was realised that their small dimension and the capability of creating microelectrode arrays[3] would make it possible to probe *in-vivo* the electrical performance of the brain.[4] From a microscopic focus, it is realised that processes and factors influencing the rate of charge transport across interfaces between chemical phases are of great importance. These processes are; rate of heterogeneous electron transfer between the electrode/ electrolyte interface surface, rate of mass transfer, ionic strength and pH of the electrolyte solution.

In this chapter, the use of a previously synthesised and characterised polymer modified, as detailed in Chapter 2, electrode is studied. Given the analytical chemistry approach of the work a study into the influence of some to the most commonly used, physiological pH buffers was conducted. Particular attention was given to the rate of heterogeneous electron transfer and mass transfer from/to the electrode/ electrolyte interface was performed.

Throughout the entire investigation, a control study was conducted whereby progesterone, a non-electroactive biocomponent, was incorporated within the PME allowing an investigation into the influence a biocomponent will exert on the overall electrochemical performance of this model system.

3.2   Apparatus

Electrochemical methods were performed using CH Instruments Model 600 and 660 electrochemical workstations. CHN analyses were performed by the Microanalytical Laboratories, UCD. Potentials were measured versus Ag/AgCl or a silver wire where indicated. The counter electrode was a 1 cm^2 platinum flag. All electrochemical measurements were carried out at 22° ± 3 °C.

3.3   Experimental

3.3.1   Preparation of polymer modified electrodes

A metallopolymer film was formed on the surface of the electrode by drop casting a constant volume of 40 μl of the desired components using a micropipette. The electrode was dried in an upright position in a solvation chamber, an airtight container containing water, over a period of 48 hrs. Incorporation of progesterone into the PVI$_{10}$–Os was achieved by taking equal volumes of diamino-propane (13.5 μmol), polyethyleneglycol (PEG) (2.3 μmol), progesterone (50 μmol) and 50 μmol of PVI$_{10}$–Os. The addition of PEG, a hydrophilic agent, ensures the solubility of PVP$_{10}$–Os in water. All chemicals were dissolved in water except progesterone, which was dissolved in ethanol. This solution was allowed to react for approx. 1 hr. and was always prepared on the same day as the electrodes. Again, a 40 μl sample was then micro-pippetted onto the surface of a freshly polished glassy carbon electrode and left drying in an upright position for 48 hrs. in a dessicator.

3.3.2   Diffusion co-efficient using cyclic voltammetry

By varying the scan rates between 0.1–0.5 Vs^{-1}, a series of voltammograms were collected using freshly prepared PMEs, described in 3.3.1. Experiments were carried out on the pure metallopolymer, PVI$_{10}$–Os in 0.05 M phosphate, Tris and HEPES buffer, pH 7.4, with 0.1 M KCl supporting electrolyte. Additional experiments were carried out using the progesterone modified polymer, PVI$_{10}$–Os–Prog, in 0.05 M phosphate buffer, HEPES and Tris pH 7.4 with 0.1 M KCl supporting electrolyte.

101

3.3.3   Diffusion coefficients using chronoamperometry

Potential step chronoamperometry was used to measure the diffusion coefficients in order to test the effects of experimental timescale on the values obtained.   Freshly prepared PMEs were used and an equilibration procedure was applied until a uniform electrochemical response was observed, when the peak currents for two successive scans are the same. From Section 3.3.2 the precise potential limits were established for the Faradaic process, where a single peak was observed between 0.100–0.500 V. These experiments confirm that the metallopolymer film is fully reduced between 0.000 and 0.100 V and is fully oxidized for potentials positive of +0.500 V. The potential step was 0.500 V with a sample time of 0.05s. Diffusion coefficients were obtained for both anodic and cathodic peak potentials. This work was carried out using 0.05 M Phosphate buffer, pH 7.4, with 0.1 M KCl supporting electrolyte.

3.3.4   Heterogeneous rate constant using Normal Pulse Voltammetry.

The same preparation and equilibration procedure is used as was mentioned in Section 3.3.3. In this experiment, the objective is to determine the heterogeneous kinetics and the transfer co-efficient, α. These values were determined using a pulse width of 0.03 s with a sample time of 0.01 s.

3.4   Results and Discussion:

3.4.1   Cyclic voltammetry:

From the literature survey, it is known that the presence of an electrolyte is essential to avoid problems associated with migrational currents. However, in addition to minimising currents due to migration, the electrolyte possesses other important functions.[5] The presence of high concentrations of ions decreases the solution resistance (R) and, hence, a drop in uncompensated resistance, is observed. Consequently, the supporting electrolyte allows an improvement in the accuracy with which the working electrode potential is controlled, which is essential when studying electrochemical response.

Apart from the physical effects of the supporting electrolytes on the electrochemical system, there are also chemical effects. These effects include controlling the pH or ionic strength, which help to control the reaction conditions of the electrochemical cell. In electroanalytical measurements, an electrolyte is used to decrease or eliminate sample matrix effects while also ensuring that the double layer remains thin with respect to the diffusion thickness. However, supporting electrolytes are present in large concentrations making it possible that they may produce Faradaic responses themselves, by reacting with the analyte of interest. One further disadvantage involving electrolytes is that their presence in high concentrations will result in altering the medium in the cell such that the response in comparison with pure medium is altered.

While the literature shows that the most common buffer to use as the supporting medium is phosphate buffer, reports exist where other buffers such as Tris buffer[6,7,8,9] or HEPES buffer[10,11,12,13,1415,16,17] are used for the investigation of various biosensors including the classical glucose biosensor.[18] Although, these buffers are often used, very little research into the effects of the buffer choice on the electrochemical responses such as charge transport or heterogeneous kinetics of biosensors has been reported. For these reasons, it was decided to investigate the effects of phosphate, Tris and HEPES buffer on the electrochemical response. The ionic strength and pH was kept constant throughout all experiments performed. The

pH range chosen for these experiments was 7.4 while an ionic strength of the buffer and the supporting electrolyte was 0.1 M and 0.05 M respectively.

Phosphate buffer

From the Chapter 2, it was established that these PVI_{10}–Os films exhibit electrochemical properties typical of electrochemically reversible surface confined species at slow scan rates. However, as illustrated in Figure 3.1, as the scan rate, v, increased, the response begins to resemble that of a solution phase redox species, i.e., the peak current depends linearly on $v^{1/2}$ and diffusional tailing is observed. Figure 3.2 shows the classical influence of semi-infinite diffusion with increase in scan rate – seen by the increase in value of ΔE_p from 0.06 to 0.1 V at 0.1 and 0.5 Vs^{-1} respectively. Theoretically[5] this value should remain at 0.059 V for a reversible single electron process, assuming a switching potential at least 0.09 V beyond E_p. A corresponding increase in FWHM can also be seen going from 0.170 to 0.200 V at 0.1 and 0.5 Vs^{-1} respectively. Again this is a deviation from the expected theoretical value of a one electron reversible redox couple – confined to the surface of the electrode – which should yield a value of 0.0906V and be independent of scan rate. Such a deviation from the theoretical expectation suggests the influence of semi-infinite diffusion on the overall electrochemical response.

The linear dependence of current on $v^{1/2}$ can be seen in Figure 3.2, showing good correlation factors. These experiments were carried out using three different electrodes and for each electrode three times, as can be seen from the error bars in Figure 3.3, the experimental error is acceptable, $\pm$ 7.5 %.
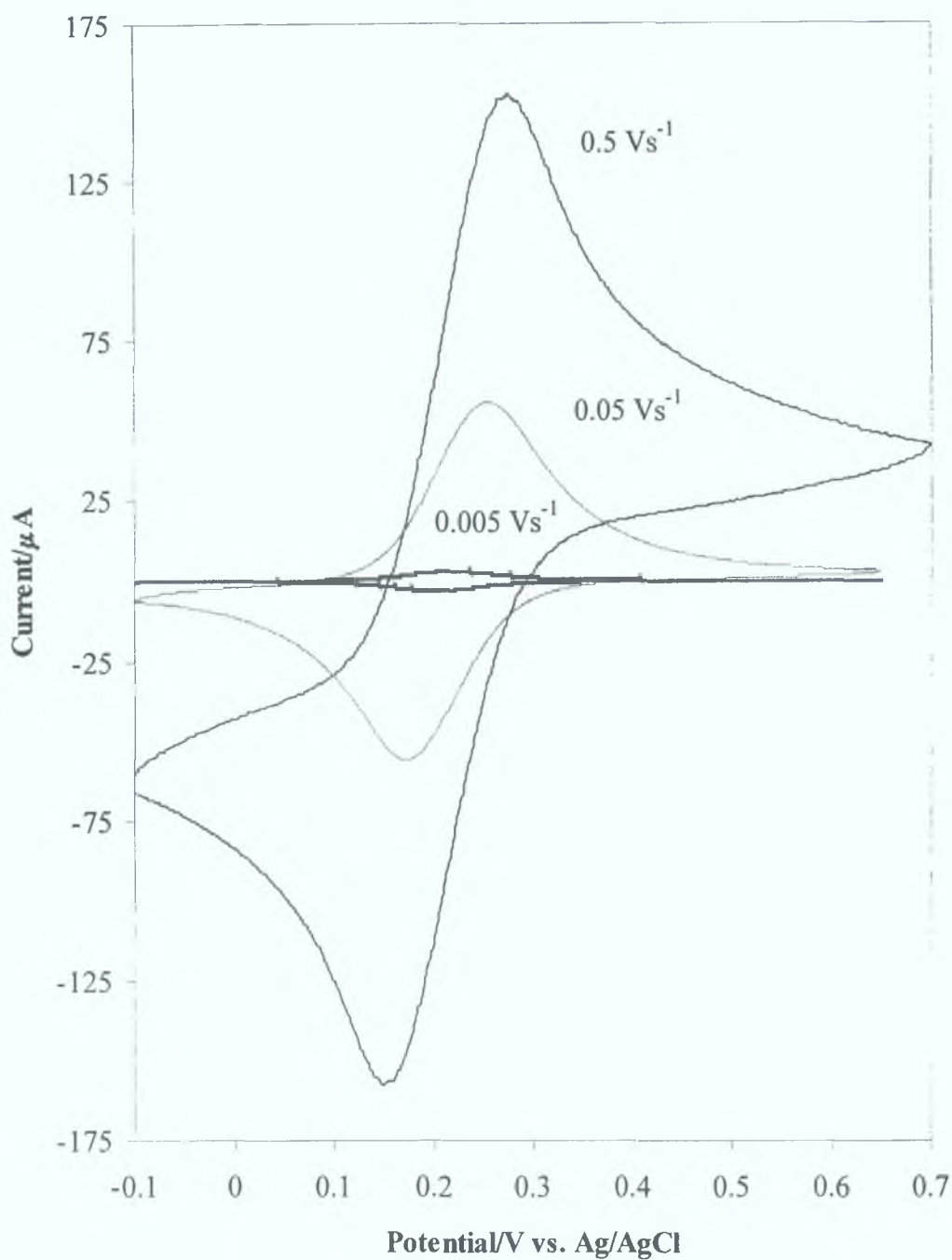
Figure 3.1. Cyclic voltammograms of PVI_{10}–Os in aqueous 0.05 M phosphate buffer, pH 7.4, with 0.1 M KCl supporting electrolyte. Surface coverage is 0.19 ± 0.02 mol cm^{-2}, WE was a glassy carbon electrode, 3mm in diameter. Scan rate was 0.005, 0.05 and 0.5 Vs^{-1}, the initial potential was –0.1 V in a positive direction.
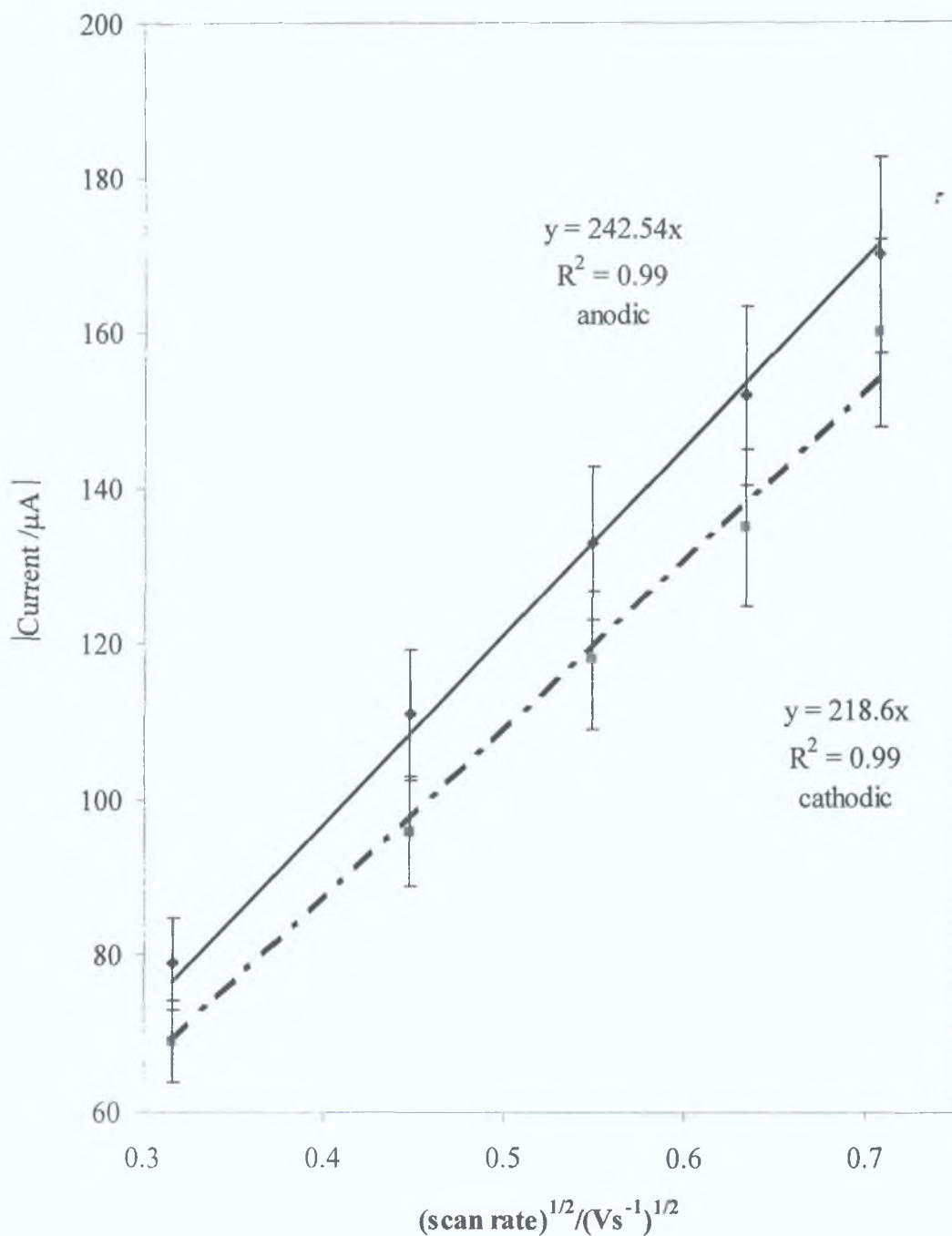
Figure 3.2. Dependence of the peak current for PVI_{10}–Os on the square root of scan rate, between 0.1 and 0.5 Vs^{-1}. WE was a glassy carbon electrode, 3 mm in diameter, in aqueous 0.05M Phosphate buffer, pH 7.4, containing 0.1 M KCl supporting electrolyte.

Tris buffer

Figure 3.3 shows the same experimental results for 0.05 M Tris buffer, pH 7.4, with 0.1 M KCl supporting electrolyte. Again, the influence of semi-infinite diffusion is apparent, with a ΔE_p of 0.045 and 0.1 V for scan rates of 0.1 and 0.5 Vs^{-1} respectively. Likewise, the FWHM shows an increased value as expected for semi-infinite diffusion response, going from 0.140 to 0.195 V at 0.1 and 0.5 Vs^{-1} respectively. The corresponding graph of i_p vs. $v^{1/2}$, Figure 3.4, shows a good correlation factor, the error bars show that the experiment was well within accepted experimental error. These results are again much larger than the expected theoretical values for a surface confined species.
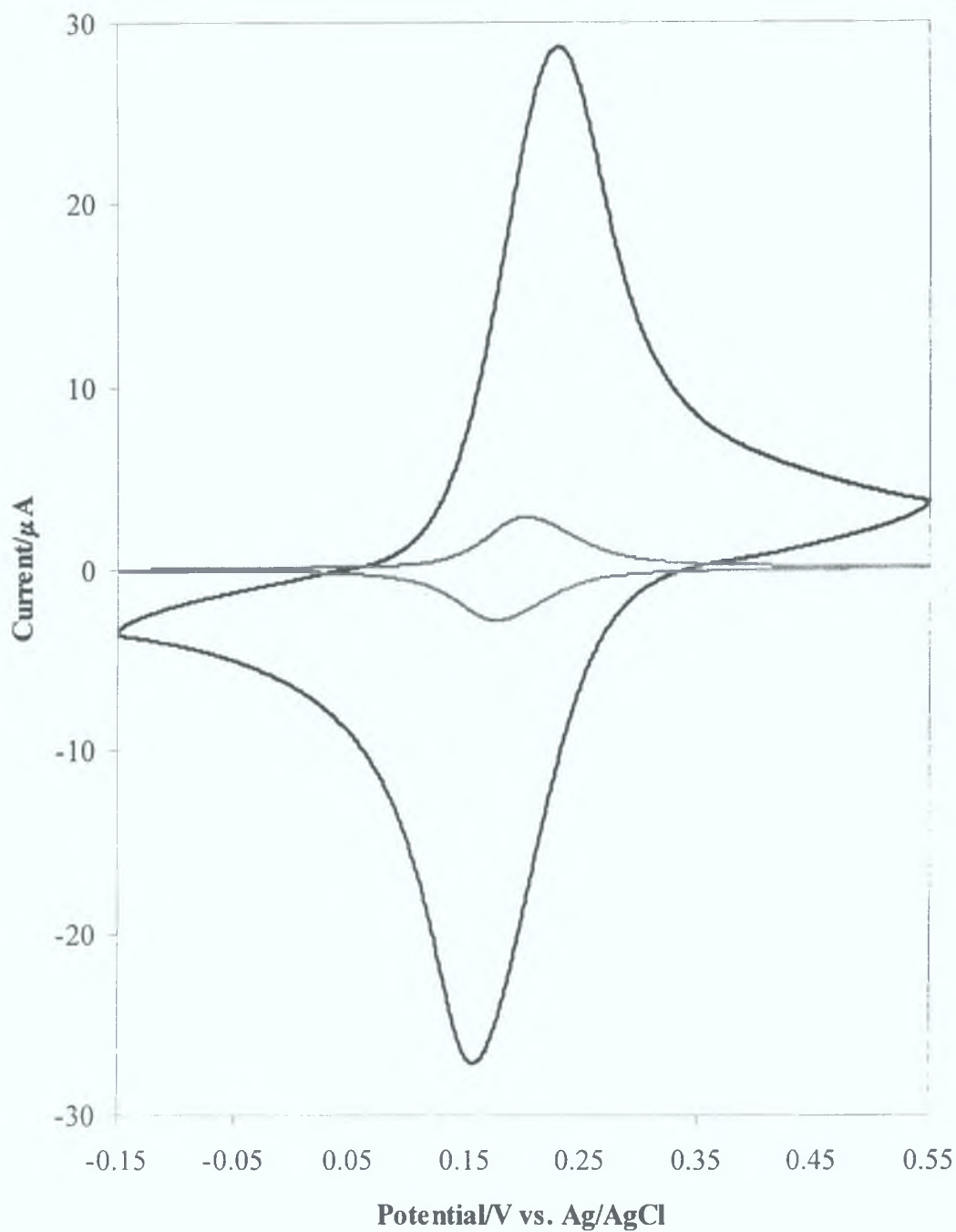
Figure 3.3. Cyclic voltammograms of a PVI$_{10}$–Os film in aqueous 0.05 M Tris buffer, pH 7.4, with 0.1 M KCl supporting electrolyte. Surface coverage is 0.091 ± 0.03 mol cm^{-2} The WE was a 3 mm in diameter glassy carbon electrode. Scan rate was 0.005 and 0.5 Vs^{-1} initial potential was –0.15 V in a positive direction.
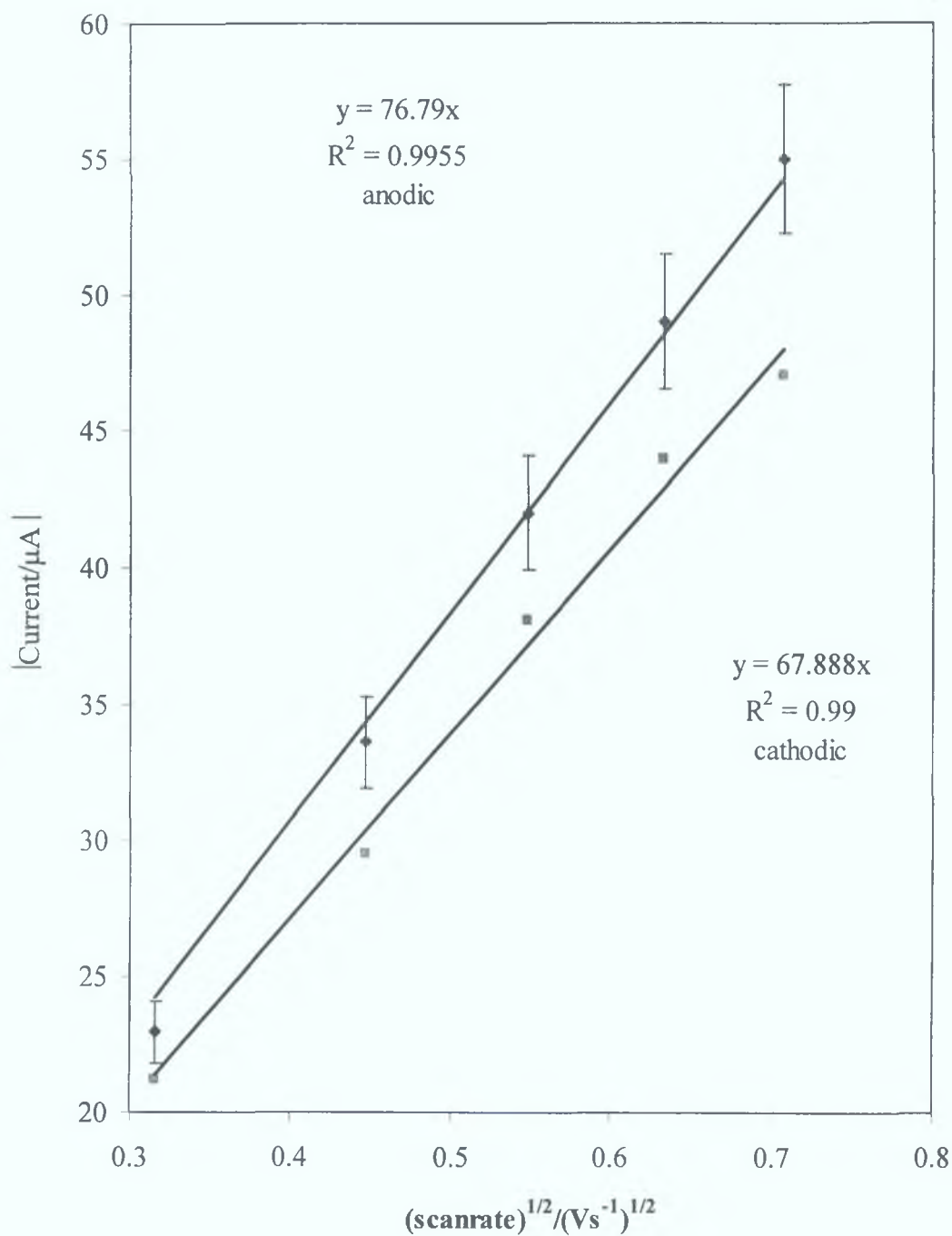
**Figure 3.4.** Dependence of the peak current for PVI_{10}–Os on the square root of scan rate, between 0.1 and 0.5 Vs^{-1}. WE was a 3 mm in diameter glassy carbon electrode, in aqueous 0.05M Tris buffer, pH 7.4, containing 0.1 M KCl supporting electrolyte.

HEPES buffer

Figure 3.5 shows a sample of the voltammograms obtained in HEPES buffer pH 7.4. In this case, a larger ΔE_p is observed 0.190 V and 0.230 V at scan rates of 0.1 and 0.5 V s^{-1} respectively. The values for FWHM are 0.220 V and 0.240 V for 0.10 and 0.50 Vs^{-1} respectively. Figure 3.6 shows the linear dependence of i_p on $v^{1/2}$ a good correlation factor and low errors of $\pm$ 5% are observed. A larger ΔE_p can be observed than in the previous two cases for phosphate and Tris buffer respectively, with a much larger value than that which is theoretically expected.

The responses of the PME in various electrolytes has been summarised in Table 3.1

Table 3.1. Summary of ΔE_p and FWHM for the various buffers, all of which are 0.05M in concentration, with 0.1M KCl supporting electrolyte.

| Buffer	Phosphate		HEPES		Tris	
Scan rate Vs^{-1}	0.100	0.500	0.100	0.500	0.100	0.500
ΔE_p V	0.060	0.100	0.190	0.230	0.045	0.100
FWHM/ V	0.170	0.200	0.220	0.240	0.140	0.195
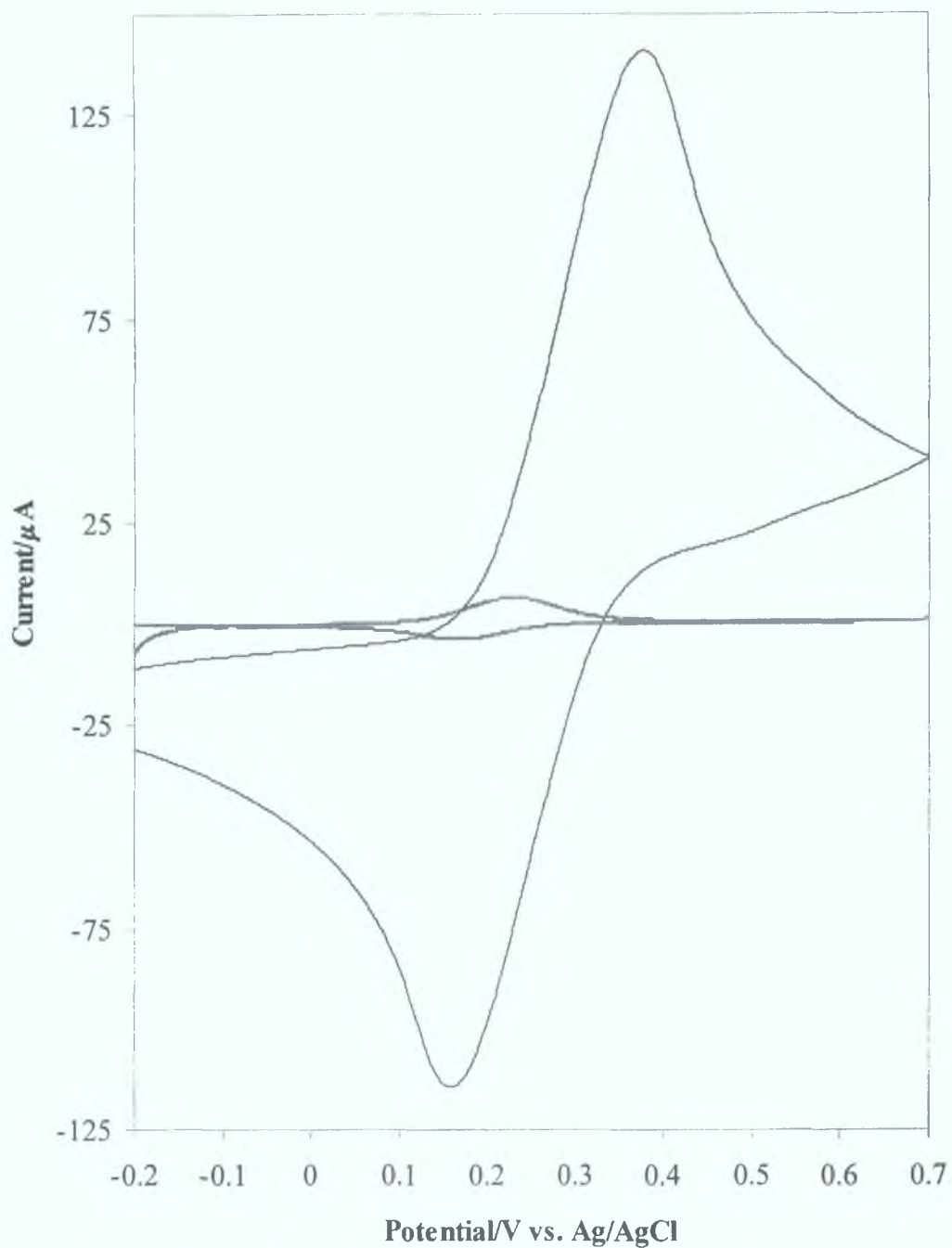
Figure 3.5. Cyclic voltammograms of PVI_{10}–Os in aqueous 0.05 M HEPES buffer, pH 7.4, with 0.1 M KCl supporting electrolyte. Surface coverage was 0.088 ± 0.03 mol cm^{-2} WE was a 3 mm, in diameter, glassy carbon was employed. Scan rate was 0.005 and 0.5 Vs^{-1} Initial potential was –0.2 V in a positive direction.
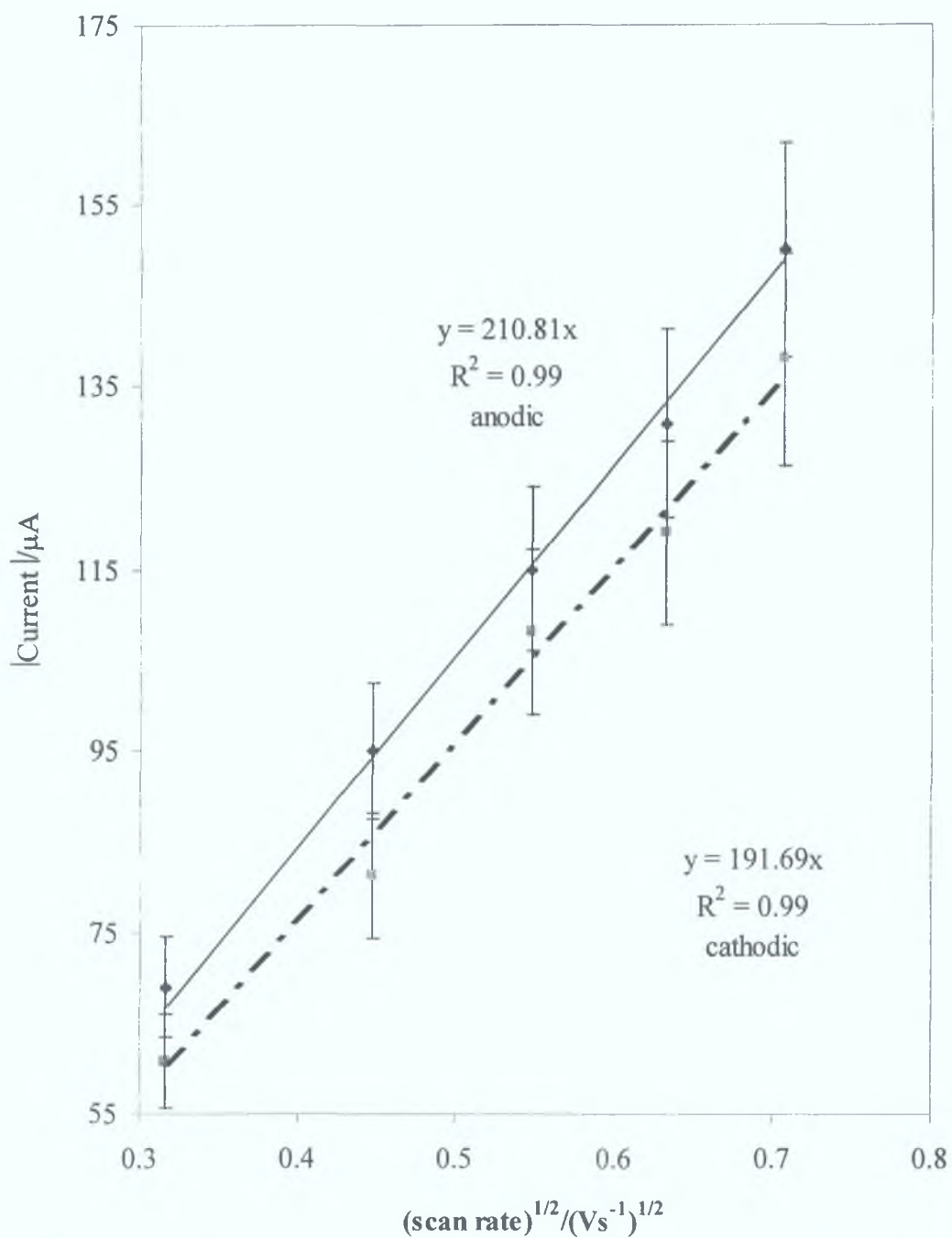
Figure 3.6. Dependence of the peak current for PVI_{10}–Os on the square root of scan rate, between 0.1 and 0.5 Vs^{-1}. WE was a 3 mm in diameter glassy carbon electrode, in aqueous 0.05M HEPES buffer, pH 7.4, containing 0.1 M KCl supporting electrolyte.

The influence of buffer choice is evident from Figures 3.1–3.6, with the most noticeable parameter being the difference in values obtained for ΔE_p and FWHM. However, it is the linear dependence of peak current on $v^{1/2}$ that makes it possible to analyse the behaviour of these PMEs using the Randles-Sevcik, Equation 3.1, and hence to determine the rate of charge propagation (diffusion co-efficient) through the film.

$$i_p = (2.69 \times 10^5)\, n^{3/2} A D_o^{1/2}\, v^{1/2} C_t \qquad\qquad \textbf{(Equation 3.1)}$$

In Equation 3.1, n is the number of electrons transferred due to either oxidation or reduction of species at the WE surface, A is the electrode area, $(0.0707\,cm^2)$, D_0 is the diffusion co-efficient, v is scan rate, and C_t is the concentration of fixed redox sites at the electrode surface. In this case, since we are interested in comparing the values between each electrolyte it was decided to determine $D^{1/2}C_t$. Equation 3.1 shows how the current is directly proportional to the concentration of the electroactive species and $v^{1/2}$, making it is possible to determine the value of $D^{1/2}C_t$, using the slopes obtained from Figures 3.2, 3.4 and 3.6, between the various buffers. Table 3.2 summarises these results.

Table 3.2. Results of $D^{1/2}C_t$ ($\times 10^{-8}$ mol cm^{-2} s$^{-1/2}$) for PVI_{10}–Os. Where the supporting electrolyte is 0.05 M aqueous, phosphate, HEPES and Tris buffer, containing 0.1 M KCl.

	Phosphate	HEPES	Tris
Anodic	1.2 ± 0.09	0.044 ± 0.003	1.11 ± 0.083
Cathodic	1.15 ± 0.086	0.033 ± 0.005	0.99 ± 0.047

From Table 3.2 it can be seen that the ratio of $i_{pa} : i_{pc}$ is not unity and hence the value for the respective diffusion coefficients is also not unity. Inzelt[19] proposed that this difference in behaviour is related to the adsorption / desorption of the solvent molecules that result in the swelling / deswelling of the polymer. As a result, of these phenomena the polymer chain and segmental motion are effective and may play a crucial role in the thermodynamic nature of the solvent. In all cases the $D^{1/2}C_t$ for the reduction process i.e. $Os^{3+} + e^- \rightarrow Os^{2+}$ is slower than for the oxidation process. It has been observed before[20] that the larger diffusion coefficient observed for an Os^{3+} system is consistent with expected steric hindrance requiring the diffusion of counterions through a triply charged oxidised matrix whereas in the case of a Os^{2+} system the counterions need to diffuse through a doubly charged reduced matrix. Such differences in charge demand that diffusion of sufficient amount of counter ions to maintain electroneutrality.

Further studies by Aberg *et al*[21] attribute this non-uniform behaviour to counter ion diffusion through the layer. Aberg *et al*[21] state that counterions such as K^+ and H^+ enter the film upon oxidation and exit upon reduction in order for the film to maintain electroneutrality. The possible counterions in this case are H^+, K^+ PO_4^{3-} or OH^- Cl^- for phosphate buffer, K^+, H^+, Na^+, OH^- or $C_8H_{17}N_2O_4^-$ Cl^- for HEPES buffer and K^+, H^+, NH_2^+ Cl^- OH^- or CH_2OH^- for Tris buffer. The number of counterions in the film is determined by the film loading and the oxidation of the redox species.

If one considers an active surface concentration[24] of 0.85 M and using Equation 3.1, it is observed that the rate of charge propagation through a PVI_{10}–Os film in the presence of buffered electrolytes is 8.14×10^{-8}, 8.16×10^{-9} and 6.15×10^{-8} $cm^2 s^{-1}$. If these results are compared with other studies that have been conducted using a PVI_{10}–Os modified electrode such as a study conducted by Aoki *et al*[22] where the value of D was measured as 2.3×10^{-9} $cm^2 s^{-1}$ in a pH 7.0 electrolyte solution it can be seen that the rate of charge propagation is higher in buffered electrolytes.

In agreement with stability studies conducted in Chapter 2, it appears that phosphate buffer is the more suitable of all buffers as it results in the fastest rate of charge propagation through the film, hence, all further studies are conducted using this buffered medium.

From the initial data presented above in Figures 3.1–3.6, it was decided to study what effects the presence of a biological component (PVI_{10}–Os–Prog.) has on the rate of charge propagation through the metallopolymer film. It is expected that some difference should arise, as the presence of a crosslinking agent (PEG) would result in a more porous "bulky" layer and hence the limits associated with counterion motion across the PME film should be reduced or even eliminated. The voltammograms shown in Figure. 3.8, illustrate the data collected in aqueous 0.05M phosphate buffer, pH 7.4, with 0.1 M KCl.

In all cases it was observed that these PVI_{10}–Os–Prog showed a linear dependence on $v^{1/2}$, for scan rates between 0.005–0.500 Vs^{-1}. These results are different from those observed for the PVI_{10}–Os polymer, which demonstrates the onset of semi-infinite diffusion at, scans rates of 0.100 Vs^{-1}. In agreement with previous reports,[23] these voltammograms suggest that in the presence of a biocomponent, the rate of counterion motion across the PME interface is slower than for PVI_{10}-Os. It is possible to attribute such behaviour to the size of the steroid molecule progesterone resulting in a more sluggish movement of counterions through the PME. The work done by Ohara[23] shows for a PVI_{10}–Os modified with glucose oxidase demonstrates the same diffusional limitations however this observation was not further researched. It is possible however that this early onset is due to the presence of a bulky biocomponent. In addition to the observed diffusional tailing the ΔE_p of 0.090 V and 0.130 V at 0.1 and 0.5 Vs^{-1} while, the FWHM shows of 0.170 and 210 V for 0.1 and 0.5 Vs^{-1} respectively.

In addition to the scan rate dependence. it can also be seen in Figure 3.7 that there is greater diffusional tailing at slower scan rates. Figure 3.8 shows the plot of i_p versus $v^{1/2}$ that exhibits a peak to peak ratio near unity with good correlation factor and small error bars. All of the above mentioned factors suggest the earlier onset of semi-infinite diffusion process in comparison to PVI_{10}-Os, especially evident by the early onset of linear dependence of i_p on $v^{1/2}$. This is in agreement with previous reports.[23] A comparison of the values for $D^{1/2}C_o$, seen in Table 3.3, show that a PME of PVI_{10}–Os–Prog exhibit a rate of charge propagation through the modified matrix that is two orders of magnitude slower when compared with PVI_{10}–Os electrodes.

As with all experimental processes, the inclusion of a control is necessary. In this case the control used is PVI_{10}–Os containing all the crosslinking reagents apart from progesterone. Table 3.3 shows that the values obtained for $D^{1/2}C_t$ for PVI_{10}–Os–crosslinking reagents lie somewhere between the values of the PVI_{10}–Os and PVI_{10}–Os–Prog, Table 3.3. From Table 3.3 it can be seen that although the presence of PEG influences the rate of charge propagation through the modified electrode, it is not the only deciding factor and the inclusion of progesterone further decreases the value of $D^{1/2}C_t$.

Table 3.3. Results of $D^{1/2}C_t$ (10^{-8} mol $(cm^{-2}s^{-1})^{1/2}$ for variations of PVI_{10}–Os PME. Results were obtained in aqueous phosphate, 0.05 M in concentration, containing 0.1 M KCl.

PME	Anodic	Cathodic
PVI_{10}-Os	1.28 ± 0.087	2.16 ± 0.081
PVI_{10}-Os with PEG	0.75 ± 0.36	6.92 ± 0.309
PVI_{10}-Os-Prog.	0.012 ± 0.02	0.011 ± 0.02
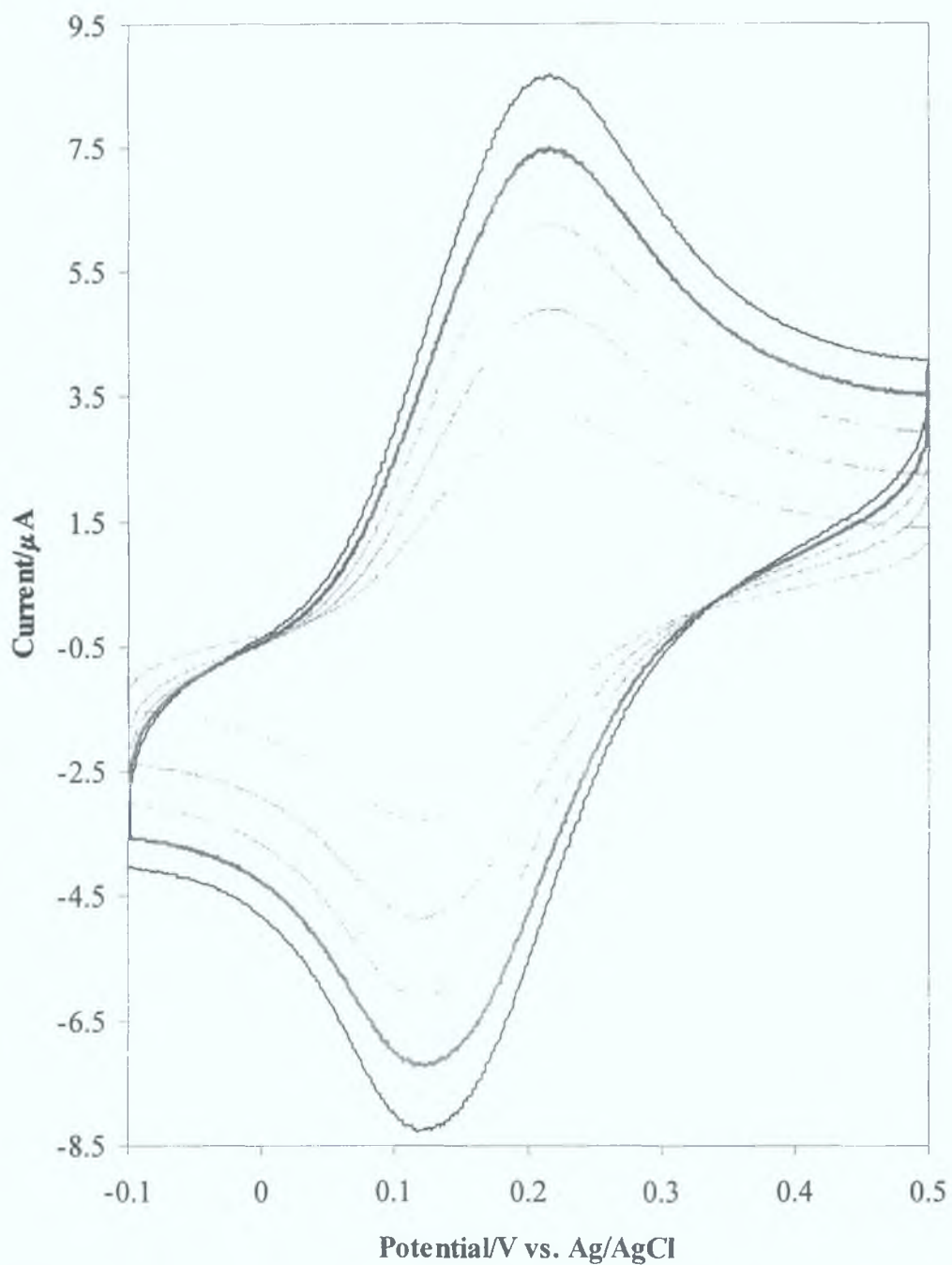
Figure. 3.7. Cyclic voltammograms of PVI_{10}–Os–Prog, in aqueous 0.05 M phosphate buffer, pH 7.4, with 0.1 M KCl supporting electrolyte. WE is a 3 mm(in diameter) glassy carbon. From outer to inner voltammograms respectively the scan rate was 0.5, 0.4, 0.3, 0.2 and 0.1 Vs^{-1} Initial potential was –0.1 V in a positive direction.
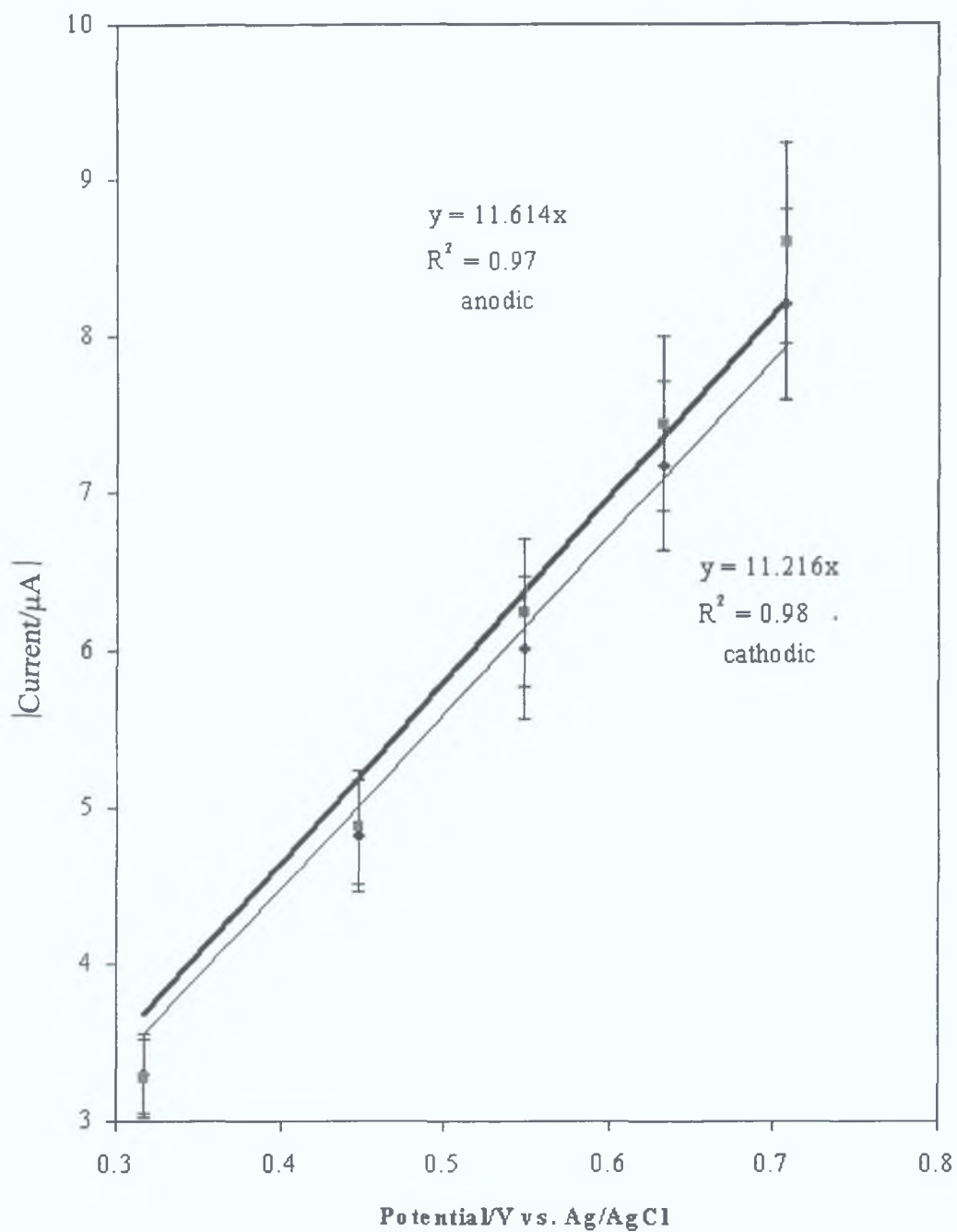
Figure.3.8. Dependence of the peak current for PVI$_{10}$–Os on the square root of scan rate, between 0.1 and 0.5 Vs^{-1}. WE was a 3 mm in diameter glassy carbon electrode, in aqueous 0.05M phosphate buffer, pH 7.4, containing 0.1 M KCl supporting electrolyte.

3.4.2   Chronoamperometry

The principle advantage of chronoamperometry over cyclic voltammetry is the ability to measure electrode dynamics under more clearly defined conditions.   In brief, chronoamperometry involves stepping the potential of the working electrode, from a value at which no Faradaic reaction occurs (V_1) to a potential at which the surface concentration of the electro-active species is effectively zero, (V_2) Figure 3.9*a*.   The current-time dependence is obtained, Figure 3.9*b*, and can be understood from concentration–time profiles, Figure 3.9*c*.   As the surface concentration of oxidised species (O) is zero at V_1, a concentration gradient is established near the surface. Immediately following the potential step, the concentration gradient is steep and the diffusion layer is thin. As time goes by the diffusion layer expands (δ_2 and δ_3 at t_2 and t_3), and hence the concentration gradient decreases.

To understand the shape of a chronoamperogram one needs to consider the concentration-distance profiles for a potential step excitation in conjunction with Faraday's law.   According to Faraday's law, the charge passed across an interface is related to the amount of material that has been converted from O to R species, and the current is related to the instantaneous rate at which this conversion occurs. It is possible to define current as the rate of charge flow giving rise to Equation 3.2:

$$Q = nFN$$ **(Equation 3.2)**

where Q is the charge passed, n is the number of electrons transferred in the reaction, F is Faraday's constant and N is the number of moles converted. The rate of conversion at time t is proportional to the electrode area making it possible to describe the flux of material to the electrode surface according to Fick's first law, Equation 3.3:

$$i_t = nFAD_o\left(\frac{\partial C_o}{\partial x}\right)_{x=0,t}$$ **(Equation 3.3)**

where i_t is the current at time t, A is the electrode area; C_o concentration of oxidised species and x is the distance from the electrode.   Examination of a chronoamperogram shows, Figure 3.9*b*, that for product O at x = 0, a decrease in the

119

slope with time or a decrease in current, this may be described using what is known as the Cottrell equation, Equation 3.4.

$$i_t = \frac{nFAC_O D_O^{1/2}}{\pi^{1/2} t^{1/2}}$$

(**Equation 3.4**)

The Cottrell equation states that the product $it^{1/2}$ should be constant for a diffusion-controlled reaction at a planar electrode. Deviation from this behaviour can be caused by a number of situations, including non-planar diffusion, convection in the cell, migration of species to the electrode surface, and above all slow charging of the electrode during the potential step. Variations of $it^{1/2}$ can signify slow attainment of the imposed potential by the electrode. Although the input voltage to a potentiostat is a square wave for a potential-step experiment, the actual charge may lag behind due to uncompensated resistance in the cell.

The length of the pulse time for these experiments is crucial, as deviations of mass transport behaviour occur over long times due to natural convection effects. Hence, great care needs to be taken in deciding on pulse length. [24]
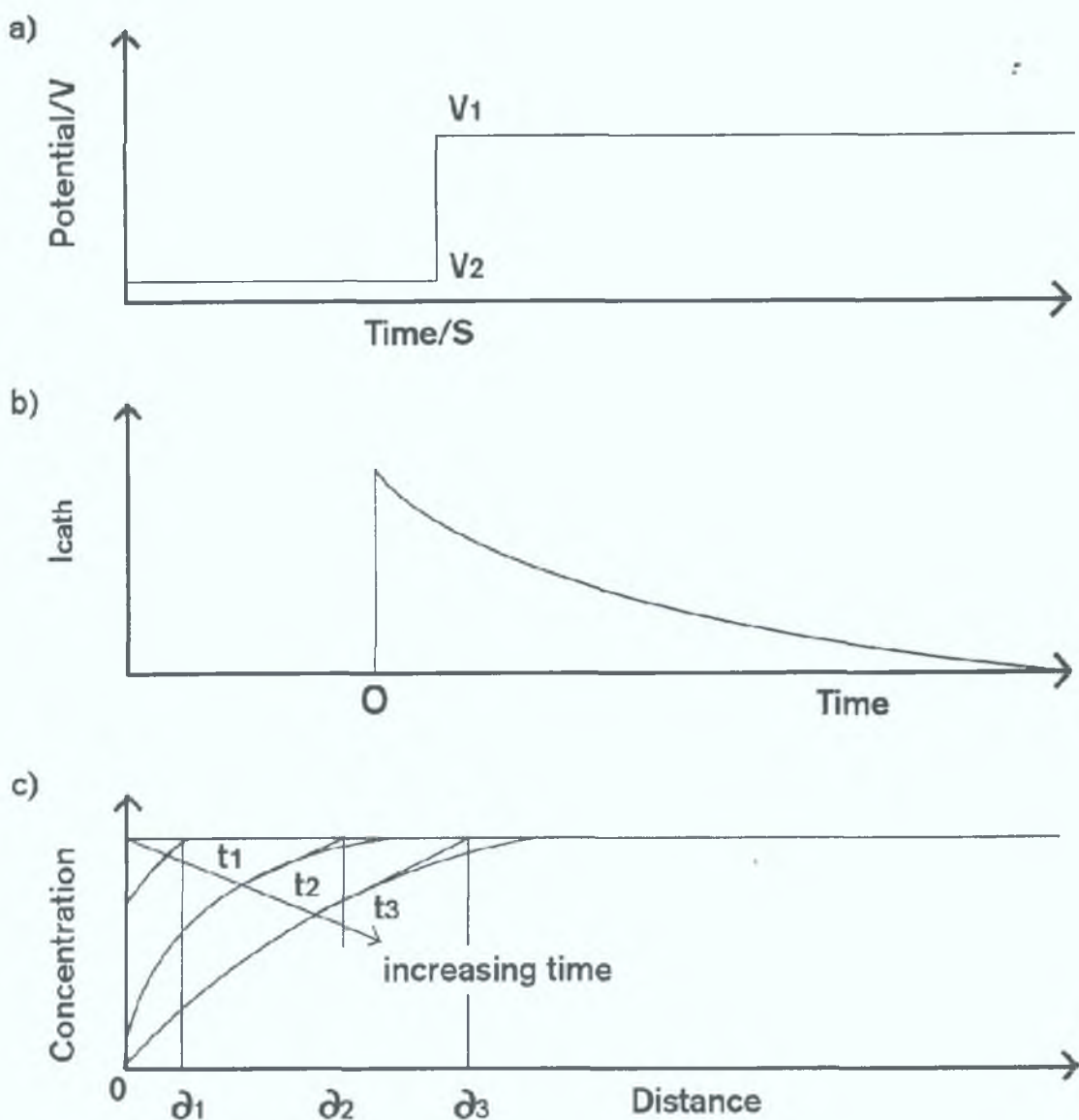
Figure 3.9. (a) Variation of applied potential with time in a potential step experiment; V_1 and V_2 are the initial and final potential respectively. (b) Plot of cathodic current against time for a classical chronoamperometric response. (c) Effect of time on the concentration profile at the surface of an electrode, δ thickness of the diffuse layer. At t_1 the concentration gradient is high, while the diffusion layer is thin, as time increases the thickness of the diffusion layer increases while the concentration of electroactive species at the electrode surface decreases

In the case of a PME where both O and R are confined to the surface the rate of oxidation is controlled by three individual processes. First, the rate at which counterions, required to maintain electroneutrality of the PME, diffuse from bulk solution and propagate the PME in order reach the electrode surface. Second, the rate at which electron transfer between the electrode and the redox species confined to the electrode surface occurs. And finally, the rate at which these counterions diffuse out of the film allowing the reduction process to occur.

Previously,[29] it was demonstrated that a variation in pulse width had effect on the slopes obtained from the Cottrell plots: hence, it was decided to work with a pulse width of 0.1s. The use of this large potential step amplitude ensures that the response obtained is not influenced by uncompensated resistance or slow interfacial kinetics.[25] Hence, in the experiments described here, the potential was stepped from 0.100 to 0.500 V, corresponding to the potential range where Faradaic current is observed in Section 3.4.1. As a precautionary measure, the contribution of charge from non-Faradaic processes was also measured in the potential region directly before (0.0–0.1 V) and after (0.5–0.6 V) the potential step region. Figures 3.10 and 3.11 show these results in 0.05 M phosphate buffer, pH 7.4, with 0.1 M KCl supporting electrolyte and, as can be seen, the contributions of current from non-Faradaic processes are indeed lower when compared to contributions for Faradaic processes. For the anodic process, this contribution is 700 ± 50 and 300 ± 30 µA. for Faradaic and non-Faradaic respectively, and for cathodic processes it is 1200 ± 100 and 300 ± 100 µA for Faradaic and non-Faradaic respectively. The large errors observed for the cathodic non-faradic response are associated with the semi-infinite diffusion.

The influence of semi-infinite diffusion is confirmed by the presence of a zero intercept, in the current–time plots. The presence of migrational effects, would be indicated by a non-zero intercept. Although not shown, a comparative study for both 0.05 M HEPES and Tris buffer, pH 7.4, with 0.1 M KCl supporting electrolyte was conducted. In both incidences, the current response was tenfold lower, than the phosphate buffer counterpart.
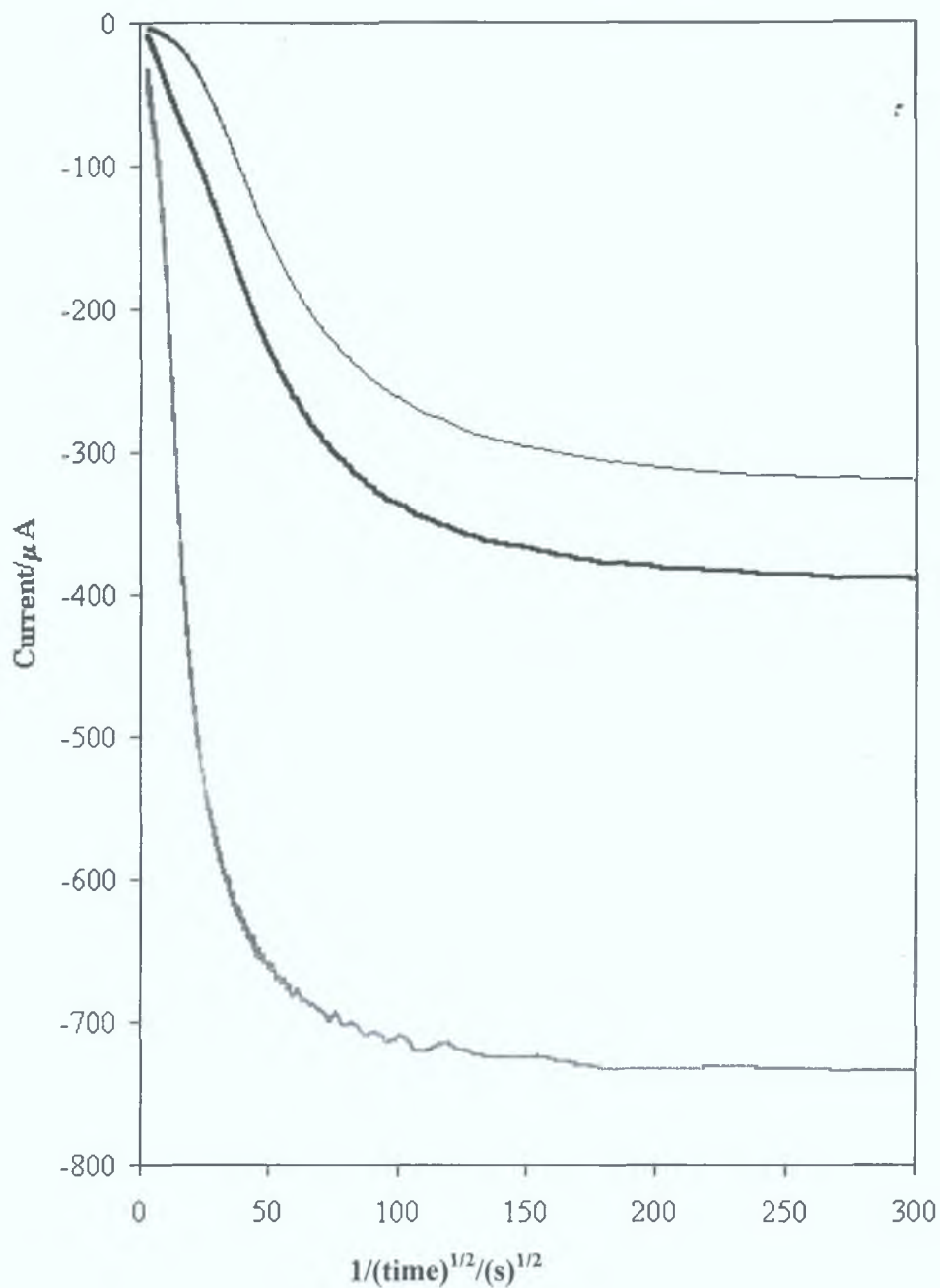
Figure 3.10. Chronoamperometry from the top: non-faradic processes, 0.100 - 0.0 V, 0.50–0.60 and faradic processes 0.1–0.5 redox area. A pulse width of 0.1s was used. WE was a 3 mm, in diameter, glassy carbon modified with PVI_{10}-Os in aqueous 0.05M phosphate buffer, pH 7.4, with 0.1 M KCl.
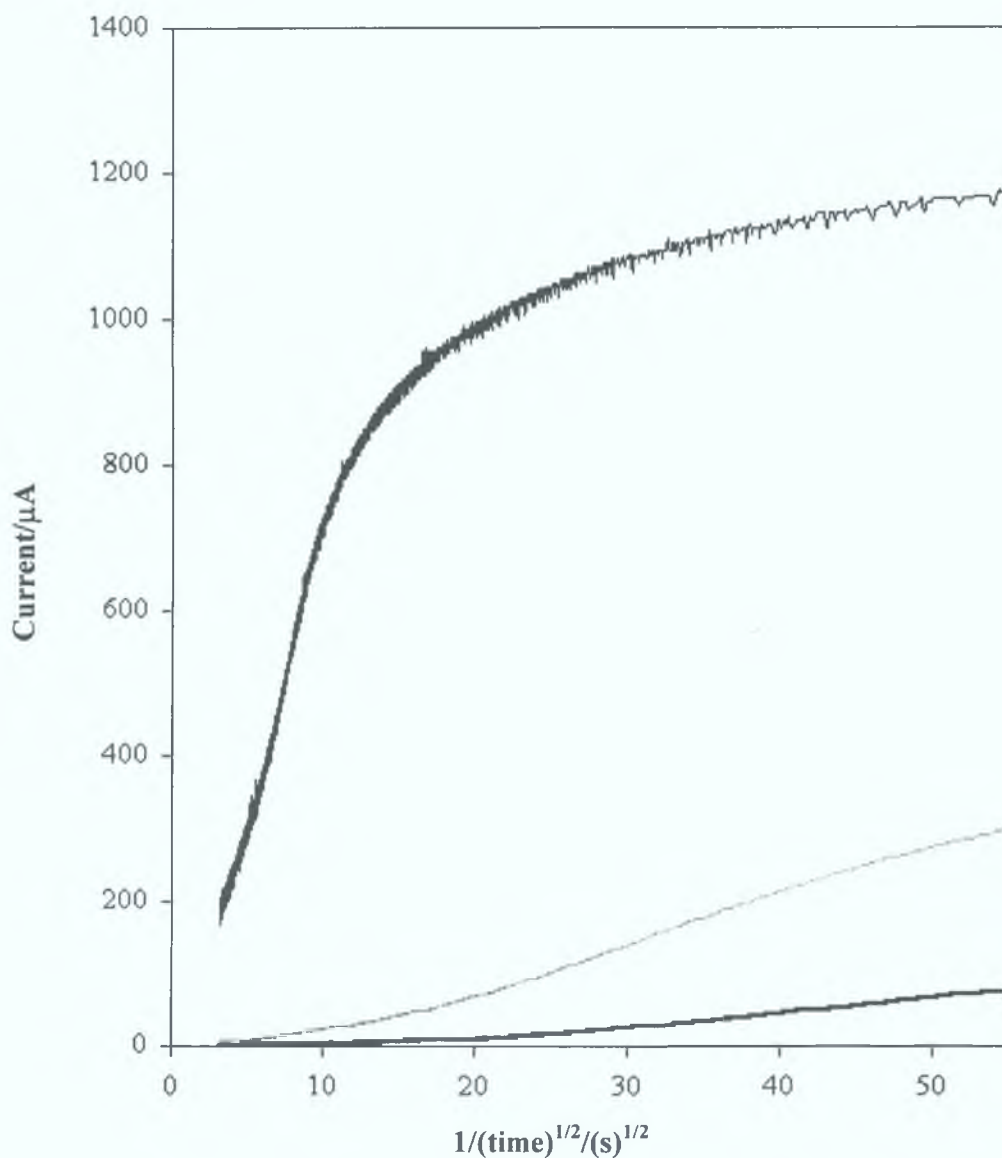
Figure 3.11. Chronoamperometry, from bottom; non-faradic processes for cathodic process, 0.00–0.10 V, 0.60–0.50 and faradic processes from 0.50–0.10. WE was a 3 mm, in diameter, glassy carbon working electrode modified with PVI_{10}–Os, in aqueous 0.5 M phosphate buffer, pH 7.4, with 0.1 M KCl supporting electrolyte. A pulse width of 0.1s was used.

Results presented in Table 3.4 demonstrate that, again, there is a variation in diffusional response between various buffers, with phosphate buffer showing the greatest rate of diffusion, followed by Tris buffer and then HEPES. What is most surprising about these results is that there is almost an order of magnitude difference between the rate of charge transport for phosphate buffer and HEPES. In agreement with the results obtained for cyclic voltammetry, Table 3.2, there is a discrepancy between the anodic and cathodic response, albeit not as large. For both cyclic voltammetry and chronoamperometry the anodic process is faster. Reasons for these discrepancies have been described in Section 3.4.1.

Although, cyclic voltammetry proves to be an invaluable technique for obtaining analytical information there are problems associated with the reliability of the results obtained for charge propagation[24,25,26,27,28]. Inzelt *et al*,[19,27] report that the difficulties associated with interpretation of the results are due to the superimposition of several different processes, including both Faradaic and non-Faradaic currents, on the resulting voltammogram, thereby making it difficult to obtain conclusive results. Because of this superimposition, the apparent rate of charge transport through a PME using cyclic voltammetry is faster. The use of a chronoamperometry can help to eliminate this problem, as the potential region is chosen to correspond directly to the potential range where faradic processes exist. Hence, assuming that a large enough pulse width is applied, it may be said that for an accurate determination of the influence of electrolyte on the rate of charge transport it is not sufficient to rely solely on cyclic voltammetry as an experimental technique.

Examination of the results presented in Table 3.4 shows that the time required to charge the PME in phosphate buffer is shorter than in the other two buffers. This is seen in the Cottrell plot as a shorter timescale for the decay of current with $1/(t)^{1/2}$.

In most incidences, the rate of charge propagation of a PME is slower by one order of magnitude, when compared with its solution phase counterpart, assuming ionic strength and pH conditions are optimised.[29,30,31,32,33,34] The rate of charge transport for solution phase PVI_{10}–Os has been evaluated in 0.1 M $LiClO_4$ at 3.2×10^{-8} mol cm s^{-2}.[34] For all results, the variation in rate of charge propagation is not as pronounced using chronoamperometry when compared with cyclic voltammetry. The data suggests that

the influence of non-Faradaic processes on the overall response is considerable when using the electrolytes mentioned here.

Table 3.4. Results obtained for the value of $D^{1/2}C_t$ (10^{-8} mol $(cm^2 \, s^{-1})^{1/2}$) in various buffers. In all cases a 0.05 M with 0.1 M KCl in concentration and a pH of 7.4 is used.

Buffer	Anodic	**Cathodic**
Phosphate	7.22 ±1.7	7.3 ± 1.69
Tris	1.12 ± 0.41	1.01± 0.41
HEPES	9.56 ± 0.77	9.76 ± 0.44

Modified electrode

Again, the rate of charge transport through a PME was determined for PVI_{10}–Os–Prog. Figure 3.12, shows a Cottrell plot of PVI_{10}–Os–Prog and PVI_{10}–Os. A difference in the current obtained for these systems is observed. From Figure 3.12 it can be seen that there is similar rates of current decay for the oxidation process. By comparing results presented in Table 3.5 with those in Table 3.4 it is possible to observe that the presence of a biocomponent results in a slower rate of charge propagation. Additionally, the presence of the PEG exerts influence over this rate. Results obtained for the control experiment do show small errors, unlike the results for cyclic voltammetry, shown in Table 3.3 where large errors were observed. Such a reduction in errors confirms that chronoamperometry is a more suitable technique for studying rates of charge transport. Additionally, unlike the results obtained for cyclic voltammetry, it can be seen that there is less discrepancy between the anodic and cathodic response suggesting the influence of the counterions on the electrochemical response when using cyclic voltammetry.

Table 3.5, Results obtained for $D^{1/2}C_t$ (10^{-8} mol $(cm^2\ s^{-1})^{1/2}$) PVI_{10}–Os–progesterone with PVI_{10}-Os and control. All data is collected in 0.05 M phosphate buffer, pH 7.4 with 0.1 M KCl supporting electrolyte.

| Electrode	Anodic	Cathodic
PVI_{10}–Os	7.2±0.2	7.3 ± 0.469
PVI_{10}–Os–PEG	1.3 ± 0.04	1.21 ± 0.0418
PVI_{10}–Os–Prog	0.099± 0.0037	0.089 ± 0.44
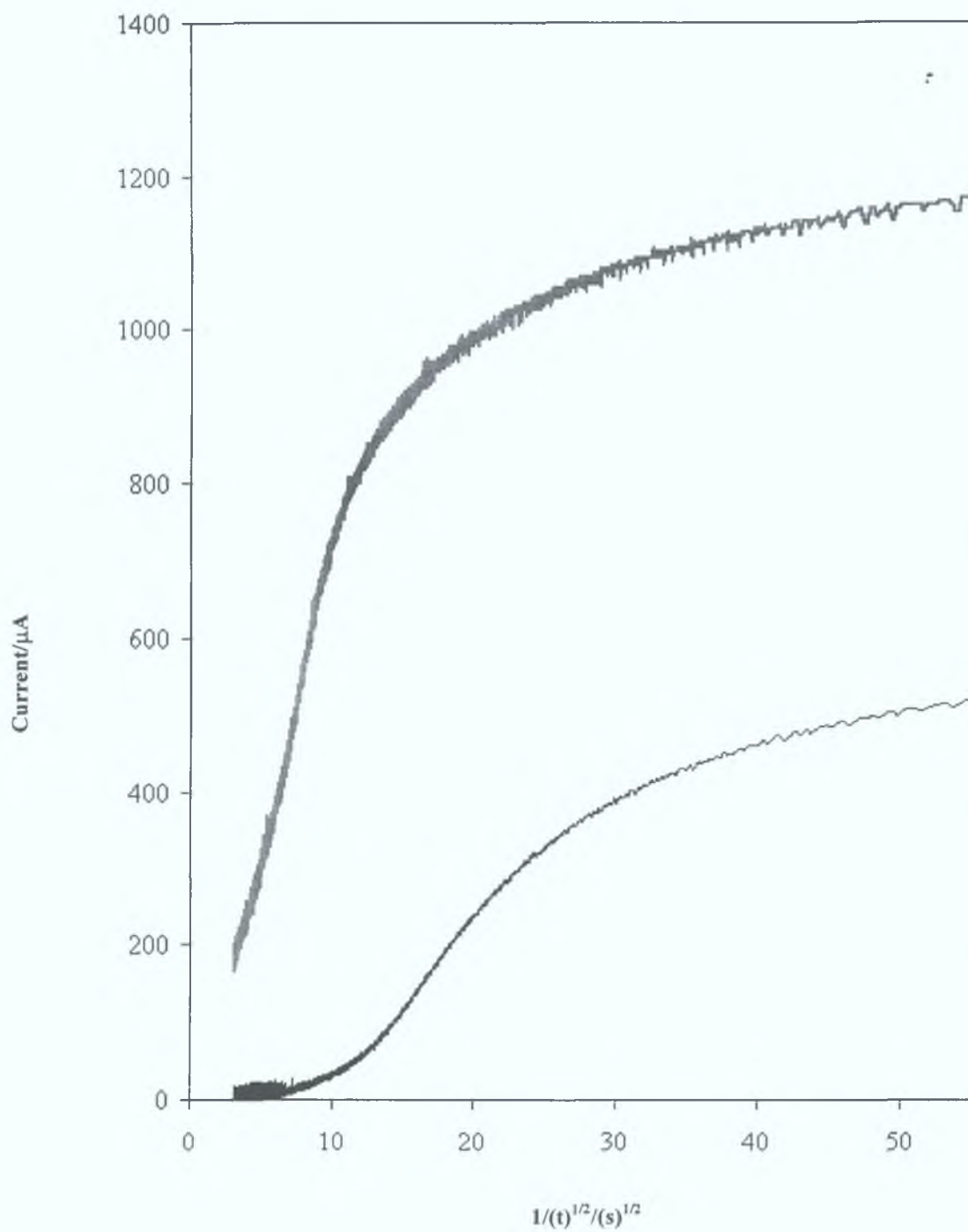
Figure 3.12. Chronoamperometry, from bottom; non-faradic processes for cathodic process, 0.00–0.10 V, 0.60–0.50 and faradic processes from 0.50–0.10. A 1.5 mm glassy carbon working electrode modified with PVI_{10}–Os–Prog, in aqueous 0.5 M phosphate buffer, pH 7.4, with 0.1 M KCl supporting electrolyte. A pulse width of 0.1s was used

3.4.3 Scanning electron microscope

The results obtained in Sections 3.4.1 and 3.4.2 demonstrate that the presence of a biocomponent has profound affects on the rate of charge propagation through a modified electrode. It was therefore decided to examine the nature of these PME using scanning electron microscopy (SEM).

There is a general consensus that film structure is likely to have a profound influence upon the properties of a PME, as it influences both the rate of charge transport of mobile species through the film and the local environment within which it undergoes mediated charge transfer reaction with polymer-bound redox sites.[34] SEM work was carried out to investigate the heterogeneous nature of the PME surface and determine if the topography of these modified electrodes does indeed exert influence over the charge transport. All magnifications are **X**10.

In Figure 3.13 an image of bare graphite electrode is shown with a relatively smooth surface. A comparison of Figure 3.13 with the modified electrodes is seen in Figure 3.14 and 3.15.

Figure 3.14 shows a SEM image of PVI_{10}–Os. Here a crystal-like structure is observed. In Figure 3.15 the SEM image contains that of PVI_{10}–OS–Prog. The overall appearance of Figure 3.15 differs very little from that of Figure 3.14 except for the appearance of large globule/node like features, more noticeable in the centre of the image. Although SEM is not regarded as a definitive analytical technique it is possible to obtain information regarding the type of surface i.e. homogeneous/heterogeneous, from the height and density of the images. From the images obtained in Figures 3.14 and 3.15 it may be said that both of these PMEs are indeed heterogeneous in nature with the PVI_{10}–Os–Prog appearing the more heterogeneous. For all images presented the electrode was scanned in the phosphate buffer at a scan rate of 0.1 Vs^{-1} for 20 cycles and left to dry overnight in a saturation chamber, as was described in Chapter 2.3.5.

SE   21-Oct-99   S3000N WD28.0mm 20.0kV x800   50um

Figure 3.13. SEM image (**X**10) of a bare graphite carbon electrode. Prior to scanning the graphite was polished and sonicated to obtain a smooth surface acceleration voltage is 2 V s^{-1}.

130

**Figure 3.14**. SEM image (X10) of PVI_{10}–Os scanned in 0.05 M phosphate buffer, pH 7.4, with 0.1 M supporting electrolyte for 20 continuous cycles at a scan rate of 0.100 Vs^{-1}. Acceleration voltage is 2 V s^{-1}.

Figure 3.15. SEM image (X10) of PVI_{10}–Os–Prog in 0.05 M phosphate buffer, pH 7.4, with 0.1 M KCl supporting electrolyte for 20 continuous cycles at a scan rate of 0.100 Vs^{-1}

### 3.4.4 Determination of heterogeneous electron transfer

Rapid electron transfer between electrodes and metallo-proteins is in general difficult to achieve within accepted analytical constraints. Because of this, most electrochemical studies of redox proteins have made use of small-molecule electroactive mediators, either free in solution or, as in the case here, confined to the electrode surface, thereby enhancing the rate of electron transfer between the electrode and the protein of interest. Many methods exist for the analysis of the rate of heterogeneous electron transfer including volumetric,[35,36,37] spectrophotometry,[38,39,40] and electrochemical monitoring.[29] Few procedures however, are capable of detecting substrate concentrations less than 10^{-6} M. This may be due a number of reasons: lack of sensitivity due to the properties of the assay components, instrumentation limitations or interferences.

The suitability of incorporating metallopolymers within PMEs for use as a biosensor has already been discussed in Chapter 1. Studies executed by Ohara[23] show the advantages of using osmium-containing PMEs for the incorporation of biocomponents. Among these advantages are the fast electron exchange dynamics, allowing the detection of rapid naturally occurring redox reactions that are not possible at an unmodified electrode surface.

Normal Pulse Voltammetry

Although cyclic voltammetry is an invaluable tool for deciphering many electrochemical properties, problems of sensitivity still limit these techniques. This is especially true for the determination of heterogeneous rate constants which require a highly sensitive method where the contribution from non-Faradaic current it negligible. Normal Pulse Voltammetry (NPV) belongs to a group of techniques known as pulse voltammetry. The excitation waveform consists of successive pulses of gradually changing amplitude between which a constant "initial" potential is applied, Scheme 3.1. The initial potential is usually chosen in a region where none of the sample components is electrochemically active. Usually the current is sampled at the end of the forward step and the remainder of the response is ignored. This sampled current is then plotted against the pulse height, Figure 3.16. The difference between successive sample currents is then plotted as a function of potential.

A close study of Figure 3.16 shows that initial pulse, Pulse 1, amplitude is insufficient to excite a Faradaic response hence the only current observed is associated with non-Faradaic processes – plateau level marked t_p. If this is then compared to a pulse recorded for Pulse 2, Figure 3.16*a*, which is large enough to excite a Faradaic response such that the measured current is as a result of Faradaic processes– rising portion of voltammogram observed in Figure 3.16*c*. All contributions associated with non-Faradaic or double layer charging have at this point decayed, as the current is sampled in the last stage of the pulse. Lastly, a pulse, Pulse 3, is taken at a point where the surface concentration is effectively zero resulting in a response which follows the Cottrell equation and demonstrated the limits to which classical chronoamperometry can be used.
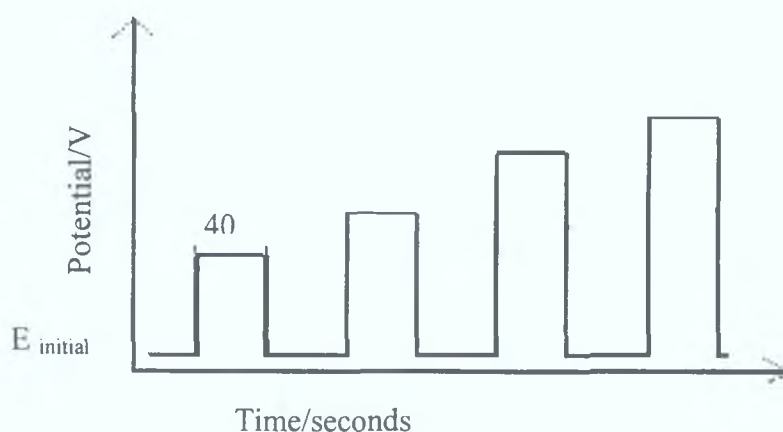
**Scheme 3.1.** Excitation waveform for normal pulse voltammetry
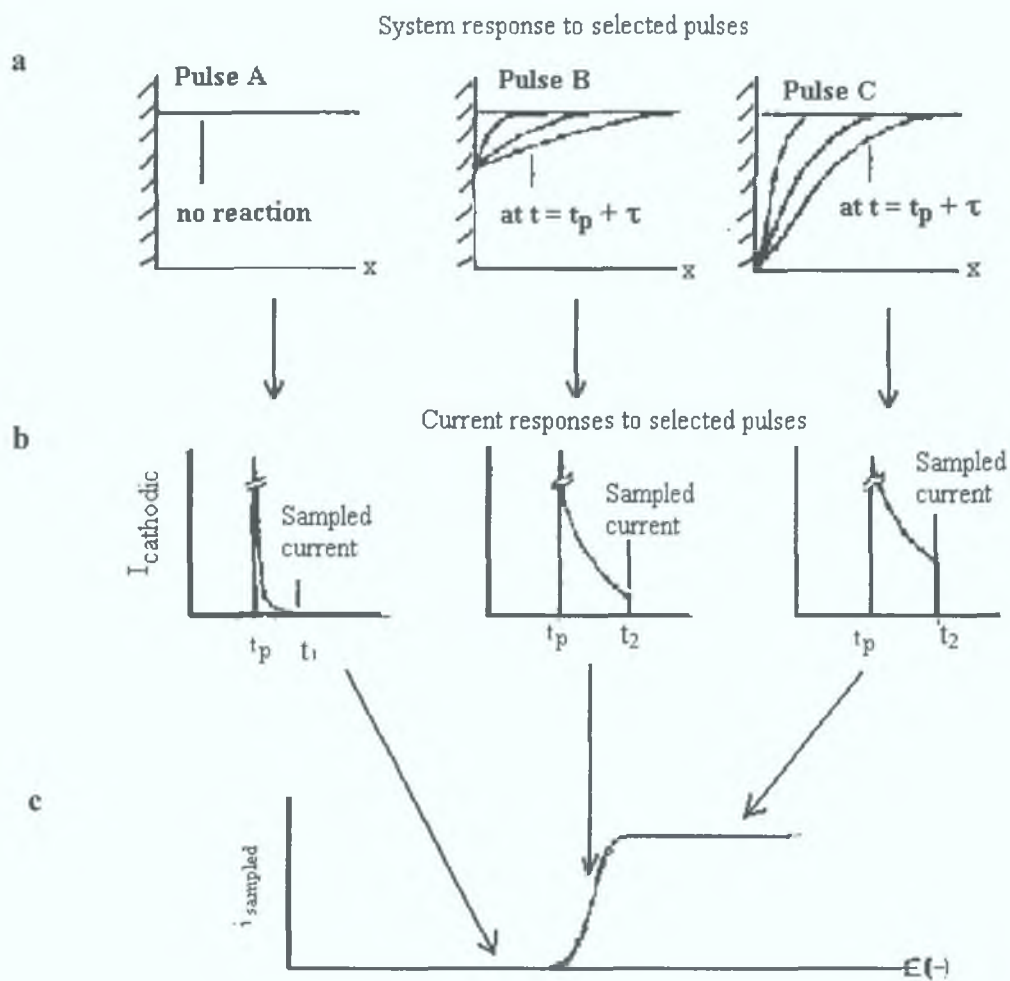
Figure 3.16. **(a)**. System response to various potential steps, **(b)** Current response to potential steps in a, i_c is cathodic current, and **(c)** plot of current vs. potential.

135

A typical sampled current voltammogram for the $Os^{2+/3+}$ oxidation within PVI_{10}–Os film in 0.05 M phosphate buffer, pH 7.4, with 0.1 M KCl electrolyte is shown in Figure 3.17. This sigmoidal–shaped wave is similar to those observed for solution phase reactants.[41] In agreement with Forster *et al*[29-31] the anodic current increases with decreasing sampling time while at the same time the half wave potentials of the voltammograms for the oxidation process shift in a positive direction with decreasing sampling times, Figure 3.17. This behaviour is accepted as being indicative of a Butler–Volmer response kinetics discussed in Chapter 1.5.[2] A detailed investigation through these films as described above strongly suggests that the response is diffusional in character and that significant migrational influence is absent. According to a method proposed by Matsuda[42] the analysis of the rising portion of the sampled current voltammogram for the process R → O + e⁻ permits determination of the standard rate constant, $k°$ and the transfer coefficient, α. The equation for the current – potential relationship is seen below, Equation 3.5:

$$E = E^* \pm \frac{RT}{\alpha nF} \ln \left\{ x \left[\frac{1.75 + x^2 [1 + \exp\pm\zeta]^2}{1 - x[1 \pm \exp(\pm\zeta)]} \right]^{1/2} \right\}$$ (Equation 3.5)

With

$$E^* = E^{1/2} \pm \frac{RT}{\alpha nF} \ln \left\{ \frac{4}{\sqrt{3}} \frac{k^* \sqrt{\tau}}{\sqrt{D_0}} \right\}$$

where, E is the electrode potential, $E_{1/2}$ is the reversible half wave potential, $k°$ is the standard heterogeneous electron transfer rate constant, τ is the sampling time, R the gas constant, T the absolute temperature, ζ a dimensionless parameter expressed as $[(nF/RT)(E - E_{1/2})]$, D_0 is the homogeneous charge transport diffusion coefficient as determined by the chronoamperometry experiments, and x is the ratio of the current at the potential E to the anodic limiting current. A plot of the right hand side (RHS) of Equation 3.5 against time should be linear, with a slope of $[(RT/\alpha nF)^{-1}]$ and an intercept E^*, Figure 3.18. This allows the relevant kinetic parameters α and $k°$ to be evaluated. For these experiments, the rate of heterogeneous electron transport is determined for the oxidation process only.

136
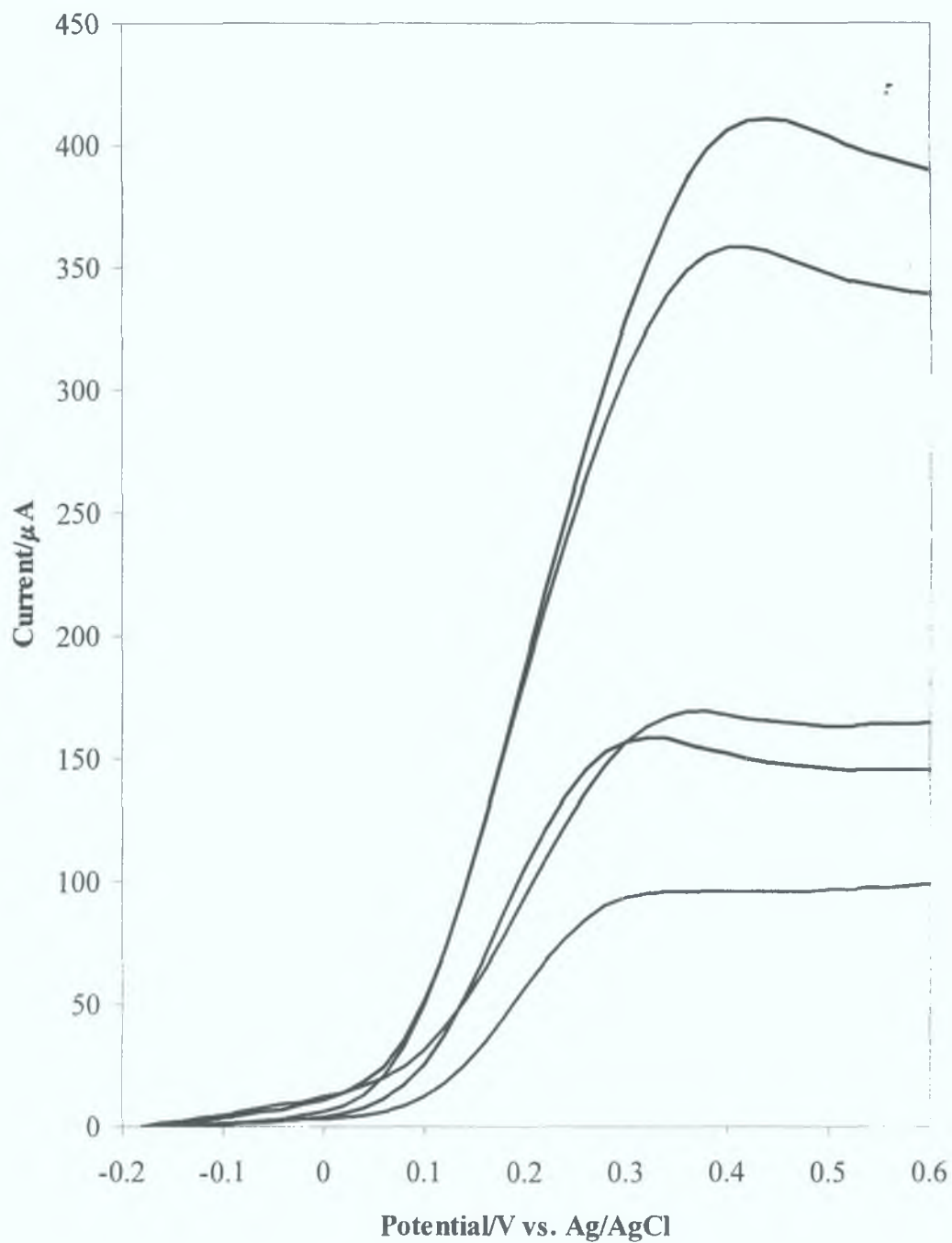
Figure 3.17. Sampled current voltammograms for the $Os^{2+} \rightarrow Os^{3+}$ reaction within PVI_{10}–Os films in 0.5 M phosphate buffer, pH 7.4, with 0.1 M KCl supporting electrolyte. Sampling times are from top to bottom 1, 2, 6, 10 and 12 ms. Surface coverage is 6.7×10^{-9} mol cm^{-2}

137
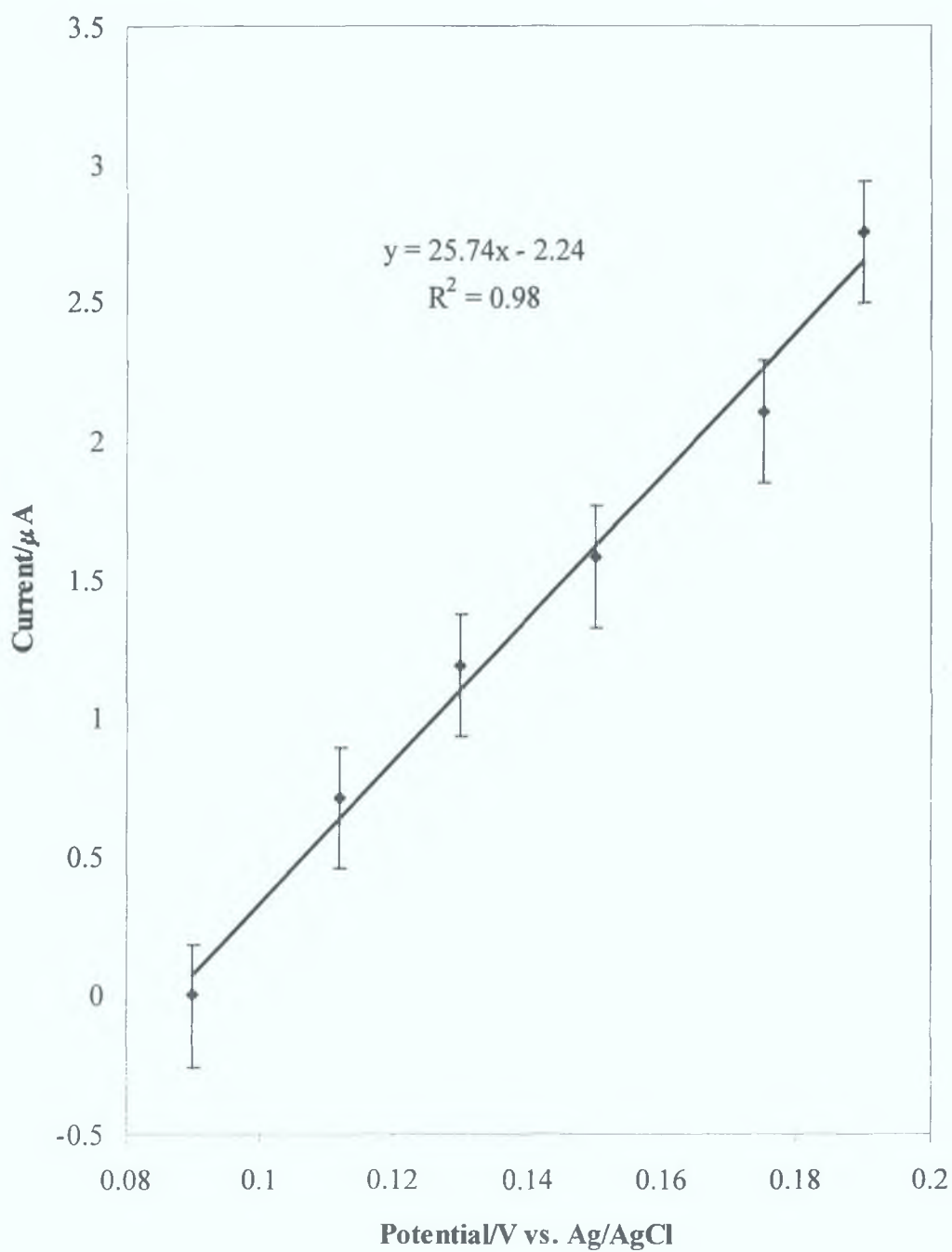
Figure 3.18. Plot of RHS of Equation 3.5 vs. time (s). For a PME of PVI_{10}–Os in 0.05 M phosphate buffer, pH 7.4, with 0.1 M KCl supporting electrolyte. Initial potential was 0 V, sampling time 4 ms, pulse width 3ms.

Analysis of all sampled voltammograms shown in shown in Figure 3.17 yielded straight lines with correlation coefficients ~0.99 and also similar slopes at the different sampling times. The consistency of these results suggests that the sample times chosen are sufficient to allow accurate determination of heterogeneous electron transfer. From the slopes in Figure 3.18 the charge transfer coefficient, α of 0.52 ± 0.05 was estimated for the oxidation process. The heterogeneous electron transfer rate constant, $k°$, obtained from the intercept of these plots can thus be estimated as 1.55×10^{-5} cm s^{-1}.

Modified electrode

The same analysis was carried out for the PVI$_{10}$–Os–Prog system with all experimental parameters kept constant. The sampled current voltammogram is shown in Figure 3.19, with the linear plot seen in Figure 3.20. From the slopes in Figure 3.20 the transfer coefficient of 0.61 ± 0.075 was estimated for the oxidation process. The heterogeneous electron transfer rate constant, $k°$, obtained from the intercept of these plots, was thus estimated as 5.11×10^{-5} cm s^{-1}.

Table 3.6. Heterogeneous electron transfer rate constant, $k°$ and transfer coefficient, α. All data was obtained using NPV in 0.05 M phosphate buffer, pH 7.4, with 0.1 M KCl supporting electrolyte.

PME	α	$10^5 \, k°$/cm s^{-1}
PVI$_{10}$–Os	0.52 ± 0.075	1.55 ± 0.12
PVI$_{10}$–Os–Prog	0.61 ± 0.075	0.51 ± 0.07
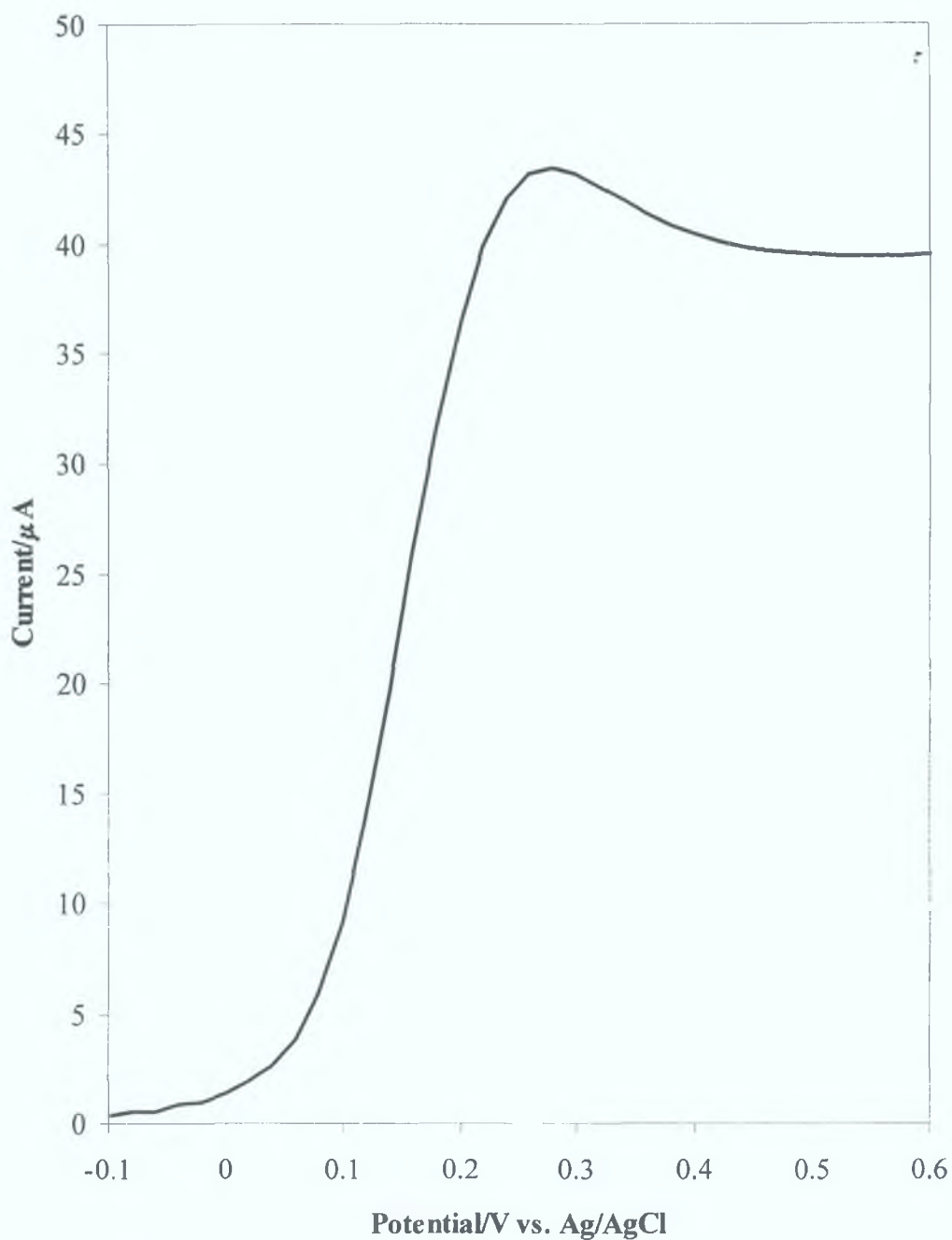
Figure 3.19. Normal pulse voltammogram of PVI_{10}–Os–Prog, in 0.5 M phosphate buffer, pH 7.4, with 0.1 M KCl supporting electrolyte. Working electrode was glassy carbon, starting potential was 0.6 V in a negative direction. Sample time of 4 ms pulse width 3ms. Initial potential was 0.6 V in a positive direction, surface coverage is 2.05 $X\ 10^{-9}$ mol cm^{-2}.
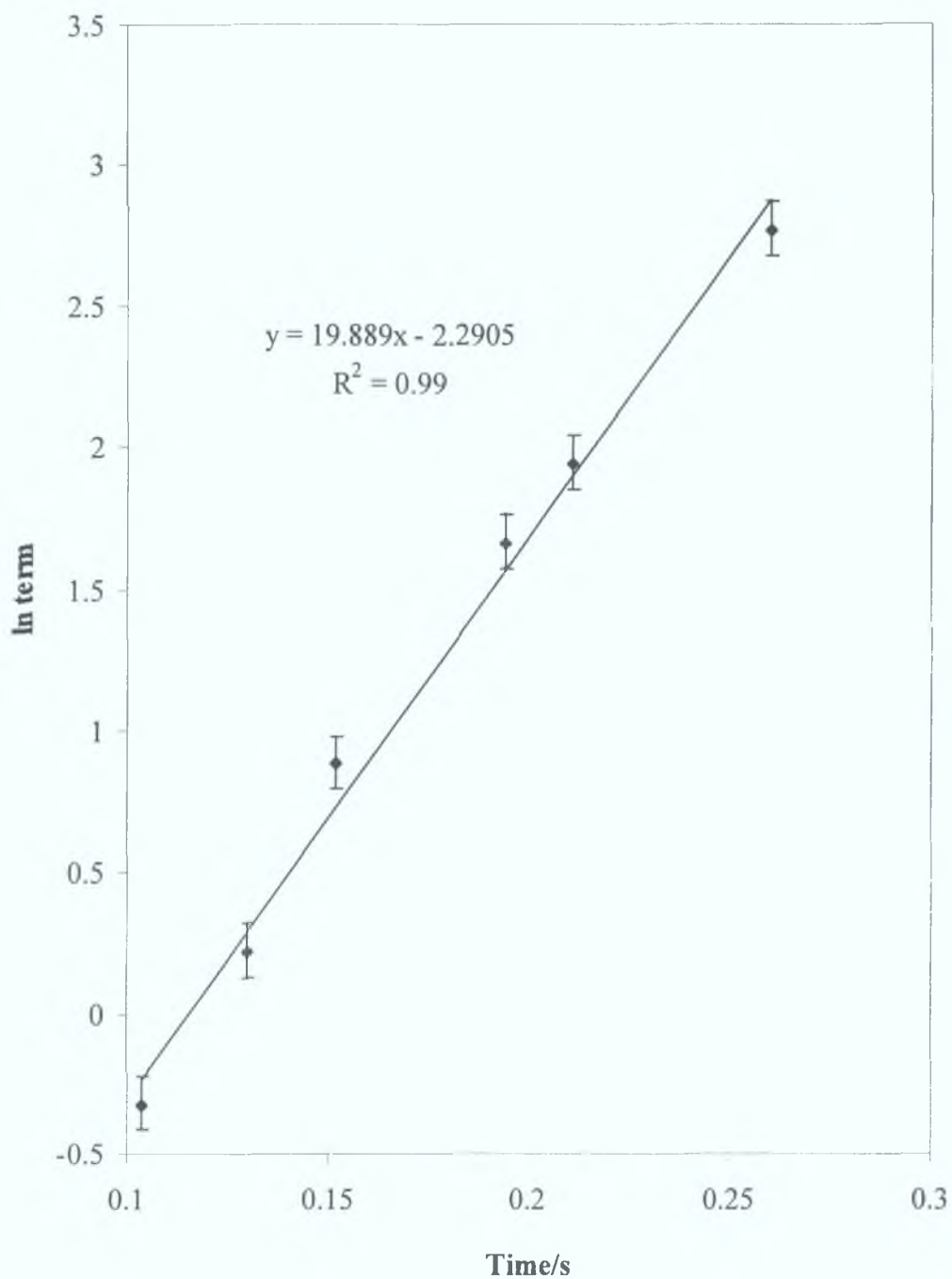
Figure 3.20. Plot of RHS of Equation 3.5 (ln term) vs. time/s. For a PME of PVI_{10}–Os–Prog, in 0.05 M phosphate buffer, pH 7.4, with 0.1 M KCl supporting electrolyte. Initial potential was 0 V, sampling time 4 ms, pulse width 3ms.

Earlier determinations[43,24,29-32] carried out with the same redox couple incorporated in a number of different polymers, yield a value of 3.4×10^{-4} cm s^{-1} for k° and a value of 0.16 ± 0.04 for the transfer coefficient, α.

The charge transport results, using phosphate buffer in Tables 3.2 and 3.3, demonstrate that the presence of a buffered electrolyte exerts influence over the rate of propagation through the modified electrode system. In agreement with the results shown in Tables 3.2 and 3.3 and literature results, the rate of heterogeneous electron transfer is slowed by a factor of ~20 for PVI_{10}–Os and a factor of ~60 for PVI_{10}–Os–Prog when compared to those results obtained by Forster[29-32] for a similar redox couple modified to the electrode surface, again $HClO_4$. In the reports by Forster the effect of electrolyte concentration and pH on the rate of heterogeneous electron transfer and transfer coefficient was illustrated.

3.5   Conclusion:

Recent work has investigated the influence of various solvents[28-33] on the rate of charge propagation through modified electrode systems. All these studies indicate the profound influence of solvent choice on the rate of charge propagation. However, to date very little information has been obtained regarding buffered systems and their influence on the electrochemical response, this is surprising when one considers the extent to which these buffers are used in electrochemical analysis. [6-15, 23, 33, 37]

In addition to this, there is a general consensus that the film structure is likely to have a profound affect upon the properties of a PME, as its' structure influences both the rate of transport of mobile species through the film and the local environment within which it undergoes a mediated charge transfer reaction with polymer-bound redox sites. Thus, slight alterations of the film studied here were made by incorporation of progesterone, a non-electroactive biocomponent, to eliminate any influence of electrochemical interferences. And as indicated in the SEM study the presence of progesterone does indeed alter the topography of the PME.

The results obtained for the effects of the most popular buffers,[6-15] used in electrochemical analysis show that the influence that they exert on the rate of charge transport is indeed significant. When these results are compared with previously collected data for various electrolytes such as $LiClO_4$ – which from previous studies in various electrolytes showed the slowest response – it is seen that the rate of charge propagation is more sluggish in all cases where a buffer is used. A difference in the value of $D^{1/2}C_t$ for the oxidation and reduction process was observed. To confirm these differences the same experiments were carried out using chronoamperometry. A comparison of the results, illustrated Tables 3.2–3.5, show a large difference between the data obtained using cyclic voltammetry and chronoamperometry.

Discrepancy between techniques has been observed previously while studying the electrochemical response obtained using cyclic voltammetry and comparing it to different techniques. These differences was often attributed to the timescale of the cyclic voltammetry experiments, but impedance spectroscopy performed at frequencies corresponding to the scan speeds used in cyclic voltammetry still exhibits such a discrepancy, which has further been shown to be potential

amplitude dependent.[44,45,46,47] Understanding the cause of this anomaly is important in the determination of the rate of charge propagation. In a study of Nafion® with incorporated $Os(bpy)_3^{3+/2+}$, charge propagation diffusion coefficients based on electroactive amount measured by cyclic voltammetry showed a strong dependence on the available concentration of electroactive species.[48] Anson et al[49] support this concentration dependence theory. Measurement by impedance spectroscopy show this concentration dependence is even more striking. A model proposed by Aberg and Sharp[21] suggests that the transfer of counterions to and from electroactive sites requires activation energies and, by necessary coupling to the electron transport, is responsible for the discrepancies observed. Such an argument can be supported by the presence of a triply and doubly charge polymer matrix, when $Os^{2+} + e^- \leftarrow\rightarrow Os^{3+}$ occurs. The model postulated by this group is based on the concept that some electroactive sites are freely accessible to counterions whereas other sites require a sufficient potential gradient in order to overcome barriers presented by the film, suggesting the presence of non-equivalent electroactive sites.

Aberg et al[21] also demonstrated that the size of the counterions involved in maintaining electroneutrality exerts influence over the observed rates of propagation. The data presented above for the various buffers is in agreement with what was put forward by Aberg et al, where the larger counterions associated with HEPES and Tris buffer result in a slower rate of charge propagation through the PME, even when a 0.1 M KCl is used. An electrochemical quartz crystal (EQCM) study[50] showed that, at the start of the oxidation process, cation expulsion occurs while anion uptake occurs at potentials more positive than E_p. In this study[50] it was suggested that contribution of counterions is a function of potential in cyclic voltammetry experiments. This could explain the discrepancy between the oxidation and reduction procedure seen for cyclic voltammetry. Also it has been observed[21] that a variation in oxidation and reduction currents is as a result of morphological changes within the modified electrode due to this counterion movement. While chronoamperometry results show that, although there is a difference between the rates of charge propagation for the oxidation/reduction process, it is well within experimental error. However, there does still exist a difference in the rates of charge propagation for the various buffers. This in agreement with Hiratsuka et al[51] who suggest, that in the presence of different counterions, the interior

144

of the polymer matrix changes resulting in a different electrochemical response associated with the accessibility of redox sites for reduction and oxidation.

From the results obtained above, it may be said that the electrochemical response in buffered electrolytes, exerts influence in the rate of charge propagation through a PME. When one considers the size of available counterions contributed by the various buffer species for maintaining electroneutrality, these results are not surprising.

It has long been established that catalytic activity of redox polymer modified electrodes may be limited by different factors: the mass transport of the substrate across the polymer film | solution interface, the diffusion of the substrate from the film | solution interface towards the electrode | film interface, the diffusion like propagation of charge and finally the rate of electron exchange between the redox mediator and the electrode.[52] Hence, further investigation into the standard heterogeneous rate constant was used to determine if the presence of a biocomponent affects the rate at which electrons are transferred within the modified electrode or if the presence of the biocomponent is influencing factor.

It is generally accepted that the rate of charge transport in such polymer films proceeds by an electron hopping process.[53] This process is in turn accompanied by the motion of charge compensating counterions, solvent and polymer chain segments. It is the interplay between these processes that will ultimately determine the rate at which charge may be transported to these materials. From the initial data presented in Tables 3.2–3.5 demonstrate that the nature of the interaction between solvent and polymer has profound influence on the electrochemical properties of PVI_{10} - Os. The enhanced responses in phosphate buffer over the other two buffers used may likely reflect more facile ion motion within the polymer film. As was previously stated the use of phosphate buffer might result in a more swollen film that facilitates ion motion through the polymer. However, a comparison of the rates of charge propagation for PVI_{10}–Os with PVI_{10}–Os–Prog show a more sluggish rate of charge transport for the latter. For this reason it was decided to examine if the rate of electron exchange proved to be a limiting factor in the overall electrochemical response. Results presented in Table 3.6 show these results.

145

The deviation of these values, from those obtained for solution phase species has been observed previously and was explained by Savéant *et al*[54] in terms of partial blocking of the electrode surface by the modified film was suggested. However, unlike the results obtained previously for various systems, which showed little or no deviation between osmium covalently attached to the electrode surface or electrostatically attached, a deviation of a factor of ~20 seen for PVI_{10}–Os and a factor of ~60 for PVI_{10}–Os–Prog.

In conclusion, it may be said that the use of buffered electrolyte systems does indeed affect the rate of both charge propagation and electron transfer through a modified electrode. The rate of transport (couple electron and counter ion motion) through a polymer matrix is affected by the nature of the counterions, notably their size, which are required to satisfy the overall electroneutrality. With the advent of nano-technologies that will allow greater assay sensitivity choosing the most appropriate electrolyte for development of biosensors will play a vital role in maximising their sensitivity.

3.6   References

1.   de Haro, C.; Mas, R.; Abadal, G.; Muñoz, J.; Perez-Murano, F.; Domínguez, C. *Biomaterials*, **2002**, *23*, 4515

2.   Bard, A. J.; Faulkner, L. R. *Electrochemical Methods: Fundamentals and Applications*, Chapter 3, 1980, p

3.   Wehrens, R.; van der Linden, W. E. *Anal. Chim. Acta*, **1996**, *334*, 93

4.   Weiya, X.; Wentao, M.; Kaiyang, L.; Jiming, H, Liaorong, S.; Hongyi, L.; Lianxin, C. *Sensors and Actuators B, Chemical*, **2002**, *86*, 174

5.   Wang, J. *Analytical Electrochemistry*, VCH publisher, New York, New York, 1994.

6.   Doong, R. A.; Tsai, H. C. *Anal. Chim. Acta*, **2001**, *434*,239

7.   Vidal, M. M.; Delgadillo, I.; Gil, M. H.; Chamarro, A. *Biosens. Bioelectron.*, **1996**, *4*, 347

8.   Brinkman, E.; Van der Dos, L.; Bantjes, A. *Biomaterials*, **1991**, *12*, 63

9.   Lund, N.; Sjöberg, F.; Guldbrans, H.; Walfridsson, H.; Edwall, G. *Int. J. Clin. Monitoring and Computing*, **1984**, *3*, 147

10.   Gäberlein, S.; Knoll, M.; Spener, F.; Zaborosch, C. *Analyst*, **2000**, *125*, 2274

11.   Mulchandani, A.; Mulchandani, I.; Kaneva, W.; Chen, H. *Biosens. Bioelectron.* **1999**. *14*, 77

12.   Mulchandani, I.; Kaneva, W.; Chen, H. *Anal. Chem.*, **1990**, *70*,5042

13.   Mulchandani, A.; Mulchandani, I.; Kaneva, W.; Chen, H. *Anal. Chem.*, **1998**, *70*, 4140

14.   Steinschaden, D.; Adamovic, G.; Jobst, R.; Glatz G.; *Sensors and Actuators B*, **1997**, *44*, 365

15.   Van Os, J.; Bult, A.; Koopal, C. G. J.; Van Bennekom, W. B. *Anal. Chim. Acta*, **1996**, *335*, 209

16.   Dart, R. D.; Vaughan, J. *Physiology*, **1992**, *451*, 365

17.   Bielen, V.; Bosteels, S.; Verdonck, F. *J. Physiol.*, **1990**, *427*, 325

18.   Katz, E.; Riklin, A.; Heleg-Shabtai, V.; Willner, A.; Bückmannare, A. F. *Anal. Chim. Acta*, **1999**, *385*, 45

19. Inzelt, G.; Pineri, M.; Schultze, J. W.; Vorotyntsev, M. A. *Electrochim. Acta*, **2000**, 2403

20. Sharp, M. *Electroanal. Chem.,* **1998**, *449*, 137

21. Aberg, S.; Sharp, M. *J. Electrochim. Acta*, **1998**, *449*, 121

22. Aoki, A.; Rajagopalan, R.; Heller, A. *J. Phys. Chem.*, **1995**, *99*, 5102

23. Ohara, J.; Rajagopalan, R.; Heller, A. *Anal. Chem.*, **1993**, *65*, 3512

24. Forster, R. J.; Kelly, A. J.; Vos, J. G.; Lyons, M. E. G. *J. Electroanal. Chem.*, **1989**, *270*, 365

25. *Laboratory Techniques in Electroanalytical Chemistry*, Kissenger, P. T.; Heineman, W. R.; **(Eds.)**, 2nd edition, Marcel Dekker Inc. 1996.

26. Wilson, R. W.; Cubitt, R.; Glidle, A.; Hillman, A. R.; Saville, P. M.; Vos, J. G. *Electrochim. Acta.*, **1999**, *44*, 3533

27. Inzelt, G.; Pineri, M.; Schultze, J. W.; Vorotyntsev, M. A. *Electrochim. Acta.*, **2000**, *45*, 2403

28. Meerholz, K.; Heinze, J. *Electrochim. Acta*, **1996**, *41*, 1839

29. Forster, R. J.; Kelly, A. J.; Vos, J. G.; Lyons, M. E. G. *J. Chem. Soc. Faraday Trans.*, **1991**, *87*, 3761

30. Forster, R. J.; Vos, J. G. *Electrochim. Acta*, **1992**, *37*, 159

31. Kelly, A. J.; Ohasaka, T.; Oyama, N.; Forster, R. J.; Vos, J. G. *J. Electroanal. Chem.*, **1990**, *287*, 185

32. Kelly, A. J.; Oyama, N. *J. Phys. Chem.* **1991**, *95*, 9579

33. Huangxian, J.; Leech, D. *Anal. Chim. Acta*, **1997**, *345*, 51

34. Kelly, D. M.; Vos, J. G. *Electrochim. Acta*, **1996**, *11*, 1825

35. Schumb, W.C.; Satterfield, C.N.; Wentworth, R.L.; *Hydrogen Peroxide*, Reinhold, New York, 1955,

36. Vogel, A. I. *Textbook of Quantitative Inorganic Analysis*, Longman, New York, 1978

37. Hurdis, E. C.; Romeyn, H. *Anal. Chem.*, **1985**, *57*, 1107

38. Atriss, J. D.; Thibert, R. J.; McInotosh, J. M.; Zak, B. *J. Microchem.* **1981**, *26*, 487

39. Frew, J. E.; Jones, P.; Scholes, G. *Anal. Chim. Acta*, **1983** *155*, 191,

40. Matsubara, C.; Kudo, K.; Kawashita, T.; Takamura, K. *Anal. Chem.*, **1985**, *57*, 1107

41. Ohsaka, T.; Oyama, N.; Yamaguchi, S.; Matsuda, H. *Bull Chem. Soc. Jpn.*, **1981**, 54, 2475

42. Matsuda, H. *Bull. Chem. Soc. Jpn.*, **1983**, *26*, 3439

43. Oyama, N.; Ohsaka, T.; Ushirogouchi, T.; Sanpei, S.; Nakamura, S. *Bull. Chem. Soc. Jpn.*, **1988**, *61*, 3103

44. Ren, X.; Pickup, P. G. *J. Electroanal. Chem.*, **1994**, *372*, 289

45. Kalaji, M.; Peter, L. M. *J. Chem. Soc. Faraday Trans.* **1991**, *87*, 853

46. Rubenstein, I.; Sabatani, E.; Rishpon, J. *J. Electrochem Soc.*, **1987**, *134* 3078.

47. Tanguy, J.; Petiot, F. *J. Electrochem. Soc.* **1987**, *134*, 795

48. Sharp, M.; Lindholm, B.; Lind, E. L.; *J. Electroanal. Chem.* **1989**, *274*, 35

49. Anson, F. C.; Blauch, D. N.; Savent, J. M.; Shu, C.-F. *J. Am. Chem. Soc.* **1991**, 113, 1922

50. Pruneanu, S.; Csahók, E.; Kertész, V.; Inzelt, G. *Electrochim. Acta*, **2000**,. *43*, 2305

51. Hiratsuka, A.; Muguruma, H.; Nagata, R.; Nakamura, R.; Sato, K.; Uchiyama, S.;. Karu, I. *J. Membrane Sci.*, **2000**, *175*, 25

52. Hoffer, E.; Steckhan, E.; Ramos, B.; Heineman, W. R. *J. Electroanal. Chem.*, **1996**, *402*, 115

53. Kauyfman, F. B.; Schroeder, A. H.; Engler, E. M. Kramer, S. R.; Chambers, J. Q. *J. Am. Chem. Soc.*, **1980**, *102*, 483

54. Amatore, C.; Savaent, J. M.; Tessier, D. *J. Electroanal. Chem.*, **1983**, *146*, 37

Chapter 4

Construction and Characterisation

of Carbon–Polymer Biocomposite

Electrodes

4.1   Introduction

The advantages of surface modified electrodes have been discussed in the previous two chapters. Due to the laborious modification techniques that are required, these surface modified electrodes have found limited application to "real world" analysis. In contrast, carbon paste electrodes (CPE) that were invented at the end of the 1980s find more common application.[1] A CPE consists of a mixture of carbon powder and a pasting liquid. The pasting liquid is chosen to be inert, pure, and electro inactive and to have low volatility and solubility in the analyte solution. Paste materials include aliphatic hydrocarbons, mixtures of hydrocarbons, aromatic compounds, and silicone oils. The carbon is chosen to have a uniform particle size, high chemical purity, low adsorption of oxygen, and insignificant electrochemical impurities. The composite typically consists of approximately 70% carbon by weight.[1] The simplicity of modification and the convenience in manipulation of this type of electrodes stimulated a further investigation into possible analytical applications. This investigation continued for numerous years in spite of the several drawbacks associated with CPEs such as, relatively poor operational stability, poor reproducibility, denaturation of the enzymes in the organic paste matrix,[2,3] leakage of enzymes and other materials and a lower sensitivity.[4]

Advances in the area of material science have opened new doors to analytical sensing. With this in mind, advancements of CPEs were achieved, by replacing the soft viscous binding agent with solid-binding agents like epoxy, Kel-F and Teflon. When these materials are mixed with conducting particles, and, allowed to cure/harden, all the merits of CPEs are produced with the additional advantages of no leaching of modifier from the electrode surface and capability to use a greater range of supporting electrolytes. Although, these electrodes have mainly found use as detectors for HPLC, it has been reported that they possess all the desired characteristics needed for a stand-alone sensor.[5]

The carbon–composite electrodes used in this study have been employed in sensor technology[19,24,28] for a number of years and have proven to be successful. From an electrochemical perspective, what is fundamentally important is that sufficient distribution of conducting graphite powder within the polymer matrix is achieved. If there is a low density of carbon within the polymer the composite will behave more like an insulator rather than conductor, rendering it useless for electrochemical applications.

Research[6] shows that a variation of the carbon content within the polymer matrix results in a sizeable shift of the working potential and variations in the residual currents with optimum performance achieved at a ratio of 1:4 (w/w) for carbon to polymer.

One consistent property of these carbon–polymer composite electrodes, which has been mentioned since the first paper[17] describing these composites appeared, is that of ultramicroelectrode (UME) behaviour, known as steady state voltammetry.[18,19,24] The importance of UMEs are well documented.[7] However, while UMEs have made a fundamental and applied impact on electrochemistry[8] unequalled by almost any other electrochemical approach in recent times, their application to sensing technology has not yet been realised. Previously this lack of application was blamed on the need for specialised expensive instrumentation, electromagnetic interferences and lack of robustness associated with their design.[9] With recent advances in engineering technology overcoming the former two drawbacks, the latter problem is currently being addressed using spontaneously assembled monolayers,[10,11,12] as a model for sensor applications, where a reduced content of analyte is required to obtain an analytical signal.

It is the consistent reporting of UME behaviour, which has instigated much of the experimental work described in this Chapter. In order to understand how this steady-state behaviour is occurring a comparative investigation into the well-known characteristics of UME was carried out on these graphite epoxy polymer composite electrodes. This characterisation involved: Scanning Electron Microscopy (SEM) to visualise the nature of dispersion of carbon within the epoxy polymer. Kinetic analysis, to determine the rate of heterogeneous electron transfer was conducted using the electrochemical technique, cyclic voltammetry. A study of the RC time constant was conducted. If the value of the RC time constant is sufficiently low – indicating a negligible contribution of charging current to the overall current obtained – it will allow these electrodes to be used for probing fast electron transfer reactions. Given the indication of UME behaviour while using these composites, the electrochemical response in a medium containing no electrolyte was also investigated as this is another property of UMEs. Also to estimate the conductivity path of the sample at various points across the surface single point resistance measurements were taken. All experiments were carried out in parallel using a glassy carbon macroelectrode whose active surface area approximates to the theoretical active surface area of these

composites while at the same time confirming the unique behaviour seen using these electrodes.

4.2 Instrumentation

Cyclic voltammetry measurements were carried out using Autolab PGSTAT 20(Eco-chemie, The Netherlands). A platinum auxiliary electrode (Crison 52-67 1) and a double junction Ag/AgCl reference electrode (Orion 900200) with 0.1 M KCl as an external reference solution was used. The carbon composite electrodes made in house as described in Section 4.4.1 were used as the working electrodes. SEM images were obtained using a HITACHI S-570 SEM. Resistance measurements were carried out using tungsten wire (tip size was 10μm) and a semi-conductor analyser from Wentworth Laboratories.

4.3 Materials and reagents

The composite electrodes were prepared using graphite powder with a particle size of 50 μm (BDH, UK), Epotek H77 (epoxy resin) and hardener (Epoxy Technology, USA). $K_3Fe(CN)_6$ and KCl were purchased from Sigma. All solutions were made up in Milli-Q water.

4.4 Experimental

4.4.1 Construction of carbon-polymer composite electrode

For every gram of graphite powder used for the composite mixture four grams of epoxy resins were mixed, yielding a ratio of 1:4 (w/w). This mixture was thoroughly hand mixed to ensure uniform dispersion of the carbon particles throughout the epoxy polymer resin. The resulting paste was placed into a PVC cylindrical sleeve body (6 mm i.d.) to a depth of 3 mm that had an electrical contact, as shown in Figure 4.1. The composite material was cured at 50 °C for one week.[13] Prior to each use, the electrode was wet with doubly distilled water and then mechanically polished with abrasive paper and alumina paper (polishing strips 301044-001, Orion) to give a smooth mirror finish. Subsequently, the working surface was dipped in 10% (v/v) aqueous nitric acid for 10 s. removing organic surface contaminants.[36] The electrode surface was then thoroughly rinsed with Milli-Q water for a further 30 s.

4.4.2 Single point conductivity experiments

Having followed the polishing procedure outlined in Section 4.4.1, the carbon disc was removed from the surrounding Teflon shroud and placed directly into the sample chamber of the semiconductor analyser. Various resistance measurements were taken at random points across the surface of the carbon disc.

4.4.3 Electrochemical experiments

After following the polishing procedure described in 4.4.1, the working electrode was immersed in a solution containing 1.6 mM $K_3Fe(CN)_6$ and 1.0 M KCl as supporting electrolyte that was previously deoxygenated with nitrogen. For steady-state investigations, the scan rate employed was 0.005 Vs^{-1}. Investigation into the rates of heterogeneous electron transfer was carried out when values of ΔE_p were greater than 0.1 V, compensation for ohmic drop was made in accordance with the values obtained in Table 4.2. In all cases a potential range of –0.600–1.200 V was used. For comparison, and to illustrate the unique behaviour of these carbon composite electrodes, control experiments was carried out using a glassy carbon macroelectrode (area $0.07cm^2$)
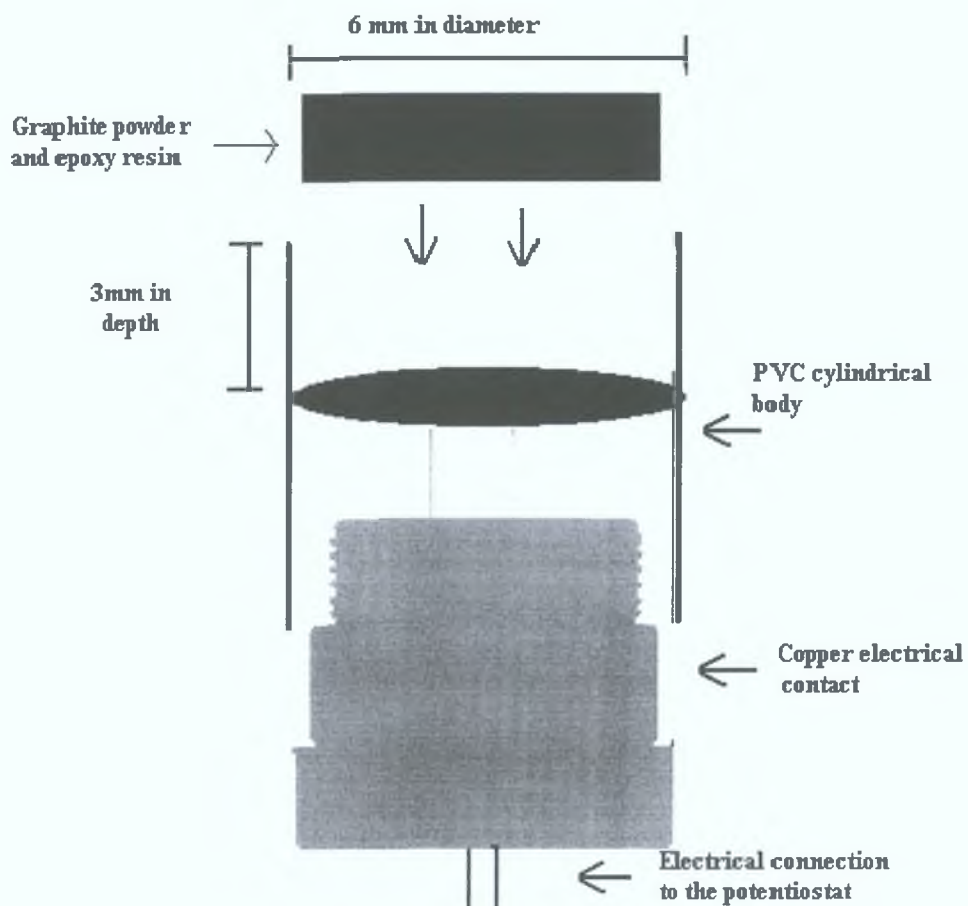
Figure 4.1. Design of a carbon–polymer biocomposite. The carbon–polymer mixture is compressed into the top of a PVC cylinder (6 mm i.d.) at the bottom an electrical connection is placed, on top of which is a copper disc, allowing electrical communication between the composite electrode and the potentiostat.

4.5   Results and discussion

4.5.1   Overview of carbon-composite electrodes

The mixing of a carbon with a binding substance is not a new science. In fact, since the concept of carbon paste electrodes was first postulated by Adams in 1958,[14,15,16] research into this field has come a long way. The first attempts at making carbon paste electrodes were instigated by the necessity to prepare an electrode that could be used in positive potential ranges where mercury electrodes could not be employed. It was thought that this alternative to a dropping mercury electrode could be set up by a capillary connected to a reservoir filled with a suspension of carbon powder in a suitable organic liquid. However, such an electrode assembly was shown to have no practical use because of high electrical resistance and instability in various medium due to too high liquid matrix content.[14]

An improvement on the problem of high electrical resistance and, therefore; electrochemical performance, of these carbon paste electrodes was postulated in 1989[17] which used carbon fibres, with dimensions in the nanometer range, cross-linked with a poly(vinyl-ferrocene). By using a polymer matrix, which upon curing hardens with time, mechanical and chemical stability of the composite is achieved thus overcoming some of the problems associated with the more traditional carbon paste electrodes. Additionally, it was reported that this new class of electrodes possessed sensitivity, selectivity and a detection limit equivalent to surface-modified electrodes.[10] Also, the signal to charging ratio(s/n) and the steady-state behaviour mimicked a classical UME. The suitability of using a polymer matrix to disperse graphite carbon is due to its plastic nature which allows the carbon content to be varied, while at the same time creating the possibility of incorporating enzymes to create biosensors.[10,11]

Since, the first paper[17] appeared on carbon–composite electrodes many research groups have devoted much time to optimising the performance of these electrodes by altering the carbon content,[18,19] polymer type[20,21] and in the case of biosensors the percentage biocomponent within the matrix.[22,23] To date two excellent reviews exist on the analytical application of carbon composite electrodes.[24,25]

The carbon–composite electrodes used in this study have been employed in sensor technology[19,24,28] for a number of years and have proven to be successful. What is fundamentally important, from an electrochemical aspect, is that sufficient distribution of conducting graphite powder within the polymer matrix is achieved. If there is an uneven distribution, within the carbon–polymer matrix there is a large chance, that the composite will behave more like an insulator rather than conductor, rendering it useless.[13] The suitability of carbon as a material for a working electrode has already been discussed in Section 1.1. Research shows that a variation of the carbon content within the polymer matrix results in a sizeable shift of the working potential and also variations in the residual currents,[26] as factors such as conductivity affect the overall performance of these electrodes, especially if the ratio of carbon: polymer is too low. Another factor, which dictates the polymer choice, is the intended application of the electrode. For instance, if an electrodes intended use is a biosensor application, the compatibility of the polymer for the biocomponent is an important consideration, especially when incorporating an enzyme within the composite.

The epoxy polymer chosen for these composites is based on a long history of successful applications as a biosensor.[27,28] In brief, epoxy resins are a family of polymers widely used for their excellent chemical properties, their good adhesion to other materials and their excellent insulating characteristics.[29]

A composite results from the combination of two or more dissimilar materials. Each individual component keeps its original properties while giving the composite distinctive chemical, physical and mechanical properties different from the original components. Classification of a composite, especially when formed from both and insulating and conductive phase, depends on the arrangement of both components within the composite. The composites used in this study are known as dispersion type composites. Regarding electrode characteristics, the most important properties are concerned with the capability of current to flow either to or from the working electrode surface. From extensive studies carried out, it is known that the electrical properties of the composite depend greatly on the nature of the components, the relative quantities of each component, i.e., graphite, polymer, and their distribution. The electrical resistance of these composites is determined by connectivity of the conducting particles within the polymer matrix. Previously,[30] a percolation curve (log resistivity vs. % graphite) was

constructed to determine to optimum quantity of each component within the matrix. In construction of a percolation curve there is a minimum threshold beyond which no conductivity is achieved. Below this critical value, the composite behaves as an insulator, due to high electrical resistance, and is not very useful from the electrochemical point of view, as a conductive substrate is essential so that current can flow. Previous studies show that a ratio of graphite: epoxy of 1:4 (w/w) is sufficient to allow maximum conductivity.[24]

4.5.1.1   Scanning electron microscopy

High-resolution microscopy, i.e., scanning electron microscopy (SEM), Scheme 4.1, is a very valuable technique to establish this distribution and heterogeneous nature of the carbon–composite electrode. In SEM a very fine "probe" of electrons with energies up to 40 keV is focused at the surface of the specimen in the microscope and scanned across it in a 'raster' or pattern of parallel lines. A number of phenomena occur at the surface under electron impact, as illustrated in Scheme 4.2; most important for scanning microscopy are the emission of *secondary electrons* with energies of a few tens eV and re-emission or reflection of the high-energy backscattered electrons from the primary beam. The intensity of emission of both secondary and backscattered electrons is very sensitive to the angle at which the electron beam strikes the surface, i.e. to topographical features on the specimen. The emitted electron current is collected and amplified; variations in the resulting signal strength as electron probe is scanned across the specimen are used to vary the brightness of the trace of a cathode ray tube being scanned in synchronism with the probe. There is thus a direct positional correspondence between the electron beam scanning across the specimen and the fluorescent image on the cathode ray tube. The magnification produced by scanning microscope is the ratio between the dimensions of the final image display and the field scanned on the specimen. Usually magnification range of SEM is between 10 to 200 000 X. and the resolution (resolving power) is between 4 to 10 nm (40 - 100 Angstroms).

Strictly speaking, SEM is not a widely accepted analytical technique. However, the principles underlying this microscopic method lend it favourable advantages to retrieve quantitative information, especially in the case of a sample containing only conducting and non-conducting material.
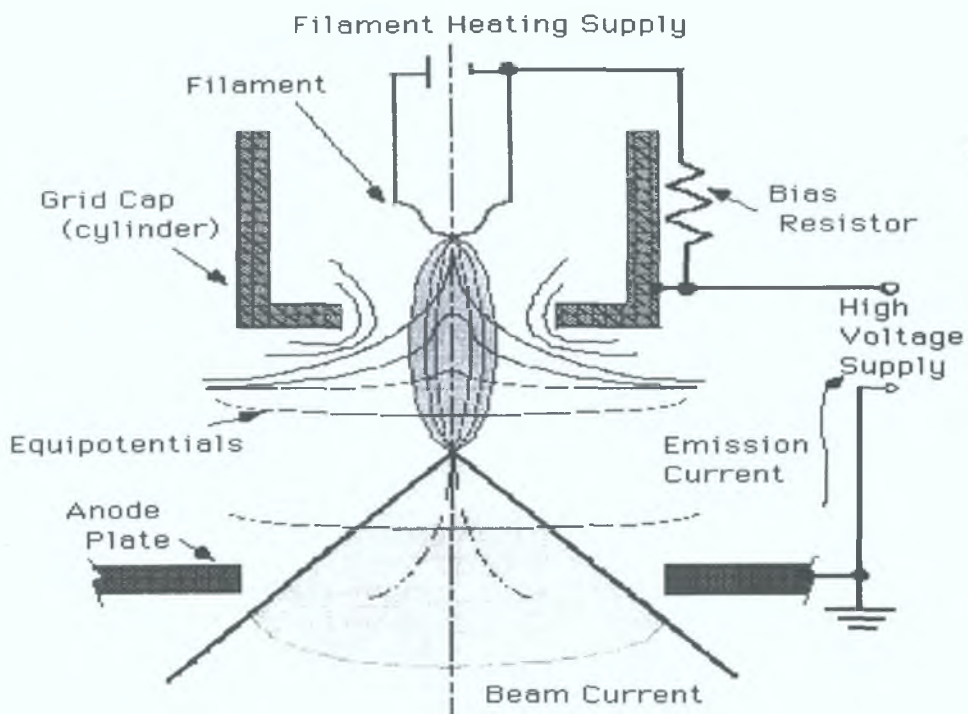
Scheme 4.1. Image of path of electron beam within the SEM
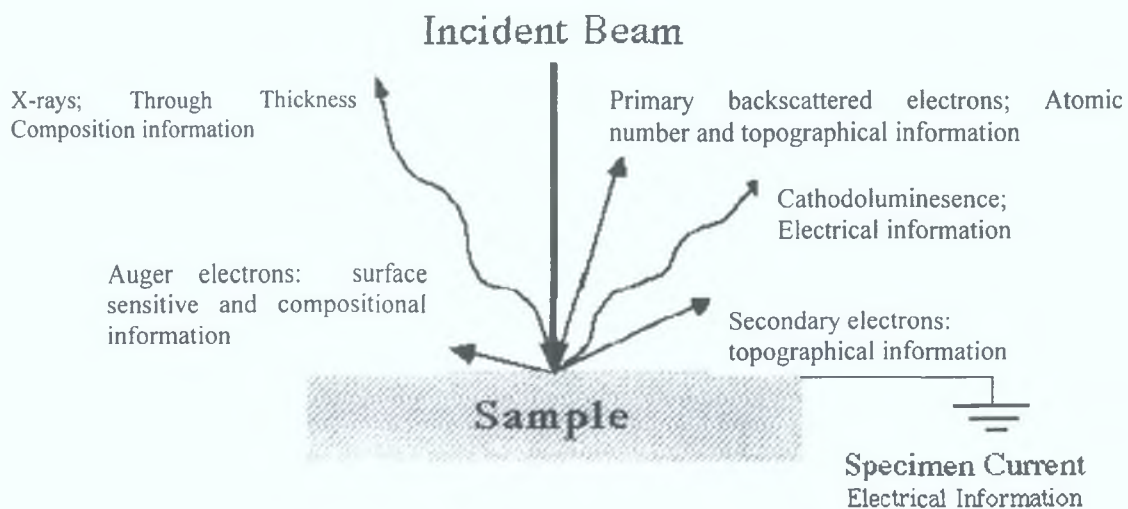
Scheme 4.2. Illustrating what occurs in an SEM sample chamber once the incident beam of electrons hits the sample and the analytical information that derived from this information SEM.

To date, microscopy work that has been carried out on carbon polymer composite electrodes, suggests that with adequate hand mixing it is possible to achieve a system whereby the carbon material is randomly distributed throughout the polymer.[17] Initial research carried out by Adams[14-16] using SEM demonstrated random distribution of carbon fibres within a polymer resin. A more recent study using conducting atomic force microscopy[31] has demonstrated that graphite epoxy composite electrodes have microscopic conducting features that justify their description as random assemblies of UME. Figure 4.2 shows an SEM image of the carbon composite electrode at a magnification X10. From previous studies it is known that the areas of a black and white SEM image which appear very bright/almost white are as a result of the back scattering of electrons, while those images which are darker are capable of conducting/absorbing the electrons which are emitted from the tip of the microscope.[32]

Considering that there are two types of material present in these carbon composite electrodes one of which is non-conducting, epoxy, while the second is conducting, graphite carbon some conclusions may be drawn. From Figure 4.2, it can be seen that there is a random dispersion of bright and dark areas within the composite material, the areas that are highlighted in black, were further studied at a magnification of 100, Figure 4. 3, and Figure 4. 4. Although, it was stated in Section 4.4.1, that these electrode were uniformly mixed, it can be seen from Figures 4.2–4.4 that at a magnification of 10 and 100 the surfaces are heterogeneous in nature, while also demonstrating the relative distribution of conducting species within an insulating polymer.
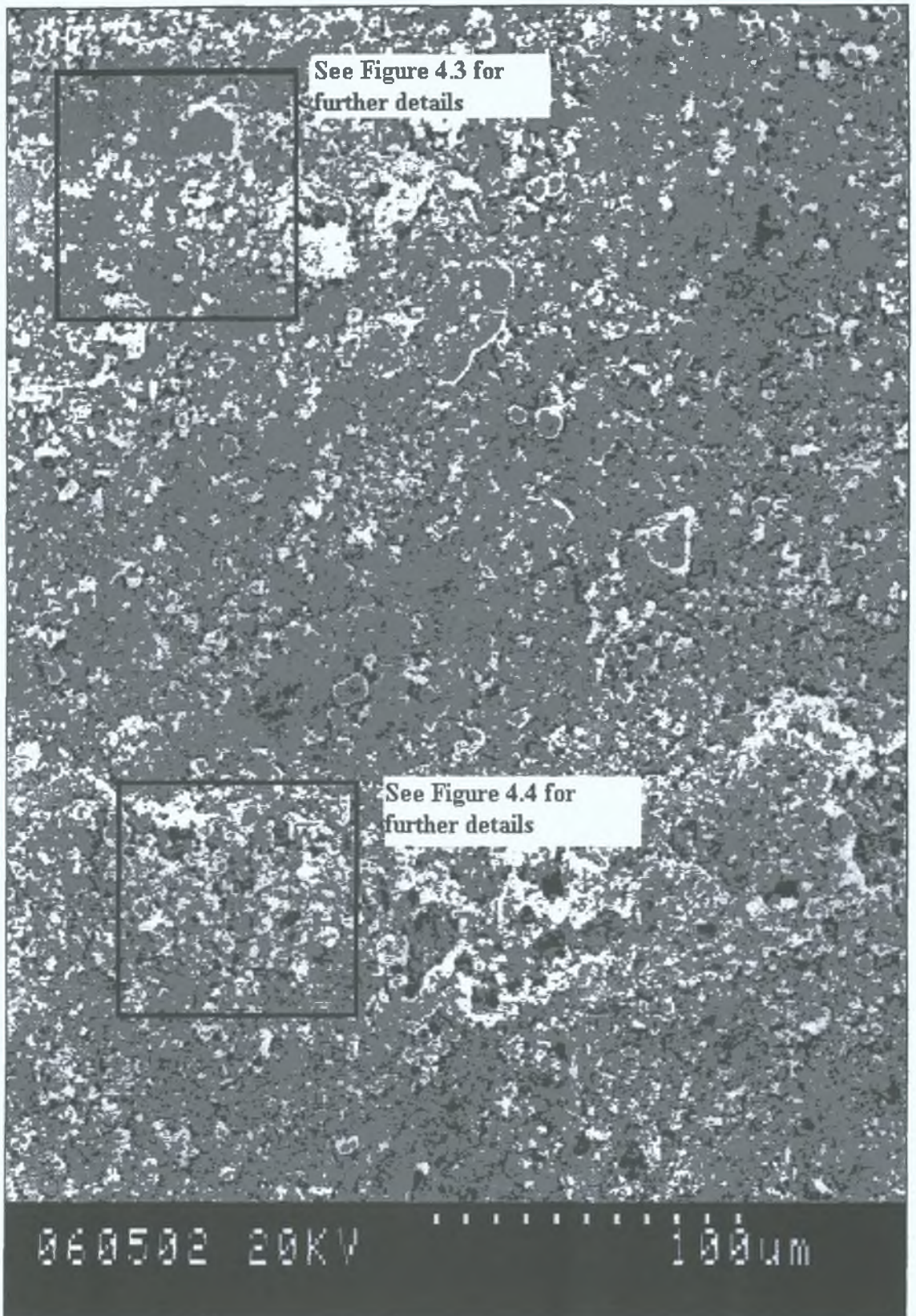
**Figure 4.2.** Image of carbon composite electrode at magnification of X10 in a nitrogen saturated SEM sample chamber. An acceleration voltage is 10 kV s⁻¹ was used.
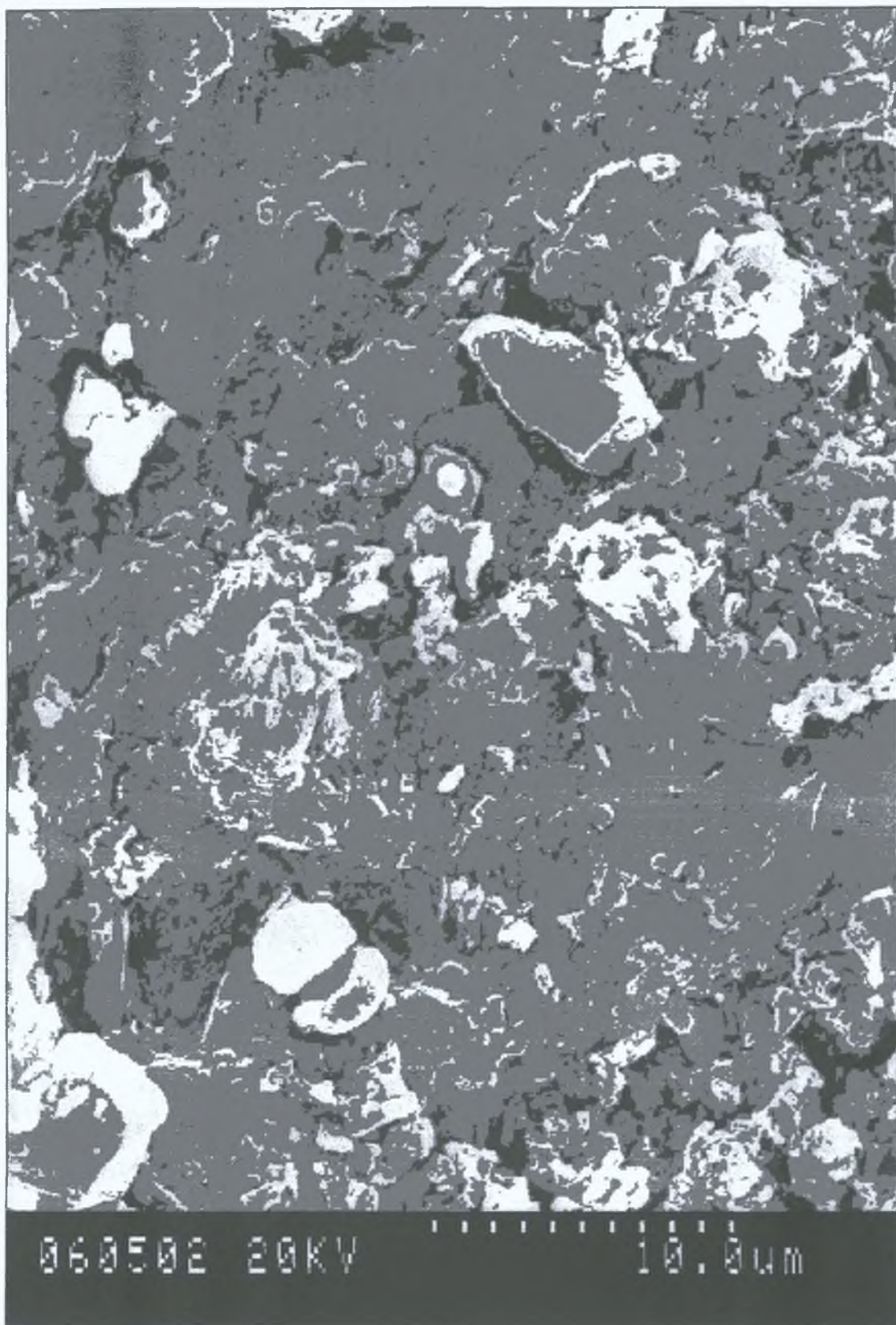
Figure 4.3. Further resolution of the high-lighted upper left hand corner, magnification **X**100 of Figure 4.2.

Figure 4.4. Further resolution of the high-lighted lower left hand corner of Figure 4.2 magnification **X**100

4.5.1.2   Single point resistance measurements:

While SEM provides invaluable information regarding the surface topography, as shown in Figure 4.1, these carbon–composite electrodes are 3 mm in depth. Moreover, since current flows either to or from the surface of working electrode it is necessary to determine the conductivity throughout the entire sample. For this reason a further study into the conductivity of these samples is essential.

It is possible that the carbon particles may not be sufficiently dispersed through the composite to achieve good conductivity, i.e., large quantities of epoxy polymer may prevent adequate conduction through out the sample. To study this phenomena, single point current measurements were taken at various points across the electrode surface.[33] Scheme 4.3, shows the design of these experiments where current flows from the base of the electrode to its surface, a tungsten wire is in place to receive any current that is flowing, and data is then collected. All measurements were taken in a Faraday cage, ensuring all currents are free from electrical interferences that may be present. Table 4.1 shows a set of random currents taken at various points from the surface of the carbon composite electrode.

A constant voltage of 0.9 V was applied to the carbon disc. The resistance measurements were derived from the classical relationship known as Ohms law: $V = iR$. As can be seen Table 4.1, a wide difference in the magnitude of the currents ranging from 7.5×10^{-6}–2.36×10^{-3} A and an inversely related resistance is observed. The former current can be attributed to areas of the composite that contain a high percentage of the polymer, which due to its insulating properties does not allow efficient flow of current. The latter current can be attributed to the graphite carbon. Also it can be seen that there are intermediate values, suggesting the presence of mixed polymer/carbon layers resulting in a convolution of currents though the electrode material. While this is not a conclusive study, it does give a good idea of individual resistance points along the surface of the composite material. As can be seen in Table 4.1, even for the most conductive regions, the values of resistance are quite large. As consequence of this high resistance there is a necessity of compensating for ohmic drop when performing any electrochemical experiments.

Tungsten tip connected to semi-conductor analyser

Carbon–polymer composite stripped of its Teflon shroud

Direction of current flow being measured by Tungsten tip
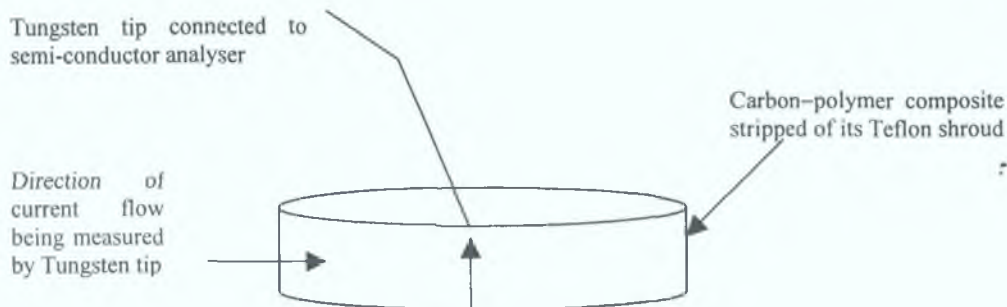
Scheme 4.3. Experimental set up of semi-conductor analyser.

Table 4.1. Collection of data for current and resistance measurements taken at random points across the surface of the carbon composite electrode.

Sample number	Current (A)	Resistance, (Ω)	Sample number	Current (A)	Resistance (Ω)
1	1.80×10^{-05}	5.56×10^{4}	7	2.36×10^{-3}	4.24×10^{2}
2	1.50×10^{-05}	6.67×10^{4}	8	2.20×10^{-3}	4.55×10^{2}
3	1.23×10^{-04}	8.13×10^{3}	9	9.00×10^{-9}	1.11×10^{8}
4	1.10×10^{-04}	9.09×10^{3}	10	7.50×10^{-12}	1.33×10^{11}
5	4.43×10^{-10}	2.26×10^{9}	11	8.20×10^{-12}	1.22×10^{11}
6	1.43×10^{-07}	6.99×10^{6}	12	7.20×10^{-12}	1.39×10^{11}

4.5.1.3 Immunity to current leakages

Quality control experiment were carried out to determine the stability and ideality of the voltammetric response of these composites. Figure 4.5, shows the response of a carbon-polymer composite electrode to continuous scanning within the potential region of − 0.6–1.2 V using 1.0 M KCl. This figure reveals that the background current is significantly sloped which is a common artefact in systems of this kind[36] . A recent report has traced this phenomenon to the occurrence of leakage currents that flow through (or over the surface of) an electrode insulation and into its back contact.[†] Distorted baselines are often an indicator of inadequate sealing. For all future analysis, carried using carbon–polymer composite electrodes, this experiment was performed and all unsuitable electrodes discarded.

[†] The term leakage current means any current that flows from the counter electrode to the working electrode lead, whilst bypassing the working electrode surface.
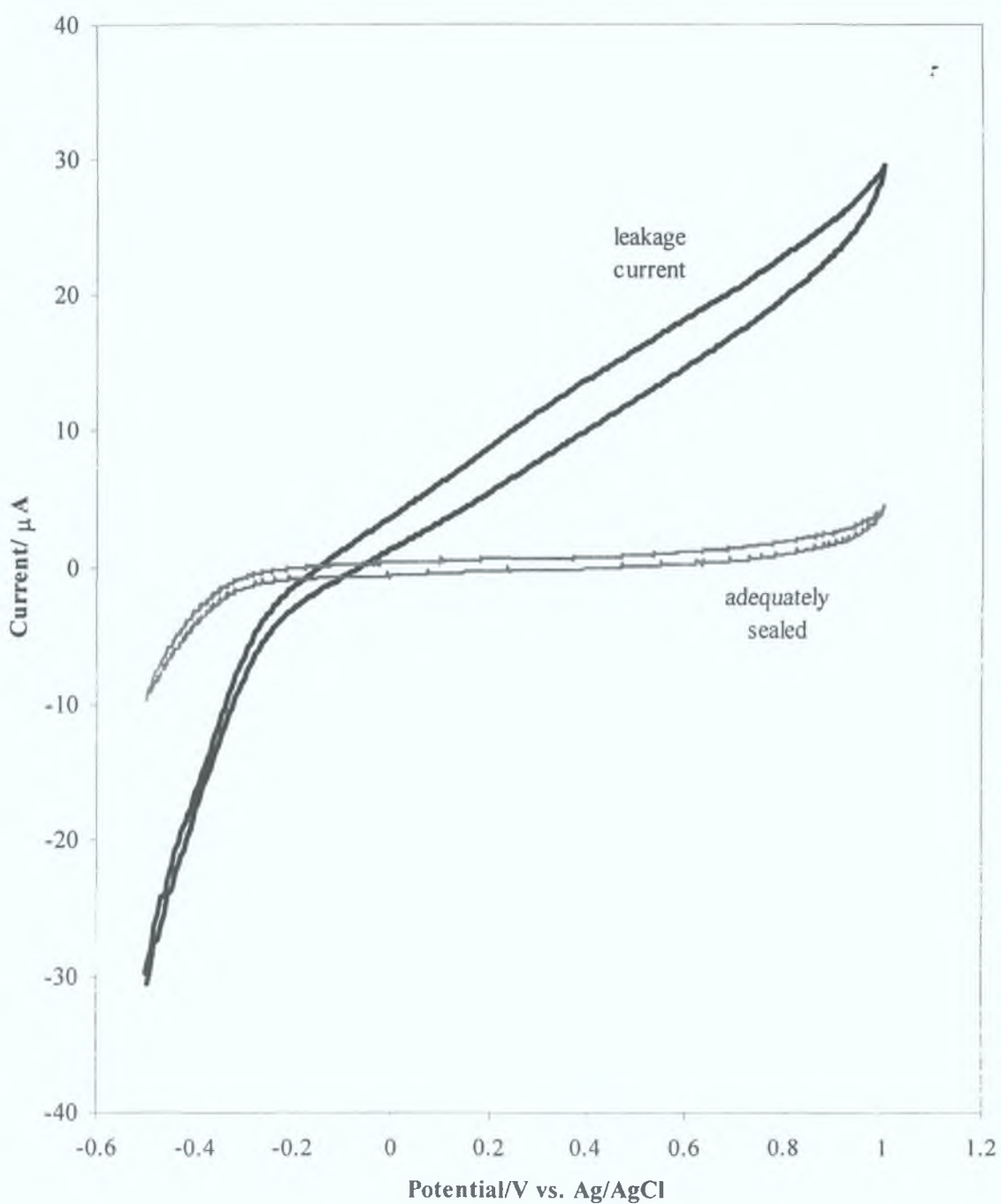
Figure 4.5. Cyclic voltammogram of a carbon–polymer–composite electrode in 1.0 M KCl as supporting electrolyte at a scan rate of 0.01 Vs^{-1}. Reference electrode is Ag/AgCl and a platinum electrode is used as the counter electrode. Initial potential is − 0.6V.

4.5.2   Electrochemical characterisation

From Section 3.4.4, it was demonstrated that the rate of heterogeneous electron transfer across the electrode/electrolyte interface can be a very rapid process e.g., 10^5 s^{-1}. It has been shown that to achieve microsecond and shorter timescales it is necessary to reduce the surface area of the working electrode to micrometer dimensions. Recent years have seen an increase in the number of publications, dealing with the theory and applications of UME, helping our understanding of their properties and has revealed many new applications.[34,35,36,37] It has been concluded that experiments using UMEs are:

- Cheap and easy to perform,

- Based on sound fundamental principles,

- Improve the quality of experimental data and expand on the range of experiments that can be carried out.

However, while proving to have many desirable properties the low current due to the reduced surface area of UME also brings new complications that were not present in traditional macroelectrode experiments. This low current output requires use of Faraday cages to shield the electrochemical experiments from interferences, e.g., background EMI, and hence may not be suitable to application as on site sensors. Microelectrode array technologies have been developed, in an effort to overcome this s/n problem. A characteristic of UME arrays is their capability to probe µs timescales, in the same manner as a UME, while generating a current similar to a traditional macroelectrode, mA and greater. In the past, the carbon composite electrodes described here have been shown to demonstrate this UMEs behaviour,[14,19,31,38] and the following section explores this phenomena and give reasons for this observed behaviour.

4.5.2.1   Steady state investigation

Figure 4.6, demonstrates a typical cyclic voltammogram of the carbon–polymer electrode in an electrolyte solution containing 0.1 M KCl as supporting electrolyte with 1.6 mM $K_3Fe(CN)_6$, using a scan-rate of 0.002 Vs^{-1}. For comparison, Figure 4.7 shows a simulated voltammogram of a UME with a radius of 25 µm, while Figure 4.8 shows a carbon macroelectrode radius 3 mm. When a comparison is made between Figures 4.6–

4.8, the similarity in wave shape between the UME, Figure 4.7, and the composite electrode, Figure 4.6 is observed. While the electrochemical response for the macroelectrode is much larger, Figure 4.8, and has a peak shape consistent with mass transfer by semi-infinite linear diffusion.

The behaviour observed in Figure 4.6 and 4.7 is known as steady-state behaviour and corresponds to the situation where the rate of depletion of active species from the surface of the electrode is equal to the rate of regeneration of active species to the electrode surface. [38]
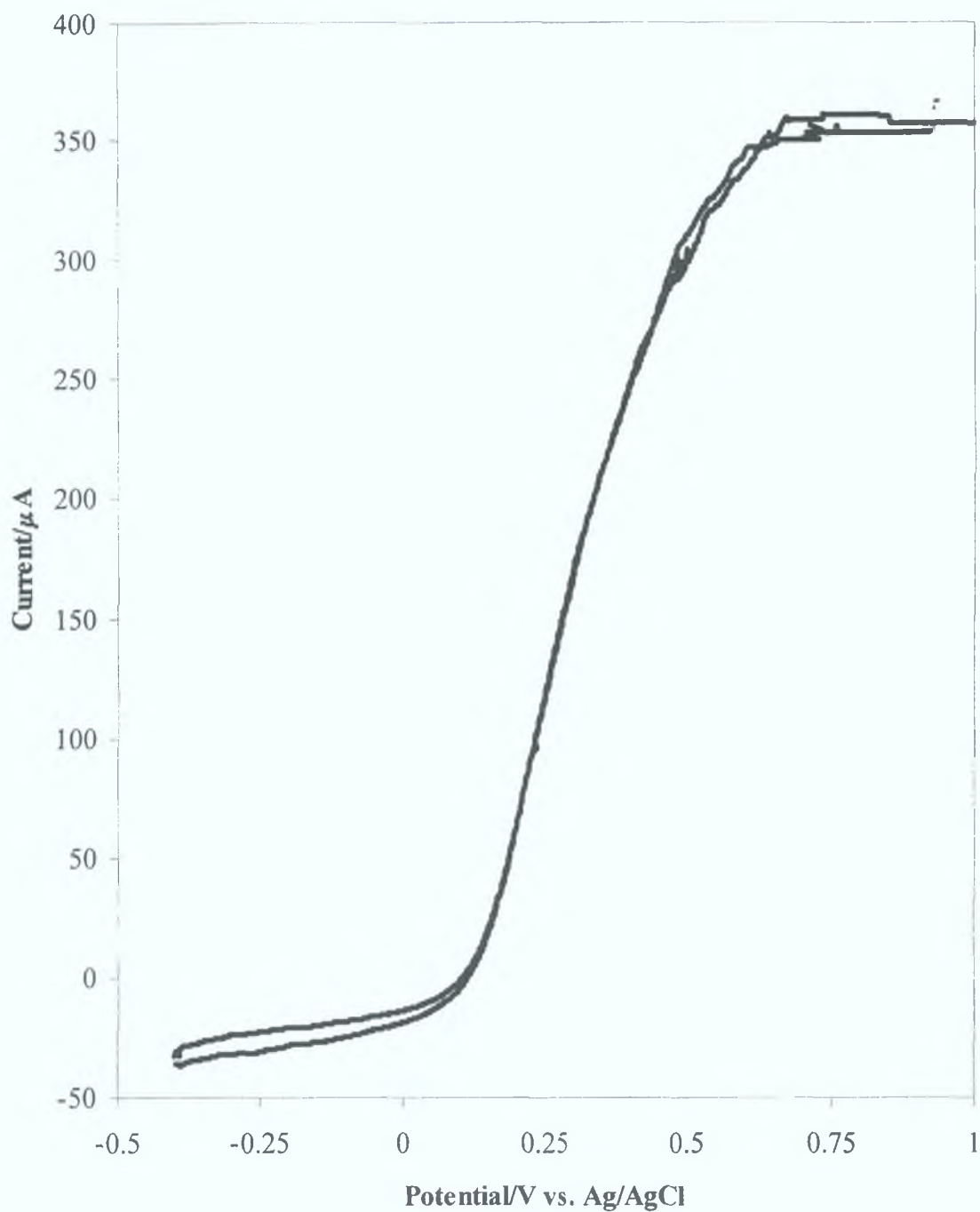
Figure 4.6. Carbon-polymer composite electrode in 1.6 mM $K_3Fe(CN)_6$ with 0.1 M KCl as supporting electrolyte at a scan rate of 0.002 Vs^{-1}. Ag/AgCl reference electrode and a Pt auxiliary electrode were used.
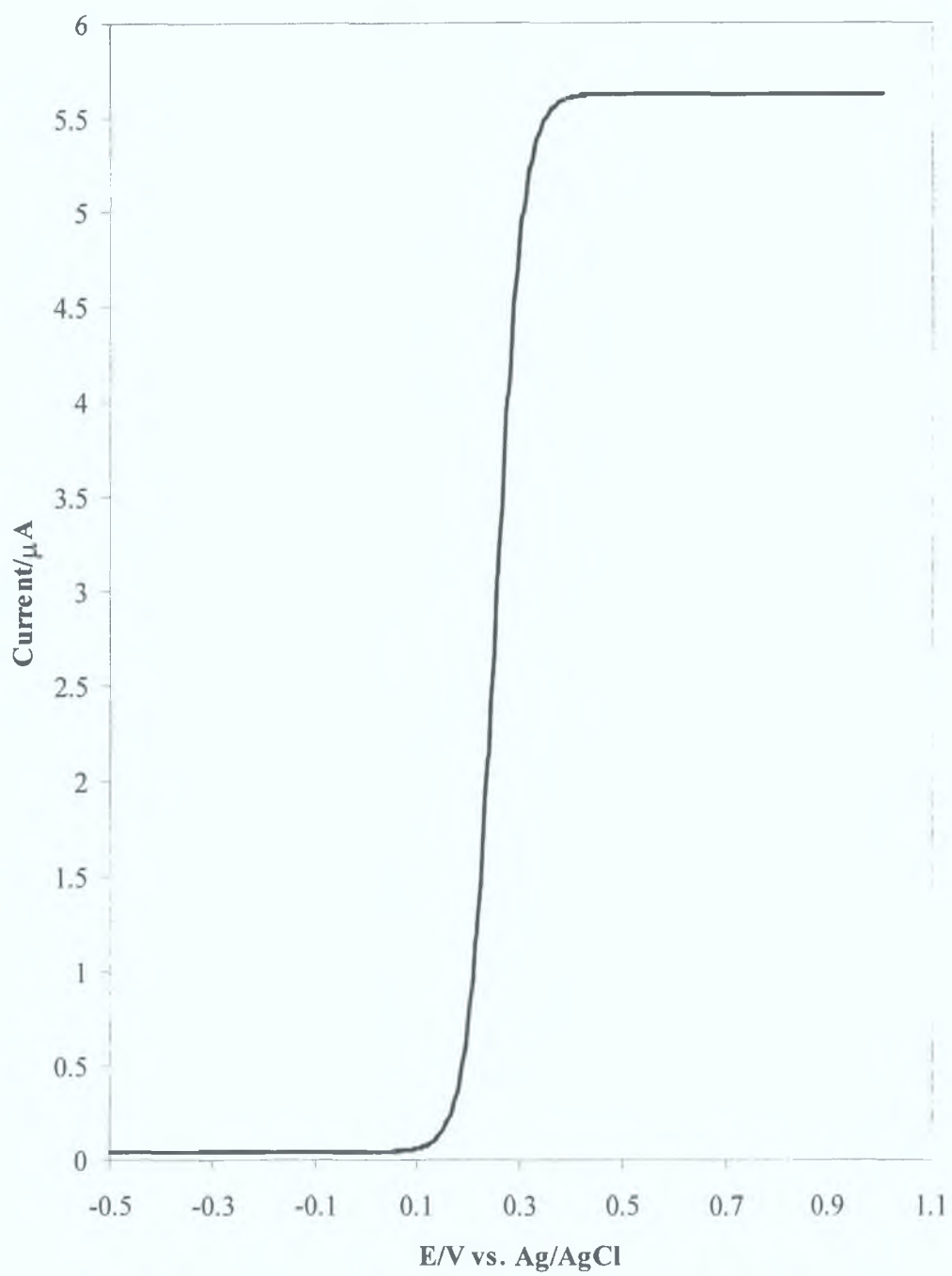
Figure 4.7. Simulated CV of UMEs under similar conditions scan rate of 0.002 Vs⁻¹.
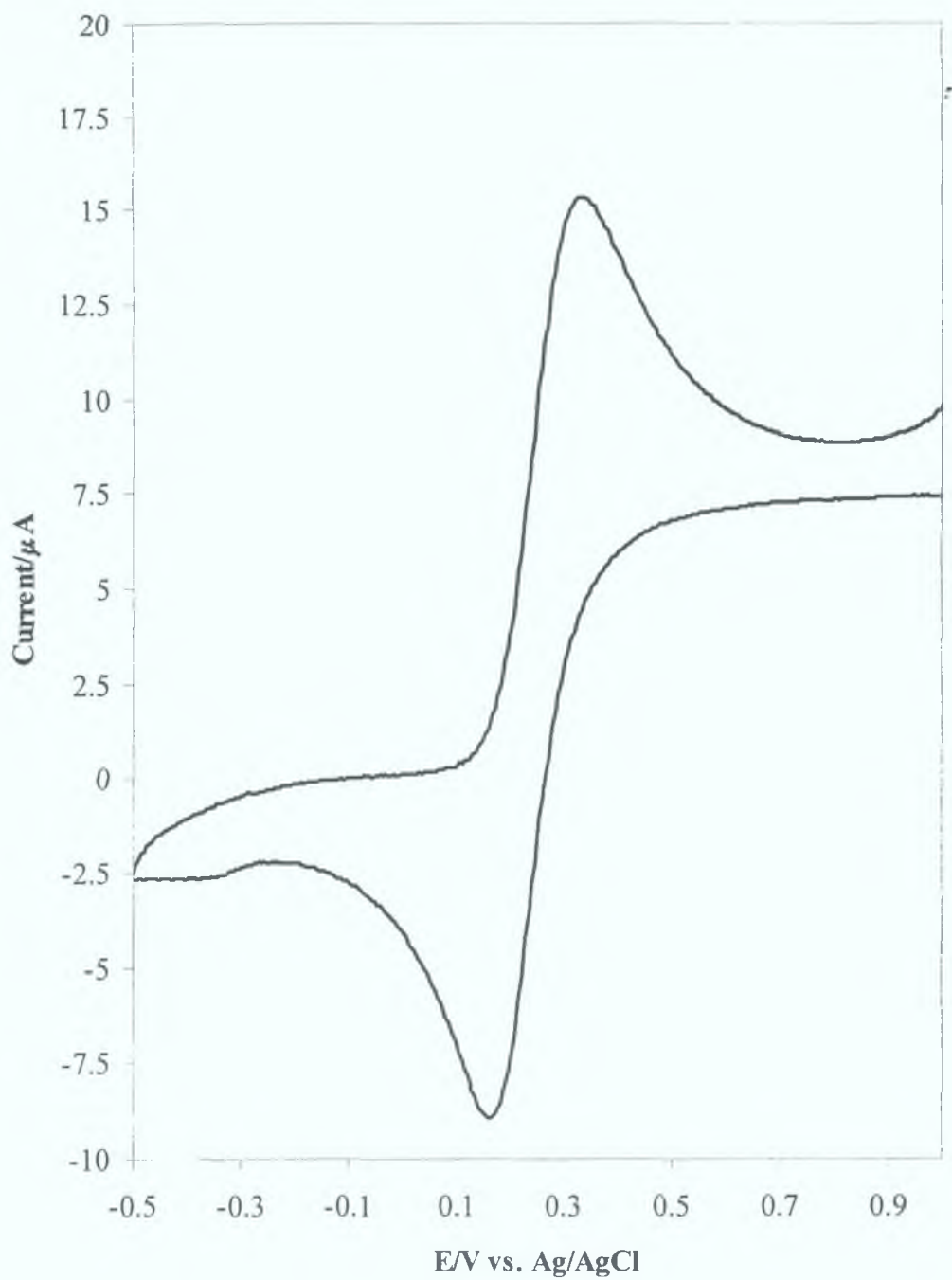
Figure 4.8. Cyclic voltammogram of glassy carbon macroelectrode in 1.6 mM $K_3Fe(CN)_6$ with 0.1 M KCl as supporting electrolyte at a scan rate of 0.005 Vs^{-1}. Ag/AgCl reference electrode and a Pt auxiliary electrode were used.

To understand how these carbon–polymer composite electrodes are capable of demonstrating behaviour traditionally associated with UMEs, it is essential that this electrochemical behaviour is discussed in terms of advantages and properties of UME, especially diffusional mass transport which is extremely efficient using UME.[34]

Application of a potential to an electrode surface, starting at a value where no electrode reaction occurs to one where the electroactive species in solution is either oxidised or reduced, results in the diffusion of species towards and away from the electrode surface generating a diffusion layer. The diffusion layer or zone can be described as the area near the electrode surface where concentrations of species differ from those of the bulk solution. Although, it is not possible to quantify exactly the thickness of this diffuse layer, it is useful to think of the diffusion layer in terms of $(D_oC_t)^{1/2}$, where D_o has units of cm s^{-1} and concentration has the units mol cm^{-3}. The diffusion layer has units of length and may be characterised by the distance that a species O can diffuse in time, t. For convenience, the term O is used here but equally applies to the species R. Application of a potential to a working electrode surface results in species O being generated.

Scheme 4.4 illustrates diffusion to a conventional disk shaped macroelectrode. There are two possible directions capable of contributing to current; diffusion with respect to the axis of symmetry, known as radial diffusion, and diffusion normal with respect to the plane of the electrode, known as linear diffusion.

Linear diffusion

Radial
diffusion
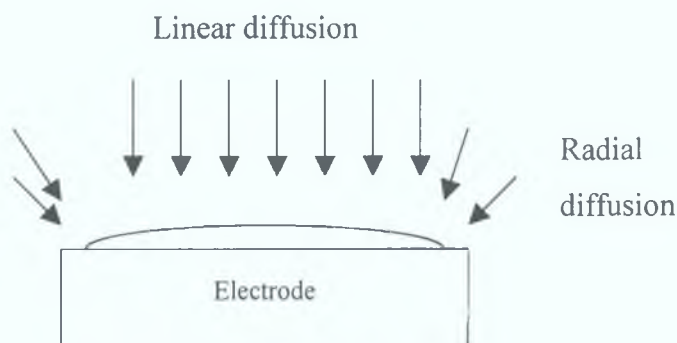
Electrode

Scheme 4.4. Showing diffusion of electroactive species to the surface of a disk shaped macroelectrode.

For a macroelectrode, semi-infinite linear diffusion to the electrode surface predominates and the contribution from radial diffusion is negligible. The time evolution of the current response corresponding to these linear and radial diffusion fields is described by Equation 4.1.

$$i_d(t) = \frac{nFAD_0^{1/2}C_0^\bullet}{\pi^{1/2}t^{1/2}} + \frac{nFAD_0C_0^\bullet}{r_0}$$ **(Equation 4.1)**

The first term dominates at short times, when the diffusion layer is comparatively thin with respect to r_0, and the second term dominates at long times when the diffusion layer grows much larger than the value of r_0. For a planar macroelectrode, the first term corresponds to the Cottrell current associated with linear diffusion, while the second term corresponds to contribution of current derived from radial diffusion. However, for macroelectrodes this steady-state current would take a significant time to achieve and hence when describing diffusion of electroactive species to the surface of a planar macroelectrode the second term is neglected.

For UMEs the situation is different, since surface area of a disk shaped UME is dramatically reduced, with respect to the surface area of a macroelectrode, the contribution of current from radial diffusion has to be considered. In the case of UMEs three timescales must be considered; short, intermediate and long times.

Short experimental timescale:

When an experiment is carried out using a short time scale, such that the diffusion layer remains thin with respect to r_0, radial diffusion does not manifest itself noticeably, and the diffusion possesses a semi-infinite linear character and the short timescale current that flows, e.g., in response to a large amplitude potential step, is described by the first part of Equation 4.1, i.e., Cottrellian behaviour. For example a UME with a radius of 5 μm and a $D_0 = 10^{-5}$ cm^2 s^{-1} the diffusion layer thickness is only 0.5 μm at a timescale of 60 μs.

Intermediate timescales:

When the experiment continues into the intermediate timeframe a diffuse layer corresponding to the approximate thickness of the electrode radius is generated, and

174

radial diffusion influences the response. Under these conditions for electrode radius of 5μm and a D_0 of 10^{-5} cm^2 s^{-1} the frame corresponds to an experimental time between 60μs and 60 ms. The diffusion layer thickness is in the range 0.5 μm and 16 μm.

Longer experimental timescale:

When the timescale becomes sufficiently long, the transient current density will decrease to a negligible value and the current will reach steady-state as shown in Equation 4.2.

$$i_{ss} = \frac{nFADC_o}{r_s}$$ (**Equation 4.2.**)

At these long times, the spherical character r_s of the electrode becomes important and mass transport is dominated by radial or spherical diffusion as illustrated in Scheme 4.4. The steady state response seen in Figures 4.6 and 4.7 arises because the electrolysis rate is equal to the rate at which molecules diffuse to the electrode surface. In the case of a disk shaped UMEs, the current response is complicated by a phenomenon known as the edge effect. Since the entire surface of a disk electrode is not uniformly accessible and the current density is not uniform across the face of the disc, but greater at the edge, which offers the nearest point of arrival to the electro-reactant drawn from a large surrounding volume. This phenomenon is known as the edge effect.[38] However, microdisks have the advantage of spherical UME in that a quasi-spherical diffusion field is established within short timescales, Equation 4.3.

$$i_{ss} = 4nFDC_o r$$ (**Equation 4.3**)

Steady-state response for carbon-composite electrodes

To explain why a steady state response is being generated by these carbon-composite electrodes it is essential to remember that 50 μm graphite particles have been distributed within a polymer matrix. Since an UME is by definition any electrode, which processes at least one critical dimension on the micron length scale, it is possible that there are

175

areas of the electrode that have individual graphite particles surrounded by a polymer matrix resulting in a random assembly of UME[31,36,39]

Consider a cyclic voltammetry experiment where only a portion of the working electrode surface is active and the potential window is wide enough so that a full redox cycle occurs i.e., oxidation and reduction of fast one electron transfer reaction such $K_3Fe(CN)_6$. Such an situation can arise when arrays of UME are fabricated by microelectronic methods, or in this incidence when the electrode is a composite material based on conducting particles embedded in a polymer material. At slow scan rates, i.e., long experimental times, the diffusion layer thickness is small compared to the size of the active graphite particle, each particle is capable of generating its own linear diffusion field, Figure 4.9a, such that the area of the overall diffusion field is the sum of the geometric areas of the individual active particles. This would explain the steady state voltammogram observed in Figure 4.6.

At intermediate timescales, the individual diffusion fields extend outside the projected boundaries, shown in Figure 4.6a, such that the radial diffusion responsible for the previously observed steady state voltammograms is augmented by a linear component, Figure 4.9b. The actual definition of slow, intermediate and long experimental timescales, depend on the distance of intersite separation. Figure 4.10, employs a scan rate of 0.500 Vs^{-1}, as can be seen there is an obvious influence of linear diffusion i.e., peak broadening, and diffusional tailing. This behaviour is suggesting partially overlapping but otherwise localised diffusion zones. Such results are in agreement with Marken and co-workers[40] who observed much the same phenomena when working with carbon nanofibres embedded in paraffin wax and mounted on a glassy carbon electrode.

At longer timescales, Figure 4.9c, the diffusion layer becomes thicker than the distances between the active zones. As a result of this increased diffusion thickness the separated fields merge into singular larger field again exhibiting linear diffusion and having an area equal to its geometric surface area. Figure 4.11, shows that for these composite electrodes a scan rate of 2 Vs^{-1}, is sufficient to generate an electrode response characteristic of a macroelectrode. This voltammogram response is most likely a mixed/linear diffusion to individual UME. For comparison Figure 4.12, shows a glassy carbon macroelectrode under identical experimental conditions as Figure 4.10. With

respect to mass-transfer response, both voltammograms in Figure 4.12 demonstrate wave shape characterised by linear diffusion. While Figure 4.13 shows that at fast scan rates the carbon composite electrode demonstrates a linear response of (scan rate)$^{1/2}$ of peak current, characteristic associated with macroelectrode behaviour and not UME, unless an extremely fast scan rate is employed.
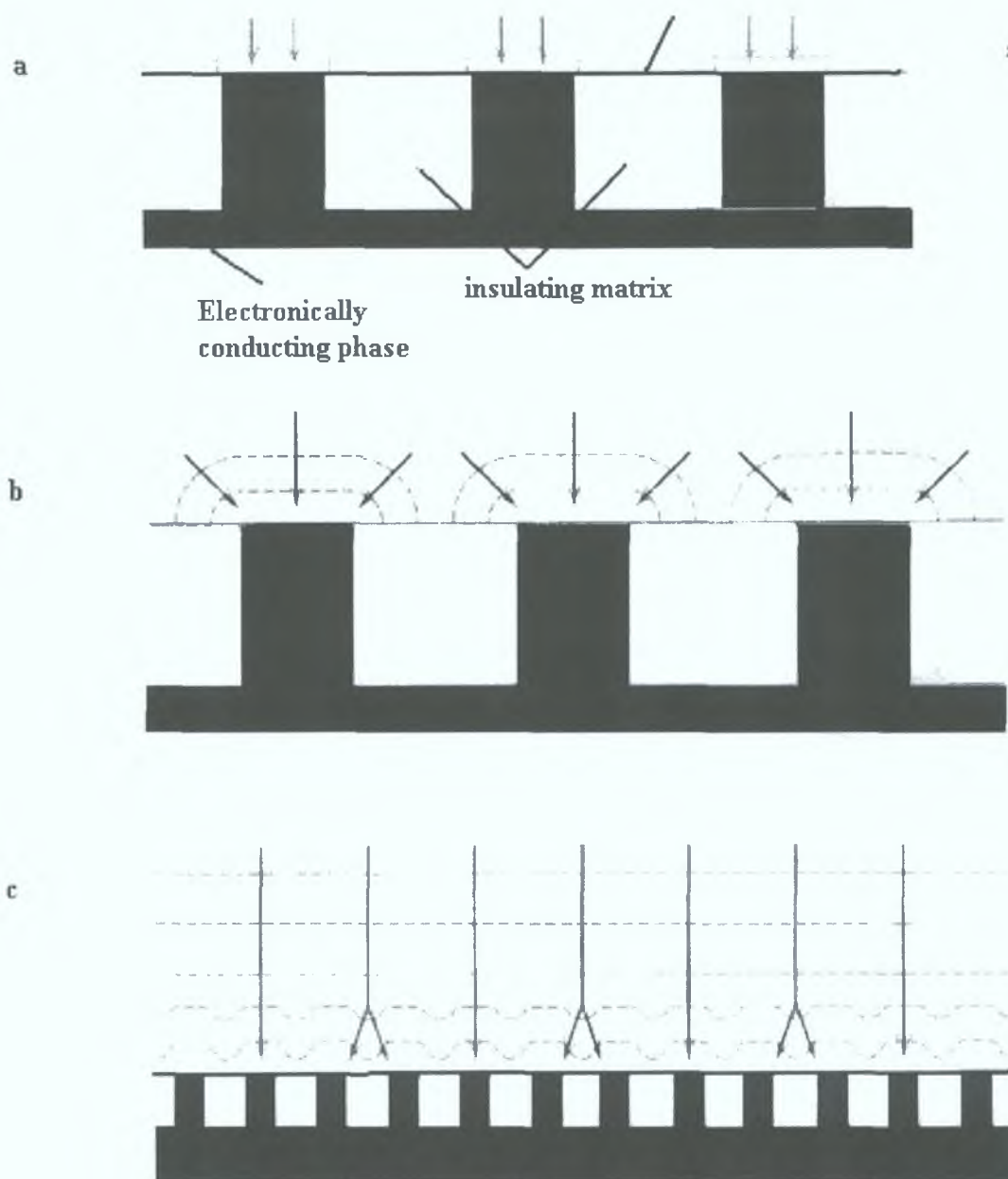
Figure 4.9. Extension of the diffusion field during chronoamperometry at an electrode with active and inactive areas on its surface. In this case the electrode is an ordered array such that active areas are of equal size and spacings but the same principles make apply to random arrays. (a) Short electrolysis times, (b) intermediate times and (c) long times. Arrows indicate flux lines to the electrode.
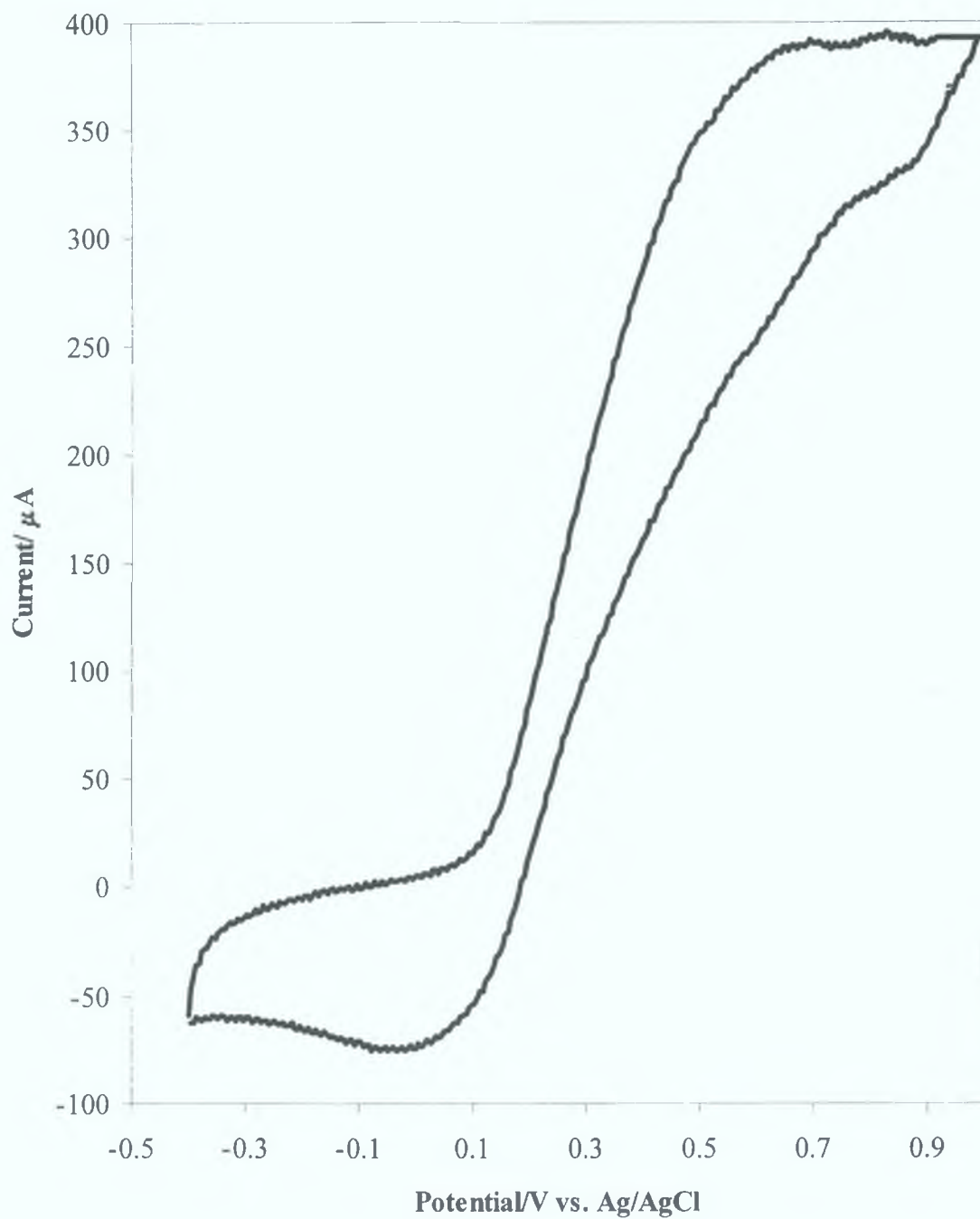
Figure 4.10. Carbon composite electrode in 1.6 mM $K_3Fe(CN)_6$ with 0.1 M KCl and a scan rate of 0.50 Vs^{-1}(outer) and 0.005 Vs^{-1}(inner). An Ag/AgCl reference electrode and Pt. auxiliary electrode were used
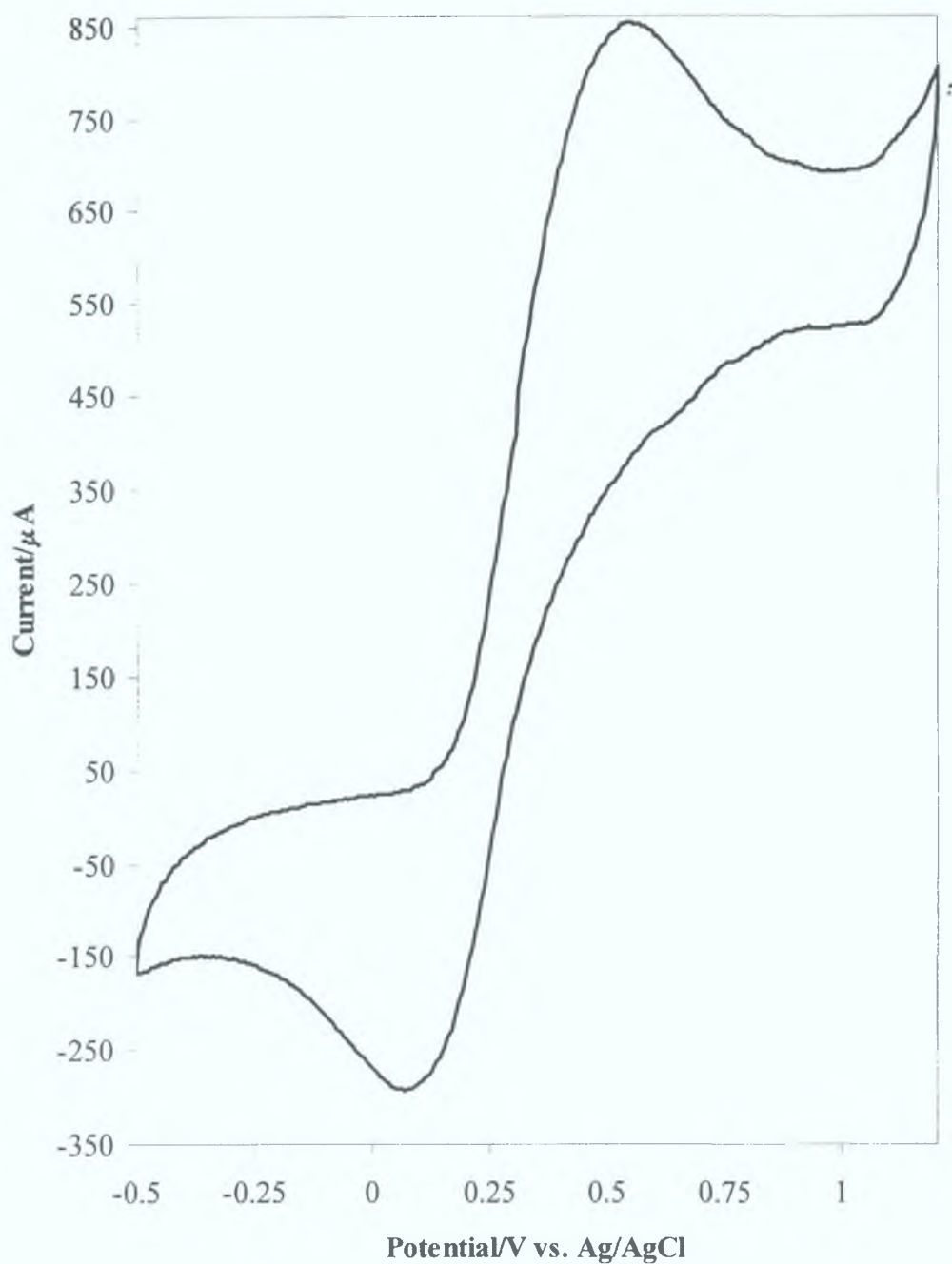
Figure 4.11. Carbon composite electrode in 1.6 mM $K_3Fe(CN)_6$ with 0.1 M KCl and a scan rate of 2 Vs^{-1}. An Ag/AgCl reference electrode and Pt. auxiliary electrode were used.
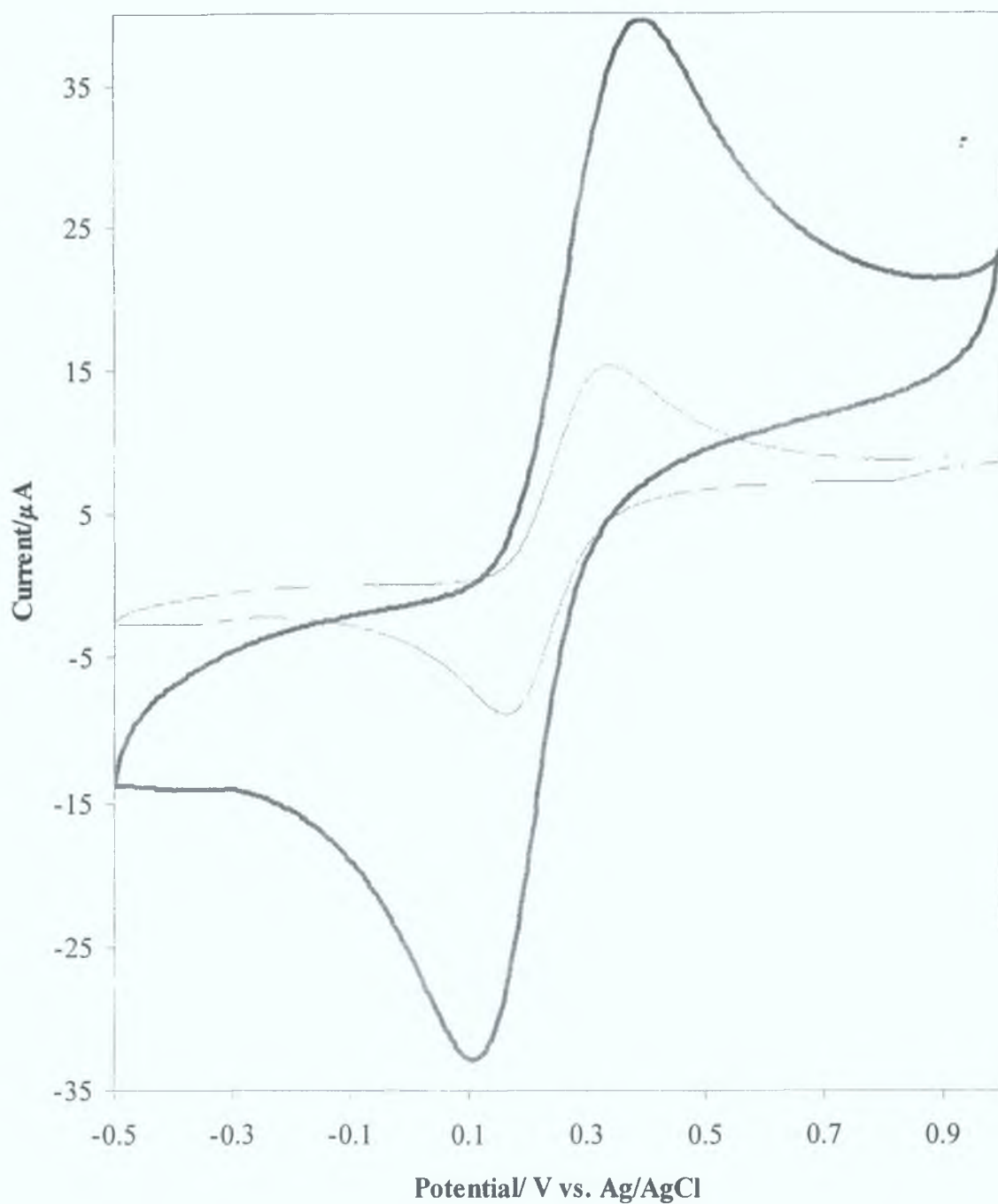
Figure 4.12. Cyclic voltammogram of Glassy carbon electrode in 1.6 mM $K_3Fe(CN)_6$ with 0.1 M KCl and a scan rate of 0.50 Vs^{-1}(outer) and 0.005 Vs^{-1}(inner). An Ag/AgCl reference electrode and Pt. auxiliary electrode were used
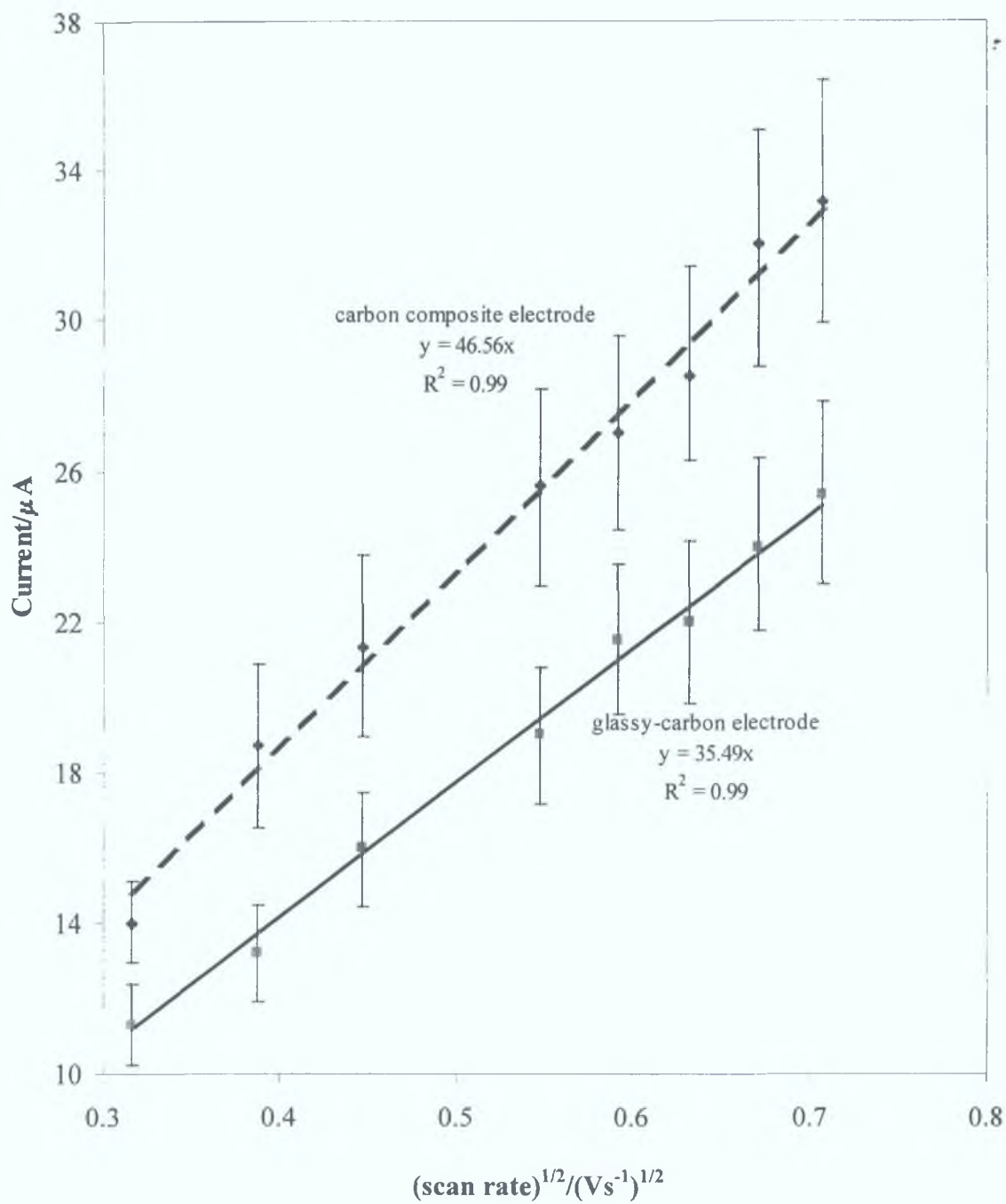
Figure 4.13. Plot of (scan rate)$^{1/2}$ vs. current. (- -) carbon composite electrode, (——) glassy carbon macroelectrode. Solution used was a 1.6 mM $K_3Fe(CN)_6$ in 0.1 M KCl.

RC time constant:

When a potential is applied across the surface of an electrode placed in an electrolytic medium, a double layer is formed in which the charge on the electrode is compensated for by a layer of oppositely charged ions from the medium.   This process is accompanied by a flow of charging current, characterised by the RC time constant, where R is the solution resistance (Ω) and C is the double layer (μF).   The RC time constant is a measure of the response time of a cell and can be an indication of electrodes being suitable for high speed measurements.[41]   Equation 4.5, illustrates that following a potential step experiment from E_1–E_2 (ΔE) the capacitive current charging decreases exponentially in time at a rate determined by RC. [42,43]

$$i_c = \left(\frac{\Delta E}{R}\right)\exp\left(\frac{-t}{RC}\right)$$
(**Equation 4.5**)

The value of C, double layer capacitance is given by Equation 4.6, where A is electrode area, i_c is the charging current associated with this double layer and v is scan rate.

$$C_{dl} = \frac{i_c}{A v}$$
(**Equation 4.6**)

From Equation 4.6 it can be seen that a reduction in surface area will result in a reduction in C while, resistance depends on the applied potential.   The overall implication of this reduced RC value is the ability to measure in a more accurate manner the rate of electron transfer, since within this time domain the influence of charging current is negligible when compared to Faradic current.   It is this characteristic which is responsible for the increased ability of UME to be used at much shorter timescales than macroelectrodes. Potential step chronoamperometry, has been used in the pass for determining the value of RC for PMEs in addition to other electrode systems.[28] According to Equation 4.5 a plot of time vs. ln(i) should be linear, with the slope providing the RC of the experiment and the intercept providing the value for resistance. The semi-log plot of five different carbon composite electrodes is shown in Figure 4.14.

The value of ΔE is 0.2 V, and occurs in a region where no Faradic activity occurs. As can be seen from Figure 4.14 none of the time vs. $\ln(i_c)$ superimpose on each other, however all results are identical to within experimental error and the majority of the variation arises from differences in the total cell resistance.   The average values of RC constant and resistance are shown below in Table 4.2, for comparison reasons values for micro and macroelectrodes are also included.

Table 4.2. Values of RC ($\Omega\mu F$) and resistance (Ω) measurements made in a phosphate buffer KCl electrolyte solution.

| electrode	RC ($\Omega\mu F$)	Resistance (Ω)
Glassy carbon	0.0533 ±0.012	10.188±0.36
Carbon composite	0.0696±0.0085	11.45±0.42
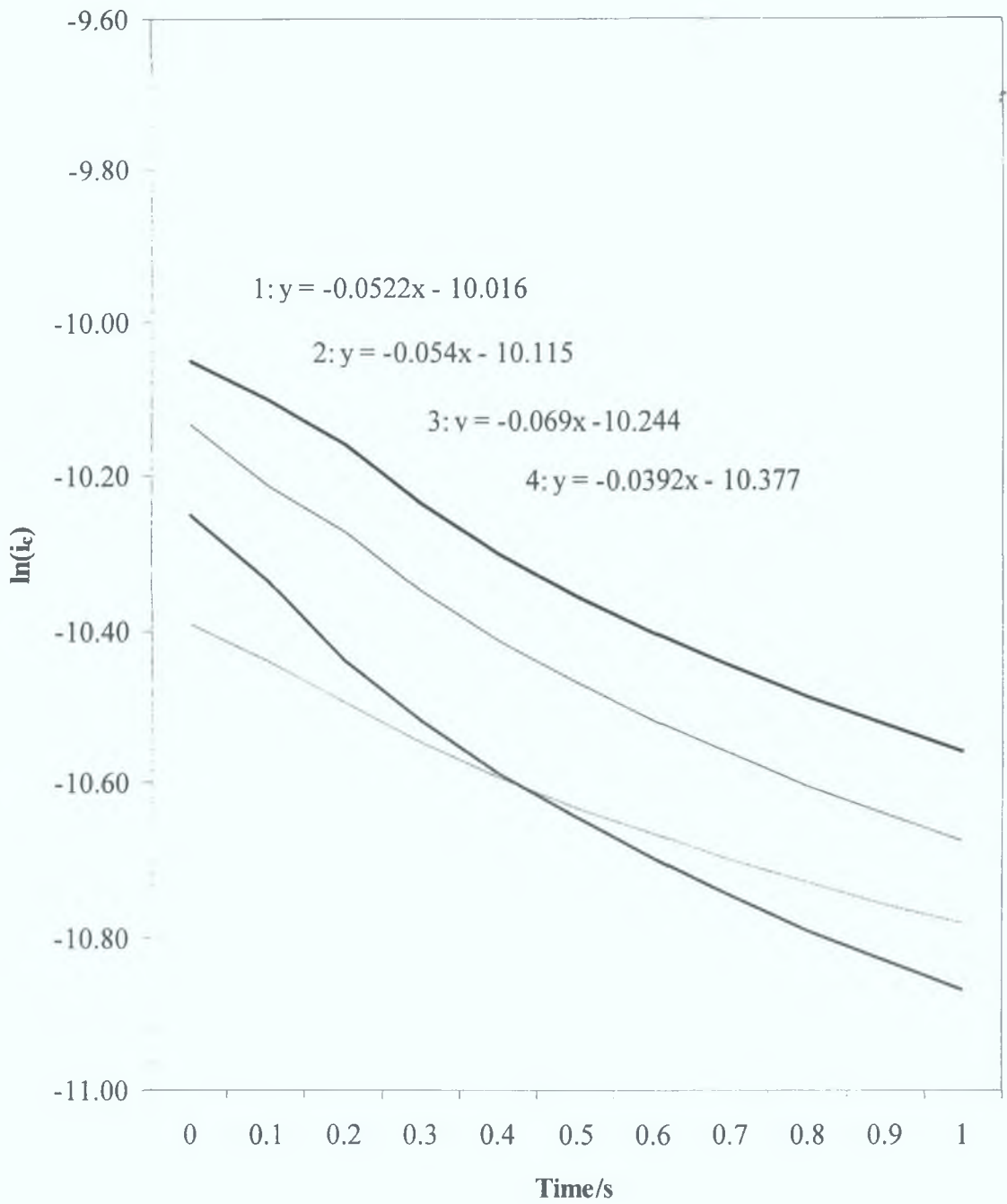
Figure 4.14 Plot of ln $i_c(t)$ vs. t, for carbon composite electrode, the potential step used for this experiment was from 0.2 to 0.4 V in 1.0 M KCl as supporting electrolyte.

4.5.3 Study in resistive media

If these carbon-composite electrodes are a true representation of a random array of UMEs it should be possible to obtain a voltammetric response in solution containing no little or no supporting electrolyte. The reasons for this capability is associated with the reduction in iR drop, otherwise known as ohmic drop. These ohmic effects are observed when Faradaic and charging currents flow through a solution generating a potential that acts to weaken the applied potential by an amount iR, where i is the total current and R is the resistance of the cell. This iR drop can lead to distorted responses. Previously it has been reported that resistance increases with decreasing size in electrode radius. This can be characterised by Equation 4.7, where R is the resistance of the solution, κ is the specific conductivity of the electrolyte and r is the electrode radius

$$R = \frac{1}{4\pi\kappa r_s}$$
(**Equation 4.7**)

Equation 4.7, reveals that the resistance increases with decreasing electrode radius. However since the currents observed using an UME are traditionally 6 magnitudes lower than a macroelectrode ohmic effects are reduced or eliminated.

It has been observed, in Section 4.5.2.1, that these carbon-polymer electrodes show UME behaviour at slow and intermediate timescales, while at longer timescales the electrochemical response is dominated by linear diffusion. Given this UME behaviour a study of the electrochemical response in resistive media was investigated. Figure 4.15, compares two voltammograms one with 0.1 M KCl as supporting electrolyte in addition to 1.6 mM $K_3Fe(CN)_6$ while the other only contains 1.6 mM $K_3Fe(CN)_6$. As can be seen there is a definite response associated with the redox couple for both situations. For comparison reasons, Figure 4.16 shows a voltammogram of a glassy carbon macroelectrode in the absence of supporting electrolyte, i.e., no KCl. Although it is possible to attain an electrochemical response associated with the redox couple $K_3Fe(CN)_6$, in the absence of deliberately added electrolyte, the current obtained is very low and the peak potentials are shifted more negative and more positive in comparison Figure 4.8 which contains electrolyte medium. It was found that increasing the scan rate beyond a value of 20 mVs^{-1} resulted in loss of this UME like behaviour.
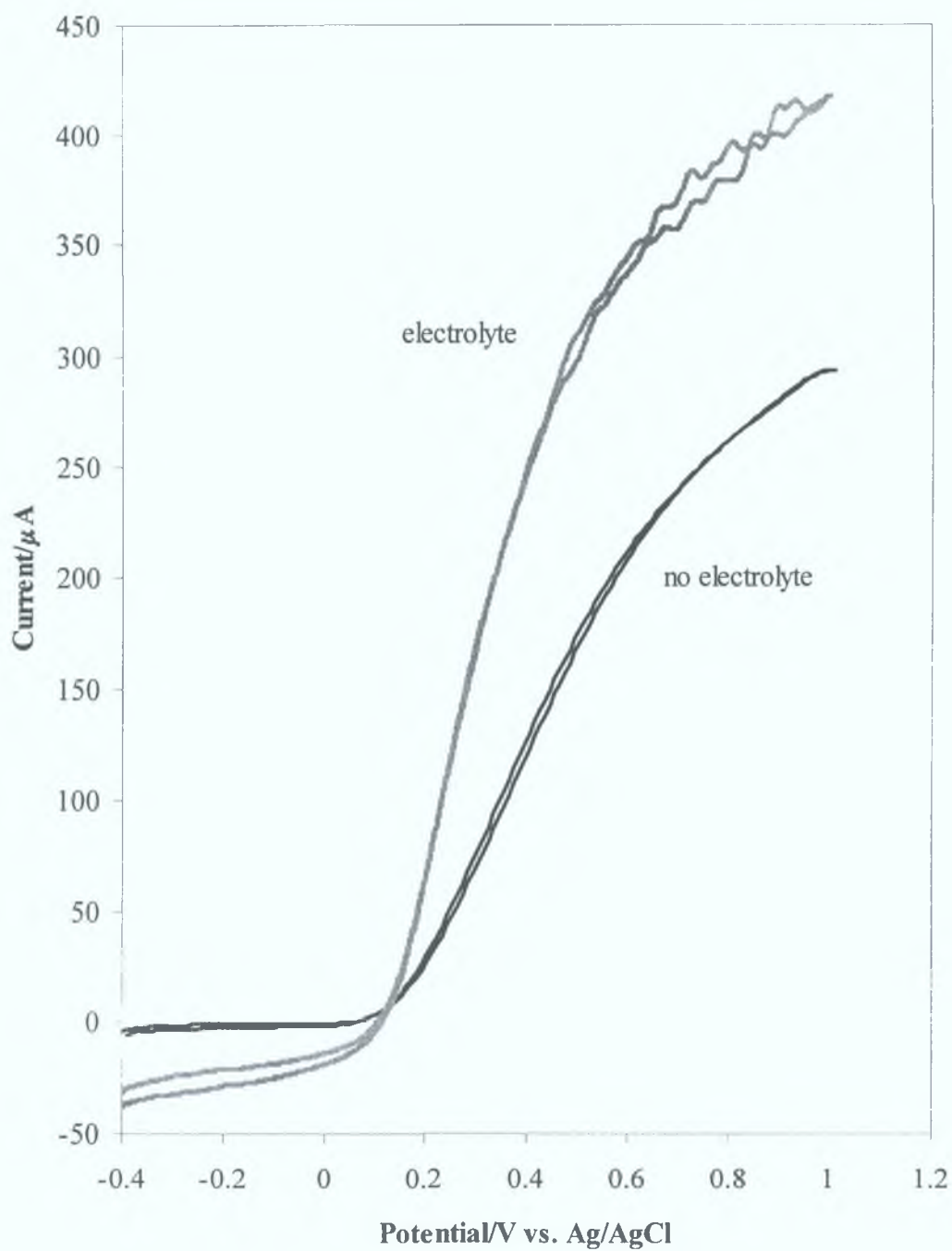
Figure 4.15. Voltammogram of carbon composite electrode both with and without supporting electrolyte, as illustrated in the text concentration of $K_3Fe(CN)_6$ is 1.6 mM. An Ag/AgCl reference and a Pt. auxiliary electrode were used in both cases
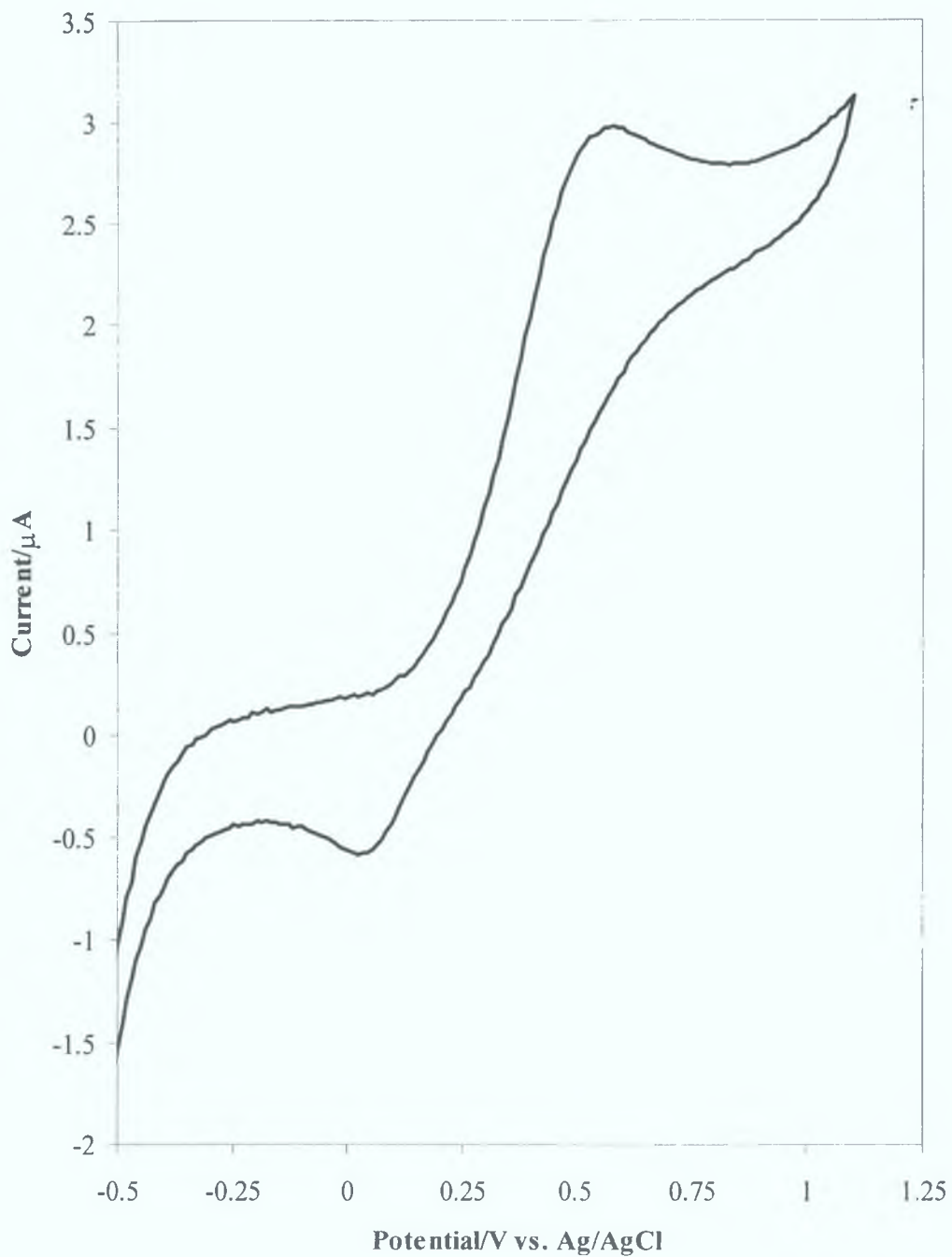
**Figure 4.16.** Voltammogram of glassy carbon electrode without supporting electrolyte, concentration of $K_3Fe(CN)_6$ is 1.6 mM. An Ag/AgCl reference and a Pt. auxiliary electrode were used in both cases

4.5.4 Determination of heterogeneous electron transfer kinetics.

As was illustrated in Figures 4.2–4.4, these electrodes are heterogeneous in nature and result in graphite islands in a sea of electrochemically inert epoxy resin. The advantages of this are apparent in Figure 4.6, for slow scan rates of 0.002 Vs^{-1} where steady-state voltammetry is observed. For longer experimental times, the carbon composite exhibits behaviour similar to that of a macroelectrode, Figure 4.11, i.e. loss of steady state behaviour, increasing ΔE_p with increased scan rate. It is known[44] that when a conducting particle is coated with a thin layer of epoxy polymer, as in the case of these carbon polymer composites, the overall effect can be reduced charge transfer reversibility across the electrode interface, or alternatively a shift from an observed Nernstian reversible system to a quasi reversible or a totally reversible system.[44]

Already explained in Section 1.5 heterogeneous electron transfer is associated with the rate at which electrons are either accepted or donated from the electrode to a species in solution or confined to the surface of the electrode. The rate of this electron transfer depends greatly on the electrode material and the ability of the electro-active species present either in solution or confined to the electrode surface to accept a donated electron. Additionally as was demonstrated in Chapter 3.5 the solvent also exerts influence. The standard heterogeneous electron transfer rate constant, $k°$, is of fundamental interest for numerous analytical and mechanistic reasons. First, the shape and magnitude of voltammograms depend on the value of $k°$. Second, the range of useful scan rates is limited by $k°$. An electrochemically reversible redox reaction will exhibit a ΔE_p 0.056/n V, once the switching potential for the reverse scan is at least 90mV beyond the peak potential. Systems with a small value for $k°$ or sluggish electron transfer can show ΔE_p values greater than 1 V. A third reason involves electro-analytical techniques requiring a mass transport limited current, such as liquid chromatography where the detection is electrochemical, under these circumstances fast electron transfer reactions are necessary, to ensure that the electrochemical species has been detected before being eluted.

From Figure 4.17 it can be seen that the electrochemical behaviour of these electrodes is not the expected reversible behaviour but rather the electrochemical response resembles behaviour known as quasi-reversible behaviour – reversible

behaviour at slow scan rates while increasing the scan rate results in the electrochemical response similar to that of a irreversible redox couple. All voltammograms have been corrected for iR drop, in accordance to Table 4.2, which is known to affect the positioning of the redox potentials. The term quasi-reversible has defined already in Chapter 2.2 to explain the behaviour of polymer modified electrode i.e., independence of E_p on scan rate, and relationship between peak current and (scan rate)$^{1/2}$ at slow scan rates, while at faster scan rates there was an dependence of E_p and peak current on scan rate i.e., quasi-reversibility.

Given the extensive analytical application of these carbon composite electrodes the heterogeneous electron rate constant, $k^°$, was investigated, using the well known method developed by Nicholson.[45] According Nicholson, the wave shape and the value of ΔE_p are functions of scan rate, diffusion coefficient (D_o) and $k^°$. Whereby, the value of $k^°$ is determined using Equation 4.8,

$$k^° = \frac{\Psi \sqrt{\pi a D_o}}{\gamma^\alpha}$$ **(Equation 4.8.)**

a is nFv/RT, Ψ is the sum of both forward and reverse rate constants ($k_f + k_b$) divided by a, γ^α is the ratio of D_0/D_R and is assumed to approximate to 1, and D_o is the diffusion co-efficient of $K_3Fe(CN)_6$. Solving of Equation 4.8. was achieved using values of ΔE_p, from Table 4.2. and the Solver option in Microsoft Excel. Knowing the values of ΔE_p, at various scan rates, it was possible to extrapolate both parameters a and Ψ and returning the value of $k^°$ using a Solver model designed in Microsoft Excel. A summary of these values can be seen in Table 4.3. As can be seen from Table 4.3 the exact value for the rate of heterogeneous electron transfer depends on the experimental timescale employed. A summary of various heterogeneous rate constants for different carbon electrode materials is given in Table 4.4.

Table 4.3. Summary of data obtained using Nicholson kinetics for a solution containing 1.6 mM $K_3Fe(CN)_6$ in 1.0 M KCl, a working electrode was the carbon composite, Ag/AgCl was the reference electrode and a Pt, auxiliary electrode were used.

Scan rate (Vs^{-1})	Ψ	ΔEp (mV)	a	K° 10^{-4} cm/s
0.5	0.0950	215	19.471	0.187
1	0.0309	312	38.943	8.59
1.5	0.0274	322	58.415	9.35
2	0.0235	335	27.260	5.47
5	0.0069	433	194.716	4.29
7.5	0.0063	439	292.075	4.90
10	0.0028	530	389.433	2.49
15	0.0028	531	584.150	3.03
20	0.0282	531	778.867	3.50

Table 4.4. Comparing the heterogeneous electron transfer rate for various carbon electrode materials.

Electrode Material	Electrolyte	K° 10^{-3} cm/s	Reference
GC[a]	1.0 M KCl	30	28
GCP[b]	1.0 M KCl	6.2	46
CPE[c]	1.0 M KCl	0.44	46
HOPG[d]	1.0 M KCl	0.001	28
CCE[e]	1.0 M KCl	0.017–0.35	Table 4.2

[a]GC: Glassy carbon electrode, values taken over a range of scan rates [b]GCP: Glassy carbon paste electrode [c]CPE: Carbon paste electrode [d] HOPG: highly ordered pyrolytic graphite. CCE: carbon composite electrode.

This sluggish electron transfer of these carbon composite electrodes has been observed previously for CPE[47] and has been attributed to the presence of the pasting liquid resulting in a decrease in the rate of electron transfer. Other theories for slower electrode kinetics have suggested that in the process of mixing graphite with the epoxy polymer a thin polymer film forms over the graphite. As a result of this film formation the distance which electrons from various graphite particles within the composite electrode are required to travel from the electrode surface to the redox species in solution is increased, and, since, the rate of electron transfer is distance dependent there *is* an observation of more sluggish electron transfer. Whatever the reason the addition of any pasting liquid or polymer is known to decrease the electron transfer rates when compared to clean carbon electrodes.[38]
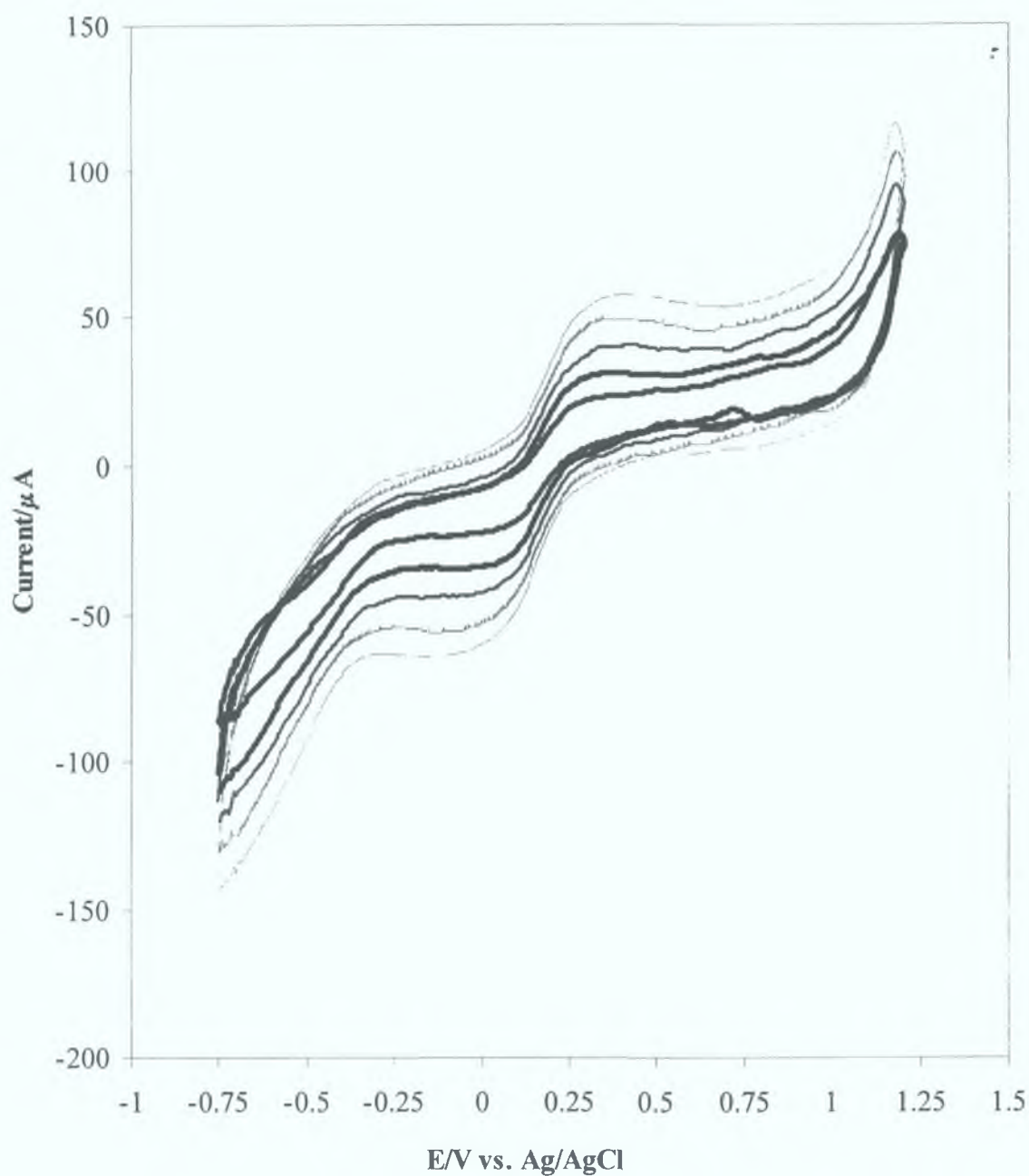
Figure 4.18. Voltammograms of carbon composite electrode in 1.6 mM $K_3Fe(CN)_6$ with 0.1 M KCl as supporting electrolyte, scan rates employed from outer to inner voltammogram were 0.500, 0.400, 0.300, 0.200, and 0.100 Vs^{-1}. Ag/AgCl reference electrode and Pt. auxiliary electrode were used

4.6 Conclusion

As was stated previously these particular carbon–polymer composite electrodes have been used successfully for analytical applications since 1993.[48,49] Additionally, other research groups report on similar carbon–polymer composites designs with many successful applications.[50,51] Possibly one of the main advantages of using carbon-polymer electrodes over their more traditional counterparts such as glassy carbon is associated with the malleability, due to the presence of polymer, of the overall composite allowing the construction of electrodes which require for a specific purpose a specific shape and size. Other advantages are associated with their analytical application especially the relatively low limit of detection, when compared with more traditional macroelectrodes.

Although, various publications [12,5,52,53] related to carbon polymer composite electrodes have mentioned the presence of UMEs array behaviour no electrochemical characterisation into this behaviour has been studied for any of the reported composites.

The concept of a UMEs was brought to the attention mainly by pioneers such as Oldham[54,55] and Savéant[56,57] both of whom contributed mathematical models capable of describing the unique steady state voltammetry of these electrodes. This unique behaviour is mainly achieved through a reduced electrode area which is smaller than the Nernst diffusion layer $(D_oC_t)^{1/2}$. A consequence of reduced surface area is the reduction in iR drop allowing very fast reactions to be studied and also offering the capability to study electrode reactions in very resistive media.[58] Additionally the capability to generate steady state currents has resulted in dramatically lowering the limit of detection, hence, enhancing the sensitivity of the electrodes and their applications to other areas of analysis. Such advantages offered to revolutionise the area of electroanalytical chemistry, but, a problem existed in that the current generated by these UME was very small, hence, specialised costly equipment was required. As a solution for this low current output it was suggested that by designing a multiple array of UME that consisted of N identically constructed UME connected in parallel, therefore, sensitivity is maintained while the current output is increased. Ideally, these UMEs arrays should yield a current amplification by a factor of N relative to a single UMEs. While, the current vs. time response should be comparable to that of a single UMEs. Studies show that while it is possible to obtain close to ideal characteristics, the actual

manufacturing and design of these devices prove to be more complicated than originally thought hence the initial concept of overcoming cost problems associated with instrumental requirements met new problems associated with design. Given the possible suggestion of UMEs array like behaviour a logical choice involved the characterisation of carbon-polymer composite electrodes, especially, when one considers the amount of analytical applications that use these devices.[12]

SEM images obtained show that even with extensive cleaning and polishing procedures these electrodes exhibit a surface that is extremely heterogeneous in nature. Studies carried out using the semi-conductor analyser demonstrates that these electrodes have a wide variation of conductivity on the surface of the electrode, suggesting a random distribution of polymer within the film.

Due to the lack of conclusive evidence which can be drawn from the two surface techniques used, the necessity to electrochemically characterise these electrodes is evident. It is worth mentioning that it was wished to investigate the surface conductivity of these electrodes using conductive-atomic force microscopy, however due to the roughness of the surface it was not possible.

Cyclic voltammetry experiments confirm the presence of three different diffusional patterns. Firstly, at slow scan rates the evidence of UMEs array behaviour is very convincing, sigmoidal shaped voltammograms are apparent at scan rates of 0.002 Vs^{-1}. In addition to these single UMEs characteristics is the high current output that can be measured with conventional laboratory equipment, this similar to what has been seen for UMEs arrays. A second or intermediate diffusional pattern was seen when the scan rates were increased above 0.500 but below 2 Vs^{-1}, in this incidence increasing the scan rate result in voltammetric broadening while maintaining a semi sigmoidal shape. It has been suggested that this behaviour is because of loss of diffusional independence. The third diffusional pattern that is observed at scan rates faster than 2 Vs^{-1}, is the presence of macroelectrode like behaviour, as is evident from peak-to-peak separation. However, unlike a macroelectrode, in the presence of a reversible one electron fast redox couple the electrochemical behaviour is quasi-reversible. Because of the overlapping of individual diffusional fields the electrochemical behaviour begins to be dominated by linear diffusion with contribution from radial diffusion being negligible, hence, electrochemical behaviour similar to that of a macroelectrode is observed.

In conclusion, from cyclic voltammetry experiments the presence of UMEs behaviour at slow scan rates is evident although this behaviour is lost as the scan rates increase. An explanation for this loss in UMEs behaviour has been explained through the necessity for sufficient spacing between individual electroactive areas within the epoxy resin. Many theoretical treatments exist which describe the necessity for sufficient spacing between active areas, however, most of these theories have been postulated for UMEs arrays, where it is possible to control the spacing between active areas, control of intersite separation is not possible for these electrodes.

The investigation into heterogeneous electron transfer rates indicates the same as was observed for the classical carbon paste electrodes: the presence of an insulating polymer layer results in a more sluggish rate of electron transfer. However, as Table 4.4 indicates the rates of electron transfer are faster than what could be expected for other carbon based electrodes.

In conclusion, from the experimental results presented above the following may be said about carbon-epoxy composite electrodes these are summarised as follows:

1) Carbon composites are capable of generating steady state currents with a higher current output.

2) The capability of these composite electrodes to carry out analysis in highly resistive media in addition to aqueous media which contains little or not electrolyte -Figure 4.15

3) A common problem in the fabrication of UME is the presence of leakage currents due to inadequate sealing. From experience of constructing these carbon composite materials, the problem was rarely encountered.

From the experimental results presented above it may be said in situations which require slow scan rate experiments, or experiments in highly resistive media the use of these carbon composite electrodes, present advantages which can be carried out on a standard lab potentiostat overcoming the need for instrumentation capable of dealing with low currents.

Although much work to date has focused on the use of graphite carbon it is possible that in situations which require metal electrodes, for self assembled monolayers

196

onto gold, that this concept of a rigid polymer support may be applied. Other possible improvements that could be suggested are a maintaining the carbon content but reducing the size of the carbon particles dispersed within the rigid matrix.

4.7   References

1.   Tess, M. E.; Cox, J. A. *J. Pharm. Biomed. Anal.*, **1999**, *19*, 55

2.   Yabuki, S.; Mitzutani, F.; Katsura, T. *Biosens. Bioelectron.* **1992**, *7*, 695

3.   Yabuki, S.; Mitzutani, F.; Katsura, T. *Sensors and Actuators B*, **1994**, *20*, 159

4.   Rajendran, V.; Csoregi, E.; Okamoto, Y.; Gorton, L. *Anal. Chim. Acta*, **1998**, 373, 241

5.   Adams, R. N. Electrochemistry at Solid Electrodes. Marcel Dekker, New York, 1969, 280

6.   Kaufmann, J. M.; Linders, C. R.; Patriarche, G. J. *Talanta*, **1988**, *35*, 179

7.   Forster, R. J. *Chem. Soc. Rev.*, **1994**, *289*

8.   Duo, R.; Pena, M. J.; Celdran, R. *J. Electroanal. Chem.*, **1996**, *404*, 99

9.   *Microelectrodes: Theory and Applications*. Vol. 197. Section 6, Montenegro, M. I.; Queiros, M. A.; Daschbach, J. L., Eds. Kluwer Academic Publishers, Boston, **1991**, p. 341

10.   Forster, R. J.; Faulkner, L. R. *J. Am. Chem. Soc.*, **1994**, *116*, 5444

11.   Forster, R. J.; Faulkner, L. R. *J. Am. Chem. Soc.*, **1994**, *116*, 5453

12.   Oliveira-Brett, A. M.; Diculescu, V.; Piedade, J. A. P. *Bioelectrochem.*, **2002**, *55*, 61

13.   Santandreu, M.; Solé, S.; Alegret, S.; Fàbregas, E. *Anal. Chem.*, **1997**, *69*, 2080

14.   Adams, R. N. *Anal. Chem.*, **1958**, *30*, 1576

15.   Olson, C.; Adams, R. N. *Anal. Chim. Acta* **1960**, *22*, 582

16.   Olson, C.; Adams, R.N. *Anal. Chim. Acta* **1963**, *29*, 358

17.   Creasy, K. E.; Shaw. B. R. *Anal. Chem.* **1989**, *61*, 1460

18.   Morales, A.; Céspedes, F.; Muñoz, J.; Fàbregas, E.; Alegret, S. *Anal. Chim. Acta*, **1996**, *332*, 131

19.   Alegret, S.; Céspedes, F.; Martorell, D.; Morales, A.; Fàbregas, E.; Centelles, E.; Muñoz, J. *Biosens. Bioelectron.* **1996**, *11*, 35

20.   Miertus, S.; Katrlik, J.; Pizzariello, A.; Stredansky, M.; Svitel, J.; Svorc, J. *Biosens. Bioelectron.*, **1998**, *13*, 911

21. Onnerfjord, P.; Emmeus, J.; Marko-Varga, G.; Gorton, L.; Ortega, F.; Domínguez, E. *Biosen. Bioelectron.* **1995**, *10*, 607

22. Wang, J.; Chen, Q. *Electroanal*, **1994**, *6*, 850

23. C. Petit, A. González-Cortes, J. M. Kaufmann. *Talanta*, **1995,** *42*, 1783

24. Alegret, S. *Analyst*, **1996**, *121*, 1751

25. Kalcher, K.; Kaufmann, J. M.; Wang, J.; Svancara, I.; Vytras, K. *Electroanal.*, **1995**, *7*, 5

26. Kaufmann, J.M.; Linders, C. R.; Patriarche, G. J. *Talanta*, **1988**, *35*, 179

27. Adélio, A. S.; Machado, C. *Analyst*, **1994**, *119*, 2263

28. Céspedes, F.; Alegret, S. *TRAC*, **2000**, *19*, 276

29. B. Ellis (Ed.) Chemistry and Technology of Epoxy Resins. 1993. Chapman and Hall, Glasgow, U.K.

30. Bergeveld, P.; van der Schoot, B.H. Sel. Electrode Rev., **1988**, 10, 5

31. O'Hara, D.; Macpherson, J. V.;. Willows, A. *Electrochem. Commun.*, **2002**, *4*, 245

32. http://www2.arnes.si

33. www.wentworthlabs.com/

34. Forster, R. J. *Chem. Rev.*, **1994**, 289

35. *Microelectrodes: Theory and Applications*. Vol. 197. Montenegro, M. I.; Queiros, M. A.; Daschbach, J. L., (Eds.) Kluwer Academic Publishers, Boston, **1991**

36. Fletcher, S.; Horne, M. *Electrochem. Commun*, **1999**, *1*, 502

37. Wrightman, R. M.; Wipf, D. O. Voltammetry at ultraUME in A. J. Bard (Ed.) Electroanalytical Chemistry, 15, Marcel Dekker, New York, 1989

38. Bond, A. M.; Oldham, K. B.; Zoski, C. G. *Anal. Chim. Acta*, **1989**, 177

39. Fletcher, S. Random assemblies of mircodisk electrodes (RAM electrodes) for nucleation studies. A tutorial review. In. *Microelectrodes: Theory and Applications*. Vol. 197. Montenegro, M. I.; Queiros, M. A.; Daschbach, J. L., (Eds.) Kluwer Academic Publishers, Boston, **1991**

40. Marken, F.; Gerrard, M. L.; Mellor, I. M. *Electrochem. Commun.*, **2001**, *3*, 177

41. Weaver, M. J.; Safford, L. K. *J. Electroanal. Chem.*, **1992**, *331*, 857

42.   Wightman, R. M.; Wipf, D. O. Electroanalytical Chemistry, vol. 15, A. J. Bard (Ed.). Marcel Dekker, New York, 1989

43.   Forster, R. J.; Vos. J. G. *Langmuir*, **1994**, *10*, 4336

44.   Bard, A. J.; Faulkner, L. R. Electrochemical Methods, Fundamentals and Applications. Wiley and Sons, New York, USA, 1980

45.   Nicholson, R. S.; Shain, I. *Anal. Chem.*, **1964**, 36, 706

46.   Wang, J.; Kirgöz, Ü. A.; Mo, J.-W.; Lu, J.; Kawde, A. N.; Muck, A. *Electrochem. Comm.,* **2001**, *3*, 203

47.   Rice, M. E.; Galus, Z.; Adams, R. N. *Electroanal. Chem,.* **1983**, *143*, 89

48.   Céspedes, F.; Martínez-Fàbregas, E.; Alegret, S. *Anal. Chim. Acta*, **1993**, *284*, 21

49.   Céspedes, F.; Martínez-Fàbregas, E.; Bartrolí, J.; Alegret, S. *Anal. Chem.* **1993,** 273, 409

50.   Wang, J.; Varughese, K. *Anal. Chem.* **1990**, *62*, 318

51.   Wang, J.; Golden, T.; Varughese, K.; El-Rayes, I. *Anal. Chem.* **1989,** *61*, 508

52.   Céspedes, F.; Martínez-Fàbregas, E.; Alegret, S. *TrAC.* **1996**, *15*, 296

53.   Pividori, M. I.; Merkoçi, A.; Alegret, S. *Analyst*, **2001**, *126*, 1551

54.   Bond, A. M.; Oldham, K. B.; Zoski, C. B. *Anal. Chim. Acta*, **1989**, *177*

55.   Oldham, K. B. *J. Electroanal. Chem.* **1981**, *122*, 1

56.   Amatore, C.; Savéant, J. M.; Tessier, D. *J. Electroanal. Chem.* **1983**, *147*, 39

57.   Amatore, C.; Savéant, J.M.; Tessier, D. *J. Electroanal. Chem.* **1983**, *146*, 37

58.   Ciszkowska, M.; Sjokek, Z. *J. Electroanal. Chem.* **1999**, *466*, 129

Chapter 5

Development of a Sequence Specific Genosensor Using Carbon-Polymer Composite Electrodes

5.1 Introduction

Staphylococcus aureus has long been recognised as one of the major human pathogens responsible for a wide range of afflictions from minor infections of the skin to wound infections, bacterial infections of the central nervous system, respiratory and urinary tracts, and infections associated with intravascular devices and foreign bodies.[1,2] Most *S aureus* are opportunistic pathogens that can colonise individuals, without symptoms, for either short or extended periods of time, causing disease when the immune system becomes compromised. Indications are that bacterial pathogens have affected human beings since prehistoric times. Before the antibiotic era *S aureus* had a high mortality rate. In 1941, the mortality rate of *S aureus* bacteria at the Boston City Hospital was reported to be 82%.[3] *S aureus* is unsurpassed by any other human pathogen in terms of its versatility of pathogenic strategies, numbers of virulence factors, and capacity to survive and multiply in a wide range of environments. The immense genetic repertoire of this bacteria for adapting to rapidly changing and uniformly hostile environments was repeatedly shown by the emergence of *S aureus* strains that acquired resistance mechanisms to virtually all anti-microbial agents shortly after their introduction into clinical practice.

The introduction of benzylpenicillin into chemotherapy in the early 1945–1946 found *S aureus* fully susceptible and several of the first success of penicillin therapy were related to the cure of formerly untreatable staphylococcal diseases.[4] However, by the mid 1950s the number of *S aureus* clinical isolates showing high level of resistance to penicillin increased rapidly, to such an extent that penicillin ceased to be a useful therapeutic agent against staphylococcal infections. The mechanism of this resistance was attributed to the acquisition of a plasmid borne penicillinase capable of degrading the antibiotic prior to it reaching its cellular targets. The effects of this "plasmid borne epidemic" was first noticed in hospital isolates but soon after penicillinase-based mechanisms found their way into the community isolates also.[5] A recent study of the *S aureus* colonising flora of 1001 healthy volunteers showed that 97% of the *S aureus* isolates recovered carried the resistant trait to penicillin.[6]

In addition to this, the power of *S aureus* to mount counter-strategies to other products of the antibiotic era besides penicillin is well documented. Records of the Danish Health Board registered the years of introduction of various antimicrobial agents.[5] According to these records, the evolutionary speed at which *S aureus* developed resistance increased. Resistance to penicillin was first reported in 1957 years,[5] eight years after being introduce, while resistance to methicillin, introduced in 1960, was first reported in 1961.[7] The first outbreak of methicillin resistance *Staphylococcus aureus* (MRSA) was reported in 1963.[8] A report from the National Nosocomial Infections Surveillance System (NNISS), recorded an increase of MRSA in large US hospitals, from 4% in the 1980s to 50% in the late 1990s. In some hospitals, resistance frequencies are as high as 80%.[9]

Molecular epidemiology has identified one common linage of all *S aureus* resistant bacteria to the acquisition 2.1kb stretch of DNA not native to the species *S aureus* and which is embedded in a larger block—up to 60 kb—of additional "foreign" DNA called the *mec* element[10] or staphylococcal chromosomal cassette (SCC*mec*),[11] which together with *mec*A is incorporated into the *S aureus* chromosome at a site-specific location.[12,13] In brief the *mec*A gene encodes for a 78 kDa penicillin-binding protein (PBP2A), which has low affinity for beta-lactum antibiotics, hence, creating resistance to target specific antibiotics.[14,15]

To date, the most efficient method of detection and identification of the *mec*A gene, after isolation and amplification from a given sample, involves the use of a technique known as pulse-field gel electrophoresis (PFGE). PFGE has been suggested as the gold standard for outbreak investigations.[16] One drawback with this technique is that the relatively long processing time, approx. 48 hr., may be too long to prevent further outbreaks.

Additional evidence that current methodologies used for detection of pathogenic bacteria are too time consuming, is the recent outbreak of foot and mouth disease in the U.K. in 2001. Detection of the presence of this virus employed an enzyme-linked immuno-sorbant assay (ELISA)[17] and involved the detection of antibodies specific to a triggered immune response within animals that have the foot and mouth virus infection. Problems with this assay are twofold. Firstly, the length of

analysis time was 48 hr. causing much stress to livestock owners and further risk of contamination of nearby farms before any culling of infected herds could commence. Secondly, using this method it was not possible to detect between antibodies due to an infection and antibodies as result of vaccination, hence, controversy existed over the use of vaccination as a tool to prevent outbreak.

The agar plate test, one of the most common methods employed to detect presence of any bacteria, requires 48 hr. for the development of colonies that may then be isolated.[18] While non-resistant *S aureus* requires only 24 hr. hence, if both resistant and non-resistant strains of bacteria are present, it can be difficult to interpret the results in a confident manner. It is known[1] that 646 of the 3,704 MRSA isolates identified between 1956–1970 demonstrated resistances to most antibiotics, including methicillin. For this reason the possibility of developing an agar plate test to identify all these individual strains of MRSA is unrealistic.

Advances in the DNA sequencing which, have been made the past decades have met with an increased interest in using methods which would be capable of detecting a specific sequence of DNA. Conveniently, in the case of *S aureus* all multiple resistant strains have a common DNA sequence absent in non-resistant strains. This is known as the *mec*A gene.[19]

As was outlined in Chapter 1.3, biosensor systems using the detection principle of enzyme labelled antibody are becoming an increasingly important route to reduce the analysis time and are proving to be very successful, easy to use and inexpensive to produce. An extensive review of these methods exists, demonstrating that detection of the hybridisation event is the most efficient choice.[20]

This chapter describes the development of a genosensor using carbon-polymer composite electrodes, as detailed in Chapter four, that have been modified with either avidin or streptavidin. Exploitation of the strong interaction between biotin–avidin or biotin–streptavidin allows immobilisation of a biotin labelled capture probe, containing the complementary DNA sequence to the target probe. Hybridisation of the target DNA to this capture probe and an antibody labelled sequence is achieved simultaneously. Upon addition of an enzyme labelled antigen, specific to the antibody labelled DNA, electrochemical detection is achieved.

Prior to detection of the MRSA *mec*A gene optimisation of the genosensor was carried out using a simple nucleotide sequence at low concentrations, indicating the capability of a one step hybridisation and immobilisation procedure. Once all parameters were optimised, the proposed sensor design was applied to detect the presence of MRSA at concentrations similar to that recovered from a polymerase chain reaction (PCR). When using PCR methods for amplifying DNA there is the possibility of more than the desired DNA sequence being present in the final sample. Since there is a danger that the incorrect sequence could hybridise to the capture probe it must be considered as an interferant and treated appropriately. Hence, detection of MRSA in the presence of a DNA sequence, identical in concentration, and differing from the target DNA by only two base-pairs was also carried out. The total experimental time, from moment of capture to moment of detection, is 120 min. Comparisons with a previous sensor design that incorporated streptavidin within the composite electrode show that the avidin based sensor reduces the analysis time and provides a more sensitive current response.

5.2   Apparatus

Amperometric measurements were performed with a LC–4C Amperometric Controller (BAS Bioanalytical System, USA). Cyclic voltammetry measurements were carried out using Autolab PGSTAT 20 (Eco-chemie, The Netherlands). A platinum auxiliary electrode (Crison 52-67 1) with a surface area of XX cm^2 and a double junction Ag/AgCl reference electrode (Orion 900200) with 0.1 M KCl as an external reference solution were used. The carbon composite electrodes, with an internal diameter of 6mm made "in house" were used as the working electrode. The incubations at controlled temperature were carried out in the eppendorf Thermomixer 5436. Both cyclic voltammetry and chronoamperometry were carried out in a 20 cm^3 electrochemical cell.

5.3 Materials and reagents

The composite electrodes were prepared using graphite powder with a particle size of 50 μm (BDH, UK), Epotek H77 (epoxy resin), and hardener (Epoxy Technology, USA). The DNA oligomers were obtained from TIB MOLBIOL (Germany). The base sequences of these oligomers can be seen below

- Biotin–DNA, (**A**), Biotin – 5´ – AAA AAA AAA AAA AAA AAA AA

- Target–DNA, (**B**), 5´–AAA AAA AAA AAA AAA AAA AAA AAA ATT TTT TTT TTT TTT TTT TTT TTT TT–3´

- Digoxigenin–DNA, (**C**), Dig–3´–TTT TTT TTT TTT TTT TTT TT–5´

- MRSA capture probe, (**D**), Biotin–3´–GTC GTT TAC CCT TGA GAT TA–5´

- Methicillin resistance *Staphylococcus aureus* (MRSA), (**E**), 5´–CAG CAA ATG GGA ACT CTA ATG GAG ATT TTT CCA AAC AAA ATA TAG ATA TT–3

- MRSA–digoxigenin labelled DNA, (**F**), 3´- GGT TTG TTT TAT ATC TAT AA–5´– Dig

- Mismatch–DNA, (**G**), 3´–GGT TTG TCT TAT AGC TAT AA–5´–Dig

The hybridisation solution (10 x SSC, 2 x Denhardt´s, 200 μg/ml chloroform extracted salmon testes DNA), Bovine serum albumin, sodium dodecyl sulphate (SDS), Tween 20, formamide and hydroquinone were purchased by Sigma. The anti-digoxigenin horseradish peroxidase (anti-Dig.–HRP), streptavidin – HRP and biotin were purchased from Roche (Germany). Tris–HCl, NaCl and hydrogen peroxide were purchased from MERCK (Germany). HCl was purchased from Panrec (Spain). Aqueous solutions were prepared from double distilled water. The electrolyte in all cases was 0.1 M phosphate buffer, pH 7.4, containing 0.1 M KCl and 1.81 mM hydroquinone. For cyclic voltammetry the scan range was from –0.75 to 1.0 V (vs. Ag/AgCl). For chronoamperometry the applied potential was –0.250 V (vs. Ag/AgCl)

5.4   Experimental

5.4.1   Construction of carbon-polymer biocomposite modified with a biocomponent

Graphite powder and epoxy resins were mixed in a ratio of 1:4 (w/w). For every gram of graphite/epoxy mixture, an additional 5, 15 or 20 mg of streptavidin or avidin were added – resulting in either a 0.5, 1.5 and 2% (w/w) streptavidin or avidin carbon-polymer biocomposite. This mixture was thoroughly hand mixed – ensuring uniform dispersion of the streptavidin and carbon throughout the polymer. Polymerisation between the Epoxy resin and hardener is achieved upon curing at 50 °C for one week. The rest of the experimental procedure followed that which has been previously described in 4.2.1

5.4.2   Determination of working potential using cyclic voltammetry

For this study a solution containing 1.81 mM hydroquinone, 0.1 M phosphate buffer, pH 7.4 with 0.1 M KCl supporting electrolyte was used. A range of scan rates between 0.05 and 1 V/s were employed the potential window ranged between -1.0–1.0 V. All electrodes were cleaned as described in 4.1.1 with the exception of the nitric acid washing step, instead the electrodes once polished were sonicated in Milli-Q water for 30s. Unless otherwise mentioned all experiments were carried out for both the avidin and the streptavidin composite electrodes.

5.4.3   Immobilisation and hybridisation procedure

The experimental procedure consists of three individual steps, as depicted in Figure 5.1*b–d*. It should be noted that the final volume of 150 µl was chosen purely because it corresponds to quantity required to ensure that the electrode is fully immersed in the solution. Firstly, to an eppendorf containing a volume of 120 µl of the hybridisation solution, previously equilibrated to 42 °C, 10µl of all oligomers **A**, **B**, **C** are deposited. The final concentration of the DNA in the eppendorf is 150 picomolar (1×10^{-12} mol l^{-1}). To this eppendorf the carbon composite electrode is then immersed and shaken gently for 60 min. The projected goal of this sensor design depends on the ability of the biotin–DNA capture probe to successfully immobilise onto the electrode surface

through a biotin–avidin or streptavidin–biotin interaction. Simultaneous hybridisation occurs between oligomer **A** and **B** and between **B** and **C**, as illustrated in Figure 5.1.*b*. . The electrode is then removed from the eppendorf and washed gently with Tris buffer pH 7.1, removing unbound DNA. When the fully prepared DNA electrodes were not in use, they were stored in Tris buffer pH 7.1 and refrigerated at 4 °C. It should be noted that although the sequences of oligomer **A** and **C** are complementary, the presence of the bulky modified components at the 5′ and 3′ ends respectively prevents hybridisation from occurring.

5.4.4   *Enzymatic labelling*

The next and most important stage of this process involves the attachment of the enzyme marker, anti-Dig – HRP to oligomer **C**, Figure 5.1.*c*. This attachment is achieved by adding 10 µl of anti-Dig – HRP (12.45 µg/µl in concentration) to 140 µl of phosphate buffered saline (PBS). Previously mentioned in Chapter 2.3.5, PBS acts as a blocking agent to prevent non-specific absorption of enzyme onto the electrode surface. This is an essential procedure to ensure the quality of the results obtained, as will be demonstrated later in Section 5.4.6.

It is known that the antigen digoxigenin attaches to its antibody, anti-digoxigenin, in controlled temperature environment of 37° C.[21] Hence, by incubating the composite electrode in an eppendorf for 40 min. at 37° C, with slight agitation, attachment of an enzyme labelled anti-digoxigenin is accomplished, as will be demonstrated in Section 5.4.5. After removing, the electrode is washed with a post incubation wash solution (10mM sodium phosphate pH 6.5, 0.5 M NaCl, 0.05 % w/v Tween 20, 0.1 % BSA 1mM EDTA) again with slight agitation. Once the immobilisation, hybridisation and enzyme labelling have been achieved, if the electrodes were not required immediately they were left standing in Tris buffer pH 7.1 and stored at 4°C.

5.4.5   *Electrochemical enzyme activity determination*

The amount of enzyme labelled antibody bound to the oligomer **C** was determined using the following electrochemical detection procedure. Experiments were carried out at 22 ± 2 °C using the hydroquinone electrolyte solution mentioned in Section 4.1.2 above.

The electrolyte was purged with nitrogen gas prior to use for at least 1 hr. Due to the sensitivity of hydroquinone to photo-oxidation, the supporting electrolyte was prepared daily. From Equation 5.1 below and Figure 5.1.d it can be seen that in the presence of HRP and at a sufficiently negative potential hydroquinone is oxidised to benzoquinone resulting in a flow of electrons which may be measured using constant potential chronoamperometry.

Firstly, it is necessary to carry out cyclic voltammetry experiments to establish the exact potential at which this reaction proceeds for these biologically modified carbon composite electrodes. Following the correct identification of the working potential using cyclic voltammetry, at a scan rate of 0.100 V/s, chronoamperometric experiments were performed at an applied potential of –0.250 V against Ag/AgCl electrode, explanation of these conditions will be give in Section 5.1.

Prior to measuring any current the sensor was allowed to equilibrate for 10 min. in the hydroquinone electrolyte solution. Once the current has stabilised H_2O_2 was added to yield a final concentration of 176 μM. This concentration of H_2O_2 was determined by standard addition method, where 50 μl of H_2O_2 (0.1M) was added to a solution containing 0.5 nmol anti-digoxigenin HRP, 176 μM corresponded to the maximum current response obtained for this concentration.[51] After, addition of the substrate, the current was again measured for a further 10 min. The electrode response is defined as the difference in current before and after the addition of H_2O_2.

$$hydroquinone + H_2O_2 \xrightarrow{\text{horseradish peroxidase}} benzoquinone + H_2O$$

$$benzoquinone + 2H^+ + 2e^- \xrightarrow{-0.250V \ vs \ Ag/AgCl} hydroquinone \qquad \textbf{(Equation 5.1)}$$
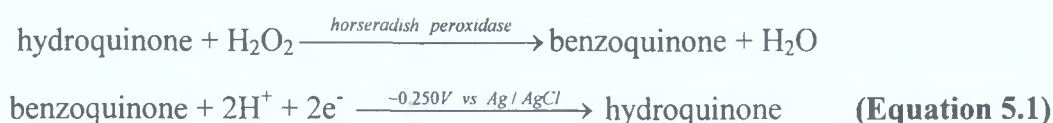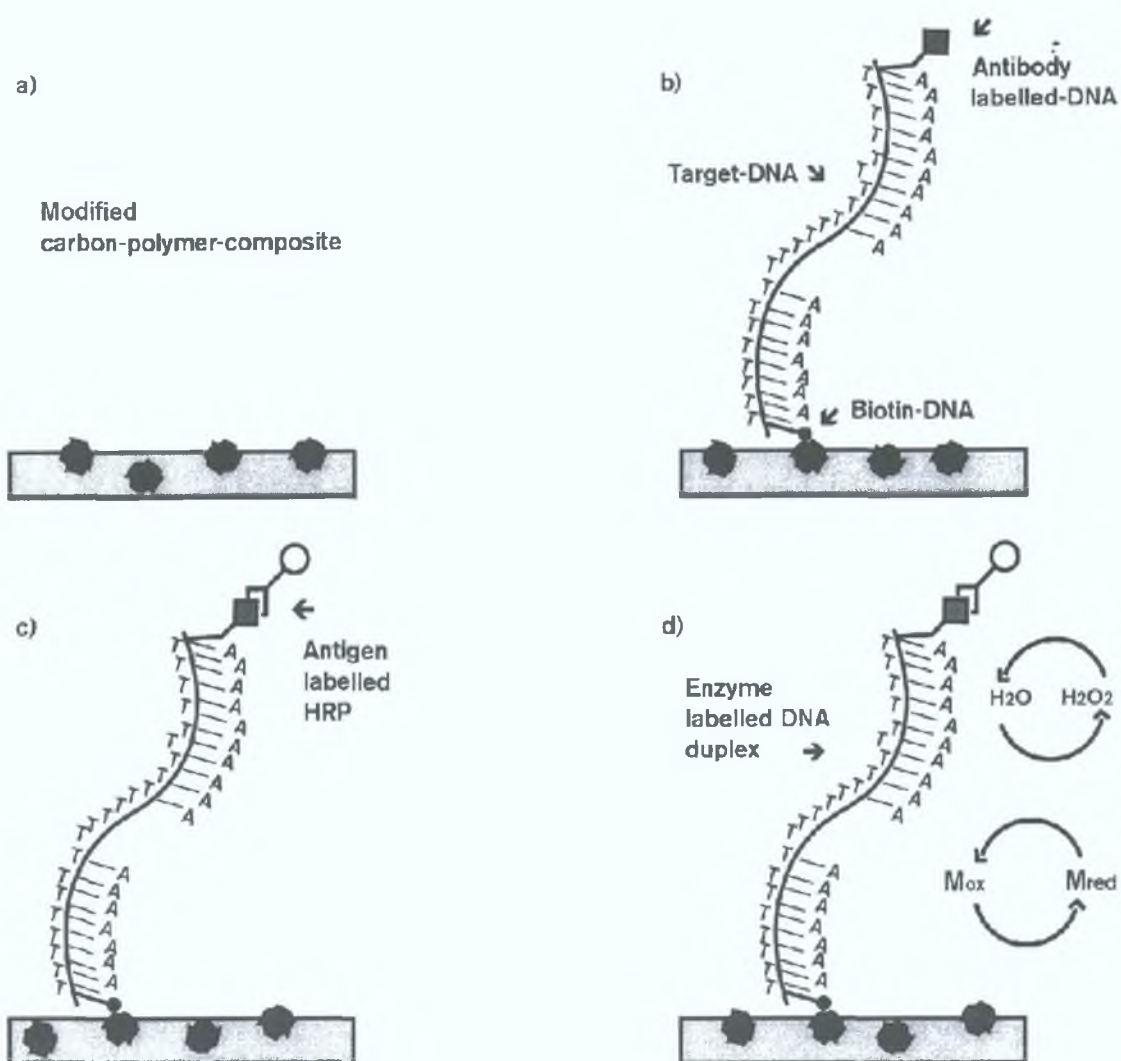
**Figure 5.1.** Schematic representation of the one step hybridisation/immobilisation of DNA to an electrode surface. (**a**) Freshly exposed modified carbon-polymer composite, (**b**) immobilisation and hybridisation step, (**c**) enzymatic labelling with antidigoxigen–HRP and (**d**) electrochemical detection using 1.81 mM hydroquinone in 0.1M phosphate buffer pH 7.4 and 0.1 M KCL and H_2O_2 with a final concentration of 176μM.

5.4.6   Non-specific adsorption evaluation

The main objective of this study is to establish that the current response is due to attachment of the antibody labelled HRP to its antigen, and not due to physical adsorption onto the electrode surface. In order to study this effect three different assays were carried out (i) carbon-polymer composites, which contain no biocomponent, were used and the same procedure as above was followed. Additionally the composite electrodes prepared above were also used. In this case, the same procedure was followed but omitting either (ii) biotin–DNA or (iii) target–DNA, allowing the selectivity of the response to be ascertained.

5.4.7   Stability study

The stability of these composite electrodes was studied over time. The procedure in this case involved immersing the composite electrodes in a 150 µl (12.45µg/µl) of a biotin–streptavidin–HRP conjugate for 60min. at 42°C with slight agitation. Choice of biotin–streptavidin–HRP sandwich assay is due to lack of commercially available biotin–HRP. Electrochemical detection was carried out as described in section 5.4.5 above for the detection of DNA/HRP conjugate.

5.4.8   Detection of MRSA – non-competitive format

Advances in DNA sequencing[22] in the past number of years are demonstrating the plausibility of using a DNA sensor, in conjunction with the polymerase chain reaction (PCR), to identify DNA sequences specific to pathogenic organism in "real time", low cost manner. For this reason the same protocol outlined in sections 5.4.3–5.4.5 was applied with slight modification. Firstly, a concentration of 150 nmol is used as this corresponds to a typical yield of amplified DNA from a short PCR amplification procedure in a time of 15 min.[6] Secondly, oligonucleotides **D–F** were used. Oligonucleotide **D** is a 50 mer sequence known as the *mec*A gene. This *mec*A gene is known to be specific to antibiotic resistant strains of the pathogen Staphylococcus *aureus.*[22] These experiments were only carried out on the avidin carbon-polymer composite electrode.

5.4.9   Detection of MRSA in the presence of a mismatch DNA – competitive format

Advances in the DNA sequencing technology has been greatly assisted by use of the amplification technique, polymerase chain reaction, (PCR). One major drawback associated with PCR is that more than the desired sequence is amplified. Hence, the purpose of this experiment is to establish if the proposed sensor is capable of distinguishing between two DNA sequences which differ very marginally in the base-pairs. Similar to Section 5.4.8, oligomers **D–F** in addition to a mismatch sequence were used, **G.** The difference in base-pairs of **G** are highlighted in bold in sequence **G.** The immobilisation, hybridisation and enzyme labelling procedure followed that outlined in Sections 5.4.3–5.4.5. The final concentration of all species is 150 nmol and all experiments were carried out on four independent electrodes.

5.5   Results and Discussion

5.5.1   Cyclic voltammetry of streptavidin carbon composite electrodes

As was established in previous chapters, cyclic voltammetry is an ideal preliminary experimental technique allowing the location of the redox potentials for a specific species to be identified. The characterisation of these electrodes has been presented in Section 4.1.1. To re-illustrate the effect of electrode material on the positioning of the peak potential and the current response Figure 5.2 shows a cyclic voltammogram for a glassy carbon and a carbon–polymer composite electrode. Where the upper curve represents the oxidation of hydroquinone to benzoquinone, while the lower curve represent the reverse reaction. Figure 5.3, shows the electrochemical response from both the streptavidin-carbon-polymer composite and avidin-carbon-polymer composite. Both of these results indicate that the chosen constant potential for subsequence chronoamperometric experiments will not cause damage to either DNA or the biocomponents present.

Results of these are presented in Table 5.1 below, highlighting the quasi-reversible nature of hydroquinone and the effects the nature of the electrode has on the overall electrochemical response.

Table 5.1. Summary of anodic (E_{pa}), cathodic (E_{pc}) peak potentials and their ΔEp values for various electrodes in a solution containing 1.81 mM hydroquinone, 0.1 M phosphate buffer pH 7.4 with 0.1 M KCl. A scan rate of 0.1 Vs^{-1} was employed, and corrections were made for influence of iR drop.

	ip_c/ip_a	Ep_a	Ep_c	ΔEp
GC^a	0.84	0.324	-0.149	0.473
CP^b	0.76	0.537	-0.266	0.837
SP^c	0.93	0.339	-0.161	0.500
AP^d	0.97	0.354	-0.206	0.560

[a]Glassy carbon electrode,[b] carbon-polymer composite electrode, [c]streptavidin-carbon-polymer electrode, [d]avidin-carbon-polymer electrode

The first observation that can be made from Figures 5.2 and 5.3 is that the current potential response for the biologically modified composite electrodes is comparable to the response for the unmodified composite electrode, suggesting there is no loss in conductivity. The second observation made Section 4.5.1.3 is due to inadequate sealing/preparation of the composite electrode resulting in stray capacitance currents. The absence of any skewed baseline indicates that there electrodes are suitable for electrochemical experiments.
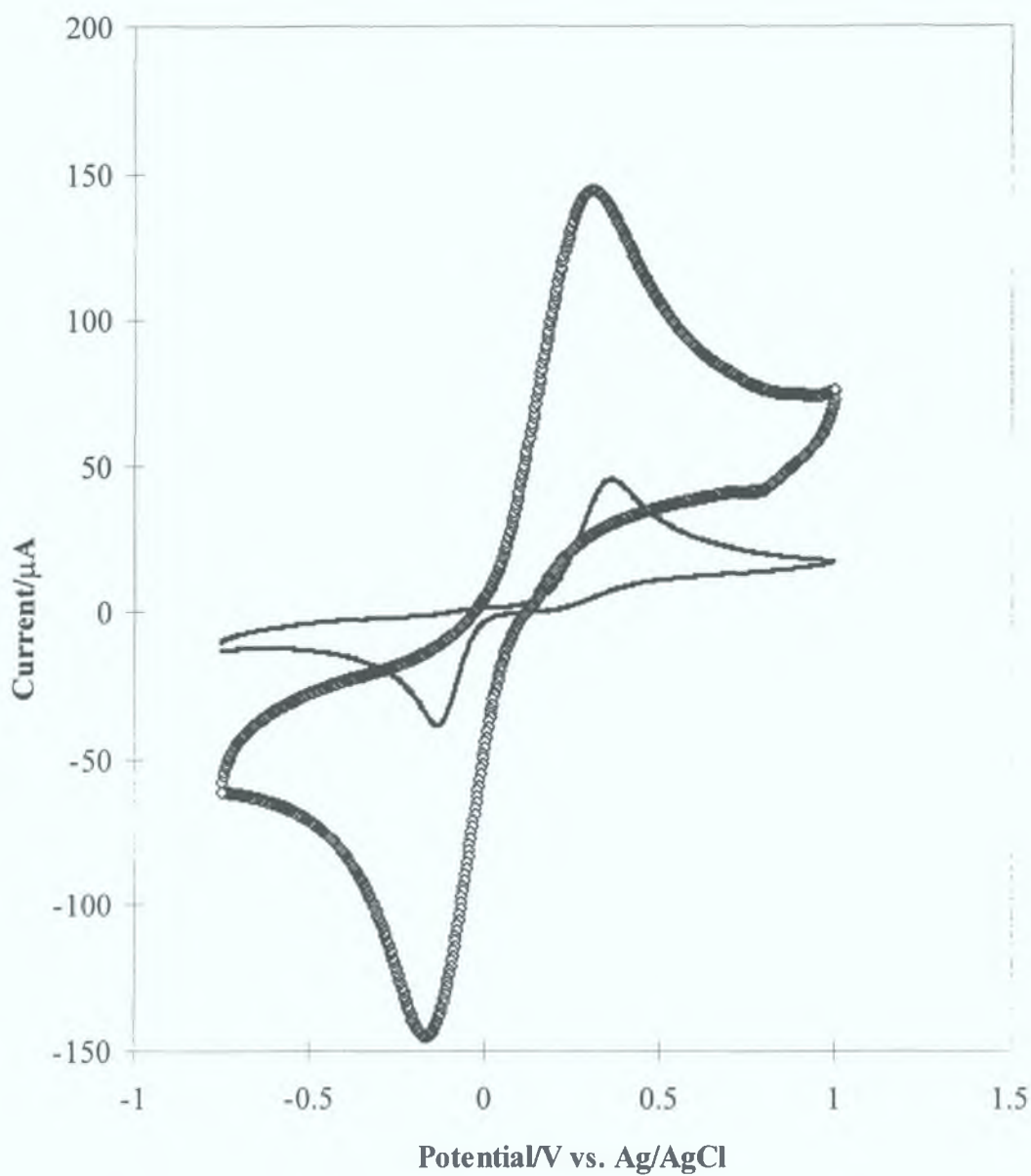
Figure 5.2. Cyclic voltammograms of carbon-polymer composite(▷) and glassy carbon electrode (—) in 1.81 mM hydroquinone with 0.1M KCl in 0.1 M phosphate buffer, pH 7.4. Ag/AgCl reference electrode and a platinum auxiliary electrode were used. Initial potential was –0.6 V in a positive direction.
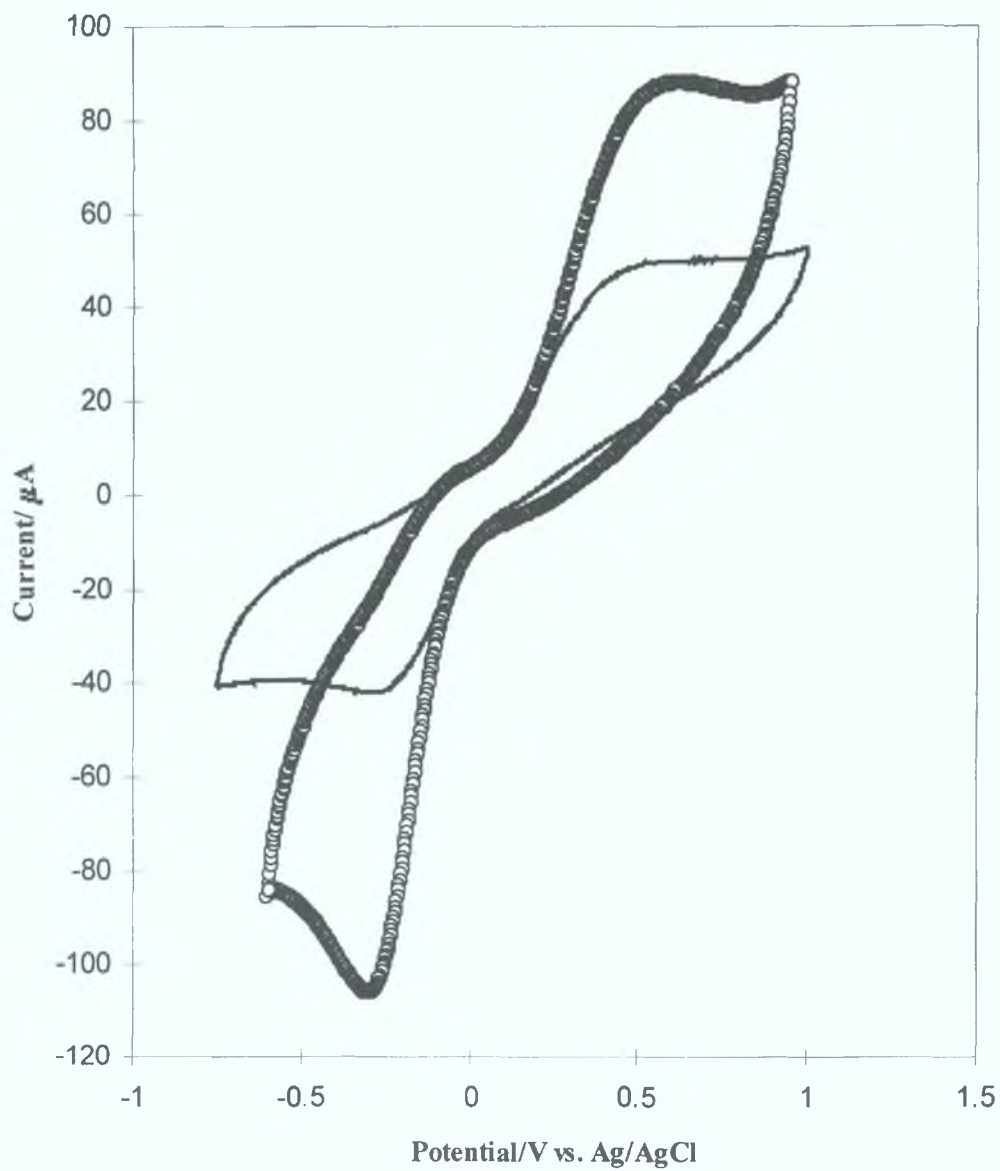
Figure 5.3. Cyclic voltammogram of (□)streptavidin-carbon-polymer and (—) avidin-carbon-composite in 1.81 mM hydroquinone with 0.1M KCl in 0.1 M phosphate buffer, pH 7.4. A Ag/AgCl reference electrode and a platinum auxiliary electrode were used. Initial potential was –0.6 V in a positive direction.

215

*5.5.2   Detection   of   horseradish   peroxidase   using   constant   potential
chronoamperometry and optimisation of streptavidin content within the carbon
composite electrode*

From Figure 5.1, it can be seen that the ultimate objective is to detect the presence of
sequence specific DNA through the use of an enzyme labelled conjugate, horseradish
peroxidase (HRP), and the previously characterised electron mediator hydroquinone.
HRP belongs to a class of enzymes defined as oxidoreductase enzymes using hydrogen
peroxidase as an electron acceptor. Of all the available oxidoreductase enzymes HRP is
one of the more common employed.[23]   In general the peroxide HRP has a total
molecular weight of 42 K_D (kilodaltons), with an isoelectric point of 3.9 and 8.8.[24] The
catalytic path of HRP in the presence of hydrogen peroxide is shown in Figure 5.4 and
Equation 5.2*a–c*.

Native peroxidase (Fe^{3+}) + H_2O_2 → Compound-I + H_2O **(Equation 5.2 a)**

Compound-I + AH_2 → Compound-II + AH*   **(Equation 5.2 b)**

Compound-II + AH_2 → Native peroxidase (Fe^{3+}) + AH* + H_2O **(Equation 5.2 c)**

The first reaction, Equation 5.2 a, involves a two electron oxidation of the ferriheme
prosthetic group of the native peroxidase by H_2O_2. This reaction results in the
formation of the intermediate compound-I (oxidation state +5) which consists of
oxyferryl iron (Fe^{4+}) and a porphyrin π radical. In the next reaction (Equation 5.2 b),
compound-I looses one oxidising equivalent upon one electron reduction by the first
electron donor AH_2 forming intermediate compound-II (oxidation state +4). The latter,
compound-II, subsequently accepts an additional electron from a second donor molecule
AH_2 (Equation 5.2.c), whereby the enzyme is returned to its native resting state,
peroxidase.[23]

There are two methods by which to detect horseradish peroxidase
electrochemically either by direct electron transfer or by mediated electron transfer. The
first method involves direct electron transfer proceeds as depicted in Figure 5.4a. It is
agreed[25,26,27,28] that the electrode current which is measured is as a direct result of

electrochemical reduction of compound-I to compound-II at the electrode surface. This conclusion is supported by the fact that the reduction starts at a potential close to the formal potentials of compound-I/-II and compound–II/HRP(Fe^{3+}), which are seen within the range of 0.63–0.69 V vs. SCE.[29,30,31,32] The heterogeneous electron transfer rate constants have been evaluated for this ferri/ferroperoxidase conversion at gold electrodes modified with viologens.[33] The values of these rate constants were found to be in the range of (1–9) x 10^{-6} cm s^{-1}. The small k^0 observed has been suggested by several authors,[25–34] to indicate that electron transfer between the electrode and the active site of HRP is a slow process.[34] In order to overcome these slow kinetics, an electron mediator is required. Mediators are small redox molecules with inherent high heterogeneous electron transfer rates.[35] In the case of the HRP enzyme, the mediator is used to deliver the electrons from the electrode surface to compound I and II, as shown in Figure 5.4 b. The chosen mediator must react rapidly with the oxidised peroxidase. Both one electron and two electron mediators can be used. Examples of one electron mediators which have been used successfully are ferrocene[36,,37,38,,39,,40,41,,42,,43] and hexacyanoferrate(II).[44,45] In this case, the protons necessary for peroxidase reaction are consumed from solution in a manner similar to direct electron transfer, Figure 5.4*b*. Exploitation of two electron-proton mediators does not require additional protons for peroxidase reaction. Mediators of this type that have been used for the construction of peroxidase-modified electrodes are phenylediamine[46,47] catechol[48] and dopamine.[49] However, the rates of these reactions prove to be slower than the optimum mediator hydroquinone,[50] which exhibits the fastest rate of electron transfer between the redox centre and active site.[23] For example the rate of electron transfer for ferrocene is 1.8 x 10^4 cm s^{-1} while the rate of electron transfer for hydroquinone is 1.2 x 10^7 cm s^{-1}. The protocol used in these experiments for the chronoamperometric detection is based on a procedure postulated by Chetcuti *et al*,[51] and proves to be very successful in this application.
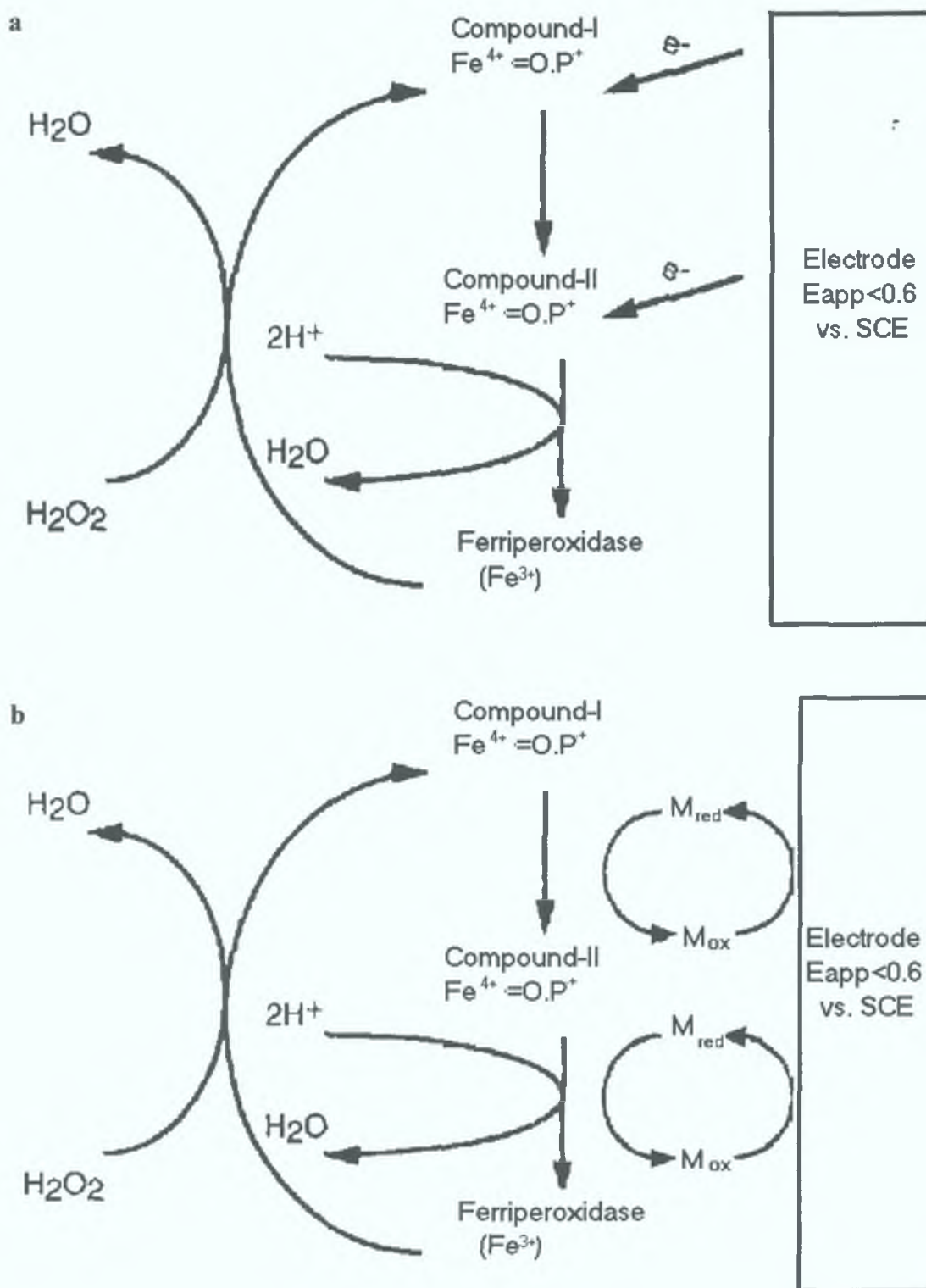
Figure 5.4. Mechanism of (A) direct (B) mediated bio-electrocatalytic reduction of hydrogen peroxidase at peroxidase-modified electrodes. M_{ox} and M_{red} are the oxidised and reduced forms of the mediator respectively. In this case M_{ox} is hydroquinone and M_{red} is benzoquinone.

Avidin or streptavidin is used in these modified electrodes for two reasons. Firstly, since a curing temperature of 50 °C is used to initiate the polymerisation reaction, many of the choices of strong protein–protein interactions could not be utilised, e.g. digoxigenin denatures at 40 °C. In contrast, both avidin–biotin and streptavidin–biotin possess a thermal stability of beyond 70 °C. Secondly, biotin–avidin have very rapid association constants, which should facilitate the possibility of a one step hybridisation and immobilisation procedure.

From previously published reports[52,53] it is known that varying the biocomponent content within a carbon-polymer matrix can adversely affect the overall electrochemical performance of a proposed sensor. This loss in electrochemical performance is attributed to the increased concentration in modified species resulting in a separation of the graphite particles; causing a loss in conductivity. This loss in conductivity is translated into a lower current response, a greater variation in current response or in the case of high modification a collapse in the current response.[52,53] For this reason, it was decided to vary the content of avidin and streptavidin within the carbon composite. The values chosen were: 1.0, 1.5 and 2 % as it is known that beyond this percentage there is a noticeable loss in sensor activity[52,53] especially when large molecules such as avidin or streptavidin are incorporated. To confirm that this was the case one batch of composite electrodes were made containing 5% (w/w) streptavidin where it was observed that upon immersion in the hybridisation solution the electrode appeared to dissolve. For these reasons no further experiments were carried out using these high loaded electrodes. Owing to the complicated and time-consuming nature of handling DNA, investigating the stability of these electrodes was achieved by dropping a small sample of biotin-streptavidin-HRP conjugate (1mg/ml) onto the surface of freshly polished composite. After drying for 1 hr. in a dessicator the electrode was then rinsed with Tris buffer. Subsequently, electrochemical detection was carried out as described in Section 5.4.5. All results presented are an average of five electrodes.

Figure 5.5 shows the electrochemical response for the various streptavidin and avidin modified composite electrodes, these results are the average of five independent electrodes. From Figure 5.5, it can be seen that a current response of 650 nA and 845 nA is observed for the carbon composite electrodes containing 2%

streptavidin and avidin respectively. While the current response was lower than this for electrodes modified with 1.5 and 1 % avidin or streptavidin. The higher current response for the 2% biologically modified electrodes confirms the use of these electrodes for all subsequent experiments. Additionally, it can be seen that over time the response diminishes. At this point it is not possible to ascertain if this reduction in electrochemical response is due to leakage of biocomponent from the carbon composite or if upon polishing the quantity of streptavidin available for binding is reduced.
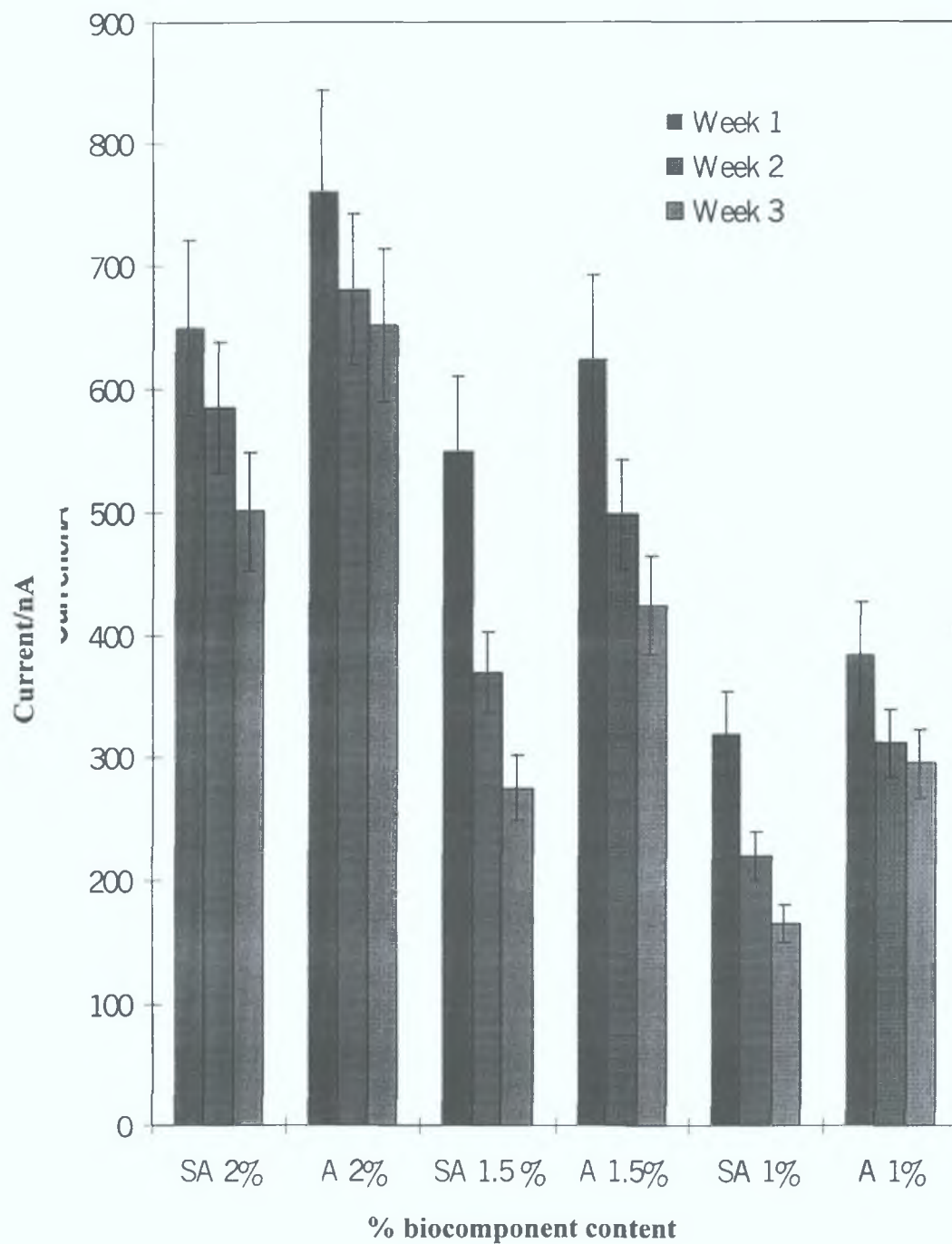
Figure 5.5. Electrochemical response for various contents of streptavidin (SA) and avidin (A) within a carbon composite electrode, using constant potential chronoamperometry held at -0.250 V. A 1.81 mM hydroquinone in an aqueous 0.1 M phosphate buffer (pH 7.4) with a 0.1 M KCl supporting electrolyte were used.

5.5.3 *Optimisation of genosensor response.*

A detailed review of the literature[54,55,56,57,58,59,60,61,62,63,64,65,66,67,68] has shown that for the more traditional methods of DNA detection, the time required from the moment of isolation by techniques such as polymerase chain reaction (PCR) to the moment of identification can take up to 48 hr. Recent attempts to shorten this time has been achieved through electrochemical means.[69,70,71,72,73,74,75,76,77,78] However, to date most studies using electrochemical methods of detection have relied on the use of a separate immobilisation step followed by a hybridisation procedure the time required for completion of these individual steps ranges from 1.5–24 hr., depending on the technique employed. As was stated earlier since the end objective is to create a sensor capable of detecting the presence of a DNA sequence specific to MRSA known as the *mec*A gene, it was decided to optimise the procedure using only the streptavidin carbon-polymer-composite electrode. Here, the intention is to exploit the well-known binding chemistry of streptavidin to a biotin–DNA, the kinetics of association for this ligand have been determined[49,79] using interface techniques such as surface plasma resonance and quartz crystal microbalance, in both cases this rate constant is reported in the region of 10^{15} M^{-1}.[80] By taking advantage of this strong binding chemistry the possible development of a one step immobilisation/hybridisation genosensor should be feasible.

Although the reduction of experimental time is an essential parameter in the development of any biosensor it is however important to establish that this reduction in the analysis time does not compromise the sensitivity of the electrochemical response. For this reason, the optimum time required for each individual step was investigated.

The first experiment involves optimising of the time required for the immobilisation of biotin–DNA onto an electrode surface, using regular intervals of 10 min. As this experiment is investigating the affects of immobilisation time, the hybridisation time was maintained constant at 60 min. This time of 60 min. is reported as an optimum time to ensure the hybridisation of target DNA to the capture probe, and based on literature reports is sufficient to allow for hybridisation to occur.[69–78]

Figure 5.6, shows results for this experiment, that used four independent electrodes. This figure shows that there is a linear increase in current with increasing

immobilisation time between 0–60 min. However, as the time increases past 60 min a levelling of the current is observed with a maximum current of 815 nA being obtained at 90 min. This current levelling suggests that all available streptavidin sites have been occupied at time longer than 90 min.

The next step in the optimisation procedure involves keeping the immobilisation time constant while the hybridisation time is varied between 0–120 min., with regular intervals of 10 min. For these experiments the optimum immobilisation time is taken from the previous experiments to be 60 min., Figure 5.6.

Figure 5.7, show the results of this study and as can be seen there is the same linear increase in current with time, as was observed in the previous incidence. In this case, the time required to reach a plateau in the current is 90 min., and a maximum current of 730 nA is obtained. From these results presented in Figures 5.6 and 5.7 it can be said that for individual experiments an optimum time of 60 min and 90 min is required for immobilisation and hybridisation, respectively.

The main objective of these experiments is to develop genosensors that require only a one step hybridisation/immobilisation procedure. Therefore, it is imperative to establish that the combination of these two individual steps into one step does not result in a compromise between sensitivity and time. To address this issue, the next stage of optimisation involves an investigation of optimum time for a one step procedure. In this incidence 10 μl of each oligomer **A–C** were equilibrated to 42 °C with 120 μl of hybridisation solution. A streptavidin–carbon–polymer composite electrode was immersed in this solution for times between 10–120 min. at regular intervals of 10 min. Figure 5.8 illustrates the results of these experiments. A linear increase of current with time is initially observed with a levelling of the current seen for times greater than 70 min, indicating maximum binding with all available streptavidin sites.

From Figures 5.6–5.8, it can be seen that the overall limiting factor is the length of time required for hybridisation of the target DNA and the antibody labelled DNA to the capture probe and procedure.[81] In brief, streptavidin is known to have a high affinity for its ligand biotin with an association constant of approx. 10^{15} M^{-1}. Additionally, it is known that these streptavidin molecules posses high thermal stability

of 75.5° C, hence, the temperatures used in this assay will not cause denaturation of any of the biocomponents present. This thermal stability is further increased upon binding to its ligand biotin.[82] A reports exists[90] that demonstrates an immobilisation time of 30 min. for biotin labelled species. In this report[90] streptavidin is immobilized onto the surface of a glassy carbon electrode in a manner similar to that describe for modification of progesterone within an osmium–polymer modified electrode in section 2.2.5. Although, the hybridisation step is the limiting factor in these experiments the results for optimum hybridisation agree with studies by other groups.[69–78,81,83]
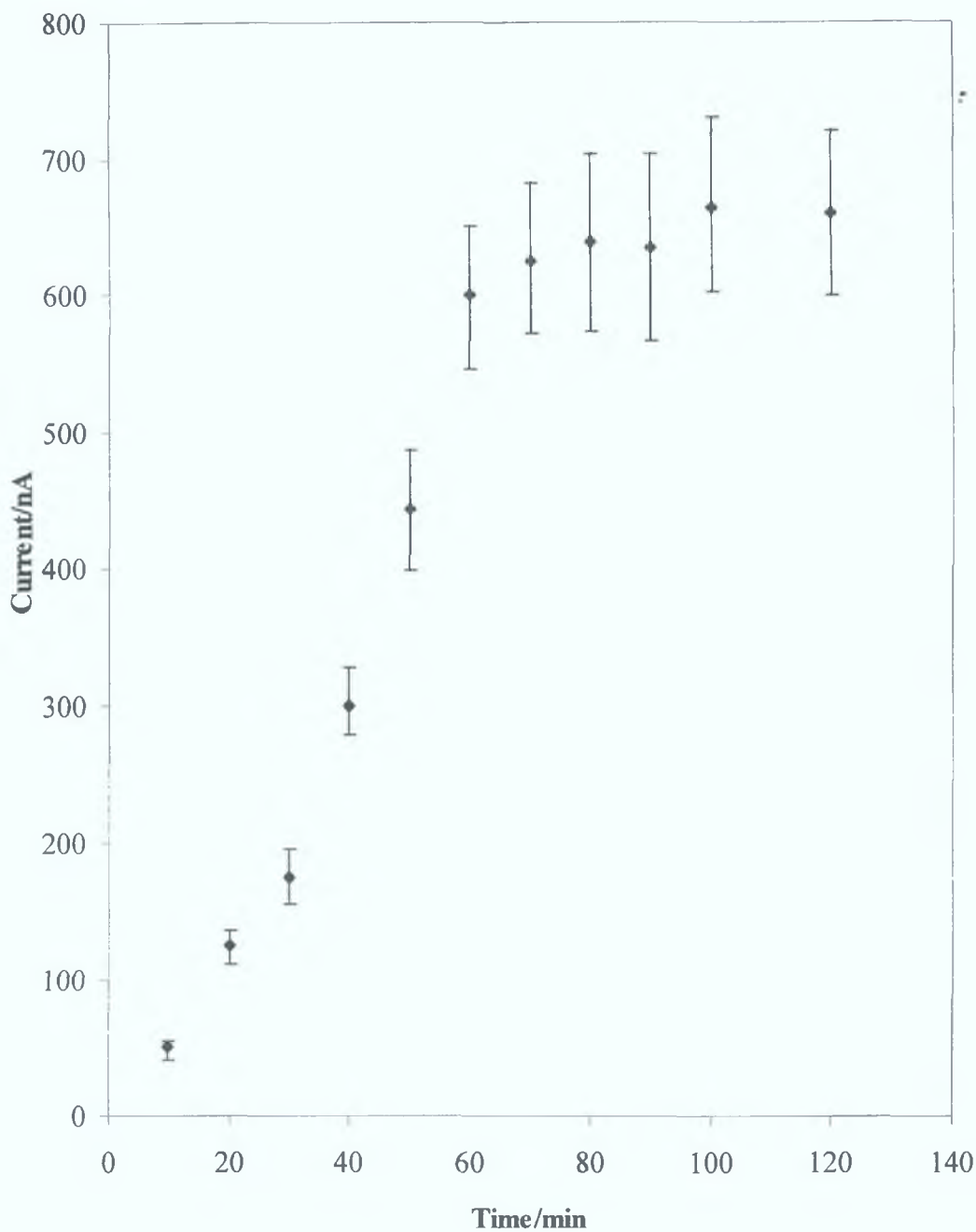
Figure 5.6. Dependence of current response with variation in immobilisation time, and a constant hybridisation time of 60 min. The working electrode was a 2% streptavidin–carbon–polymer biocomposite. All experiments were carried out at a constant potential of −0.250 V in a 1.81 mM hydroquinone solution containing an aqueous 0.1 M phosphate buffer pH 7.4 with 0.1 M KCl supporting electrolyte.
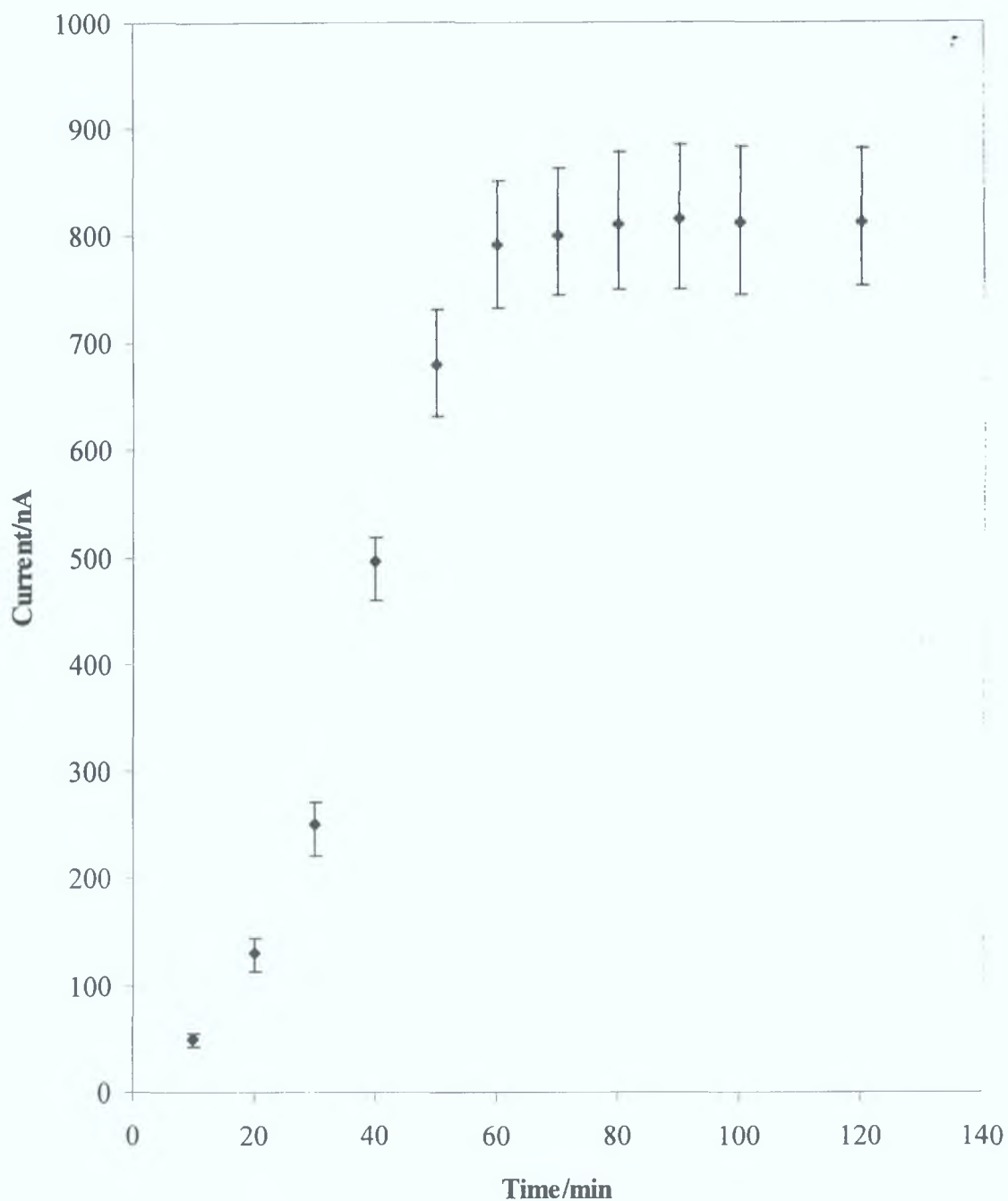
Figure 5.7. Dependence of current response on a varying hybridisation time, with a constant immobilisation time of 60 min. The working electrode was a 2% streptavidin–carbon–polymer biocomposite. All experiments were carried out at a constant potential of –0.250 V in a 1.81 mM hydroquinone solution containing an aqueous 0.1 M phosphate buffer pH 7.4 with 0.1 M KCl supporting electrolyte

226
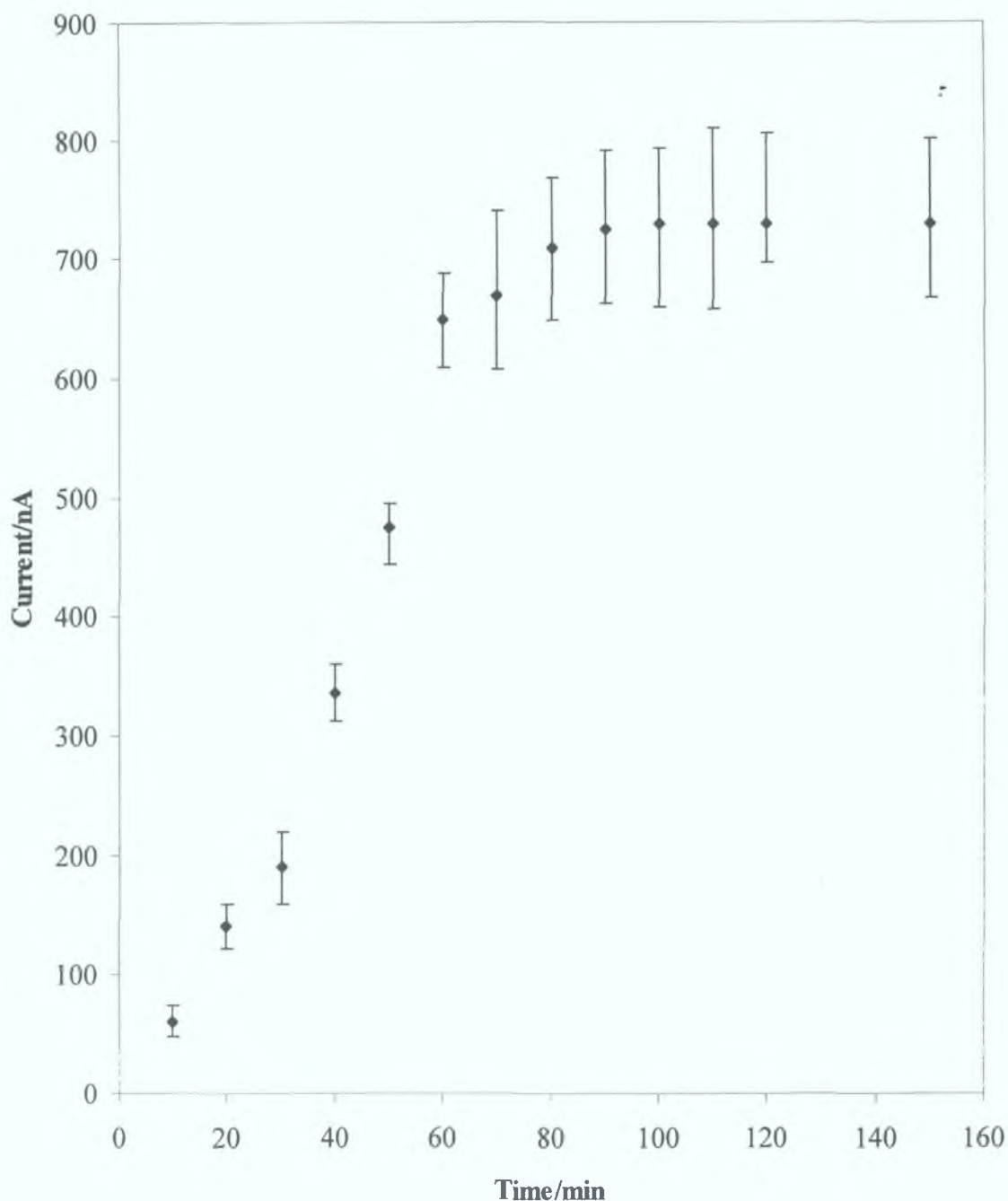
5.5.4   ***Figure 5.8.***   *Dependence of current response on a varying both immobilisation time and hybridisation time.   The working electrode was a 2% streptavidin–carbon–polymer biocomposite.   All experiments were carried out at a constant potential of –0.250 V in a 1.81 mM hydroquinone solution containing an aqueous 0.1 M phosphate buffer pH 7.4 with 0.1 M KCl supporting electrolyte*

5.5.4   Non-specific adsorption study

A common problem encountered with traditional enzyme immunoassays such as ELISA, is non-specific adsorption[84] of the enzyme onto the microtitre plate. This is also an issue that needs to be addressed in the development of the ideal genosensor based on enzyme labelling techniques. Scheme 5.1 illustrates the two possible sources of non-specific adsorption in this system. First, the electrochemical response associated enzyme marker anti-Dig-HRP may arise from direct adsorption onto the carbon composite electrode and not through hybridised DNA. Second, the hybridised DNA may directly adsorb onto the carbon composite electrode surface–in contrast to direct attachment to the exposed streptavidin molecule.

a) direct adsorption of enzyme onto carbon surface
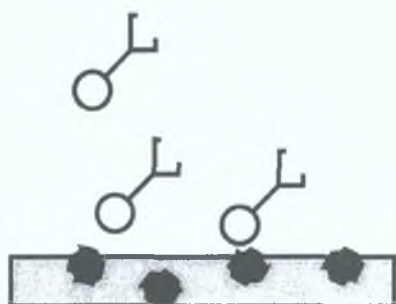
b) direct adsorption of DNA duplex onto electrode surface
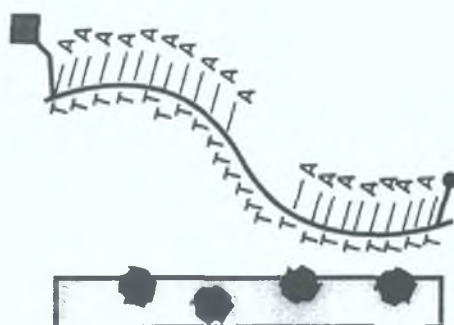
Scheme 5.1. Possible sources of non-specific adsorption onto the electrode surface

Figure 5.9 shows the results for the non-specific adsorption assays described in Section 5.4.6, carried out at a constant potential of –0.250 V, in 1.81 mM hydroquinone, 0.1 M phosphate buffer with 0.1 M KCl. The first of these three assays was carried out at an unmodified carbon–composite electrode, to probe the extent of non-specific adsorption of the biotin–DNA onto the carbon-composite surface. Second, a streptavidin-carbon-polymer biocomposite was used in which the biotin-DNA was omitted, to establish if non-specific attachment of the target–DNA or Dig–DNA occurs. Third, a streptavidin-carbon-polymer biocomposite was used omitting the target–DNA to test whether a significant fraction of the electrochemical response is from non-specific adsorption of

Dig–DNA onto the carbon surface. From Figure 5.9, it can be seen that issues pertaining to non-specific adsorption do indeed influence the current obtained, maximum contribution coming from assay (ii). If these results are compared with assay (iv) in – the current response associated the proposed genosensor assay – it is observed that the contribution to the overall analytical response is less than 10% in all cases and within experimental error.
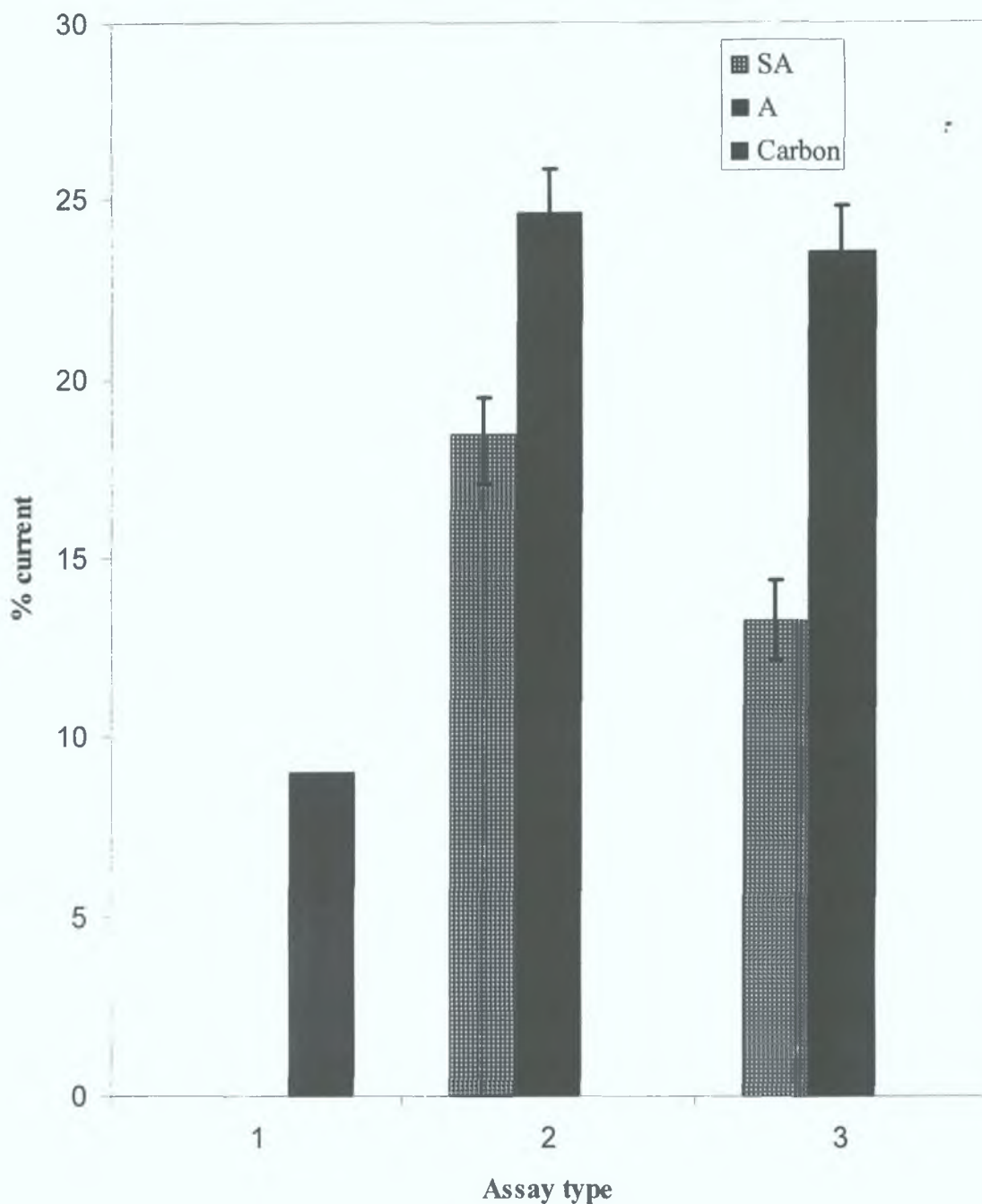
Figure 5.9. Non-specific adsorption of (1) biotin–DNA onto surface of a carbon composite electrode, (2) target–DNA and Dig–DNA onto the surface of a streptavidin (SA) and avidin (A) carbon–polymer composites and (3) biotin–DNA and Dig–DNA onto the surface of a SA and A carbon–polymer composite. All experiments were carried out in 1.81 mM hydroquinone in aqueous 0.1 M phosphate buffer, pH 7.4, and 0.1 M KCl, at a constant applied potential of –0.250 V.

5.5.5   *Stability of carbon-polymer composite over time*

When developing and optimising any biosensor intended for a "real world" application the stability of the response with time needs to be investigated. The extensive use of these carbon composite electrodes in other areas of analytical chemistry[85] has revealed a problem with their stability over time. As the biocomponent is not chemically confined within the composite electrode, the possibilities exist of either loss of biocomponent stability due to denaturation or leaching into either the electrolyte solution or the hybridisation solution. In order to study the stability of these electrodes a batch of four electrodes was prepared and experiments carried on a weekly basis, over a twelve-week period. After each experiment a quick polishing procedure was implemented, removing previously bound biotin–streptavidin–HRP and the electrodes were then left in an upright position and stored at 4 °C. Prior to carrying out any experiments, the electrodes were polished to a mirror finish revealing fresh streptavidin that is available for binding. This polishing procedure overcomes the need to break the strong bond formed with the biotin–DNA target.

Since the main parameter being analysed in this section involves the availability and stability of the biocomponent for binding, it was decided to investigate the stability using biotin–streptavidin–HRP conjugate and not DNA, where electrochemical detection was carried out as described previously in Section 5.1. Again, the problem of non-specific adsorption are investigated, whereby all experiments were carried out in parallel using a blank carbon-composite electrode. All results are an average of four independent electrodes. From Figure 5.10 it can be seen that the contribution due to non-specific adsorption of the biotin–streptavidin–HRP conjugate results in a current response relatively consistent over time with a current of less than 150 nA being observed in all cases. Figure 5.10 shows the results obtained for the streptavidin and the avidin composite, after subtracting the response associated with non-specific adsorption. These results show a variation with time ranging from a maximum value of 800 nA for week one to a minimum value of 185 nA at week 11. The response associated with the avidin carbon-composite shows the same decrease

231

over time. However the current response appears to be more consistent for the first four weeks when compared with the streptavidin–carbon–composite electrode.

While it is essential to remember there is no uniform dispersion of streptavidin within the carbon composite and, hence, one electrode may expose more streptavidin than another upon polishing and give rise to the fluctuations in currents observed. Taking the random dispersed nature of these composites into account the variation of streptavidin that is available for binding decreases over time. The results in Figure 5.10 suggest that there may be a problem with either streptavidin with time or a loss of streptavidin from the electrode through leeching.

By comparing the results obtained in Figure 5.10 for both the streptavidin and avidin carbon–polymer electrodes it can be seen that there is a greater stability for the avidin electrode over the streptavidin, with a relative standard deviation 7.5–10 %. Again there is a discrepancy between weeks that can be attributed to the random nature of dispersion.

A study of the pK_a values for both streptavidin and avidin suggest that streptavidin should be the more stable of the two composite types as its pK_a is well outside the pH range employed in these experiments. However, it was observed that upon excessive use of these electrodes the streptavidin appeared to swell to a greater extent that the avidin electrodes. As streptavidin is the larger of the two molecules this swelling could be the result of a more porous carbon–polymer structure.
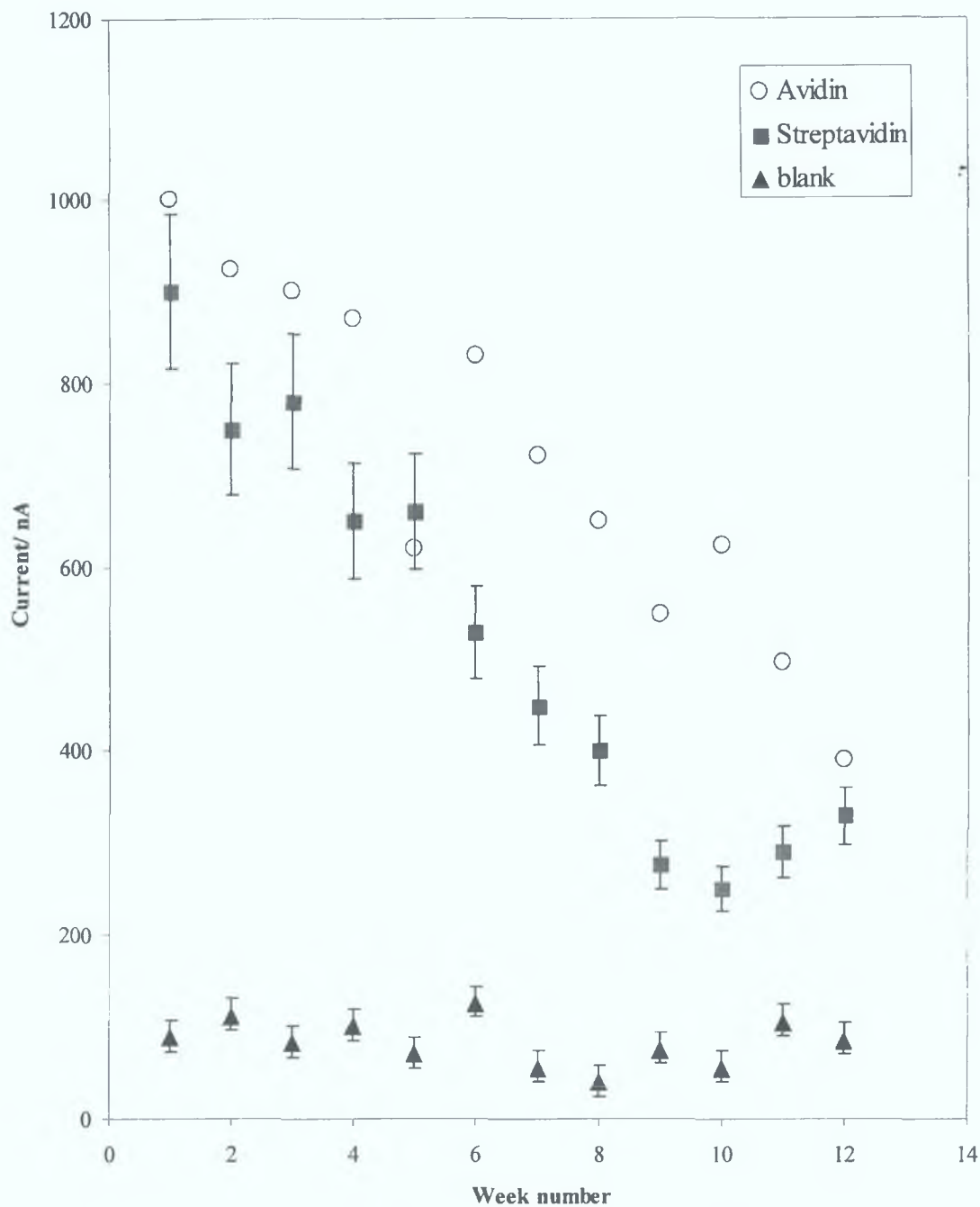
Figure 5.10. Stability of carbon–composite electrodes over a 12 week period. (▲) Non-specific adsorption of biotin–streptavidin–HRP onto a carbon-polymer composite electrode, electrochemical response for adsorption of biotin–HRP onto a 2 % streptavidin–carbon–polymer composite electrode (■) and a 2 % avidin–carbon–composite electrode (○). All experiments were carried out at –0.250 V in an aqueous 1.81 mM hydroquinone solution containing 0.1 M phosphate buffer, pH 7.4, and 0.1 M KCl as the supporting electrolyte.

In Sections 5.5.3–5.5.5, it has been demonstrated that the proposed sensor design is capable of generating an analytical signal in response to the presence of a hybridised DNA strand. However, the target DNA sequence, **B**, used in optimising this genosensor was very simple and therefore it is not possible to establish if exact hybridisation has occurred. In reality the nature of a DNA strand rarely exhibits such constant base-pairing as is used in the first part of this assay. Therefore it is essential that this proposed sensor design is applied to a real sample, MRSA.

The chosen target DNA used for this study is oligonucleotide **E,** this sequence corresponds to the *mec*A gene of MRSA and was obtained from the national centre of biotechnology information.[86] The concentration used in these assays corresponds to a typical concentration yield from a 15 min PCR amplification procedure. A non-specific adsorption study was carried out in the same manner as described in 5.4.6. The electrode of choice for these assays was the avidin–carbon-polymer composite as it exhibits less randomness between analytical response for varying weeks. Moreover it is a much more stable electrode, as shown in Figure 5.10.

Previous literature reports,[45–51] involving the development of a genosensor capable of detecting a hybridised DNA strand, shows that a gentle washing procedure with a buffered solution is sufficient to remove unbound DNA from the electrode. The reason for this careful approach in reduction of non-specific adsorption is attributed to the fragile nature of immobilised DNA onto the electrode surface, especially where physical adsorption methods takes place.[87,88,89]

On the contrary avidin–biotin interactions are one of the strongest known protein–ligand interactions[82] and should therefore withstand a stronger washing. Hence, when carrying out the non-specific adsorption studies both a vigorous and gentle washing procedures were implemented. In the case of the rigorous washing step the electrode when removed from the hybridisation solution is washed under a continuous stream of Tris buffer, from a wash bottle, pH 7.1, for 60 s. Whereas, the gentle washing procedure involved slight agitation in a mixer at room temperature. Results shown in Figure 5.11 illustrate a successful reduction in current associated with non-specific adsorption of ~30%, when a vigorous washing step is employed. Not only does this

data enhance the quality of the response but also indicates the strength of the avidin–biotin–DNA binding. All further assays were carried out using this vigorous washing step.
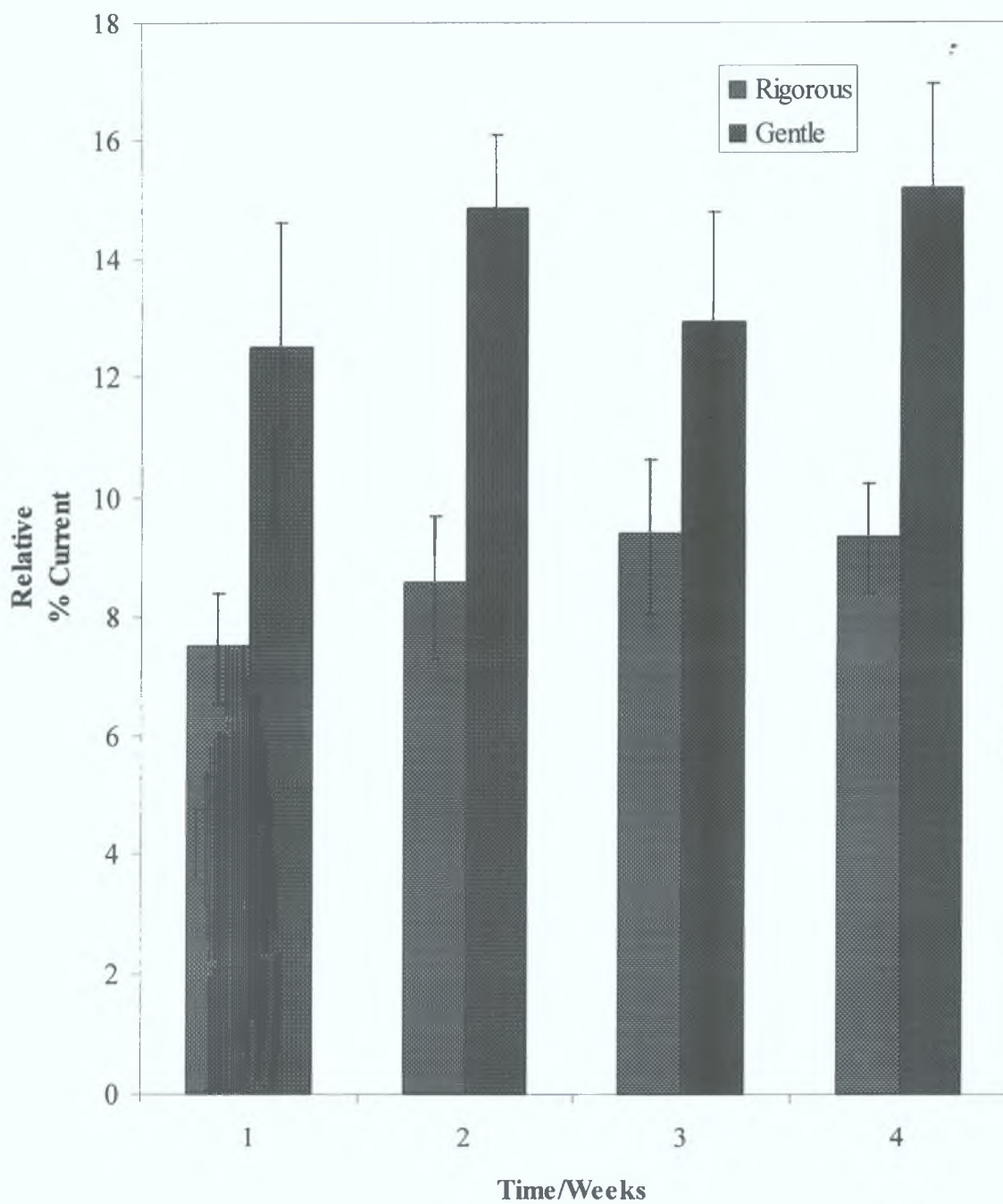
Figure 5.11. Results of non-specific adsorption using a vigorous and gentle washing procedure, all assays are carried out without the target DNA. All experiments were carried out in an aqueous 1.81 mM hydroquinone, in 0.1 M phosphate buffer pH 7.4 and 0.1 M KCl.

5.5.7   Non-competitive format

Figure 5.12 shows the results for a non-competitive assay. The data illustrates the capability of this sensor design to elicit an response from a β-lactamase resistance DNA strain. A significant increase in current response with an increasing concentration is observed from 800 nA to 100 μA for an increased concentration of 150 pmol to 150 nmol. Unlike the streptavidin composite, the current response does not decrease in an orderly manner over time, but as can be seen in Figure 5.12 for week two there is an *increase* in the analytical signal. As there is no way of ensuring how many of the four available binding sites on the avidin molecule will be exposed at the electrode surface for binding with the biotin–DNA probe, this random variation in current response suggests fluctuation in available avidin binding sites exposed to the biotin labelled probe. A recently published paper[90] incorporating avidin within an osmium polymer in a manner similar to that described in Section 2.3.5 confirms the non-quantitative nature of using an avidin–biotin interaction. However, no reports exist that suggest a person can carry MRSA resistant bacteria without being affected by its pathogenicity, therefore a qualitative assay is sufficient.

5.5.8   Competitive format

Traditionally, products recovered from a PCR amplification procedure have required a purification step[91] to remove any interferences, including the enzymes used throughout the reaction. Also, there is a problem associated with inaccurate amplification or amplification of additional DNA sequence in addition to the core gene. However, until some new method is proposed, PCR will remain the gold standard for amplification of DNA as its advantage of speed have undeniably revolutionised and aided DNA sequencing.

For these reasons a competitive assay also known as a mismatch assay was carried out by including a DNA sequence which differed by two mismatch base-pairs, i.e., oligomer **G**.

The intention of this competitive format assay is to establish the selectivity of the genosensor to a specific DNA sequence in the presence of a mismatch DNA

sequence. Results for this competitive assay are presented in Figure 5.12 and are an average of four electrodes. As can be seen the current response is similar to what was obtained for the non-competitive assay. The similarity between the two assays shown in Figure 5.12 indicate the ability of the proposed genosensor to differentiate between different sequences, even if only two mismatch base-pairs are present in a sequence. Such differentiation capability allows, with confidence, the identification of a disease causing pathogen in the presence of similar sequences.
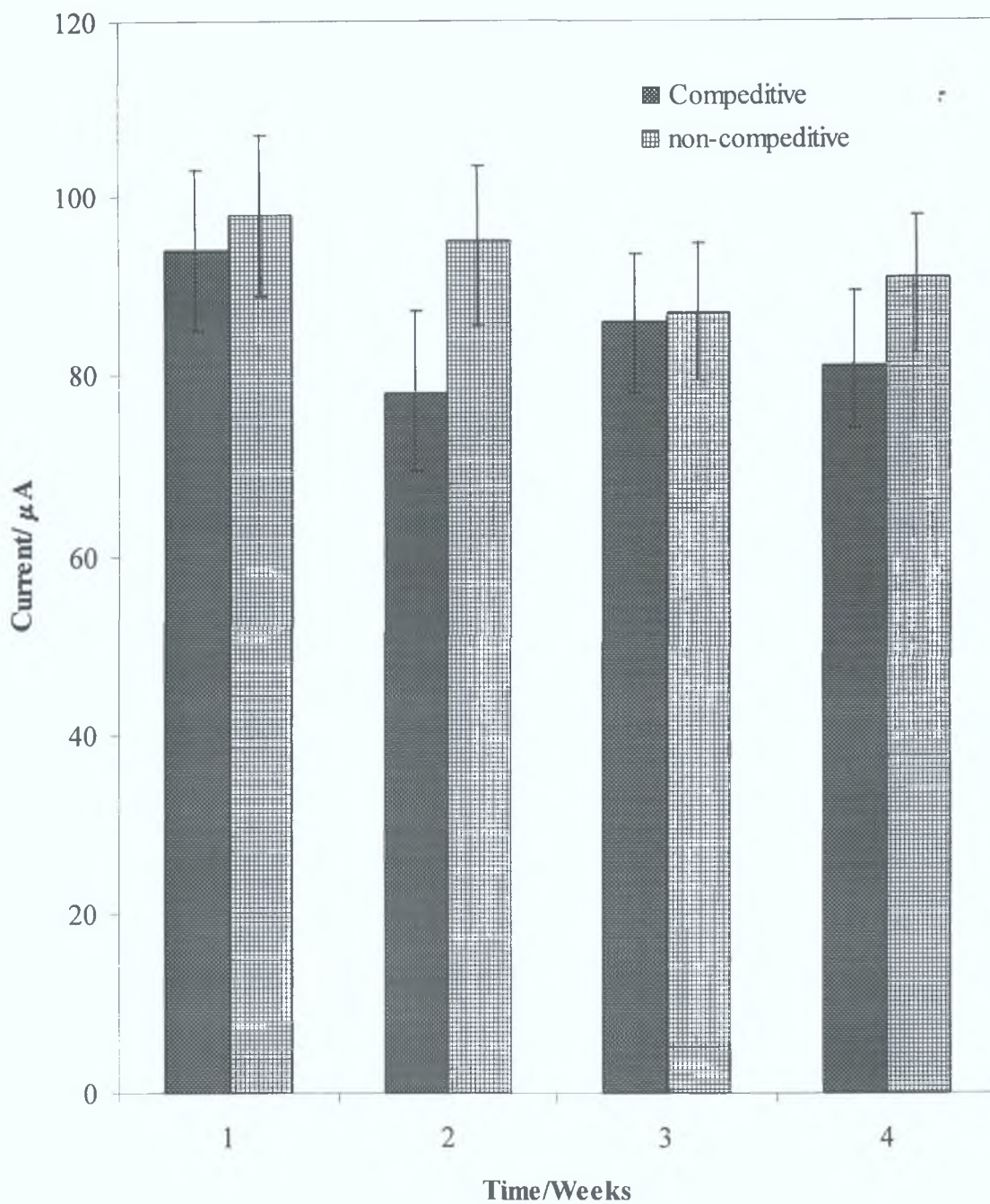
Figure 5.12. Current response after applying a constant potential of −0.250 V for an avidin–carbon composite electrode, using a vigorous washing procedure. The assay was carried out both in the presence and absence of a mismatched DNA sequence. All experiments were carried out in 1.81 mM hydroquinone in 0.1 M phosphate buffer pH 7.4 and 0.1 M KCl

5.6 Conclusion

The overall conclusion that can be drawn from the above experimental results is that it is possible to develop a reproducible, quantitative sequence specific genosensor exists. In Figures 5.2–5.9 the sensor response was optimised using a simple DNA sequence. As illustrated in Figure 5.5 a 2% (w/w) biocomposite was sufficient to yield an analytical signal in response to the presence of an HRP labelled DNA. Any higher biocomponent content did not result in a stable carbon-composite electrode. In the study of non-specific adsorption, Figure 5.9, it was confirmed that the current response is not dominated by physical adsorption of the enzyme labelled anti-digoxigenin, but rather that the proposed sensor design outlined in Figure 5.1 is successful.

Figures 5.3 indicated that the location of the working redox potential at which Equation 5.1 proceeds did not adversely affect or influence any of the biocomponent species present.

Interestingly, while both avidin–biotin and streptavidin–biotin are known for their strong protein–ligand interactions, as shown in Figure 5.10 the avidin–carbon–polymer composites overall preformed better than streptavidin. The exact reasons for this are still unclear but it is possibly associated with the molecular conformation of streptavidin being more bulky and gives rise to a more porous composite electrode and hence absorption of water or other reagents causing swelling and disruption of the carbon polymer matrix. The experimental timescale used in the above procedure is shortened by the rapid kinetics of association between the biotin labelled capture probe and the modified component. Figures 5.6–5.8 indicate that although there is a greater current response when a two step approach is used it is not significant enough to justify a lengthening of analytical time. Hence a total analysis time of 120 min is achieved.

One of the main obstacles for successful application of genosensors is the how to regenerate the surface in order for the electrode to be used more than once. Most reported genosensor designs are not suitable for an analytical lab environment, as methods demand too many different steps requiring a level of expertise to employ them. The proposed genosensor solves this problem of surface regeneration by using a bulk modification method whereby upon use of a simple polishing procedure a fresh active layer of biocomponent is ready for a new oligonucleotide–biotin interaction with a new

240

capture probe. The advantage of this type of sensor regeneration over DNA denaturation is that with each new surface a different capture probe can be immobilised allowing for a different DNA assay to be carried out. However, as shown in Figure 5.10 one drawback of using this approach is that it is very difficult to control the exact availability of binding sites hence complicating the exploitation of these sensors for quantitative analysis.

Having optimised the procedure for immobilising and hybridising the DNA to the electrode surface the real test was to see if it could detect the presence of MRSA both in the presence and absence of a mismatch DNA sequence. Results in Figure 5.12 show that this was indeed possible, and again the results for non-specific adsorption were only 10% of the total analytical current.

While the quality of the analytical response associated with these genosensor varies too much for them to be considered as a new gold standard for sequence specific DNA further progress in the field of screen printing technology may see such a concept being utilised as an preliminary method of analysis for detection of pathogenic bacteria and aid with the decision on how to act when confronted with suspected outbreaks of potentially fatal diseases.

Further work using a bulk immobilisation could involve trying to incorporate antibodies within the composite electrode and using an antigen labelled DNA as a capture probe. It would also be interesting to investigate the capability of these electrodes to detect DNA amplified from a polymerase chain reaction, or DNA isolated from pathogenic species to establish the capability of these electrodes to be used for a real time assay.

5.7   Reference

1   *The Staphylococci in Human Disease.* Crossley, K. B.; Archer, G. L. (Eds.) Churchill Livingstone New York, **1997.**

2.   Emori, T. G.; Gaunes, R. P. *Clin. Microbiol. Rev.* **1993**, *6*, 428.

3   liveira, D. C.; Tomasz, A; de Lencastre, H. *Lancet,* **2002**, *2*, 180.

4   Abraham, E. P.; Gardener, A .D.; Chain, E. *Lancet,* **1941**, *ii*, 177.

5   Jessen, O.; Rosendal, K.; Bunlow, P.; Faber, V.; Eriksen, K. R. *N. Engl. J. Med.,* **1969**, *281*, 627.

6   Sa-Leao, R.; Sanches, I. S.; Couto, I.; Alves, C. R.; de Lencastre, H. *Microb. Drug Resist.,* **2001**, *7*, 237.

7.   Jevons, M. P. *BMJ,* **1961**, *1*, 124

8   Stewart, G. T.; Holt. R. J. *BMJ,* **1963**, *1*, 308

9   Wenzel, R. P.; Nettleman, M. D.; Jones, R. N.; Pfaller, M. A. *Am. J. Med.,* **1991**, *91*, 221S

10.   Beck, W. D.; Berger-Bachi, B.; Kayser, F. H. *J. Bacteriol.,* **1986**, *165*, 373

11.   Katayama, Y.; Ito, T.; Hiramatsu, K. *Antimicrob. Agents Chemother.,* **2000**, *444*, 1549

12   Katayama, Y.; Ito, T.; Hiramatsu, K. *Antimicrob. Agents Chemother.,* **1999**, *43*, 1449

13   Katayama, Y.; Ito, T.; Hiramatsu, K. *Antimicrob. Agents Chemother.,* **2001**, *45*, 1323

14   Hartman, B.; Tomasz, A. *Antimicrob. Agents Chemother.,* **1981**, *19*, 726

15   Ubukata, K.; Nonoguchi, R.; Katsuhashi, M.; Konno, M. *J. Bacteriol.,* **1989**, *171*, 2882

16   Tenover, F. C.; Arbeit, R.; Archer, G. *J. Clin. Microbiol.,* 1994, *32*, 407

17   British Ministry for Agriculture

18   Zubay, . *Microbial Methods of Detection,*

19   www.cdc.com

20   Pividori, M. I.; Merkoci, A.;. Alegret, S. *Biosen. and Bioelectron.* **2000**, *15*, 291

21   Pividori, M. I.; Merkoci, A.;. Alegret, S. *Biosen. and Bioelectron.*, **2001**, *16*, 1132

22   www.ncbi.nlm.nih.gov

23   Ruzgas, T.; Csöregi, E.; Emnéus, J.; Gorton, L.; Marko-Varga, G. *Anal. Chim, Acta*, **1996**, *330*, 123

24   *Peroxidases in Chemistry and Biology*: Everse, J.; Everse, K. E.; Grisham,
M.   B. (Eds.) Vol. 1, 2, CRC Press, Boca Raton, **1991**, 620

25   Bogdanovskaya, V. A.: Tarasevich, M. R.; Hintsche, R.; Scheller, F. *Bioelectrochem. Bioenerg.*, **1988**, *19*, 581

26   Tarasevich, M.; Hintsche, R.; Scheller, F. *Bioelectrochem. Bioenerg.*, **1978**, *5*, 18

27   Durliat, H.; Courteix, A.; Comtat, M.; *Bioelectrochem., and Bioeng.*, **1989**, *22*, 81

28   Csöregi, E.; Gorton, L.; Marko-Varga, G. *Anal. Chim. Acta*, **1993**, *273*, 59

29   Armstrong, F. A.; Lannon, A. M. *J. Am. Chem. Soc.*, **1987**, *109*, 7211

30   Dryhurst, G.; Kadish, K. M.; Scheller, F.; Renneberg, R. *Biological Electrochemistry*, Academic Press, New York, **1982**

31   Yamazaki, I.; Tamura, M.; Nakajuma, R. *Mol. Cell. Biochem.*, **1981**, *40*, 143

32   Farhangrazi, Z. S.; Fosset, M. E.; Powers, L. S.; Ellis, W. R. *Biochemistry*, **1995**, *24*, 2866

33   Razumas, V.; Gudavicius, A.;. Kulys, J. *J. Electroanal. Chem.*, **1986**, *198*, 81

34   Razumas, V.; Jasaitis, J.;. Kulys, J. *Bioelectrochem. Bioenerg.*, **1984**, *12*, 297

35   Barnett, P. N.; Tebbutt, P.; Whitaker, R.G. *Prog. React. Kinetics*

36   Epton, R.; Hobson M. E.; Marr, G. *J. Organomet. Chem.*, **1978**, *149*, 231

37   Tatsuma, T.; Okawa, Y.; Wantabe, T. *Anal. Chem.*, **1989**, *61*, 2352

38   Smit, M. H.; Cass, A. E. G. *Anal. Chem.*, **1990**, *62*, 2429

39 Schubert, F.; Saini, S.; Turner, A. P. F.; Scheller, F. *Sens. Actuators, B*, **1992**, *7*, 408

40 Tsai, W-C.; Cass, A. E. G. *Analyst*, **1995**, *120*, 2249

41 Cooper, J. M.; Bannister, J. V.; McNeil, C. J. *J. Electroanal. Chem.* **1991**, *312*, 155

42 Lobo, M. J.; Miranda-Ordieres, A. J.; Costa-García, A.; Tuñon-Blanco, P. *Electroanalysis*, **1996**, *10*, 932

43 Wang, J.; Reviejo, A. J.; Angnew, L. *Electroanalysis*, **1993**, *5*, 575

44 Scott, D. L.; Paddock, R. M.; Bowden, E. F. *J. Electroanal. Chem.*, **1992**, *341*, 307

45 Wang, J.; Varughese, K. *Anal. Chem.*, **1990**, *62*, 318

46 Adeyoju, O.; Iwuoha, E. I.; Smyth, M. R. *Electroanalysis*, **1995**, *7*, 924

47 Wang, J.; Lin, M. S. *Electroanalysis*, **1989**, *1*, 43

48 Pantano, P.; Morton, T. H.; Kuhr, W. G. *J. Am. Chem. Soc.*, **1991**, *113*, 1862

49 Yang, X.; Guilbault, G. G.; Suleiman, A. A. unpublished results

50 Domínguez-Sanchez, P.; Tuñon-Blanco, P.; Fernández-Alvarez, J. M.; Smyth, M. R.; O' Kennedy, R. *Electroanalysis*, **1990**, *2*, 303

51 Chetcuti, A. F.; Wong, D. K. Y. *Anal. Chem.*, **1999**, *71*, 4065

52 Cèspedes, F.; Martinez-Fabregas, E.; Alegret, S. *TRAC*, **1996**, 296

53 Cèspedes, F,; Alegret, S. *TRAC*, **2000**, *19*, 4, 276

54 Gilbert, N.; Corden, S.; Ijaz, S.; Grant, P. R.; Tedder, R. S.; Boxall, E. H. *J. Viro. Methods*, **2002**, *100*, 37

55 Pitel, P.H.; Pronost, S.; Cjatagnon, G.; Tainturier, D.; Fortier, G.; Baller. J.J. *Vetinary Parasitology*, **2001**, *102*, 269

56 Lüdicke, F.; Stalberg, A.; Vassilakos, P.; Major, A. L.; Campana, A. *J. Pediatric and Adolescent Gynecology*, **2001**, 14, 171

57 Wagnerr, H. J.; Schläger, F.; Claviex, A.; Bucsky, P. *European J. Cancer*, **2001**, *37*, 15, 1583

58 Davies, M. J. *Trends in Biotech.*, **2001**, *19*, 8, 287

59   Spinillo, A.; Debiaggi, M.; Zara, F.; De Santolo, A.; Polatti, F.; Filice, G. *Obstetrics and Gynecology,* **2001**, *97*, 999

60   Zabzdyr, J. L.; Lillard, S. J. *J. Chrom. A.*, **2001**, *911*, 269

61   Olatunbosun, O.; Deneer, H.; Pierson, R. *Obstetrics and Gynecology*, **2002**, *97*, 357

62   Krishnan, M.; Namasivayam, V.; Lin, R.; Pal. R.; Burns, M.A. *Current Opin. Biotech.*, **2002**, *12*, 92

63   Kido, C.; Murano, S.; Tsuruoka, M. *Gene*, **2000**, *259*, 123

64   Husnjak, K.; Grce, M.;. Magdic, Ñ.; Pavelic, K. *J. Virol. Methods*, **2000**, *88*, 125

65   Anke, J.; van Eekelen, M.; Shammas, F. V.; Wee, L.; Heikkilä, R.; Osland, A. *Clinical Biochem.*, **2000**, 457

66   Barman, S. P.; Lunsford, L.; Chambers, P.; Hedley, M. L. *J. Controlled Release*, **2000**, 337

67   Pawlotsky, J. M.; Bastie, A.; Hézode, C.; Lonjon, I.; Carthuy, F.; Rémiré, J.; Dhumeaux, D. *J. Virolo. Methods*, **2000**, *85*, 11

68   Taypay, L. M.; Cesar, E.; Nadala, B.; Loh, P. C. *J. Virolo. Methods*, **1999**, *82*,   39

69   Chiti, G.; Marrazza, G.; Mascini, M. *Anal. Chim. Acta*, **2001**, *47*, 155

70   Shamansky, L. M.; Brandon-Davis, C.; Stuart, J. K.; Kuhr, W. G. *Talanta*, **2001**, *55*, 909

71   Lee, T.-Y.; Shim, Y.-B. *Anal. Chem.*, **2001**, *73*, 5629

72   Armistead, P. M.; Thorp, H. H. *Anal. Chem.*, **2001**, *73*, 558

73   Wang, J.; Kawde, A.-N. *Anal. Chim. Acta*, **2001**, *431*, 219

74   Alfonta, L.; Singh, A. K.; Willner, I. *Anal. Chem.*, **2001**, *73*, 91

75   Xu, C.; Cai, H.; He, P.; Fang, P. *Analyst*, **2001**, *126*, 62

76   Eckart, K.; Speiss, J. *J. Am. Soc. Mass Spectrom.*, **1995**, *6*, 912

77   Yang, M.; Yau, H. C. M.; Chen, H. N. *Langmuir*, **1998**, *14*, 6121

78   Ruan, C.; Kong, J.; Deng, J. *Anal. Chim. Acta*, **2000**, 89

79   Wilchek, M.; Bayer, E. A. *Anal. Biochem.*, **1988**, *171*, 1

80.   Gonzalez, M.; Argarana, C. E.; Fidelio G. D. *Biomolec. Engine.***1999,** *16*, 67

81   Sano, T.; Cantor, C. R. *Proc. Natl. Acad. Sci. USA,* **1995**, *92*, 3180

82   M. González, M.; Argaraña, C. E.; Fidelio, G. D. *Biomolecular Engineering*, **1999**, *16*, 67

83   Pividori, M. I.; Merkoçi, A.; Alegret, S. *Biosens. Bioelectron.*, **2001**, *16*,
1133

84   Tijssen, P. (Ed). *Laboratory techniques in Biochemistry and Molecular Biology,* Vol. 15, Elservier, New York, 1985

85   Alegret, S.; Alonso, J.; Bartrolí, J., Céspedes, F.; Martínez-Fàbregas, E.; de Valle, M. *Sensors and Materials,* **1996**, *8*, 147

86.   www.ncbi.nlm.nih.gov

87   Nedorezova, P. M.; Galashina, N. M.; Tsvetkova, V. I.; Sukhova, T. A.; Saratovskikh, S. L.; Dyachkovskii, F. S.; Babkina, O.N. *Eur. Polym. J.*, **1996**, *32*, 1161

88   Mishima, Y.; Montanka, J.; Ikeda, J. *Anal. Chim. Acta.*, **1997**, *345*, 45

89   Dinh, V. *Sens Actuators, B*, **1998**, *51*, 52

90   Campbell, C. N.; Gal, D.; Cristler, N.; Banditrat, C.; Heller, A. *Anal. Chem.* **2002**, *74*, 158

91   Jurinke, C.; van den Boom, D.; Collazo, V.; Luchow, A.; Jacob, A.; Koster, H. *Anal. Chem.*, **1997**, *69*, 904

Chapter6

Overview, General Conclusions

and Future Work

Overview

This thesis addresses problems that will face sensing technology if the current trend towards miniaturisation continues, whereby factors such a buffer choice and modification methods will play a major role. Two electrode systems are considered. The first uses the classical surface modification of an electrode with a polymer, redox metal and progesterone. The second method investigates bulk modified electrodes and their capability to allow immobilization of DNA onto the electrode surface. Electrochemistry is the primary technique used to probe the performance of these electrodes; the rate of electron transfer, rate of charge propagation, RC time constant. Scanning electron microscopy, UV/vis, CHN, and HPLC are used to characterize the components of the modified electrodes.

General Conclusion and Future Work

Current advances in science are indicating that nanotechnology and genetics will be the route to the future especially, regarding the analysis of disease causing pathogens. Nanotechnology can now provide instruments capable of detecting picoampre currents, probing timescales in the nanosecond time domain, hence; reducing the limit of detection and probe fast reactions that were previously not possible. Developments in genetics have resulted in the capability of providing information pertaining to the sequences of DNA causing pathogens.

If the knowledge provided by geneticists can be optimised it should be possible to detect almost immediately a single strand of DNA specific to a disease causing pathogen. As to what methods are available that can utilize both advances in nanotechnology and genetics the obvious answer is sensor technology, since microelectrodes are themselves promising to revolutionize this branch of electrochemistry.

The first Chapters of this thesis are dedicated to what influence if any the supporting electrolyte and presence a biocomponent can have on the overall electrochemical response, if the classical polymer modified electrodes were to be used for micro sensing technologies. The results obtained suggest that choice of buffer can result in a sluggish rate of charge transport, while the presence of a non-electroactive biocomponent can cause sluggish electron transfer through the PME. Given the present sensor targets this will not cause a problem, however if the intention is to

248

implement sensors to study fast electron transfer reactions, as in the case of reactive oxygen species known to cause damage at various points in-vivo, for any in-vitro study the choice of buffer may play an important role.

From work carried out in the 1980s and 1990s regarding sensors it was realized that an ideal sensor would be capable of repeated use and possess a high signal/noise ratio allowing detection limits to be improved. Carbon composite electrodes offer these advantages since they are composed of a random array of carbon microparticles embedded in a rigid polymer matrix. An electrochemical investigation into the properties of these electrodes confirms a constantly mentioned property known as steady state behaviour. The advantage of such a phenomena is the reduced limit of detection if compared with other surface modified macroelectrodes. While this behaviour is often mentioned as unique to microelectrodes, and, many authors have assumed that these composite electrodes are examples of microelectrode arrays. The electrochemical study conducted in this thesis indicates otherwise as an RC time constant and a rate of heterogeneous electron transfer proved to be greater than that obtained for macroelectrodes. Therefore, restricting the possibility of using these electrodes to study fast electron exchange reactions.

While none of the above polymer modified electrodes appear to solve the problem, of how to take sensing technology into nanodimension, Chapter five illustrates how these composite electrodes are possible to modify with a protein (avidin or streptavidin) and in combination with molecular biology it is possible to create a sensing probe that can immobilize a specifically labelled DNA sequence (biotin–DNA) allowing subsequent hybridisation with a target DNA probe (MRSA). Utilizing the low signal/noise ratio of these composites it is possible to detect the presence of DNA at very low concentrations. The process of bulk immobilization allows repeated use of these electrodes, where different capture DNA probes may be immobilized onto the electrode surface. However, the possibility of designing biologically modified carbon composite microelectrodes contained within micro capillary tubing are unlikely, unless improvements can be made regarding resistance and rate of heterogeneous electron transfer.

However, in terms of future work utilizing composite designs, an area which is showing great promise in recent years, is that of screen printing technology. In this method an ink is pasted over a conductive material and one use sensors are produced. If material science can improve the currently available inks and improvements can be

made on the binding of these inks to the conductive substrate the possibility of rapid one off use sensors capable of low limits of detection, may be realised.

250